U.S.NRC
United States Nuclear Regulatory Commission
Protecting People and the Environment

NUREG/CR–6909, Rev. 1

Effect of LWR Water Environments on the Fatigue Life of Reactor Materials

Final

Office of Nuclear Regulatory Research

AVAILABILITY OF REFERENCE MATERIALS IN NRC PUBLICATIONS

NRC Reference Material

As of November 1999, you may electronically access NUREG-series publications and other NRC records at the NRC's Public Electronic Reading Room at http://www.nrc.gov/reading-rm.html. Publicly released records include, to name a few, NUREG-series publications; *Federal Register* notices; applicant, licensee, and vendor documents and correspondence; NRC correspondence and internal memoranda; bulletins and information notices; inspection and investigative reports; licensee event reports; and Commission papers and their attachments.

NRC publications in the NUREG series, NRC regulations, and Title 10, "Energy," in the *Code of Federal Regulations* may also be purchased from one of these two sources.

1. **The Superintendent of Documents**
   U.S. Government Publishing Office
   Mail Stop SSOP
   Washington, DC 20402-0001
   Internet: http://bookstore.gpo.gov
   Telephone: 1-866-512-1800
   Fax: (202) 512-2104

2. **The National Technical Information Service**
   5301 Shawnee Road
   Alexandria, VA 22161-0002
   http://www.ntis.gov
   1-800-553-6847 or, locally, (703) 605-6000

A single copy of each NRC draft report for comment is available free, to the extent of supply, upon written request as follows:

U.S. Nuclear Regulatory Commission
Office of Administration
Publications Branch
Washington, DC 20555-0001
E-mail: distribution.resource@nrc.gov
Facsimile: (301) 415-2289

Some publications in the NUREG series that are posted at the NRC's Web site address http://www.nrc.gov/reading-rm/doc-collections/nuregs are updated periodically and may differ from the last printed version. Although references to material found on a Web site bear the date the material was accessed, the material available on the date cited may subsequently be removed from the site.

Non-NRC Reference Material

Documents available from public and special technical libraries include all open literature items, such as books, journal articles, transactions, *Federal Register* notices, Federal and State legislation, and congressional reports. Such documents as theses, dissertations, foreign reports and translations, and non-NRC conference proceedings may be purchased from their sponsoring organization.

Copies of industry codes and standards used in a substantive manner in the NRC regulatory process are maintained at—

The NRC Technical Library
Two White Flint North
11545 Rockville Pike
Rockville, MD 20852-2738

These standards are available in the library for reference use by the public. Codes and standards are usually copyrighted and may be purchased from the originating organization or, if they are American National Standards, from—

American National Standards Institute
11 West 42nd Street
New York, NY 10036-8002
http://www.ansi.org
(212) 642-4900

Legally binding regulatory requirements are stated only in laws; NRC regulations; licenses, including technical specifications; or orders, not in NUREG-series publications. The views expressed in contractor-prepared publications in this series are not necessarily those of the NRC.

The NUREG series comprises (1) technical and administrative reports and books prepared by the staff (NUREG-XXXX) or agency contractors (NUREG/CR-XXXX), (2) proceedings of conferences (NUREG/CP-XXXX), (3) reports resulting from international agreements (NUREG/IA-XXXX), (4) brochures (NUREG/BR-XXXX), and (5) compilations of legal decisions and orders of the Commission and Atomic and Safety Licensing Boards and of Directors' decisions under Section 2.206 of NRC's regulations (NUREG-0750).

NUREG/CR–6909, Rev. 1

U.S.NRC
United States Nuclear Regulatory Commission
Protecting People and the Environment

Effect of LWR Water Environments on the Fatigue Life of Reactor Materials

Final

Manuscript Completed: January 2017
Date Published: March 2018

Prepared by
Omesh Chopra[1] and Gary L. Stevens[2]

[1] Argonne National Laboratory
9700 South Cass Avenue, Argonne, IL 60439

[2] Electric Power Research Institute
1300 West W.T. Harris Boulevard, Charlotte, NC 28262

Appajosula Rao, NRC Project Manager

NRC Job Codes V6069/V6269

Office of Nuclear Regulatory Research

ABSTRACT

The American Society of Mechanical Engineers Boiler and Pressure Vessel Code (ASME Code) provides rules for the design of Class 1 components of nuclear power plants. Figures I-9.1 through I-9.6 of Appendix I to Section III, "Rules for Construction of Nuclear Facility Components," of the ASME Code specify fatigue design curves for applicable structural materials. However, the ASME Code design curves do not explicitly address the effects of light-water reactor (LWR) water environments. The existing fatigue strain vs. life (ε–N) data illustrate potentially significant effects of LWR water environments on the fatigue resistance of pressure vessel and piping steels. Under certain environmental and loading conditions, the fatigue lives of reactor components in water relative to those in air can be a factor of approximately 12 lower for austenitic stainless steels, approximately 3 lower for nickel-chromium-iron alloys, and approximately 17 lower for carbon and low-alloy steels. The original version of NUREG/CR-6909, "Effect of LWR Coolant Environments on the Fatigue Life of Reactor Materials—Final Report," issued February 2007, which is the technical basis document for Regulatory Guide 1.207, "Guidelines for Evaluating Fatigue Analyses Incorporating the Life Reduction of Metal Components Due to the Effects of the Light-Water Reactor Environment for New Reactors," issued March 2007, summarizes the work performed at Argonne National Laboratory on the fatigue of piping and pressure vessel steels in LWR environments. That document evaluates the existing fatigue ε–N data to identify the various material, environmental, and loading parameters that influence fatigue crack initiation and to establish the effects of key parameters on the fatigue lives of these steels. The report presents fatigue life models for estimating fatigue lives as a function of material, loading, and environmental conditions and describes the environmental fatigue correction factor (F_{en}) for incorporating the effects of LWR environments into ASME Code Section III fatigue evaluations. The report also presented a critical review of the ASME Code Section III fatigue adjustment factors of 2 on stress (or strain) and 20 on life and assessed the possible conservatism in the choice of these adjustment factors.

This report provides updates and improvements to the F_{en} approach based on an extensive update to the fatigue ε–N data from testing and results available over the past decade since this report was first published. The updated expressions also address concerns from interested stakeholders related to (1) the constants in the F_{en} expressions that result in F_{en} values of approximately 2 even when the strain rate is very high or the temperature is very low, (2) the temperature dependence of F_{en} for carbon and low-alloy steels, and (3) the dependence of F_{en} on water chemistry for austenitic stainless steels. The F_{en} methodology was validated by comparing the results of five different experimental datasets obtained from fatigue tests that simulate actual plant conditions with estimates of fatigue usage adjusted for environmental effects using the updated F_{en} expressions. The potential effects of dynamic strain aging on cyclic deformation and environmental effects are also discussed.

FOREWORD

This report summarizes, reviews, and quantifies the effects of the light-water reactor (LWR) environments on the fatigue lives of reactor materials, including carbon steels, low-alloy steels, nickel-chromium-iron (Ni-Cr-Fe) alloys, and austenitic stainless steels. The primary purpose of this report is to provide the background and technical bases to support the revision of Regulatory Guide 1.207, "Guidelines for Evaluating Fatigue Analyses Incorporating the Life Reduction of Metal Components Due to the Effects of the Light-Water Reactor Environment for New Reactors," issued March 2007.

The original version of this report included a review of the fatigue strain vs. life (ε–N) data available at that time for carbon steels, low-alloy steels, Ni-Cr-Fe alloys, and austenitic stainless steels to define the potential effects of key material, loading, and environmental parameters on the fatigue lives of the steels. This database was used to update the fatigue life models in use at the time to estimate the fatigue curves as a function of key material, loading, and environmental parameters. The original version of this report also provided a procedure for incorporating environmental effects into fatigue evaluations. This revision of the report incorporates additional fatigue ε–N data available since the original publication of this report, most particularly from Japan, into the database and updates the fatigue life models. In addition, feedback from interested stakeholders obtained since the original publication of this report has been evaluated and incorporated in the report, as appropriate.

The database summarized in this report demonstrates that the previously published guidance in Regulatory Guide 1.207 for incorporating the LWR environmental effects in fatigue life evaluations should be revised. Toward that end, this report maintains the previously established methods for establishing reference air fatigue curves and defines updated environmental fatigue correction factors for use in evaluating the fatigue lives of reactor components exposed to LWR water environments.

The database described in this revised report has been used to verify that the previously developed fatigue design curves in air are consistent with the available fatigue data. Specifically, the existing curves from American Society of Mechanical Engineers Boiler and Pressure Vessel Code (ASME Code), Section III, "Rules for Construction of Nuclear Facility Components," are appropriate for austenitic stainless steels (e.g., Types 304, 316, and 316NG) and nickel-based alloys and are conservative for carbon and low-alloy steels. Revision 1 of Regulatory Guide 1.207 endorses the fatigue design curves presented herein for incorporation in fatigue analyses for new and operating reactors.

TABLE OF CONTENTS

LIST OF FIGURES

LIST OF TABLES

EXECUTIVE SUMMARY

Cyclic loadings on a reactor pressure boundary component occur because of changes in mechanical and thermal loadings as the system goes from one load set (e.g., pressure, temperature, moment, and force loading) to another. Subsection NB, "Class 1 Components," of Section III, "Rules for Construction of Nuclear Facility Components," of the American Society of Mechanical Engineers Boiler and Pressure Vessel Code (ASME Code) contains rules for the design of Class 1 components of nuclear power plants and recognizes fatigue as a possible mode of failure in pressure vessel steels and piping materials. ASME Code Section III fatigue analysis procedures consider all fatigue cycles based on the anticipated number of thermal and pressure transients. In addition, for each load cycle or load set pair, an individual fatigue usage factor is determined by the ratio of the number of cycles anticipated during the design lifetime of the component, as specified by the Owner, to the number of allowable cycles. Figures I-9.1 through I-9.6 of Mandatory Appendix I to Section III of the ASME Code specify fatigue design curves that define the allowable number of cycles as a function of applied stress amplitude. Those fatigue design curves have evolved significantly since the initial publication of ASME Code Section III in 1963. However, Paragraph NB-3121 of the 2011 Addenda to ASME Code Section III continues to state that the effects of water environments on the fatigue resistance of materials were not addressed in the fatigue design curves. Therefore, the effects of water environments on the fatigue resistance of materials used in operating pressurized-water reactors and boiling-water reactors, whose components were designed in accordance with ASME Code Section III, may not adequately address long-term environmental effects on fatigue based on the data available at the time the fatigue design curves were derived.

The current design fatigue curves in air contained in ASME Code Section III were based primarily on strain-controlled fatigue tests of small polished specimens at room temperature in laboratory air environments. Best-fit curves to the experimental test data were first adjusted to account for the effects of mean stress and then lowered by a factor of 2 on stress and 20 on cycles (whichever was more conservative) to obtain the design fatigue air curves. These factors were not intended as "safety margins"; instead, they were intended as "adjustment factors" that were applied to the experimental laboratory data to obtain estimates of the fatigue lives of actual reactor components. Recent fatigue strain vs. life (ε–N) data obtained primarily in the United States and Japan demonstrate that light-water reactor (LWR) environments have potentially significant effects on the fatigue resistance of materials. Specimen lives obtained from laboratory tests in simulated LWR environments were much shorter than those obtained from corresponding tests in an air environment.

The original version of NUREG/CR-6909, "Effect of LWR Coolant Environments on the Fatigue Life of Reactor Materials—Final Report," issued February 2007, evaluates the existing fatigue ε–N data for carbon and low-alloy steels, wrought and cast austenitic stainless steels (SSs), and nickel-chromium-iron (Ni-Cr-Fe) alloys in air and LWR environments to identify the various material, environmental, and loading parameters that influence fatigue crack initiation. The results of those evaluations were used to establish the effects of key parameters on the fatigue lives of steels. The fatigue lives of materials were decreased in LWR environments; the magnitude of the reduction depended on the temperature, strain rate, and dissolved oxygen (DO) level in the water and, for carbon and low-alloy steels, the sulfur content of the steels. For all steels, environmental effects on fatigue lives were significant only when critical parameters (temperature, strain rate, DO level, and strain amplitude) met certain threshold values. Environmental effects were moderate (e.g., less than a factor of 2 decrease in fatigue lives) when any one of the threshold conditions was not satisfied. The threshold values of the critical

parameters and the effects of other parameters (such as water conductivity, water flow rate, and material heat treatment) on the fatigue lives of the steels were also discussed.

This report reevaluates the fatigue ε–N data for nuclear power plant piping and pressure vessel steels presented in the original version of NUREG/CR-6909 using a much larger database. The results were updated to include this reevaluation and to address concerns from interested stakeholders about the environmental fatigue correction factor (F_{en}) methodology for incorporating environmental effects into ASME Code Section III fatigue cumulative usage factor evaluations. This report summarizes the resulting effects of various material, loading, and environmental parameters on the fatigue lives of steels. Note that, as with the original evaluation, the reevaluation in this report was still based on various compositions of wrought Type 304 and 316 SSs, associated weld metals, and a few heats of CF-8M cast austenitic SSs. The reevaluation did not consider other grades of austenitic SSs, particularly the titanium- or niobium-modified SSs, which have better fatigue resistance. Therefore, fatigue lives based on the proposed fatigue design curve are expected to be conservative for SSs with improved fatigue resistance, such as the titanium- or niobium-modified steels.

The results indicate that the ASME Code Section III mean air curve for low-alloy steels is in good agreement with the available experimental data and that the ASME Code Section III mean air curve for carbon steels is conservative. In addition, the best-fit mean air curve used to develop the fatigue design air curve for austenitic SSs in ASME Code Section III editions before publication of the 2009 Addenda is not consistent with the experimental data at strain amplitudes of less than 0.5%; fatigue lives predicted by the ASME Code Section III mean air curve were longer than those obtained from experiments. Therefore, in the initial version of NUREG/CR-6909, new fatigue design air curves were developed for carbon and low-alloy steels and austenitic SSs that were based on the Argonne National Laboratory (ANL) fatigue life models and were consistent with the fatigue ε–N data available at that time. The air design curves were extended up to 10^{11} cycles using available high-cycle fatigue data. In 2009, the ANL design air curve for austenitic SSs was adopted into Mandatory Appendix I to ASME Code Section III. The reevaluation of the fatigue ε–N behavior of austenitic SS materials using a much larger database indicates that the air fatigue design curves previously developed by ANL are consistent with the available fatigue data and do not warrant any modifications. However, the present report modifies the extension of the air fatigue design curves for carbon and low-alloy steels up to 10^{11} cycles to be consistent with the extension of the current ASME Code Section III fatigue design curve beyond 10^6 cycles.

The reevaluation results also indicate that the fatigue data for Ni-Cr-Fe alloys were not consistent with the current ASME Code mean air curve for austenitic SSs. The rather limited fatigue ε–N data for Ni-Cr-Fe alloys, such as Alloys 600, 690, and 800 and their welds, are consistent with the best-fit mean air curve for austenitic SSs at fatigue lives less than 10^4 cycles and show longer fatigue lives than the predicted values for fatigue lives greater than 10^4 cycles. However, a separate air fatigue design curve was not developed for Ni-Cr-Fe alloys, and the current ASME Code fatigue air design curve for austenitic SSs, which is based on the ANL model, was used to represent the fatigue ε–N behavior of Ni-Cr-Fe alloys and associated weld metals. The data also indicate that the fatigue resistance of Inconel 718 is superior to that of the other Ni-Cr-Fe -alloys. The slope of the Inconel 718 fatigue ε–N curve is flatter, and the fatigue limit is higher than those for austenitic SSs. Therefore, the current ASME Code fatigue air design curve for austenitic SSs curve is conservative for representing the fatigue ε–N behavior of Inconel 718.

The fatigue lives of carbon and low-alloy steels, austenitic SSs, and Ni-Cr-Fe alloys were decreased in LWR environments. The reduction depended on some key material, loading, and environmental parameters. The fatigue ε–N data were consistent with the much larger database on enhancement of crack growth rates in these materials in LWR environments. The key parameters that influenced fatigue lives in these environments (e.g., temperature, DO level in the water, strain rate, strain (or stress) amplitude, and, for carbon and low-alloy steels, sulfur content of the steel) were identified. In addition, the functional form of the dependence of fatigue lives on these parameters and the range of the values of these parameters within which environmental effects were significant was defined. If these critical loading and environmental conditions exist during reactor operation, environmental effects may be significant and should be included in any relevant ASME Code Section III fatigue evaluations.

The initial version of NUREG/CR-6909 developed fatigue life models to predict the fatigue lives of small smooth specimens of carbon and low-alloy steels, wrought and cast austenitic SSs, and Ni-Cr-Fe alloys as a function of material, loading, and environmental parameters using the existing fatigue ε–N database. The functional form and bounding values of these parameters were based on experimental observations and data trends. An approach was presented that incorporates the effects of LWR coolant environments into the ASME Code Section III fatigue evaluations based on the F_{en}. The fatigue usage for a specific stress cycle or load set pair derived using the ASME Code Section III fatigue design air curves was multiplied by the F_{en} to account for environmental effects. Note that the F_{en} approach described in this report is only applicable for use as part of an ASME Code fatigue evaluation. Further, this report does not address any conservatisms associated with the ASME Code fatigue evaluation procedures.

The present report updates the F_{en} expressions using a much larger fatigue ε–N database, primarily derived from extensive additional data provided from Japan. The updated expressions also address comments provided by interested stakeholders related to (1) the constants in the F_{en} expressions that result in an F_{en} value of approximately 2 even when the strain rate is very high or the temperature is very low, (2) the temperature dependence of F_{en} for carbon and low-alloy steels, and (3) the dependence of F_{en} on water chemistry for austenitic SSs.

This report also briefly describes the mechanisms for fatigue cracking in air and LWR water environments. Fatigue life is conventionally divided into two stages—initiation and propagation. In LWR environments, the initiation stage involves the growth of microstructurally small cracks characterized by decelerating crack growth. The propagation stage involves the growth of mechanically small cracks characterized by accelerating crack growth. The available fatigue ε–N data indicated that LWR environments affect both the initiation and propagation of fatigue cracks. Two mechanisms are described in this report that potentially enhance both fatigue crack initiation and fatigue crack growth rates in LWR environments—slip oxidation/dissolution and hydrogen-induced cracking. The potential effects of dynamic strain aging on cyclic deformation and environmental effects are also discussed.

This report also presents a critical review of the ASME Code Section III fatigue adjustment factors of 2 on stress and 20 on life and assesses the possible conservatism in the choice of adjustment factors. Although these factors were intended to be conservative, they were not considered to be safety margins in the work presented in this report. Instead, these factors cover the effects of variables that influence fatigue lives but were not investigated in the experiments that were used to obtain the air fatigue design curves. Data available in the literature were reviewed to evaluate the factors on cycles that are needed to account for such differences and uncertainties. Monte Carlo simulations were performed to determine the factor on cycles needed to obtain a fatigue design curve in air that provided a conservative estimate of

the number of cycles required to initiate a fatigue crack in reactor components. The results presented in the original version of NUREG/CR-6909 indicate that, for carbon and low-alloy steels and austenitic SSs, the current ASME Code Section III requirements for a factor of 20 on cycles to account for the effects of material variability and data scatter, size, surface finish, and loading history may be decreased by at least a factor of 1.7. Thus, to reduce conservatism, fatigue design curves were developed based on the ANL fatigue life models, and those curves were then adjusted for mean stress effects and by factors of 2 on stress and 12 on cycles. These adjustments were made to account for the effects of (1) material variability and data scatter, (2) size, (3) surface finish, and (4) loading sequence. For this report, the range of these four parameters were modified, and Monte Carlo simulations were repeated to determine the factor on cycles needed to obtain fatigue design curves in air. The results indicate that, for carbon and low-alloy steels and austenitic SSs, factors of 2 on stress and 10 on cycles are adequate to develop air fatigue design curves from the best-fit mean air curves. However, until these results are further validated with applicable fatigue data ε–N data, the air fatigue design curves presented in this report are based on factors of 2 on stress and 12 on life.

The F_{en} methodology was also validated by comparing the results of several experimental datasets obtained from fatigue tests that simulated actual plant conditions with estimated fatigue usage using the updated F_{en} expressions. The datasets represent fatigue tests with changing strain rate or temperature, or both; complex loading that simulated a pressurized-water reactor safety injection transient; spectrum loading (i.e., random strain amplitudes); and pipe U-bend tests. In all cases, the results indicate that the predicted fatigue lives were in good agreement with the experimental values; the differences between the experimental and predicted fatigue lives were within a factor of 2, which is within the experimental data scatter. The predicted fatigue lives for the tests with the complex strain loading cycle were lower than the experimental values by a factor of about 2. The reason for this deviation was not clear but may be unique to the specific test loading cycle. Nonetheless, although the predicted lives were all lower, the estimated values were within the range of data scatter.

This report also presents a detailed procedure for incorporating environmental effects into ASME Code Section III fatigue evaluations. This procedure applies to any component exposed to the LWR environment that requires an ASME cumulative usage factor calculation either as part of its design, for the component's safety basis, or as part of the plant current licensing basis, unless otherwise justified. This procedure allows evaluation using either a modified rate or an average rate approach. F_{en} calculations based on an average strain rate for the transient are expected to yield conservative estimates of fatigue lives as long as the calculations use appropriate temperatures selected in accordance with the recommended procedures in Section 4.4. Using an average transient temperature within the average strain rate approach does not always yield a conservative estimate of F_{en}. Therefore, an average temperature should only be used if it has been demonstrated that it yields a comparable or conservative estimate of F_{en} compared to the F_{en} obtained using the modified rate approach. The ASME Code Section III fatigue design curves for carbon and low-alloy steels and austenitic SSs apply to various grades and compositions of materials having a wide range of tensile strength. Furthermore, the criterion used in establishing the fatigue design curve ensures that the proposed curve bounds 95% of the available fatigue data with 95% confidence. In addition, the mean stress correction for the design curves is based on a conservative value of mean stress at room temperature. Finally, the fatigue loading in laboratory specimens is uniformly tensile, which is more severe than in many applications where the loading decreases through the thickness. Therefore, the design curves should be conservative for most materials and applications, particularly at reactor operating temperatures where mean stresses are likely to be lower.

The criteria used for establishing the adjustment factors to account for the parameters that influence fatigue life, but were not considered in the experimental data used to develop the fatigue design curves (Section 5), also yield conservative values of fatigue life in applications. These adjustment factors may be further optimized. It should be stressed that other factors (e.g., component size) may lead to decreases in fatigue life in applications compared to laboratory testing. Therefore, any modifications of the design curves or adjustment factors should be performed holistically to develop a technical basis that addresses all the sources of conservatism and uncertainty mentioned above. Further, guidance should be provided for using the high-cycle portion of the design curves for mechanical loading. This guidance is necessary because strain-controlled fatigue test data are used to develop the ASME Code strain vs. life fatigue design curves, and these must be converted to pseudo-stress vs. life curves in most applications.

Revision 1 of this report represents a comprehensive and detailed expansion of the Revision 0 manuscript that incorporates significant additional background, test data, and test data descriptions. In addition, the content layout of the report was revised for clarity. As a result, the changes made to the Revision 0 manuscript are not specifically identified throughout the text of this revision.

ACKNOWLEDGMENTS

The authors are indebted to the Japan Nuclear Regulatory Authority (formerly the Japan Energy Safety Organization) for sharing its enormous fatigue strain vs. life database for use in the evaluations documented in this report. The authors are deeply indebted to Dr. Robert Tregoning for preparing the final manuscript of this report and his help in addressing and incorporating the public comments. The authors are also grateful to Dr. William J. Shack for his invaluable input and guidance in preparing this report. The authors acknowledge Dr. Appajosula Rao for his help in preparing and publishing this report and Dr. Yogen Garud for his contributions and helpful comments. This work was cosponsored by the Office of Nuclear Regulatory Research, U.S. Nuclear Regulatory Commission (NRC) (Gary L. Stevens, Project Manager), and the Electric Power Research Institute (EPRI) as Cooperative Nuclear Safety Research under the Environmentally Assisted Fatigue Effects Addendum to the NRC/EPRI Memorandum of Understanding, under NRC Job Codes V6069 and V6269.

ABBREVIATIONS AND ACRONYMS

ANL	Argonne National Laboratory
ANN	artificial neural network
ASME	American Society of Mechanical Engineers
ASME Code	American Society of Mechanical Engineers Boiler and Pressure Vessel Code
ASTM	American Society for Testing and Materials
ATR	Advanced Test Reactor
BTP	branch technical position
BNCS	Board on Nuclear Codes and Standards
BWR	boiling water reactor
^{o}C	degrees Celsius
CGR	crack growth rate
CLEE	cyclic life environmental effects
cm^3/kg	cubic centimeters per kilogram
CT	compact tension
CUF	cumulative usage factor
CVCS	chemical and volume control system
CW	cold worked
da/dN	fatigue crack growth rate (expressed as the change in crack depth, da, divided by the number of applied cycles, dN)
DO	dissolved oxygen
DSA	dynamic strain aging
E	Energy
EAC	environmentally assisted cracking
EBR II	Experimental Breeder Reactor II
ECP	electrochemical potential
EFD	environmental fatigue data
EFT	environmental fatigue testing
EPR	electrochemical potentiodynamic reactivation
EPRI	Electric Power Research Institute
ETR	Experimental Test Reactor
ε–N	fatigue strain vs. life
F_{en}	environmental fatigue correction factor
^{o}F	degrees Fahrenheit
FAP	fatigue action plan
GE	General Electric Company
GSI	generic safety issue
H	Hydrogen
HS	hydrosulfide ion
HAZ	heat affected zone
He	Helium
HWC	hydrogen water chemistry
ID	internal diameter
IG	Intergranular
in.	Inches
IHI	Ishikawajima-Harima Heavy Industries
INEL	Idaho National Engineering Laboratory
JAPEIC	Japan Power Engineering and Inspection Corporation

JNES	Japan Nuclear Energy Safety Organization
JNUFAD	revised and renamed fatigue database “FADAL” from Japan
KWU	Kraftwerk Union Laboratories
L/h	liters per hour
LEFM	linear elastic fracture mechanics
LWR	light-water reactor
LWR water environment	light-water reactor water environment
μS/cm	microsiemens per centimeter
MA	mill annealed
MEA	Materials Engineering Associates
MeV	million electron volts
MHI	Mitsubishi Heavy Industries
m	Meters
μm	Micrometers
mm	Millimeters
MnS	manganese sulfide
MOU	memorandum of understanding
MPa	Megapascals
m/s	meters per second
MPA	Materialprufungsanstalt
MSC	microstructurally small crack
N	number of cycles
N_{air}	number of cycles in air
N_{water}	number of cycles in water environment
NASA	National Aeronautics and Space Administration
n/cm^2	neutrons per centimeter squared
Ni-Cr	Nickel-chromium
Ni-Cr-Fe	nickel-chromium-iron
Ni-Fe-Cr	nickel-iron-chromium
n/m^2	neutrons per meter squared
NPS	nominal pipe size
NRC	U.S. Nuclear Regulatory Commission
NWC	normal water chemistry
OD	outer diameter
ORNL	Oak Ridge National Laboratory
ppb	parts per billion
ppm	parts per million
PSB	persistent slip band
psi	pounds per square inch
PVRC	Pressure Vessel Research Council
PWR	Pressurized-water reactor
R_a	average surface roughness (μm)
R_q	root-mean-square value of surface roughness (μm)
R_t	maximum height of the surface roughness profile (μm)
RCS	reactor coolant system
RG	regulatory guide
RHR	residual heat removal
RMS	root mean square
RT	room temperature (77°F [25°C])

S	Sulfur
S^{2-}	sulfide ion
SICC	strain-induced corrosion cracking
SS	stainless steel
T	Temperature
TENPES	Thermal and Nuclear Power Engineering Society
Ti	Titanium
TG	Transgranular
TMI	Three Mile Island
UTS	ultimate tensile strength
VTT	Valtion Teknillinen Tutkimuskeskus (Technical Research Center of Finland)
VVER	Voda-Vodyanoi Energetichesky Reaktor (Russian PWR)
WRC	Welding Research Council
YS	monotonic yield strength

1 INTRODUCTION

The structural integrity of a metal component may gradually degrade when it is subjected to cyclic loading, even at magnitudes less than the design static loads, caused by a well-known degradation mechanism called fatigue. The mechanism of fatigue can damage flaw-free components by causing them to develop cracks during service. Subsection NB "Class 1 Components," of Section III, "Rules for Construction of Nuclear Facility Components," of the American Society of Mechanical Engineers Boiler and Pressure Vessel Code (ASME Code), which contains rules for the design of Class 1 components for nuclear power plants, recognizes fatigue as a possible mode of failure in pressure vessel steels and piping materials. Fatigue is a major consideration in the design of rotating machinery and aircraft in which the components are subjected to a very large number of cycles (i.e., high-cycle fatigue). In these situations, the primary concern is the endurance limit, which is the stress level below which an infinite number of cycles can be applied without fatigue failure. However, cyclic loadings on a reactor pressure boundary component occur because of changes in mechanical and thermal loadings as the system goes from one load state to another. The number of cycles applied during the design life of the component seldom exceeds 100,000 and is typically less than a few thousand (e.g., low-cycle fatigue). The main difference between high-cycle and low-cycle fatigue is that the former involves little or no plastic strain, whereas the latter involves strains in excess of the yield strain. Therefore, design curves for low-cycle fatigue are based on tests in which strain rather than stress is the controlled variable.

Subarticles NB-3200, "Design by Analysis," and NB-3600, "Piping Design," of ASME Code Section III describe the fatigue evaluation procedures. The ASME Code fatigue analysis considers all transient loads based on the anticipated number of thermal and pressure transients, and for each load cycle or load set pair, an individual fatigue usage factor is determined by the ratio of the number of cycles anticipated during the lifetime of the component to the allowable cycles. Figures I-9.1 through I-9.6 of Mandatory Appendix I to ASME Code Section III specify fatigue design curves for various materials that define the allowable number of cycles as a function of applied stress amplitude. The cumulative usage factor (CUF) is the sum of the individual usage factors for all load set pairs, and ASME Code Section III requires that at each location, the CUF, which is calculated based on Miner's rule, must not exceed unity for acceptable fatigue design.

Although the ASME Code Section III rules apply to Class 1 components, those fatigue design rules are sometimes applied to other classes of components to provide a robust fatigue design in situations where known fatigue issues exist or fatigue duty is high (e.g., Class 2 pressurized-water reactor (PWR) feedwater nozzles). As such, the methods described in this report are intended to apply to all components exposed to any water environment in a light-water reactor (LWR) that uses the fatigue calculation procedures from ASME Code Section III. References made to an "LWR environment" throughout this report refer to any water environment at a temperature greater than 50°C in an LWR power plant and encompasses both steady-state and transient conditions, such as during a reactor shutdown.

This revision represents a comprehensive and detailed expansion of the Revision 0 manuscript (i.e., the original version of NUREG/CR-6909, "Effect of LWR Coolant Environments on the Fatigue Life of Reactor Materials—Final Report," issued February 2007, as depicted throughout this report) that incorporates significant additional background, test data, and test data descriptions. In addition, the content layout of the report was revised for clarity. As a result, the

changes made to the Revision 0 manuscript are not specifically identified throughout the text of this revision.

1.1 Definition of Fatigue Life

Before discussing the fatigue design curves used in the ASME Code Section III fatigue CUF analysis, the use of the term "fatigue life" in this report should first be described. American Society for Testing and Materials (ASTM) Designation E 1823-09a, "Standard Terminology Relating to Fatigue and Fracture Testing,"[1] issued March 2009, defines fatigue life as "the number of cycles of a specified character that a given specimen sustains before failure of a specified nature occurs. Fatigue life, or the logarithm of fatigue life, is a dependent variable." Accordingly, the ASME Code fatigue design curves [i.e., stress amplitude (S_a) vs. number of cycles (N) curves] are generally considered to represent the allowable number of cycles to failure. However, note that ASTM Standard E1823-09a states that fatigue life is "failure of a specified nature." Furthermore, Section 8.9 of ASTM Standard E606-04, "Standard Practice for Strain-controlled Fatigue Testing,"[2] issued July 2005, states that the definition of failure may vary with the ultimate use of the fatigue life information, and provides the following acceptable alternatives for determination of failure:

(i) *Separation*: Total separation or fracture of the specimen into two parts at (1) some location within the uniform section of the uniform-gauge specimen, or (2) the vicinity of the minimum diameter in the hourglass specimen.

(ii) *Modulus Method*: For any specified number of cycles, N, during a fatigue test, the modulus for unloading following a peak tensile stress is defined as E_{NT} and the modulus for loading following a peak compressive stress is E_{NC}. Failure is defined as the number of cycles where the ratio E_{NT}/E_{NC} reaches one-half the value for the first cycle (i.e., is reduced by 50%). However, if total separation occurs first, as in item (i) above, fatigue life is defined by the number of cycles to separation.

(iii) *Microcracking*: The existence of surface microcracks (e.g., as observed optically or by replicas) that are larger than some preselected size consistent with the test objective.

(iv) *Force (Stress) Drop*: Failure is defined as the ability of a test specimen to sustain a tensile force (or stress). Failure is often defined as the point at which the maximum force (stress) or elastic modulus (as measured when unloading from a peak tensile stress) decreases by approximately 50% because of the presence of cracks. The exact method and the percentage drop should be documented.

In the fatigue strain vs. life (ε–N) data used to develop the original ASME Code best-fit or mean-data curves, failure was primarily defined as total separation or fracture of the specimen into two parts. In the fatigue tests performed during the last four decades, failure was defined according to the force (stress) drop method. In most of these tests, fatigue life was defined in terms of the number of cycles for the tensile stress to decrease 25% from its peak or steady-state value (i.e., 25% load drop). For the typical 9.5-mm diameter cylindrical specimens used in these studies, this load drop corresponded to the number of cycles needed to produce approximately 3-mm-deep cracks in test specimens.

Based on the foregoing discussion and the results of the majority of the test data evaluated, fatigue life is defined in this report as the number of cycles of a specified strain amplitude that a specimen can sustain before the formation of a 3-mm-deep crack (i.e., an "engineering crack"). Thus, the fatigue life of a material can be described in terms of three parameters: strain or stress, cycles, and crack depth. The best–fit curve to the existing fatigue ε–N data describes, for a given strain or stress amplitude, the number of cycles needed to develop a 3–mm deep crack. This number of cycles also equates to a 25% load drop in a solid 9.5-mm test specimen, and is assumed to equate to crack initiation in an actual component. Using this definition, a calculated fatigue CUF of less than unity provides reasonable assurance that a fatigue crack has not formed in a component, and indicates that the probability of forming a crack in the component is low.

1.2 Air Fatigue Design Curves in ASME Code Section III

The ASME Code fatigue design curves, as given in Mandatory Appendix I to ASME Code Section III, are based on strain–controlled tests of small polished specimens at room temperature in air. The data are typically obtained from fatigue tests conducted in accordance with ASTM Standard E606-04. This practice covers the determination of fatigue properties of nominally homogeneous materials by the use of uniform gauge section specimens subjected to axial strain-controlled, fully reversed (strain ratio, R, equal to -1) cycling. The practice also applies to hourglass specimens. The practice may be adapted to guide more general testing where strain or temperature may be varied according to application specific histories. The presentation and analysis of data are performed in accordance with ASTM Standard E468, "Standard Practice for Presentation of Constant Amplitude Fatigue Test Results for Metallic Materials,"[3] issued October 2004, and ASTM Standard E739, "Standard Practice for Statistical Analysis of Linear or Linearized Stress-Life (S–N) and Strain-Life (ε–N) Fatigue Data,"[4] issued May 2006. The guidance in Volume 8, "Fatigue Data Analysis,"[5] issued 1985, of the *Metals Handbook* can also be used. ASTM Standard E1823, "Standard Terminology Relating to Fatigue and Fracture Testing,"[6] issued March 2009, defines the terms related to fatigue testing.

The design curves were developed from the best–fit curves to the experimental fatigue ε–N data, which are expressed in terms of the Langer equation[7] of the form

$$\varepsilon_a = A1(N)^{-n1} + A2, \tag{1}$$

where ε_a is the applied strain amplitude, N is the fatigue life, and A1, A2, and n1 are coefficients of the model. Equation 1 may be written in terms of stress amplitude S_a instead of ε_a. The stress amplitude is the product of ε_a and elastic modulus E (i.e., $S_a = E \cdot \varepsilon_a$) (stress amplitude is one-half the applied stress range). The current ASME Code best-fit or mean curve described in ASME Code Section III criteria document[8] for various steels is given by

$$S_a = \frac{E}{4\sqrt{N_f}} \ln\left(\frac{100}{100 - A_f}\right) + B_f, \tag{2}$$

where E is the elastic modulus (MPa), N_f is the number of cycles to failure, and A_f and B_f are constants related to reduction in area in a tensile test (percent) and endurance limit of the material at 10^7 cycles (MPa), respectively.[7] The current Code mean curves were obtained from Equation 2 and A_f and B_f values of 68.5% and 149.2 MPa, 61.4% and 265.4 MPa, and 72.6% and 299.9 MPa, respectively, for carbon steels, low-alloy steels, and austenitic stainless steels

(SSs).[8] Thus, using an elastic modulus of 206,843 MPa for carbon and low-alloy steels and 179,264 MPa for austenitic SSs, the mean curves are expressed for carbon steels, as

$$S_a = 59{,}734\ (N_f)^{-0.5} + 149.2, \quad (3)$$

for low-alloy steel, as

$$S_a = 49{,}222\ (N_f)^{-0.5} + 265.4, \quad (4)$$

and for austenitic SSs, as

$$S_a = 58{,}020\ (N_f)^{-0.5} + 299.9. \quad (5)$$

The fatigue ε–N data are typically expressed by rewriting Equation 1 as

$$\ln(N) = A - B \ln(\varepsilon_a - C), \quad (6)$$

where A, B, and C are constants; C represents the fatigue limit of the material; and B is the slope of the log-log plot of fatigue ε–N data. The ASME Code mean-data curves (i.e., Equations 3-5) may be expressed in terms of Equation 6 as follows. The fatigue life of carbon steels is given by

$$\ln(N) = 6.726 - 2.0 \ln(\varepsilon_a - 0.072), \quad (7)$$

and for low-alloy steels by

$$\ln(N) = 6.339 - 2.0 \ln(\varepsilon_a - 0.128). \quad (8)$$

For austenitic SSs, the fatigue life corresponding to the fatigue design curve originally published in ASME Code Section III prior to the 2009 Addenda is given by

$$\ln(N) = 6.954 - 2.0 \ln(\varepsilon_a - 0.167), \quad (9)$$

and, as derived in Section 3.2.6, the fatigue life corresponding to the fatigue design curves in the 2009 Addenda and later editions of the ASME Code is given by

$$\ln(N) = 6.891 - 1.920 \ln(\varepsilon_a - 0.112), \quad (10)$$

where strain amplitude ε_a is in percent. The ε–N curve for austenitic SSs is also used for nickel-chromium-iron (Ni-Cr-Fe) alloys (e.g., Alloy 600).

The best-fit or mean-data curves (e.g., Equations 7-10) provide an estimate of the fatigue life that would lead to failure in 50% of the population under a given loading. However, this report includes a rigorous evaluation for defining an adjustment factor to derive the fatigue design curve from the mean-data curve, to account for the variability resulting from data scatter, size, surface roughness, and loading sequence.

Another term that is often used in ASME Code Section III fatigue evaluations is fatigue limit (or endurance limit), which is defined as "the limiting value of the median fatigue strength as the fatigue life, N_f, becomes very large."[1] However, certain materials (e.g., carbon and low-alloy steels and austenitic SSs) and environments preclude the attainment of a fatigue limit. Therefore, in the

literature, fatigue limit is typically defined as a value of stress, S_N, for failure at a specified number of cycles, N (e.g., at 10^6 or 10^{11} cycles).

The above ε–N curves describe the formation of engineering fatigue cracks in small, smooth test specimens in an air environment. To use the small-specimen data for actual reactor components, the best-fit ε–N curves for specimen data must be adjusted to account for the effects of variables that are known to affect fatigue life but were not accounted for in the small-specimen data. Such variables include mean stress, surface finish, size, and loading history. Furthermore, the best-fit curve represents the average behavior of the material. To obtain a curve that ensures a low probability for formation of fatigue cracks, the small specimen curve must also be adjusted to account for data scatter and material variability.

The procedure used to develop the ASME Code fatigue design curves from the best-fit (or mean-data) curves for small specimens is as follows. First, the best-fit curves are adjusted to account for the effects of mean stress. This is necessary to account for mean stress effects that were not considered during specimen testing, such as weld residual stress. Mean stress was accounted for using the modified Goodman relationship given by

$$S'_a = S_a \left(\frac{\sigma_u - \sigma_y}{\sigma_u - S_a} \right) \quad \text{for } S_a < \sigma_y \,, \tag{11}$$

and

$$S'_a = S_a \qquad \text{for } S_a > \sigma_y \,, \tag{12}$$

where S'_a is the adjusted value of stress amplitude, and σ_y and σ_u are the monotonic yield and ultimate strengths of the material, respectively. Equations 11 and 12 assume the maximum possible mean stress and typically give a conservative adjustment for mean stress. The original ASME Code Section III fatigue design curves were obtained by reducing the fatigue life at each point on the adjusted best-fit curve by a factor of 2 on strain (or stress) or 20 on cycles, whichever was more conservative.

As described in the ASME Code Section III criteria document,[8] the factors of 2 and 20 are not safety margins, but rather adjustment factors that were applied to the small–specimen data to account for the effects of variables that are known to affect fatigue life but were not accounted for in the small-specimen data. These factors include (1) data scatter and material variability, (2) the differences in surface condition and size between the test specimens and actual reactor components, and (3) random load cycles as compared to constant strain cycles used to obtain the fatigue ε–N data.

1.3 Subfactors Included in ASME Code Section III Air Fatigue Design Curves

In comments about the initial scope and intent of the ASME Code Section III fatigue design procedures, Cooper[9] states that the factor of 20 on life was regarded as the product of the following three subfactors:

(1)	scatter of data (minimum to mean):	2.0
(2)	size effect:	2.5
(3)	surface finish, atmosphere, and other such subfactors:	4.0

Although the ASME Code Section III criteria document[8] states that these factors were intended to cover such effects as environment, Cooper[9] further states that the term “atmosphere” was intended to reflect the effects of an industrial atmosphere compared to an air-conditioned laboratory, which are different

than the effects of a specific water environment. In addition, surface finish represented surface roughness of an industrial-Grade component surface compared to that of a polished test specimen. Subsubarticle NB-2160 (or Subsubarticle NG-2160 for core support structures) of ASME Code Section III states, “It is the responsibility of the Owner to select material suitable for the conditions stated in the Design Specifications (NCA-3250), with specific attention being given to the effects of service conditions upon the properties of the material.” Paragraph NCA-3252 of ASME Code Section III specifies the minimum contents of the design specifications. Subparagraph NCA-3252(a)(3) states that the design specifications shall include “the environmental conditions, including radiation.” The environmental conditions that are likely to influence the properties of materials used in nuclear power plant structures and components include temperature, water environment, and neutron irradiation.

Furthermore, Paragraph NB–3121 of ASME Code Section III (or Paragraph NG-3121 for core support structures) states, “It should be noted that the tests on which the fatigue design curves (Figures I-9.0) are based did not include tests in the presence of corrosive environments which might accelerate fatigue failure.” Paragraph B-2131 in Nonmandatory Appendix B, “Owner’s Design Specifications,” to ASME Code Section III states that the Owner's design specification should provide information about, “any reduction to design stress intensity values, allowable stress, or fatigue design curves that is necessitated by environmental conditions.”

1.3.1 Effects of Water Environment on Fatigue Lives

Existing fatigue ε–N data (Figure 1-1) illustrate potentially significant effects of light water reactor (LWR) coolant environments on the fatigue resistance of carbon and low-alloy steels, wrought and cast austenitic SSs, and Ni-Cr-Fe alloys.[10-75] Small-scale laboratory fatigue test data indicate that under certain reactor operating conditions, the fatigue lives of carbon and low-alloy steels can be a factor of 17 lower in the water environment than in air. Therefore, the factors in the ASME Code may be less conservative than originally intended.

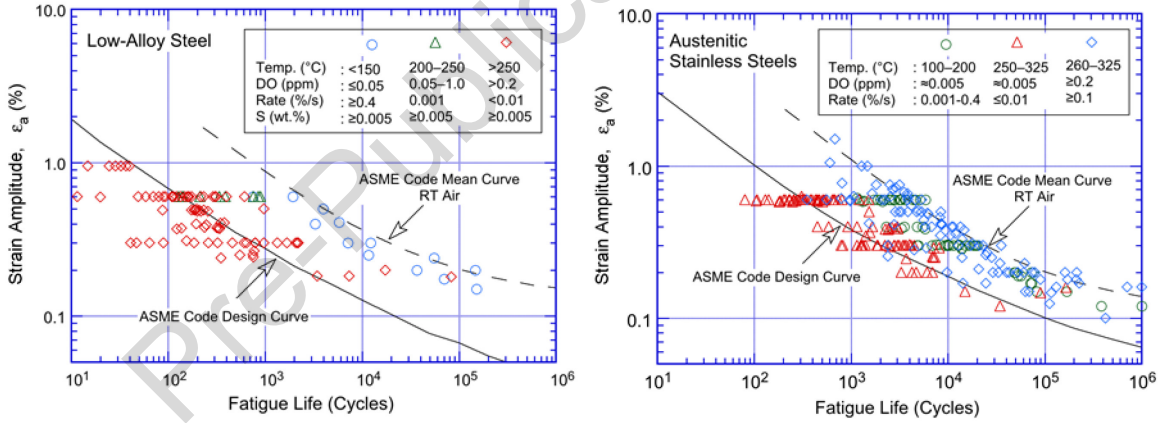

Figure 1-1 Fatigue ε–N data for low-alloy steels and austenitic SSs in water compared to the ASME Air Design Curve; RT = room temperature [77°F (25°C)].

The fatigue ε–N data are consistent with the much larger database on enhancement of crack growth rates (CGRs) in these materials in simulated LWR environments. The key parameters that influence fatigue life in these environments are temperature, the dissolved–oxygen (DO) level in the water, strain rate, strain (or stress) amplitude, and, for carbon and low-alloy steels, the sulfur content of the steel. The range of the values for these parameters within which environmental effects are significant has also been defined. If these critical loading and environmental conditions exist during reactor operation, then environmental effects may be

significant and should be included in any associated ASME Code fatigue evaluations. Experience with nuclear power plants worldwide indicates that the critical range of loading and environmental conditions that leads to environmental effects on formation of fatigue cracks can and do occur during plant operation.[56,76-92] Therefore it is important that component design considers environmental effects to prevent premature fatigue failures.

Experience with operating nuclear power plants worldwide reveals that many reactor component failures were attributed to fatigue; examples include piping, nozzles, valves, and pumps.[76-83] In most cases, these failures were associated with thermal loading due to thermal stratification and striping, or mechanical loading due to vibratory loading that was not originally considered in the component design. Thermal stratification was typically caused by the injection of low-flow, relatively cold feedwater during plant startup, hot standby, and variations below 20% of full power, whereas thermal striping was caused by rapid, localized fluctuations of the interface between hot and cold feedwater. In addition, for most of these cases, the additional thermal loading had high through-wall stress gradients that are not considered in the development of the ASME Code design air fatigue curves (see Section 1.5, item xxi). Considering through-wall stress gradients instead of assuming uniform stress in analyses may significantly increase the calculated fatigue lives of components.

The original design basis analyses for most U.S. nuclear power plants typically did not include thermal loading caused by flow stratification or striping. Regulatory evaluation indicated that high-cycle thermal–stratification loading can occur in PWR surge lines as a result of in-surge and out-surge during heatup/cooldown transients.[93] During heatup or cooldown, when, the pressurizer water is heated to approximately 227°C (440°F), the hotter water can flow at a very low rate from the pressurizer through the surge line to the hot–leg piping over the cooler water layer in the piping. The thermal gradients between the upper and lower parts of the pipe can be as high as 149°C (300°F). As a result, all U.S. PWRs performed revised fatigue analyses to address thermal stratification effects in surge lines. Furthermore, corrosion effects caused by a high-temperature aqueous environment may also aggravate the effect of these loadings. The increased fatigue duty caused by such thermal loading increases the importance of evaluating environmental effects.

The mechanism of cracking in feedwater nozzles and piping was attributed to corrosion fatigue or strain–induced corrosion cracking (SICC).[84-86] Hickling and Blind summarized case histories and identified conditions that lead to SICC in low-alloy steels in LWR systems. An Electric Power Research Institute (EPRI) report presented a review of significant occurrences of corrosion fatigue damage and failures in various nuclear power plant systems.[56] Shah et al. presented an assessment of the U.S. experience related to PWR primary system leaks observed during the period 1985 through 1996.[88]

Hirschberg et al. summarized the operating experience regarding thermal fatigue of nonisolable piping connected to PWR reactor coolant system (RCS).[87] Significant cracking occurred in nonisolable sections of the safety injection system and residual heat removal (RHR) system piping connected to the PWR coolant system.[89,90] At Joseph M. Farley Nuclear Plant, cracking occurred in the heat affected zone (HAZ) of the weld between the first elbow and the horizontal pipe, approximately 0.9 m (36 in.) from the RCS cold–leg nozzle. At Tihange Nuclear Power Station, the crack was located in the base metal of an elbow, approximately 0.6 m (24 in.) from the RCS hot–leg nozzle. At the Genkai Nuclear Power Plant (Genkai), cracking occurred in the RHR suction line at the weld between the first elbow downstream of the hot–leg nozzle and the horizontal pipe section. Cracking due to thermal fatigue also occurred in the safety injection system at Dampierre Nuclear Power Plant, Units 1 and 2 plants, and in the chemical and

volume control system (CVCS) in Obrigheim Nuclear Power Plant. In all cases, thermal cycling was caused by interaction of hot RCS fluid from turbulent penetration at the top of the pipe, and cold valve leakage fluid that stratified at the bottom of the pipe. At Genkai, the valve internals alternately shrunk and expanded causing periodic leakage of hot fluid through the stem packing and leak-off line into the elbow.

However, thermal stratification can occur even in the absence of valve leakage. The results of fatigue monitoring indicate that many PWR plants measured thermal–stratification cycling in the RHR suction line because of turbulence penetration of the hot leg fluid extending into the horizontal pipe section, which then stratified due to normal convection. [87] For thermal stratification, the length of the vertical pipe section of the RHR suction line must be short enough for the hot fluid to reach the horizontal pipe section, and the length of the horizontal pipe section must be long enough to cause sufficient heat losses for stratification to develop. A typical temperature gradient of 49°C (120°F) was observed for typical cases of stratification, and temperature gradients as high as 177°C (350°F) were measured in some plants.

Nonisolable leaks due to thermal-stratification cycling also occurred in reactor coolant loop drain lines, excess letdown lines, and makeup/high pressure injection lines at the Three Mile Island Nuclear Station (TMI), Loviisa Nuclear Power Plant, Unit 2, Mihama Nuclear Power Plant (Mihama), and Oconee Nuclear Station (Oconee).[87,88] A leak in the cold–leg drain line [1.5 in. or 2 in. nominal pipe size (NPS)] occurred in the weld between the first elbow downstream of the loop nozzle and the horizontal pipe section at TMI, and in the elbow extrados at Oconee. In both cases, thermal stratification was caused by turbulence penetration of the RCS fluid periodically extending into the horizontal section and it stratified due to heat loss because the pipe was not insulated. The same mechanism caused a leak in the 2 in. NPS excess letdown line at Mihama. Although the Mihama line was insulated, stratification still occurred because the length of the horizontal section to the isolation valve was very long, thus resulting in significant heat loss.

Thermal fatigue caused leaks in a connecting pipe and shell of the regenerative heat exchanger in the CVCS at Tsuruga Nuclear Power Plant (Tsuruga), Unit 2,[91,92] and in a 250–mm pipe section of the heat exchanger bypass on the RHR system at Civaux Nuclear Power Plant, Unit 1.[76] Thermal-hydraulic mockup tests indicate that at Tsuruga, superposition of low-frequency temperature gradients caused by changes in the flow pattern and high frequency temperature fluctuations resulting from mixing of the bypass flow and main flow caused thermal fatigue. [91,92]

Cracking also occurred in austenitic SS channel heads in an experimental test loop used for stress corrosion cracking studies in a simulated PWR environment.[94] Cracks were observed in a region that was subjected to temperature fluctuations between 170°C and 190°C at a frequency of 0.05 Hz. The cracks initiated on the inner surface; the cracking morphology was essentially transgranular with fatigue–like striations visible in some regions of the fracture surface. Thermal fatigue, with possible effects of the PWR coolant environment, was determined to be the root cause of these failures.[94]

Such cracking in nonisolable pipe sections due to thermal cycling was generally termed as high-cycle fatigue, i.e., it occurs at stress levels that correspond to allowable fatigue cycles of 10^5 or higher. The current understanding of turbulent penetration is not sufficient to accurately predict the frequency of thermal cycling associated with that phenomenon. Environmental effects on fatigue crack initiation may be significant in low-DO water at stress levels above the threshold value and at strain rates less than 0.4%/s.

Lenz et al.[85] showed that in feedwater lines, the strain rates are 10^{-3} to 10^{-5} %/s due to thermal stratification and 10^{-1} %/s due to thermal shock. They also reported that thermal stratification is the primary cause of crack initiation resulting from SICC. Stephan and Masson[95] subjected a full–scale mockup of the steam generator feedwater system to various regimes of stratification. After 4,000 cycles of applied loading, destructive examination performed between two locations where stable states of stratification occurred revealed small cracks, 1.4 to 2.0 mm deep, in the weld region. The fatigue usage factors calculated with elastic and cyclic elastic–plastic computations gave values of 1.3 to 1.9. Because the average DO level in the water was approximately 5 ppb, which corresponds to the maximum admissible value under normal operating conditions (power greater than 25% nominal power) in French PWRs, environmental effects on life were expected to be minimal and environmental fatigue correction factors were not applied in the computations of the fatigue usage factor.

Full–scale mockup tests designed to generate thermal stratification in a pipe in a laboratory confirmed the applicability of laboratory data to component behavior.[96] The material, loading, and environmental conditions were simulated on a 1:1 scale using only thermohydraulic effects. Under the conditions of strain rate and strain range typical of thermal stratification in these piping systems, the coolant environment has a significant effect on fatigue crack initiation.[12,29,30]

Finally, a study conducted on SS pipe bend specimens in simulated PWR primary water at 240°C concluded that reactor coolant environment has a significant effect on the fatigue life of SSs.[97-99] Relative to fatigue lives in an inert environment, lives in a PWR environment at strain amplitudes of 0.4% and 0.6% were decreased by factors of 2.9 and 1.4 at strain rates of 0.0005%/s and 0.01%/s, respectively. These values show very good agreement with the values predicted from the Argonne National Laboratory (ANL) models presented later in this report for incorporating environmental effects into the ASME Code Section III fatigue evaluations.

1.3.2 Effects of Neutron Irradiation

The potential effects of neutron irradiation on the fatigue life of reactor structural materials such as low-alloy pressure vessel steel, austenitic SSs, and Ni-Cr-Fe alloys and their weld metals, are not fully characterized. Irradiation effects were not included in the ASME Code Section III fatigue evaluations performed for reactor core support structures and reactor internal components. The majority of the existing data on the effects of neutron irradiation resulted from fatigue crack growth tests on austenitic SSs that were irradiated in fast reactors [primarily Experimental Breeder Reactor II (EBR-II)] at test temperatures of 427 (800°F) and 593°C (1100°F).[100-104] The CGR test results indicated that for Type 304 and 316 SS irradiated at 405-410°C (760-770°F) to 1.2×10^{22} n/cm^2 (E>0.1 MeV) fluence, the fatigue CGRs at 427°C (800°F) were up to a factor of 2 higher than those for unirradiated material at low values of stress intensity factor range (ΔK) [less than 40 ksi in$^{1/2}$ (43.9 MPa m$^{1/2}$)], but were lower for higher ΔK values. These observations were reversed at 593°C (1100°F). Crack growth rates were comparable or lower at higher values of ΔK. A similar behavior was observed for Type 316 weld metal. Tests on Type 304 and 316 SSs irradiated in a thermal reactor [the Advanced Test Reactor (ATR)] at 288°C (550°F) to 1.8×10^{21} n/cm^2 (E>0.1 MeV) and tested at 427°C (800°F) showed superior resistance to crack growth; CGRs were 25 to 50% lower than those for unirradiated material.[105] Based on these studies EPRI concluded that "[t]he work of several researchers suggest that neutron irradiation does not result in a further reduction in fatigue properties and in some cases suggest an improvement."[106]

Other limited fatigue ε–N data on materials irradiated under LWR conditions and tested at LWR operating temperatures also showed significant differences in the microstructure and

microchemistry of LWR irradiated materials, and materials irradiated in fast neutron test reactors. Specifically, cavities and helium (He) bubbles were observed in austenitic SSs irradiated at a temperature of 320°C (608°F) to high neutron fluence levels in PWRs. Such microstructures could lead to embrittlement of the material.[107] Therefore, fatigue data on LWR irradiated materials should be developed to further quantify the effects of neutron irradiation on fatigue lives.

Fatigue ε–N data on irradiated Type 308 SS weld metals showed moderate decreases in fatigue lives in the low-cycle regime and superior fatigue lives in the high-cycle regime.[108] Similar effects from neutron irradiation were also observed on the room-temperature fatigue ε–N behavior of Type 347 SSs irradiated in the Engineering Test Reactor (ETR) at 60°C (140°F) to total integrated fast flux (>1 MeV) exposures of 5.5×10^{25}, 1.1×10^{26}, and 1.6×10^{26} n/m^2, as shown in Figure 1-2(a).[109] Neutron irradiation decreased the room-temperature fatigue lives of Type 347 SSs at high strain amplitudes (above 0.35%) and had beneficial effects on fatigue lives at low strain amplitudes (below 0.25%). The decreases in fatigue lives increased with increased total neutron doses. The reductions in fatigue lives were likely related to the irradiation-induced decreases in ductility of the materials.

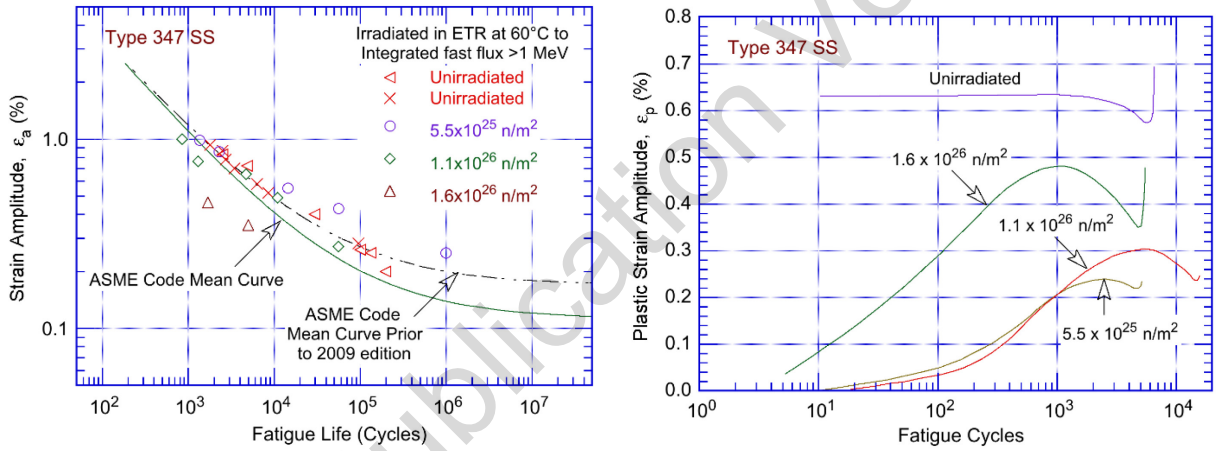

Figure 1-2 The effects of neutron irradiation on fatigue lives of Type 347 SSs at room temperature: (a) the fatigue ε–N behavior, and (b) variations in plastic strain amplitude as a function of fatigue cycles (Ref. 109).

The fatigue test results also indicated significant differences in the cyclic hardening behavior of the irradiated materials relative to unirradiated materials. Typically, at room temperature, austenitic SSs exhibited strain softening after the initial cyclic hardening during the first ten cycles. For the irradiated Type 347 SSs, although total strain was held constant, the plastic strain varied significantly during the fatigue tests, as shown in Figure 1-2(b). The plastic strains were insignificant initially and increased gradually during the fatigue tests due to strain softening until a later stage where plastic strains started to decrease due to secondary strain hardening and formation of fatigue cracks in the specimens. The extent of strain softening increased with increased neutron doses (Figure 1-2(b)). The rapid increases in plastic strains near the end of the tests were associated with specimen fracture. In contrast, the unirradiated Type 347 SSs exhibited slight strain hardening and plastic strain decreased at a very low rate; the materials later showed faster decreases in plastic strains because of secondary strain hardening and formation of fatigue cracks. Thus, the impact of irradiation on fatigue life is not readily apparent from these data because of several competing factors.

The fatigue ε–N data on cold-worked (CW) Type 316 SS tube materials and solution-annealed Type 304 bar materials removed from an operating PWR are shown in Figure 1-3 and Figure 1-4, respectively.[110] The data were obtained in simulated PWR water at 325°C (617°F) on CW Type 316 SS tube specimens with a 6.48 mm outer diameter and a 0.71 mm wall thickness. The tube specimens were irradiated to fluence values of less than 10^{22}, 2 - 6x10^{25}, and greater than 3x10^{26} n/m^2 (E > 0.1 MeV), while the 5.08-mm diameter cylindrical specimens of Type 304 SS were irradiated to fluence levels ranging from 5x10^{25} to 10^{26} n/m^2 (E > 0.1 MeV). However, the baseline fatigue data for the unirradiated materials for the same heats of SSs were not available. To determine the possible effects of specimen configuration (i.e., solid cylindrical vs. thin-walled tube specimens), fatigue tests using the two specimen geometries were conducted on another heat of CW Type 316 SS in air at 325°C. The results indicated that the fatigue strengths of the solid specimens were 1.4 times those of the cylindrical tube specimens. The ASME Code Section III best-fit mean air curves for austenitic SSs are also shown in Figure 1-3 and Figure 1-4 for comparison. Based on these test results, the authors concluded that "[t]he fatigue life of irradiated SS was longer than that of unirradiated SS in the range of this research, that is, strain amplitude was less than 0.6%. This increase in fatigue strength was considered due to an increase of tensile strength after irradiation."

In the absence of sufficient baseline fatigue data on unirradiated materials, the above conclusion that the fatigue lives of irradiated materials are longer than those of unirradiated materials is not fully justified. For example, the fatigue lives of irradiated Type 304 SSs in air are close to the ASME Code Section III best-fit mean curves. However, the effects of neutron irradiation are not available because there is insufficient fatigue ε–N data in air on unirradiated materials for these heats of Type 304 SSs. The fatigue data for irradiated CW Type 316 SSs were obtained on thin-walled tube specimens, and were not consistent with the ASME Code Section III mean air curve for austenitic SSs because the majority of the data were obtained from solid cylindrical specimens. The experimental ε–N behavior showed a lower ε–N slope than that for the ASME Code Section III mean curve (Figure 1-3). Even after adjusting by a factor of 1.4 on strain to account for the effect of specimen geometry, the fatigue lives in air at 0.3% strain amplitude fall to the right of the ASME Code Section III mean curve, whereas, the fatigue lives at 0.6% strain amplitude are significantly to the left. The primary reason for this inconsistency is likely caused by inadequate specimen size (tube specimens with a 0.71-mm thick wall) for fatigue tests performed at high strain amplitudes. However, the fatigue data in Figure 1-3 and Figure 1-4 show that fatigue lives of austenitic SSs were decreased in a PWR primary water environment. Except for the data on CW Type 316 SSs irradiated to a fluence greater than 3x10^{26} n/m^2, the data for irradiated materials and the data for irradiated Type 304 SSs show lower fatigue lives in PWR primary water environment compared to those in air. The effects of the environment increase with decreasing strain rates.

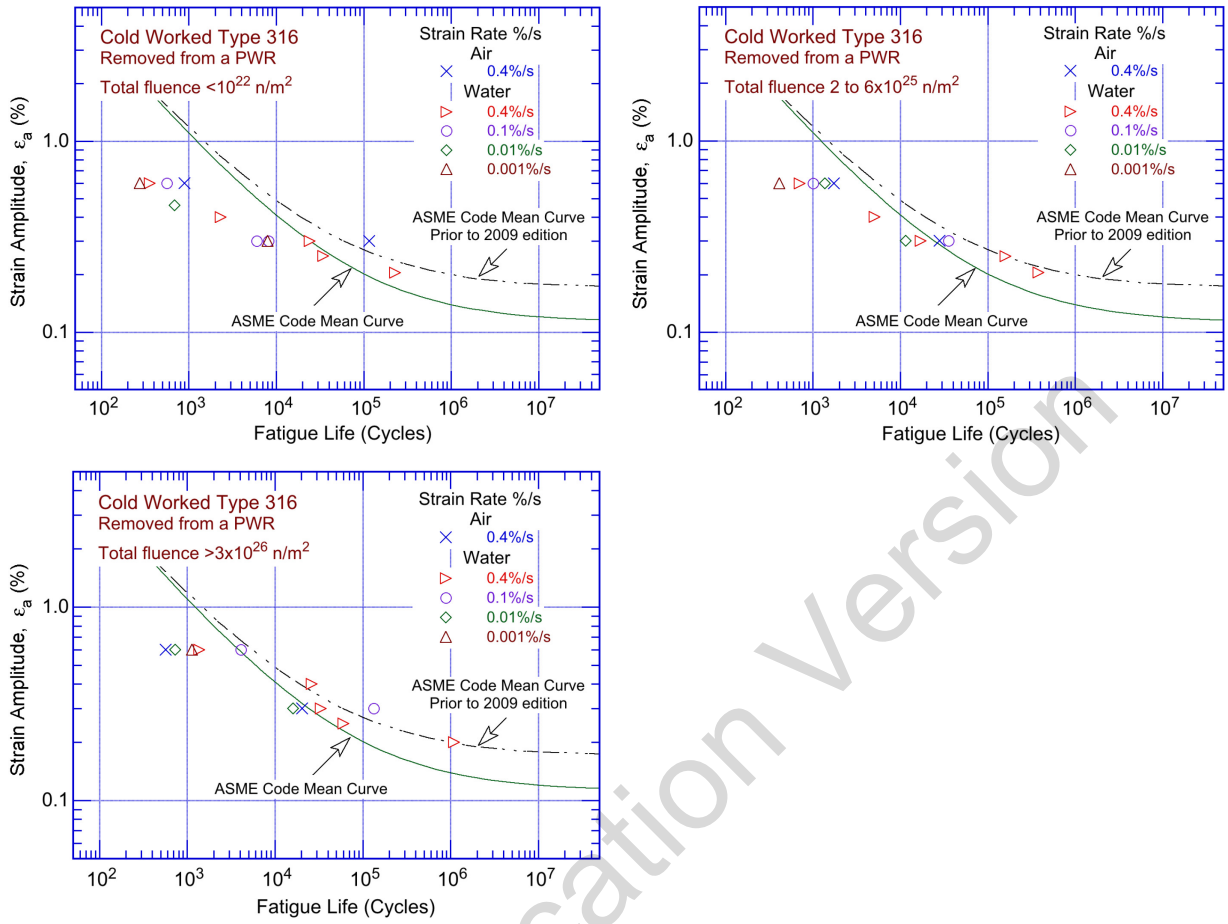

Figure 1-3 Strain amplitude vs. fatigue life data in 325°C air and simulated PWR primary water environments for CW Type 316SS irradiated to (a) less than 10^{22}, (b) 2-6x10^{25}, and (c) greater than 3x10^{26} n/m^2 (E > 0.1 MeV) (Ref. 110).

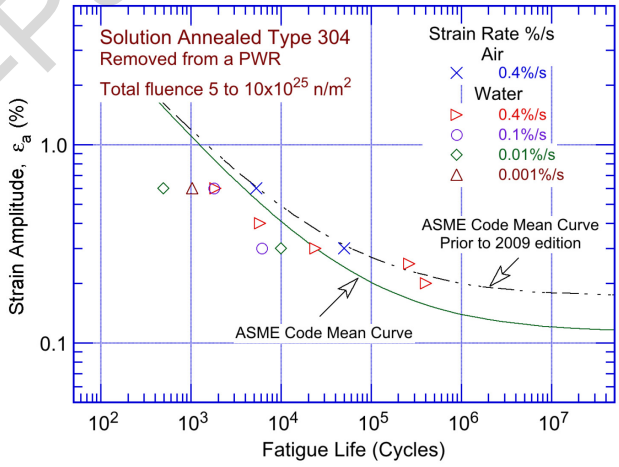

Figure 1-4 Strain amplitude vs. fatigue life data in 325°C air and simulated PWR primary water environments for Type 304 SS irradiated to 5x10^{25}–10^{26} n/m^2 (E > 0.1 MeV) (Ref. 110).

The limited available data are inconclusive with regard to the impact of irradiation on the fatigue lives of materials exposed to LWR environments. Although some small-scale laboratory fatigue ε–N test data indicate that neutron irradiation decreases the fatigue lives of austenitic SSs, particularly at high strain amplitudes, quantifying the impact of irradiation on the prediction of fatigue lives is not possible because of the limited data currently available. Additional fatigue data on reactor structural materials irradiated under LWR operating conditions are needed to determine whether neutron irradiation causes measurable effects on the fatigue lives of these materials and, if so, to better define how those impacts may be quantified. In the absence of such data, the methods described in this report are considered appropriate for application to materials exposed to significant levels of irradiation, such as SS reactor internals components, when mandated by regulation or required by the current licensing basis.

1.4 Modeling of Environmental Effects

In 1991, the U.S. Nuclear Regulatory Commission (NRC) issued a draft Branch Technical Position (BTP) for fatigue evaluation of nuclear plant components for license renewal. The BTP raised a concern about the adequacy of the ASME Code in addressing environmental effects on fatigue resistance of materials for operating PWRs and boiling water reactors (BWRs), whose primary–coolant pressure boundary components were constructed as specified in ASME Code Section III. In 1993, the Commission directed the NRC staff to treat fatigue as a potential safety issue within the existing regulatory process for operating reactors. The staff developed a Fatigue Action Plan (FAP) to resolve three principal issues: (1) adequacy of fatigue resistance of older vintage plants designed to the United States of America Standard B31.1 that did not require an explicit fatigue analysis of components, (2) effect of LWR environments on the fatigue resistance of primary pressure boundary materials, and (3) appropriate corrective action required when ASME Code fatigue allowable limits are exceeded (i.e., when the CUF is greater than unity).

Idaho National Engineering Laboratory (INEL) assessed the significance of ANL-developed interim fatigue design curves, by performing fatigue evaluations of a sample of components in the reactor coolant pressure boundary.[111] In all, six locations were evaluated from facilities designed by each of the four U.S. nuclear steam supply system vendors. Selected components from older vintage plants designed according to the B31.1 code were also included in the evaluation. Conservatism in the original fatigue evaluations (e.g., actual loading cycles instead of assumed cycles) was removed, and fatigue usage was evaluated with a fatigue design curve that considered the effects of the coolant environment. The results indicated that most of the locations had a CUF of less than the ASME Code limit of 1.0 for 40 years. The risk to reactor coolant pressure boundary components from failure due to fatigue was assessed under Generic Safety Issue (GSI) 78, "Monitoring of Fatigue Transient Limits for the Reactor Coolant System," and GSI 166, "Adequacy of Fatigue Life of Metal Components," in NUREG-0933, "Resolution of Generic Safety Issues," dated March 29, 2012."[112] Based on these studies, it was concluded[113] that no immediate action was necessary to address the three fatigue issues identified in the FAP. A risk study indicated that fatigue failure of piping was not a significant contributor to core damage frequency. Based on the risk assessment, a backfit to incorporate environmental effects into the fatigue analyses of operating plants was not justified.[114]

However, because the NRC studies were less certain that the conservatism in the original fatigue calculations could be used to account for an additional 20–years of operation, the NRC staff recommended that environmental effects be considered by evaluating the sample locations in the INEL study (NUREG/CR-6260, "Application of NUREG/CR-5999 Interim Design Curves to Selected Nuclear Power Plant Components," issued March 1995) [111] for plants pursuing license renewal. GSI 190, "Fatigue Evaluation of Metal Components for 60-year Plant Life, documents

these recommendations.[112] Based on probabilistic analyses and sensitivity studies, interactions with the industry, and various programs available to licensees to manage the effects of aging, the NRC concluded that no generic regulatory action was required. For some components, although cumulative probabilities of crack initiation and through-wall cracks approached 1.0 for the renewal period, the maximum failure rate was generally low, in the range of 10^{-2} through-wall cracks per year.

In addition, the predicted failure rates were generally associated with high CUF locations and components with thin walls; in most cases, any leakage that might result from these through-wall cracks was estimated to be small and not likely to lead to core damage. However, the calculations that supported the resolution of this issue indicated the potential for an increase in the frequency of pipe leaks as plants continue to operate. Thus, the NRC staff recommended that aging management programs for license renewal should address component fatigue, including the effects of the reactor coolant environment. However, note that, when the INEL study was performed, it was not known that the effects of high-temperature water environment on fatigue cracking of austenitic SSs are greater in low-DO environments than they are in high-DO environments. Thus, the six sample locations evaluated in the INEL study may not necessarily be the bounding locations for some plants, and fatigue CUF evaluations should include additional plant-specific component locations along with those considered in NUREG/CR-6260, including the effects of the environment.

In 1991, the ASME Board on Nuclear Codes and Standards (BNCS) requested that the Pressure Vessel Research Council (PVRC) examine the existing worldwide ε–N data and develop recommendations for the ASME. The PVRC compiled and evaluated fatigue ε–N data related to the effects of LWR coolant environments on the fatigue life of pressure boundary materials; Van Der Sluys and Yukawa summarized the results.[115,116] The staff agreed with the concept of using an environmental fatigue correction factor (F_{en}) approach to obtain fatigue usage reflecting environmental effects for ASME Code Section III fatigue evaluations. This information was forwarded to the appropriate ASME Code committee.[117]

An analysis of the existing fatigue ε–N data and the procedures for incorporating environmental effects into ASME Code Section III fatigue evaluations were presented in several review articles[115,116,118-126] and ANL reports.[10,12,13,45-47] The fatigue ε–N data in air and LWR environments were also examined from the standpoint of fracture mechanics and CGR data.[127,128] Section 2.0 of this report presents further details. The key material, loading, and environmental parameters that influence the fatigue lives of carbon, low-alloy, and austenitic SSs were identified, and the range of these key parameters where environmental effects are significant, was defined. Two approaches were proposed for incorporating the environmental effects into ASME Section III fatigue evaluations for primary pressure boundary components in operating nuclear power plants: (1) develop new fatigue design curves for LWR applications, or (2) use an environmental fatigue correction factor to account for the effects of the coolant environment.

In the first approach, following the same procedures used to develop the fatigue design curves in ASME Code Section III, environmentally adjusted fatigue design curves were developed from fits to experimental data obtained in LWR environments. Interim fatigue design curves that address environmental effects on the fatigue life of carbon, low-alloy, and austenitic SSs were first proposed by Majumdar et al.[129] However, as mentioned above, the “interim” fatigue design curve for austenitic SSs was based on little or no data in low-DO environments. As a result, at the time of the development of the interim design curves, it was not known that the effects of high-temperature water environment on fatigue lives are greater in low-DO environments than in

high-DO environments. Keisler et al.[130] developed fatigue design curves based on a more rigorous statistical analysis of experimental data. These design curves were subsequently revised based on updated ANL models.[10,12,45,46] However, in LWR environments, the fatigue life of carbon and low-alloy steels, Ni-Cr-Fe alloys, and austenitic SSs depends on several loading and environmental parameters. Therefore, such an approach requires the development of several design curves to cover all possible environmental conditions encountered during plant operation. Depending on the number of such design curves for the desired loading and environmental conditions, development of additional curves may be a significant undertaking.

The second approach, proposed by Higuchi and Iida in 1991,[19] considers the effects of reactor coolant environments on fatigue life in terms of an F_{en} that is defined as the ratio of fatigue life in air at room temperature to that in water under reactor operating conditions. To incorporate environmental effects into fatigue evaluations, this approach requires multiplying the fatigue usage factor for a specific stress cycle or load set pair, based on the ASME Code Section III design fatigue curves, by the F_{en}. Specific expressions for F_{en}, based on the ANL fatigue life models, were developed.[10,45] Such an approach is relatively simple for application to previously developed fatigue analyses and is recommended in this report. A similar methodology was also developed in Japan by the Environmental Fatigue Data (EFD) Committee of the Thermal and Nuclear Power Engineering Society (TENPES) under the Environmental Fatigue Testing (EFT) Project. The EFT was also supported by the Japan Power Engineering and Inspection Corporation (JAPEIC) and the Japan Nuclear Energy Safety (JNES) Organization, and some utilities.[131-135] Updated technical results appear in JNES-SS-1005 "Environmental Fatigue Evaluation Method for Nuclear Power Plants," issued March 2011.[136] All of these data were considered in the results documented in this report.

In 2007, the original version of NUREG/CR-6909,[137] which is the technical basis document for NRC Regulatory Guide 1.207, "Guidelines for Evaluating Fatigue Analyses Incorporating the Life Reduction of Metal Components Due to the Effects of the Light-Water Reactor Environment for New Reactors," Revision 0, issued March 2007, presented an overview of the existing fatigue ε–N data for carbon and low-alloy steels, Ni-Cr-Fe alloys, and wrought and cast austenitic SSs in air and LWR environments. The existing fatigue ε–N data were evaluated to (1) identify the various material, environmental, and loading parameters that influence fatigue cracking, and (2) establish the effects of key parameters on the fatigue lives of these steels. Fatigue life models, presented in earlier reports for estimating fatigue life as a function of material, loading, and environmental conditions were updated using the fatigue ε–N database available at that time. The report also described the F_{en} approach for incorporating effects of LWR environments into ASME Code Section III fatigue evaluations, and presented a critical review of the ASME Code fatigue adjustment factors of 2 on stress (or strain) and 20 on life to assess the possible conservatism in the choice of adjustment factors. The F_{en} methodology was identified as applicable to all reactor coolant pressure boundary components exposed to reactor water that require an ASME Code Section III fatigue CUF calculation.

This report presents a revision to the original version of NUREG/CR-6909 in its entirety. The F_{en} expressions were updated using a much larger fatigue ε–N database. The additional data include the JNES data summarized in JNES-SS-1005 on carbon and low-alloy steels, wrought and cast austenitic SSs, and Ni-Cr-Fe alloys, and their associated weld metals, tested in air and LWR environments, [136] and fatigue ε–N test results from the open literature on several heats of carbon and low-alloy steels tested in BWR environments.[138-146] Most of the data evaluated for this report were obtained from completely reversed, axial, strain-controlled tests on small laboratory specimens. The results from a small number of bending tests were also considered for austenitic

SSs in air (see Table 3-6 in Section 3.2.1), Ni-Cr-Fe alloy steels in air (see Table 3-9 in Section 3.3), and carbon and low-alloy steels in water (see Table 4-1 in Section 4.1.1). These data were included to improve the best-fit evaluation of the fatigue life data. Section 3.2.2 includes figures that support the use of these bending test data for austenitic SSs, which show that the bending test data points fall evenly on both side of the best fit curve of all the data. Only a small number of high-cycle fatigue tests conducted in load control were considered.

The updated environmental fatigue expressions in this report also address comments from interested stakeholders related to (1) the constants in the F_{en} expressions that results in a F_{en} value of approximately 2 even when the strain rate is very high or temperature is very low, (2) the temperature dependence of F_{en} for carbon and low-alloy steels, and (3) the dependence of F_{en} on water chemistry for austenitic SSs. Finally, the updated methodology described in this report applies to any component exposed to the LWR environment that requires an ASME CUF calculation as part of its design, if required by the safety basis for the component, or if it is required by the plant current licensing basis, unless otherwise justified. Note that the F_{en} approach described in this report is only applicable for use as part of an ASME Code fatigue evaluation.

In addition, the report evaluates the appropriateness of a strain threshold and the possible effects of hold periods. It also discusses the potential effects of dynamic strain aging (DSA) on cyclic deformation and environmental effects.[147-153] The F_{en} methodology proposed in this report was validated by comparing the results of five different experimental datasets obtained from fatigue tests that simulate actual plant conditions with estimates of fatigue usage adjusted for environmental effects using the updated F_{en} expressions. The five datasets represent fatigue tests with (1) changing strain rate or temperature, or both,[154] (2) complex loading (actual PWR transient),[155-157] (3) spectrum loading (random strain amplitudes),[158,159] (4) thermal fatigue of a stepped pipe,[160] and (5) pipe U-bend tests.[98,99] Appendix C to this report presents a sample application of F_{en} using the methodology in ASME Code Section III, Subarticle NB-3200 that is intended to address some of the practical issues identified by interested stakeholders associated with the F_{en} calculations.[161]

1.5 Bases and Assumptions

This section describes the bases and assumptions used to develop the air fatigue design curves, the F_{en} relationships, and the guidance for addressing environmental effects in a fatigue evaluation as documented in this report. It is recognized that additional research may lead to further improvements in the modeling and analysis of environmental fatigue effects. Therefore, documentation of these assumptions and bases is intended to inform further research efforts that may be undertaken in the future.

The following represents the major assumptions or bases for the work documented in this report:

(i) **Light-Water Reactor Water Environment.** This term, (and other similar terms such as LWR reactor coolant environment, reactor coolant environment and LWR environment) which is used throughout the report, represents any transient or steady-state water environment in a light-water commercial nuclear power plant where the component of interest is exposed to water above 50°C. Environmental effects on fatigue life can occur in any such environment. Examples of systems in commercial nuclear power plants where such an environment is present include the primary pressure boundary system, the secondary side system, and the service water system. The terms “PWR environment” and “BWR environment” (and other similar terms) are also used

throughout the report to describe testing conditions that have been used to simulate steady-state water environments in PWR and BWR reactor coolant systems, respectively.

(ii) **Definition of Fatigue Life.** As discussed extensively in Section 1.1, fatigue life is described in this report as the number of cycles of a specified strain amplitude that a specimen can sustain before the formation of a 3-mm-deep crack (i.e., an "engineering crack"). However, the total fatigue life consists of two parts: (1) crack initiation (Stage I, for crack sizes up to approximately 0.2 mm) and crack propagation (Stage II, for crack growth from approximately 0.2 to 3.0 mm), as indicated in Figure 2-4. Using this definition, a calculated fatigue CUF less than unity provides reasonable assurance that a fatigue crack has not formed in a component, and indicates that the probability of forming a crack in the component is low.

The 3-mm crack depth is not intended to define the size of crack-like defects in actual components for flaw tolerance or other related analyses, particularly in thin-walled components (such as steam generator tubes). Obviously, a 3 mm definition of crack initiation is not an appropriate definition of fatigue life in thin-walled components where such a crack could result in a leak or even structural failure. Rather, fatigue life in a component or structure should be defined as the formation of an engineering-sized crack, which is the intent and use of this definition in this report. Consequently, as indicated in Section 4.2.12, the method may not be conservative for specimens with less than a 3 mm wall thickness. The report also recognizes that once such an engineering-sized crack has formed, the component or structure still has remaining life before it structurally fails, leaks, or cannot perform its intended function. The remaining life can be assessed through a defect fatigue crack growth analysis to determine margins and appropriate mitigation measures. The details and acceptance criteria of such an analysis are outside the scope of report; however, ASME Code Section XI addresses such topics.

(iii) **Modulus of Elasticity.** In developing the air design fatigue curves, the studies documented in this report assumed Young's modulus, E, values consistent with existing ASME Code design fatigue curves to convert all available strain data to stress. No attempts were made to determine new and more accurate E values for developing the new air design curves. Because the strain vs. fatigue life data used in developing the ASME Code fatigue design curve is applicable up to reactor operating temperatures, the conversion of strain to stress at higher temperatures should use elastic moduli values applicable at these temperatures. ASME Code Section III requires this practice. Note that the ASME Code Section III fatigue design curves are expressed as pseudo-stress amplitude (in ksi or MPa) vs. the number of fatigue cycles, where the pseudo-stress amplitude is the product of applied strain amplitude and room-temperature modulus of elasticity.

(iv) **Material Tensile Properties.** In developing the air design fatigue curves, the studies documented in this report assumed yield strength, YS, and ultimate tensile strength, UTS, values consistent with existing ASME Code design fatigue curves for performing mean stress adjustments. Limited investigation indicated that this assumption for strength values was accurate to within approximately 10% to 20% of the values obtained by averaging available tensile property data for some of the test data for low-alloy and carbon steels, respectively. No attempts were made to determine new and more accurate YS and UTS values for developing the new air design curves.

(v) **Environmental Loading.** In developing the environmental design fatigue curves, the studies documented in this report were based on available fatigue test data on small-scale laboratory specimens, the majority of which were performed under constant temperature, water chemistry, and uniform strain rate. The effects of varied temperature, water chemistry, strain rate, transient hold times, and other important test parameters on fatigue life were not investigated.

(vi) **Testing Procedures for High-Cycle Fatigue.** The ASME Code, Section III fatigue design curves for structural materials are based on strain-controlled, completely reversed, fatigue tests on smooth cylindrical test specimens in air. Typically, these tests are conducted at a strain rate of 0.4%/s. Therefore, to reduce test duration, fatigue tests at low strain amplitude (i.e., fatigue lives > 10^5 cycles) are often conducted at higher strain rates under load control. However, structural materials such as austenitic SSs or carbon steels strain harden during the initial 200–500 cycles to reach a steady-state condition where the cyclic stress remains essentially constant during the rest of test. As a result, load-controlled fatigue tests conducted at constant load result in very high strains during the initial fatigue cycles, which results in lower fatigue lives compared to tests under constant strain condition. Therefore, such tests are started under strain control and are switched later to load control after a steady-state condition is achieved.

(vii) **Material Grouping.** In developing both the air design fatigue curves and the environmental fatigue correction factors for LWR environments, the studies documented in this report were based on the following large material groupings: carbon and low-alloy steels, austenitic and cast SSs, and Ni-Cr-Fe alloys and their weld metals. Table B-1, Table B-2, and Table B-3 in Appendix B to this report list the applicable material grades covered by these groupings. This approach is consistent with the grouping used in the fatigue curves in ASME Code Section III. Fatigue curves were not developed for specific materials or for subsets of materials within the aforementioned broader groupings that share common properties. An example of such a subset is obtained by grouping ferritic materials as a function of their ultimate tensile strength. The development of both material-specific and property-specific fatigue curves is possible as long as an appropriate technical basis is established. The fatigue design curve in air and the F_{en} approach are applicable to the materials listed in Table B-1, Table B-2, and Table B-3, with the exception of Inconel 718. For Inconel 718, the SS fatigue design curves in either this report or in ASME Code Section III should be used but it is recognized that these design curves are conservative for Inconel 718. Environmental fatigue data are also not available for Inconel 718; therefore, this report does not include an F_{en} for Inconel 718. Further, additional data are required to develop unique curves for other Ni-Cr-Fe alloys in LWR environments. However, as demonstrated in Section 4.3, the existing Ni-Cr-Fe data (except for Inconel 718) are generally well predicted by the curves for SS alloys.

(viii) **Weld Data.** In developing the air design fatigue curves, the studies documented in this report were based on larger material groupings (as discussed in item vii) that included data for weld metals as opposed to developing fatigue curves for specific weld materials. Fatigue data on sensitized material were used to estimate the effects of heat affected zones (HAZs) on fatigue life. The analysis in this report is based on consideration of all available weld data. Although there is less weld data than base material data, the weld data analyzed generally falls within the statistical distribution of the base metal data. Section 3.2.9 notes some possible bias between the weld data and the design curves; however, it is not considered to be significant enough to warrant a separate weld metal curve without the development of additional data.

(ix) **Hardening.** The effects of material hardening, such as due to cold work or similar effects, were not investigated.

(x) **Radiation.** Limited test data indicate that neutron irradiation generally increases material strength, which may improve the fatigue lives of materials, especially in the high-cycle regime. In the absence of data that address neutron irradiation effects more completely, the methods described in this report are considered appropriate for application to materials exposed to irradiation, such as SS reactor internals components.

(xi) **Dynamic Strain Aging.** The potential effects of dynamic strain aging (DSA) discussed throughout this report, particularly in Sections 2.2.1.3 and 2.2.2.3, are provided for information. None of the evaluations contained in this report include these effects. The information is presented to identify an area that requires further research.

(xii) **Material Variability and Data Scatter.** The effects of material (heat-to-heat) variability and data scatter on fatigue life were addressed as part of the life reduction factor applied in the development of the air design fatigue curve based on limited available data (see Section 5). However, it is recognized that some of the scatter and variability results from the variety of materials that are covered both in this report and in the fatigue curves in ASME Code Section III and are a function of the material groupings selected (see item vii on material grouping for additional information). A more detailed, separate treatment of material (heat-to-heat) variability and data scatter effects was not investigated.

(xiii) **Surface Finish.** In developing the mean air fatigue curves, the studies documented in this report were based on available fatigue test data on small-scale laboratory specimens, the majority of which were polished. Consistent with ASME Code Section III, the effects of surface roughness on fatigue life were addressed as part of the life adjustment factor applied in the development of the air design fatigue curve based on the limited available data. The surface roughness values considered are representative of component surface finishes. Section 5.3 provides additional detail. A more detailed treatment of surface finish effects was not investigated.

(xiv) **Loading Sequence.** In developing the air design fatigue curves, the studies documented in this report were based on available fatigue test data on small-scale laboratory specimens loaded under constant, uniaxial membrane loading. The effects of loading sequence on fatigue life compared to actual components were addressed as part of the life adjustment factor applied in the development of the air design fatigue curve based on limited available data (see Section 5). A more detailed treatment of loading sequence effects was not investigated.

(xv) **Size and Geometry.** In developing the air design fatigue curves, the studies documented in this report are based on available fatigue test data on small-scale laboratory specimens. The effects of size and geometry on fatigue life compared to actual components was addressed as part of the life adjustment factor applied in the development of the air design fatigue curve based on limited available data (see Section 5). A more detailed treatment of size and geometry effects was not investigated.

(xvi) **Development of Adjustment Factors.** As documented in Section 5, several material, loading, and environmental factors affect fatigue life. Many of these factors have been addressed by the construction of the ASME Code, Section III fatigue design curves and the F_{en} method. Of those remaining factors, two of them—surface preparation and

reactor water flow rate—are not explicitly considered but are expected to be conservatively addressed by the design curves and F_{en} method. Section 5 explicitly considers the effects of the remaining four factors—material variability and data scatter, size and geometry, surface finish, and loading sequence. As discussed in this section, at higher cyclic fatigue lives, only the single dominant factor for a given set of conditions affects fatigue life. At lower cyclic fatigue lives, all factors affect fatigue life. These effects are conservatively considered to be independent even though some factors may be correlated. The current data are insufficient to develop quantitative correlation factors needed for a more rigorous analysis. As discussed in Section 5, a Monte Carlo analysis has also been used to determine the adjustment factors to account for the fact that most service conditions will not lead to the worse-case combination of these factors.

(xvii) **Factor of Two on Strain (or Pseudo-Stress).** In developing the air design fatigue curves, the studies documented in this report assumed a factor of 2 reduction on strain (or pseudo-stress). The factor of 2 reduction was selected to be consistent with ASME Code practices. At present, the adjustment factor of 2 on strain is used to account not only for data scatter, size, surface finish, and loading sequence, but also for the potential effects of a combination of temperature and strain rate on secondary hardening and dynamic strain aging. These effects are not cumulative within the high-cycle fatigue region, and only the most dominant of these effects controls the net adjustment factor. However, these parameters principally affect the growth of microstructurally small cracks, and their significance depends on the operating conditions, environment, material, and the fabrication process. Therefore, the effect that dominates is a function of material and environmental conditions. The factor of 2 on strain is sufficient to account for the dominant effect within the high-cycle fatigue region. It is recognized that, based on existing data, a factor of 2 on strain may be conservative for some materials, especially when the loading cycles exceed 10^4. Given sufficient data, it may be possible to refine this factor either generically or for specific materials.

(xviii) **F_{en} Assumptions.** As mentioned previously in the report, the F_{en} approach has been developed for use with ASME Code, Section III fatigue evaluation procedures. It is recognized that other design and evaluation procedures are used internationally. The use of the F_{en} approach with any other procedure has not been evaluated in this report. Further, the F_{en} approach presumes that the slope of the strain (or stress) vs. life fatigue curve is the same in air and water environments. Based on the totality of the data in this report, this assumption appears reasonable. If environmental effects increase with decreasing strain, the use of an adjustment factor would be a function of strain and the concept becomes more complex. It is not clear whether the apparent increase in environmental effects with decreasing strain is a true strain dependence or just an artifact of the dataset being used to evaluate environmental effects. Most of the fatigue data on austenitic SSs in PWR environments are for low-carbon Type 304L or 316NG materials. As mentioned in the report, the slope of the fatigue strain vs. life curve in air for these low-carbon SS materials is steeper than that for the high-carbon SS materials. Additional data are needed to investigate this topic more completely.

(xix) **Limits of Validity.** The report defines the limits of validity for all parameters affecting the F_{en} relationships for each of the materials investigated. In some cases, the limits of applicability have been extended a small amount beyond the limits defined in the applicable tests so that the relationships cover most anticipated LWR operating conditions. For example, for carbon and low-alloy steels, the maximum temperature of the data presented in the report was 290°C (see Table 4-1), but the upper temperature

limit of the F_{en} expressions is 325°C. In other cases, extension of the limits was judged to be reasonable based on limited review of other test data not explicitly presented in the report. Additionally, the cyclic limits of the air design fatigue curves were selected to match the limits currently defined in the ASME Code, Section III fatigue design curves.

(xx) **Applicability of Method and Future Work.** The fatigue design curves developed in this report for carbon and low-alloy steels and austenitic SSs are applicable to various grades and compositions of materials having a wide range of tensile strength. Furthermore, the criterion used in establishing the fatigue design curve ensures that the proposed curve bounds 95% of the available fatigue data with 95% confidence. In addition, the mean stress correction for the design curves is based on a conservative value of mean stress at room temperature. Finally, the fatigue loading in laboratory specimens is uniformly tensile which is more severe than in many applications where the loading decreases through the thickness. Therefore, the fatigue design curves should be conservative for most materials and applications, particularly at reactor operating temperatures where mean stresses are likely to be lower.

The criteria used for establishing the adjustment factors to account for the parameters that influence fatigue life that were not considered in the experimental data used to develop the fatigue design curves (Section 5) are also expected to yield conservative estimates of fatigue life in most applications. These adjustment factors may be further optimized. Note that other factors (e.g., component size) may lead to decreases in fatigue life in field applications compared to laboratory testing. Therefore, any modifications of the design curves or adjustment factors should be performed holistically to develop a technical basis that addresses all the sources of conservatism and uncertainty mentioned above.

Guidance should be provided for using the high-cycle portion of the curves for mechanical loading. This guidance is necessary because strain-controlled fatigue test data are used to develop the ASME Code ε–N fatigue design curves, and these must be converted to pseudo-stress vs. life curves in most applications.

(xxi) **Gradient Effects.** As mentioned previously, both the air fatigue design curves and the F_{en} method used to account for the effects of the LWR environment are based on small-scale laboratory specimens tested under uniaxial membrane loading. It is recognized that fatigue transients in components and structures are typically not uniaxial and also vary through the component thickness as a result of bending or other localized effects. The effects of through-thickness gradient loading or multiaxial loadings on fatigue life were not specifically investigated in this report. However, it is recognized that such effects often increase the number of cycles needed both to form an engineering-size crack (i.e., the definition of fatigue life used in this report) and the subsequent growth of such a crack through the component thickness. Therefore, the current design curves and F_{en} method are generally expected to be conservative with respect to these effects.

(xxii) **Use of Method.** Generally, the provisions of this document can be used to predict fatigue lives of any component, or portion of a component, that is exposed to water and has been evaluated for CUF using the rules in either Subarticles NB-3200 or NB-3600 of ASME Code, Section III, or in another applicable subarticle. Use extends to both Class 1 and non-Class 1 components. Such components may include piping, pumps, valves, and reactor internals components.

(xxiii) **Use of F_{en} in NB-3600 Analyses.** Generally, much of the discussion, examples, and the sample problem in this report reference the method in Subarticle NB-3200 of ASME Code Section III. The majority of evaluations that address environmental fatigue effects are expected to be performed using Subarticle NB-3200 methods. Although the experience with application of F_{en} methods to evaluations in Subarticle NB-3600 of ASME Code Section III is more limited, there are examples evaluations using Subarticle NB-3600 methods available in the literature (e.g., H.S. Mehta, EPRI Report 107943, June 1998). In addition, at the time of publication of this report, ASME committees were evaluating sample problems using Subarticle NB-3600 methods and considering further ASME guidance on the use of these methods. Therefore, the authors believe that the F_{en} methods in this report are equally applicable to Subarticle NB-3600 methods.

(xxiv) **ASME Code Class 1 Fatigue Exemption.** Generally, if the ASME Code, Section III provisions in Subparagraph NB-3222.4(d) for components not requiring analysis for cyclic service are satisfied using the air design curves in this document, an F_{en} assessment is not required for those components.

(xxv) **ASME Code Procedures.** It is generally recognized that some of the ASME Code, Section III methods for computing CUF are conservative. For example, load pairing in ASME Code fatigue calculations generally assumes the most severe ordering. Analysts address some of these conservatisms when fatigue calculations are revised or revisited. Section 4.3 of NUREG/CR-6260 cites several examples of such conservatisms. This report did not address conservativisms when computing CUF using ASME Section III methods.

(xxvi) **Clad Components.** The interiors of LWR reactor vessels and nozzles made of carbon and low-alloy steel are typically clad with stainless steel. This report does not address separate treatment of cladding. ASME Code Section III requirements (Paragraph NB-3122) specify that no structural strength shall be attributed to the cladding in satisfying primary stress limits, but the thermal and stress analyses shall consider the presence of the cladding when determining the secondary and peak stresses for the base material. Thus, consistent with the discussion in Section 4.2.2 of NUREG/CR-6260, it is appropriate to neglect fatigue of the cladding and compute the CUF and CUF_{en} for the base metal in most fatigue analyses.

2 MECHANISM OF FATIGUE

2.1 Formation of an Engineering Crack in Air

Deformation and microstructural changes in the surface grains of metals are responsible for fatigue cracking. During cyclic straining, the irreversibility of dislocation glide leads to the development of surface roughness. Strain localization in persistent slip bands (PSBs) results in the formation of extrusions and intrusions. With continued cycling, microcracks ultimately form in PSBs or at the edges of slip-band extrusions. At high strain amplitudes, microcracks form in notches that develop at grain, twin, or phase boundaries (e.g., ferrite/pearlite) or by cracking of second-phase particles (e.g., sulfide or oxide inclusions).

Once a microcrack forms, it continues to grow along its primary slip plane or a PSB as a Mode II (shear) crack in Stage I growth (where the orientation of the crack is usually at 45° to the stress axis). At low strain amplitudes, a Stage I crack may extend across several grain diameters before the increasing stress intensity of the crack promotes slip on planes other than the primary slip plane. A dislocation cell structure normally forms at the crack tip. Because slip is no longer confined to planes at 45° to the stress axis, the crack begins to propagate as a Mode I (tensile) crack, normal to the stress axis in Stage II growth. At high strain amplitudes, the stress intensity is quite large and the crack propagates entirely by the Stage II process. Stage II crack propagation continues until the crack reaches an engineering size. Figure 2-1 shows the two stages of fatigue crack growth in smooth specimens.

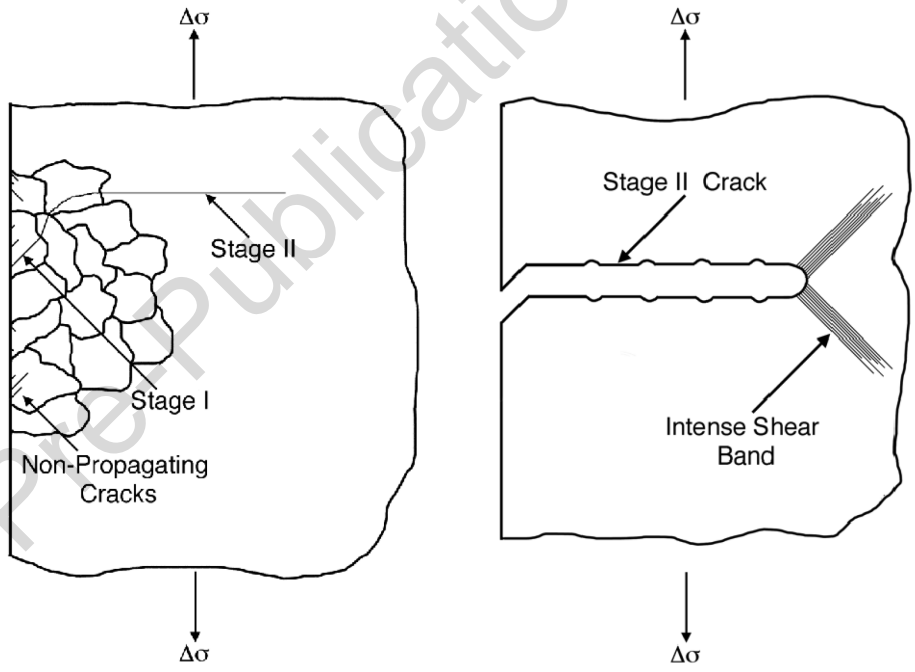

Figure 2-1 Two stages of fatigue crack growth in smooth test specimens.

In air or mildly corrosive environments, Stage II cracking is characterized by fatigue striations. Figure 2-2 illustrates the process of Stage II fatigue crack growth and formation of fatigue striations[162]. As tensile load is applied, slip bands form at the double notch or “ears” of the crack tip (Figure 2-2(b)). The slip bands widen with further straining, causing blunting of the crack tip

(Figure 2-2(c)). Crack surfaces close during compressive loading and slip is reversed, producing ears at the edges of the blunt crack tip (Figure 2-2(d) and Figure 2-2(e)). The ears are observed as fatigue striations on the fracture surface. However, there is not necessarily a 1:1 correlation between striation spacing and fatigue cycles. At high strain amplitudes, several striations may be created during one cycle, whereas at low strain amplitudes, one striation may represent several cycles.

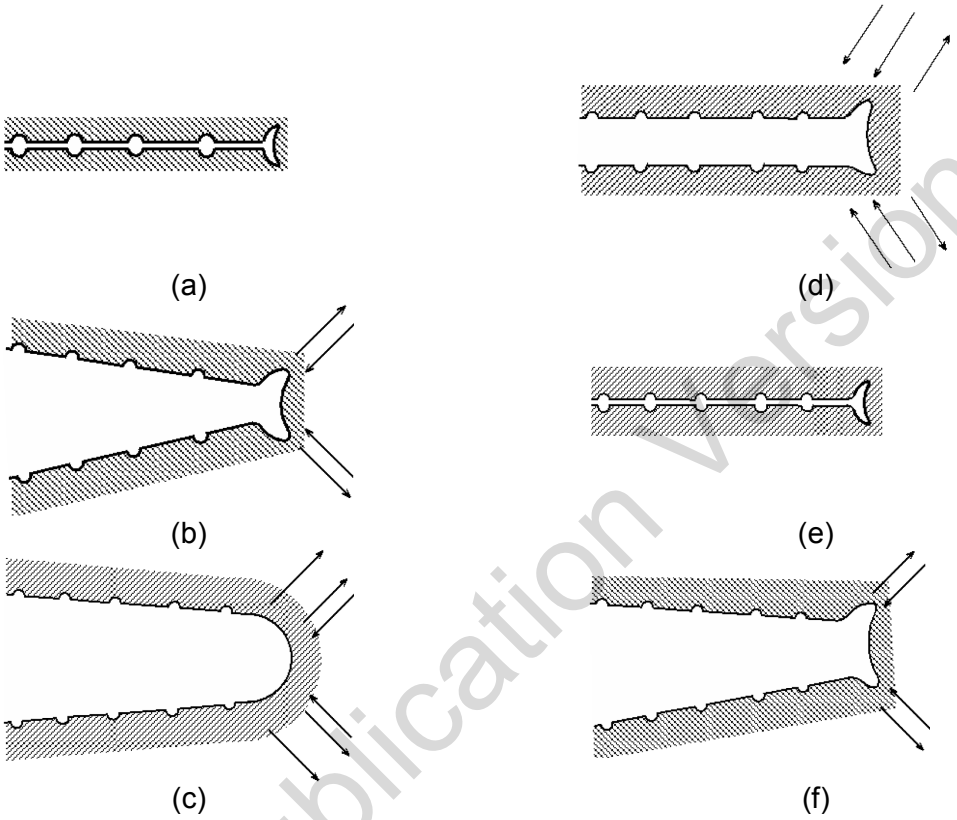

Figure 2-2 Schematic illustration of the plastic blunting process of fatigue crack growth in Stage II: (a) zero load, (b) small tensile load, (c) maximum tensile load with widening of slip bands, (d) crack closure and formation of "ears" at crack tip, (e) maximum compressive load, and (f) small tensile load in the subsequent cycle.

Thus, the formation of surface cracks and their growth as shear and tensile cracks (Stages I and II growth) to an "engineering"-size (e.g., a 3-mm-deep) crack constitute the fatigue life of a material, which is represented by the fatigue strain vs. life (ε–N) curves. Fatigue life is conventionally divided into two stages: (1) initiation, which is expressed as the number of cycles required to form microcracks on the surface, and (2) propagation, which is expressed as the number of cycles required to propagate the surface cracks to an engineering size. Thus, the definition of a cumulative usage factor (CUF) value of unity, as described in Section 1.1, conventionally includes both initiation and some amount of propagation.

An alternative approach considers fatigue life of engineering structures and components to be entirely composed of the growth of short fatigue cracks (i.e., cracks less than "engineering" size).[163,164] For polycrystalline materials, the time for the formation of surface cracks is negligible. During cyclic loading, surface cracks, 5 μm or longer, form early in life at surface

irregularities that either already exist or were produced by slip bands, grain boundaries, second-phase particles, or other such features (Figure 2-3)[11,165-167] Thus, fatigue life may be considered to constitute propagation of cracks from 10 to 3000 μm long, and fatigue damage in a material may be considered as the current size of the fatigue crack.[164] However, the growth rates of short cracks cannot be predicted accurately from fracture mechanics methodology based on the range of stress intensity factor (ΔK) alone. Under the same ΔK loading, short fatigue cracks (i.e., cracks having lengths comparable to the unit size of the microstructure) grow at a faster rate than longer fatigue cracks.[168] In addition, shorter cracks can grow at ΔK values below those predicted from linear elastic fracture mechanics (LEFM). The differences between the growth rates of short and long cracks are attributed to interactions with microstructural features, contributions of crack closure with increasing crack length, effects of mixed mode crack propagation, and an inadequate characterization of the crack tip stress/strain fields associated with short cracks.

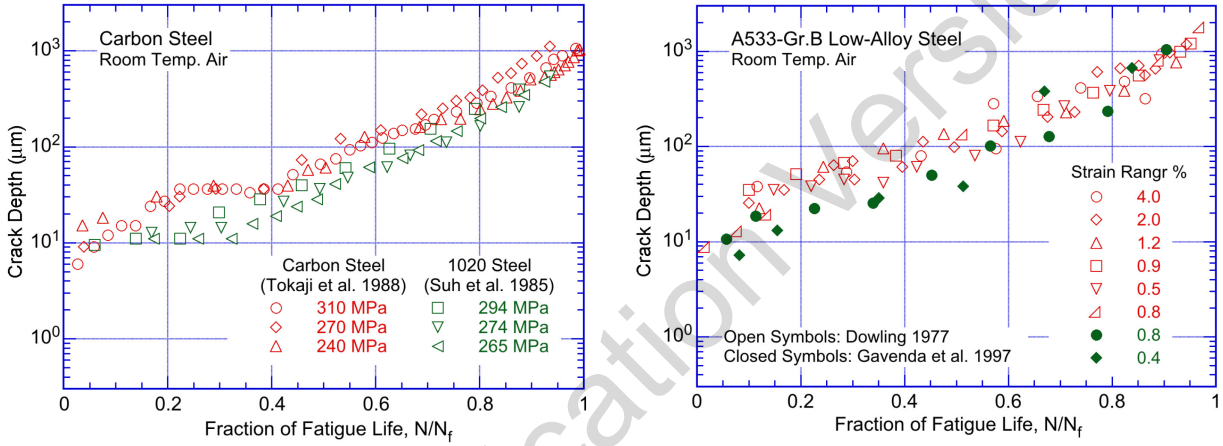

Figure 2-3 Crack depth plotted as a function of fractional life for carbon and low-alloy steels tested in air (Refs. 11 and 165-167).

Figure 2-4 shows a schematic illustration of the two stages of fatigue crack growth including (a) initiation, and (b) propagation. The initiation stage involves growth of "microstructurally small cracks" (MSCs), characterized by decelerating crack growth (Region AB in Figure 2-4(a)). The propagation stage involves growth of "mechanically small cracks," characterized by accelerating crack growth (Region BC in Figure 2-4(a)). The MSCs correspond to Stage I cracks and grow along slip planes as shear cracks in the early stage of growth. The growth of the MSCs is very sensitive to microstructure.[11,166-171] For MSCs, microstructural effects are strong because of Stage I growth (i.e., crystallographic growth). The growth rates are markedly decreased by grain boundaries, triple points, and phase boundaries. In ferritic-pearlitic steels, fatigue cracks initiate and propagate preferentially in the ferrite phase that forms as long allotriomorphs at prior austenite phase boundaries.[166,170,171] The ferrite/pearlite phase boundaries act as strong barriers to crack propagation, and growth rates decrease significantly when small cracks grow into the pearlite from the ferrite.[166] Limited data suggest that microstructural effects are more pronounced at negative stress ratios; the compressive component of the applied load plays an important role in the formation of Stage I facets and formation of cracks.[169]

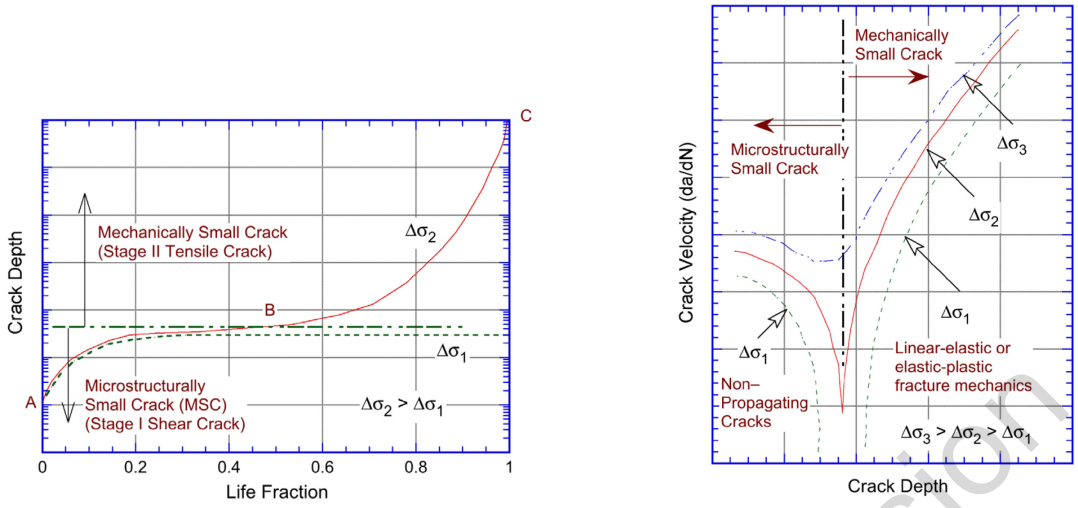

Figure 2-4 Schematic illustration of (a) growth of short cracks in smooth specimens as a function of fatigue life fraction, and (b) crack velocity as a function of crack depth.

Fatigue cracks greater than a critical size show little or no influence of microstructure and are considered mechanically small cracks.[169] Mechanically small cracks correspond to Stage II (tensile) cracks, which are characterized by striated crack growth, with the fracture surface normal to the direction of maximum principal stress. The growth of mechanically small cracks is characterized in terms of the J-integral range (ΔJ) and crack growth rate (CGR) data in air and light-water reactor (LWR) environments. The CGRs estimated from smooth specimen ε–N data show good agreement with CGRs obtained on fracture mechanics compact tension (CT) specimens in air and water environments.[13]

Various criteria, summarized in Section 5.4.1 of NUREG/CR-6717, "Environmental Effects on Fatigue Crack Initiation in Piping and Pressure Vessel Steels," issued May 2001,[12] are used to define the crack depth for transition from microstructurally to mechanically small cracks. The transition crack depth is a function of applied stress (σ) and the microstructure of the material. For completely reversed fatigue straining, the transition from an MSC to a mechanically small crack for several materials is estimated to be approximately eight times the unit size of the microstructure,[169] actual values may range from 150 to 250 μm.

At low stress levels ($\Delta\sigma_1$) (Figure 2-4(a)), the transition from MSC growth to accelerating crack growth does not occur. This circumstance represents the fatigue limit for a smooth specimen. Although cracks can form below the fatigue limit, they grow to engineering size only at stresses greater than the fatigue limit. The fatigue limit for a material is applicable only for constant loading conditions. Under variable loading conditions, MSCs can grow at high stresses ($\Delta\sigma_3$) (Figure 2-4(b)) to depths larger than the transition crack depth, and then continue to grow at stress levels below the fatigue limit ($\Delta\sigma_1$).

As discussed in Section 1.1, fatigue life is described in this report as the number of cycles of a specified strain amplitude that a specimen can sustain before the formation of a 3-mm-deep crack (i.e., an "engineering crack"). This is assumed throughout this report to equate to crack initiation in an actual component. Using this definition, a calculated fatigue CUF less than unity

provides reasonable assurance that a fatigue crack has not formed in a component, and indicates that the probability of forming a crack in the component is low.

2.2 Fatigue Cracking in LWR Environments

The available small-scale laboratory fatigue test data indicate a significant decrease in fatigue life of reactor structural materials in LWR environments. The extent of environmental effects depends on the applied strain, temperature, strain rate, dissolved oxygen (DO) in the water, and for carbon and low-alloy steels, the sulfur content in the steel. Although the structure and cyclic hardening behavior of carbon and low-alloy steels are distinctly different, there is little or no difference in susceptibility to environmental degradation of fatigue life of these steels. Reduction in fatigue life in LWR water environments may arise from easy formation of surface microcracks consisting of the growth of MSCs (i.e., the initiation stage) or an increase in growth of mechanically small cracks, or both (i.e., propagation stage). The following sections discuss the formation and growth characteristics of fatigue cracks in detail for carbon and low-alloy steels and wrought and cast austenitic stainless steels (SSs). Similar information for nickel-chromium-iron (Ni-Cr-Fe) alloys is very limited.

2.2.1 Carbon and Low-Alloy Steels

Carbon and low-alloy steels tested in air show slight discoloration, while those tested in water develop a gray/black corrosion scale and are covered with magnetite (Fe_3O_4) at all DO levels. Hematite (α-Fe_2O_3) forms on these materials at DO levels above 200 parts per billion (ppb).[20,22,172] The amount of hematite increases with increasing DO levels in the water.[20] Studies on the pitting behavior of carbon and low-alloy steels[173,174] in high-purity water indicate that pitting corrosion does not occur in these steels at reactor operating temperatures in low-DO pressurized-water reactor (PWR) environments (typically less than 0.01 parts per million (ppm) DO), and at temperatures above 200°C in water that contains 0.1–0.2 ppm DO, which represents normal boiling-water reactor (BWR) water chemistry. However, even under these conditions, micropits form in both types of steels due to dissolution of manganese sulfide (MnS) inclusions[18] or by anodic reaction in the sulfur-contaminated matrix[175] close to sulfide inclusions. These micropits and cavities can act as stress raisers and provide preferred sites for the formation of fatigue cracks.

2.2.1.1 Effects of Surface Micropits

The strain rate effects in water are such that fatigue life decreases with decreasing strain rate. These effects are often explained by a higher density of micropits at lower strain rates. Some investigators argue that the longer test durations for slow strain rate tests result in a higher density of micropits and, therefore, shorter periods for the formation of surface microcracks.[18] However, if the presence of micropits was responsible for the reduction in fatigue lives of carbon and low-alloy steels in LWR environments, then specimens pre-exposed to high-DO water followed by testing in air should also show a decrease in fatigue life.

Figure 2-5 shows a comparison of the fatigue lives of carbon and low-alloy steels tested in high-DO water at 288°C with the fatigue lives of carbon and low-alloy steels preoxidized at 288°C for 30–100 hours in water with 0.6–0.8 ppm DO and then tested in either air or low-DO water with less than 0.01 ppm DO.[40,41,176] Runouts, in this and subsequent figures, are identified in the traditional manner of using arrows after the data-point. The fatigue lives of the preoxidized specimens were identical to those of the unoxidized specimens; life was expected to decrease if surface micropits facilitate the formation of fatigue cracks. Only a moderate

decrease in life was observed for both preoxidized and unoxidized specimens tested in low-DO water. Furthermore, if micropits were responsible for the decrease in fatigue lives in LWR environments, then the fatigue limit of these steels should be lower in water than in air.

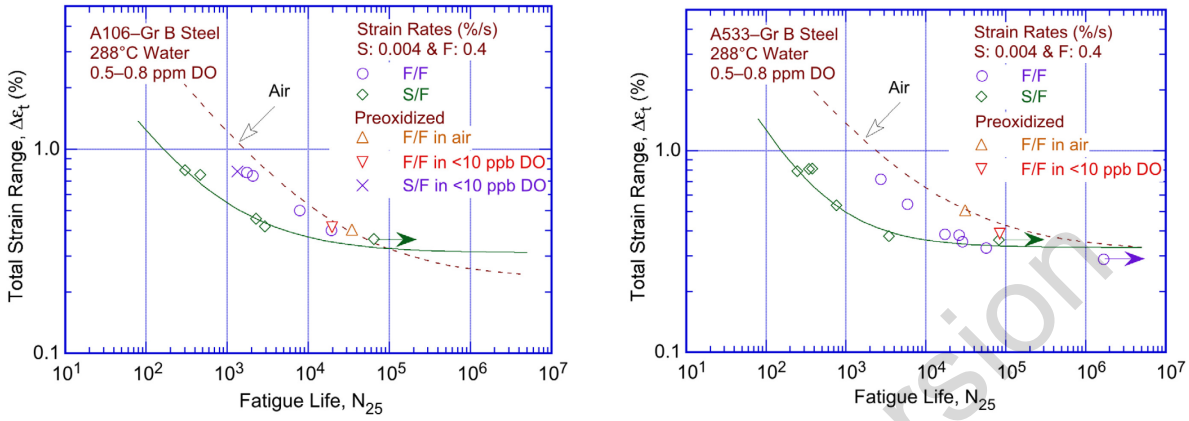

Figure 2-5 Fatigue life of carbon and low-alloy steel specimens in high-DO water at 288°C compared with the fatigue life of specimens preoxidized in high-DO water and tested in either air or low-DO water at 288°C (Refs. 40, 41, and 176) (Runouts, in this and subsequent figures, are identified in the traditional manner of using arrows after the data-point).

The extent of fatigue cracking, as measured by the number of cracks with depths greater than 10 μm, along longitudinal sections of carbon and low-alloy steel specimens as a function of strain range in air, simulated PWR, and high-DO water was also investigated.[176] The results indicated that, with the exception of low-alloy steel tested in simulated PWR water, the water environment had no effect on the frequency (number per unit gauge length) of cracks. For similar loading conditions, the number of cracks in the specimens tested in air and high-DO water was identical, although fatigue lives were lower by a factor of approximately 8 in water. If the reduction in life was caused by enhanced crack nucleation, the specimens tested in high-DO water should have shown a higher number of cracks. Detailed metallographic evaluations of the fatigue test specimens[176] also indicated that, irrespective of environment, cracks in carbon and low-alloy steels nucleated along slip bands, carbide particles, or at the ferrite/pearlite phase boundaries.[11,176]

2.2.1.2 Mechanisms of Corrosion Fatigue

The environmental enhancement of fatigue crack growth in pressure vessel steels in high-temperature oxygenated water and the effects of sulfur content, loading rate, and flow velocities are well documented.[177-189] Dissolution of MnS inclusions changes the water chemistry near the crack tip, making it more aggressive. This results in enhanced CGRs because either (1) the dissolved sulfides decrease the repassivation rate, which increases the amount of metal dissolution for a given oxide rupture rate;[189] or (2) the dissolved sulfide poisons the recombination of hydrogen (H) atoms liberated by corrosion, which enhances H uptake by the steel at the crack tip.

The enhanced CGRs in LWR environments are attributed to either slip oxidation/dissolution[189-193] or hydrogen-induced cracking mechanisms.[194-196] For the slip oxidation/dissolution mechanism, a critical concentration of sulfide (S^{2-}) or hydrosulfide (HS^{-}) ions, which are

produced by the dissolution of sulfide inclusions in the steel, is required at the crack tip for environmental effects to occur. The crack tip is supplied with S^{2-} and HS^{-} ions as the advancing crack intersects the sulfide inclusions, and the inclusions dissolve in the high-temperature water environment. S^{2-} ions are removed from the crack tip by one or more of the following processes: (1) diffusion due to a concentration gradient, (2) ion transport due to an electrochemical potential (ECP) gradient, (3) pumping action due to cyclic loading on the crack, and/or (4) fluid flow induced within the crack due to the flow of water outside the crack. The morphology, size, and distribution of sulfide inclusions and the probability of advancing the crack to intercept the sulfide inclusions are important parameters affecting growth rates of carbon and low-alloy steels in LWR environments.[183,185-188]

The requirements for a slip dissolution model are that a protective oxide film is thermodynamically stable to ensure that a crack will propagate with a high aspect ratio without degrading into a blunt pit and that a strain increment occurs to rupture that film and thereby expose the underlying matrix to the environment (Figure 2-6). Once the passive oxide film is ruptured, crack extension is controlled by dissolution of freshly exposed surfaces and by the oxidation characteristics. The effect of the environment increases with decreasing strain rate. The mechanism assumes that environmental effects do not occur during the compressive load cycle because during that period water does not have access to the crack tip. Ford et al.[191,192] proposed that the average environmentally assisted CGR, $\overline{V}_t$ (centimeters per second), is related to the crack tip strain rate, $\dot{\varepsilon}_{ct}$, by the relationship

$$\overline{V}_t = A(\dot{\varepsilon}_{ct})^n \,, \tag{13}$$

where the constants A and n depend on the material and environmental conditions at the crack tip. There is a lower limit of crack propagation rate associated either with blunting when the crack tip cannot keep up with the general corrosion rate of the crack sides, or with the fact that a critical level of S^{2-} ions cannot be maintained at the crack tip. For example, the latter condition may occur when the CGR falls below a critical value such that a high concentration of S^{2-} ions cannot be maintained at the crack tip. The critical crack growth rate at which this transition occurs depends on the DO level, flow rate, and sulfur (S) content of the steel.

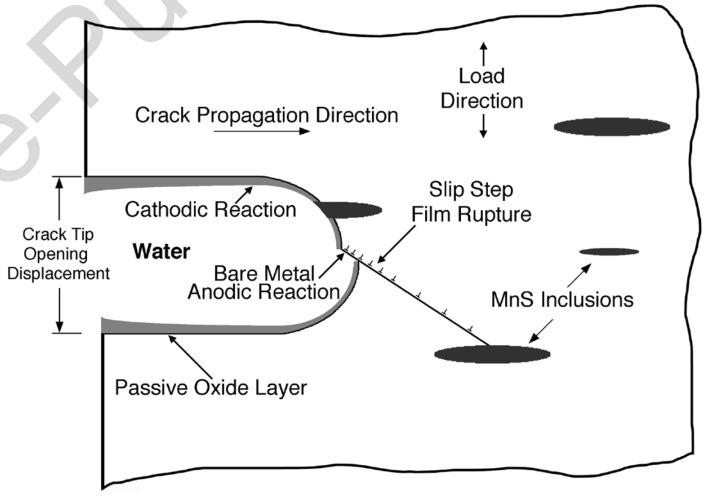

Figure 2-6 Schematic illustration of slip oxidation/dissolution process.

The average critical velocity, $\bar{V}_{in}$, (millimeters per second), for initiation or cessation of environmentally assisted cracking (EAC), was shown to depend on the balance between sulfide supply rate and mass transport away from the crack tip.[178,182] Initiation of EAC requires a critical concentration of sulfide ions at the crack tip, which is supplied with sulfide ions as the advancing crack intersects the sulfide inclusions, and the inclusions dissolve in the high-temperature water. Crack growth studies in high-temperature, low-DO environment (i.e., less than 0.05 ppm DO) indicate that $\bar{V}_{in}$ is given by

$$\bar{V}_{in} = \frac{1.27 \times 10^{-6}}{a}, \quad (14)$$

where a is the crack depth (millimeters). Thus, for a 2.54-mm crack depth, a minimum average crack velocity of 5×10^{-7} mm/s is required to produce the S^{2-} ion concentration for environmental effects on crack growth to be pronounced.[182] In addition, the critical velocity must be maintained for a minimum crack extension of 0.33 mm to achieve the concentration of S^{2-} ions needed for initiating environmental enhancement of growth rates.[178] Equation 14 indicates that the minimum crack velocity to initiate environmental effects increases with decreasing crack depth. For crack depths between 0.01 and 3 mm, crack velocities in the range of 1.27×10^{-4} to 4.23×10^{-7} mm/s are required to cause a measurable reduction in fatigue lives of carbon and low-alloy steels in low-DO water. For smooth cylindrical fatigue specimens, these growth rates are not achieved under the loading conditions typically used for fatigue ε–N data, which suggests that environmental effects on fatigue lives in low-DO environments are not significant. This behavior is consistent with the existing fatigue ε–N data; for most compositions of carbon and low-alloy steels, only moderate reductions in fatigue life (less than a factor of 2) are observed in 288°C water containing less than 0.01 ppm DO, which is within the data scatter.

In addition, consistent with the slip dissolution mechanism assumption mentioned previously, it is assumed that environmental enhancement of crack propagation does not occur during the compressive load cycle because, during that period, the water does not have access to the crack tip due to crack closure. The total crack advance during a fatigue cycle is given by the summation of crack advance in air due to mechanical factors, and crack advance during the tensile load cycle (i.e., increasing strain) from a slip-dissolution mechanism, once the tensile strain increment exceeds the fracture strain of the oxide.

Hydrogen-induced cracking (Figure 2-7) of carbon and low-alloy steels is caused by hydrogen produced by the oxidation reaction at the crack tip that is partly absorbed into the metal; it interacts with MnS inclusions and leads to the formation of cleavage cracks at the inclusion matrix interface. Crack extension occurs by linkage of the cleavage cracks. Other hydrogen-induced fracture processes may also enhance growth rates in LWR environments. According to the decohesion mechanism, significant accumulation of hydrogen at or near the crack tip decreases the cohesive interatomic strength of the lattice.[197] Hydrogen-induced bond rupture ahead of the crack tip links up with the main crack resulting in discontinuous, but enhanced crack growth. Furthermore, adsorbed hydrogen lowers the surface energy of the metal, thus facilitating crack growth at a lower fracture stress level. In addition, hydrogen can cause localized crack tip plasticity by reducing the stress required for dislocation motion.[198] Note that the hydrogen produced at the crack tip by this mechanism is not related to the hydrogen content of the bulk fluid; as a result, hydrogen content of the bulk fluid is not a parameter in the environmental fatigue correction factor (F_{en}) expressions.

Both the slip-oxidation/dissolution and hydrogen-induced cracking mechanisms are dependent on oxide rupture rates, passivation rates, and liquid diffusion rates. Therefore, it is difficult to

differentiate between the two mechanisms or to establish their relative contribution to crack growth rates in LWR environments. However, fatigue crack morphologies in test specimens indicate that both the slip-oxidation/dissolution and hydrogen-induced cracking mechanisms are important for environmental effects of the fatigue lives of carbon and low-alloy steels in LWR environments. A change in fracture appearance from ductile striations in air to brittle facets or cleavage-like fracture in LWR environments lends the greatest support for hydrogen–induced cracking.[142,143,187,195,196]

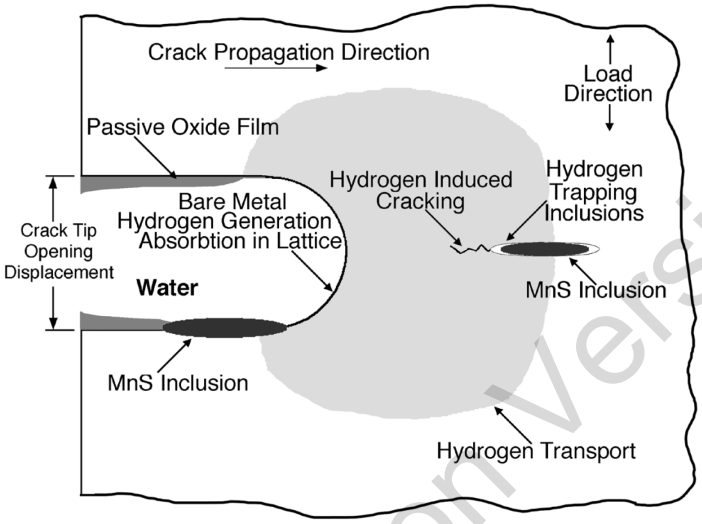

Figure 2-7 Schematic illustration of hydrogen-induced cracking of low-alloy steel.

The fatigue crack morphologies of carbon and low-alloy steels in a BWR environment also show a strong dependence and change with strain rate. At high strain rates, surface crack morphology is predominantly a zigzag pattern and is inclined to the loading axis, whereas entirely straight crack morphology normal to the loading axis is observed at slow strain rates.[10,139,143] Figure 2-8 shows the surface crack morphology in A106-Gr. B carbon steel tested in air and high-DO water at 288°C. In addition, high strain rates lead to a rough fracture surface with the typical fan-like or quasi-cleavage cracking pattern, and slow strain rates result in a flat, nondescript fracture surface.[139,142] Figure 2-9 shows the propagation of fatigue cracks in A106-Gr. B carbon steel. In air, fatigue cracks grow along relatively soft ferrite regions and avoid the hard pearlite regions. In contrast, in a high-DO BWR environment, fatigue cracks appear to grow straight, normal to the stress axis, and through both the soft ferrite and the hard pearlite regions. Such crack growth characteristics are consistent with the slip-oxidation/dissolution mechanism and crack extension by anodic dissolution of the matrix in a corrosive environment.

Wu and Katada[142] attributed the change in crack morphology to a change in the corrosion fatigue mechanism from hydrogen-induced cracking to a slip-oxidation/dissolution mechanism with decreasing strain rate. The authors reasoned that, during cyclic loading in high-temperature water, plastic deformation induces slip bands at the crack tip along the maximum shear or preferred slip directions. The extrusion of slip bands may rupture the protective oxide film at the crack tip. The slip bands are the favored path for hydrogen transportation, and the interfaces between the matrix and inclusions or precipitations in the region of maximum hydrostatic tension are the preferred traps for hydrogen. Thus, hydrogen tends to accumulate at these sites and embrittle them. As a result, at high strain rates, fatigue cracking preferentially occurs along the

slip bands or preferred slip directions and the matrix/inclusions interfaces, which results in macroscopically tortuous fatigue cracks and a rough fracture surface. However, at low strain rates, fatigue crack growth in high-temperature water is controlled by the film-rupture/oxidation-dissolution mechanism, which results in macroscopically straight fatigue cracks and a relatively flat, featureless fracture surface.

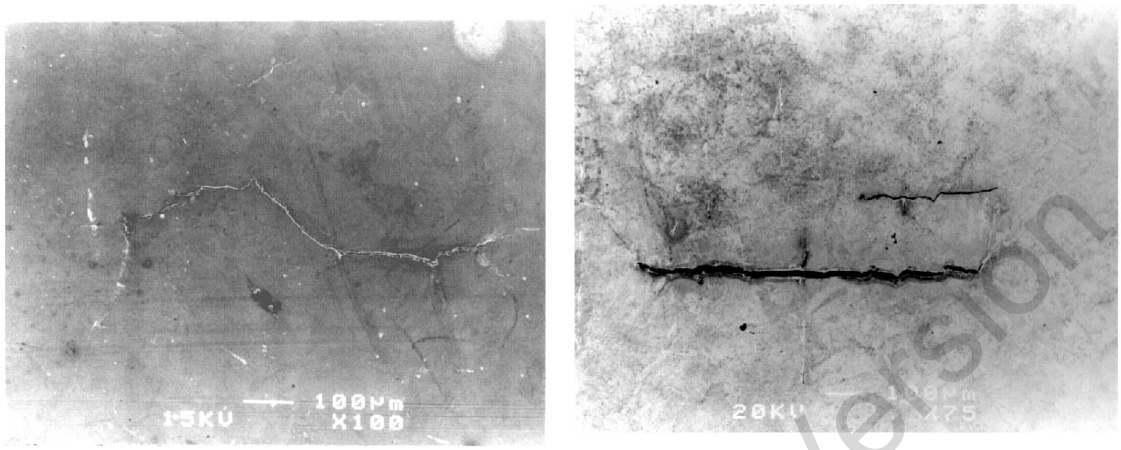

(a) (b)

Figure 2-8 Fatigue cracks on gauge surfaces of A106–Gr. B carbon steel tested in (a) air and (b) high-DO water at 288°C (Ref. 10).

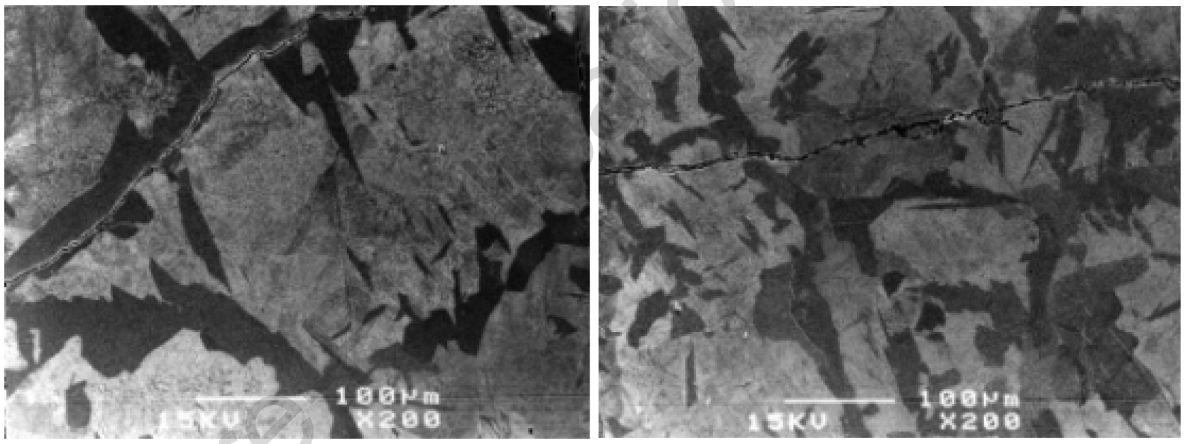

(a) (b)

Figure 2-9 Fatigue cracks along longitudinal sections of A106—Gr. B carbon steel tested in (a) air and (b) high-DO water at 288°C (Ref. 10).

2.2.1.3 Effects of Dynamic Strain Aging

Several studies showed that dynamic strain aging (DSA) may play a significant role in the cyclic deformation process of carbon and low-alloy steels in LWR environments.[147-151] DSA occurs in alloys containing solutes that segregate strongly to dislocations resulting in strong interactions between the solute and the stress-strain field of the dislocations, which leads to dislocation pinning (Figure 2-10). In carbon and low-alloy steels, the occurrence of DSA is due to interstitial elements such as nitrogen and carbon. DSA is sufficiently rapid to occur during fatigue straining

and produces a variety of inhomogeneous deformations such as serrated yielding, jerky or serrated flow, or other such deformations. These effects depend on temperature and strain rate.

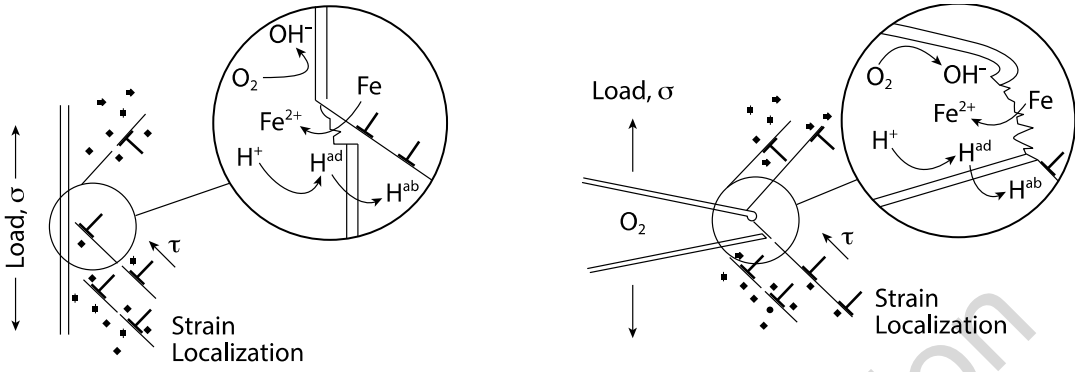

Figure 2-10 (a) Fatigue crack initiation and (b) crack growth in DSA susceptible low-alloy steel exposed to a high-temperature water environment (Ref. 147).

Under certain combinations of temperature and strain rate conditions, DSA may significantly affect the EAC behavior of carbon and low-alloy steels by increasing the monotonic yield and tensile strength, the strain hardening exponent, the creep rate, and the crack-tip strain and strain rate.[149] DSA also results in planar deformation, an increase in dislocation density and inhomogeneous localization of deformation. These factors favor brittle crack extension and rupture of the protective oxide film, thereby enhancing crack advance by either anodic dissolution or hydrogen embrittlement processes. In high-temperature water, the synergistic interactions between EAC and DSA during fatigue straining may be rationalized as follows:[149]

- Hydrogen vacancies produced by the corrosion reaction at the crack tip enter the steel and hydrogen diffuses to strong trapping sites inside the crack-tip maximum hydrostatic stress region (e.g., MnS inclusions) ahead of the crack tip.
- These sites act as initiation sites for local quasi-cleavage cracking, as well as void formation, and these microcracks link with the main crack.
- In addition, at a given macroscopic strain caused by external loads, the microscopic strain in steels that are susceptible to DSA is higher because of strain localization to small areas, which leads to higher rates and larger steps of oxide film rupture. As a result, the slip oxidation/dissolution process enhances fatigue crack initiation or fatigue CGRs.
- Such interactions, however, occur only under certain conditions of temperature, strain rate, and DO level in the environment.

In carbon and low-alloys steels, the interaction of nitrogen and dislocations during plastic deformation reduces plasticity, which causes strain localization in the material.[147] Small areas can deform plastically adjacent to areas that might be blocked by nitrogen/dislocation interactions. For a given macroscopic strain, the microscopic strain is higher due to strain localization in steels that are susceptible to DSA. Thus, because of strain localization, stress concentrations at active slip planes lead to higher rates and larger steps of oxide rupture and, simultaneously, to a decreased repassivation rate.[147,148] Consequently, both crack initiation and growth rates may be enhanced in carbon and low-alloy steels.

2.2.1.4 Crack Growth Rates in Smooth Fatigue Specimens

Studies on the formation and growth characteristics of short cracks in smooth fatigue specimens in LWR environments indicated that the decrease in fatigue life in LWR environments is caused primarily by the effects of the environment on the growth of MSCs (i.e., cracks less than 200 μm deep) and, to a lesser extent, on the growth of mechanically small cracks.[10,11]

Figure 2-11 shows measured crack lengths as a function of fatigue cycles and fraction of fatigue life for smooth cylindrical specimens of A533-Gr. B low-alloy steel in air, simulated PWR environment, and high-DO water. Figure 2-12 shows an example of the growth of a surface crack in A533-Gr. B steel tested in air at room temperature, and shows the fracture surface and probable crack front for the crack. The results indicate that, for this example, three cracks merged to form the final fracture surface. The primary crack initiated near an inclusion and reached a surface length of approximately 100 μm after 3,062 cycles (i.e., approximately 50% of the fatigue life). Two secondary cracks merged with the primary crack after approximately 5,700 and 6,000 cycles. Crack depth was determined by dividing the surface crack length by pi (π).

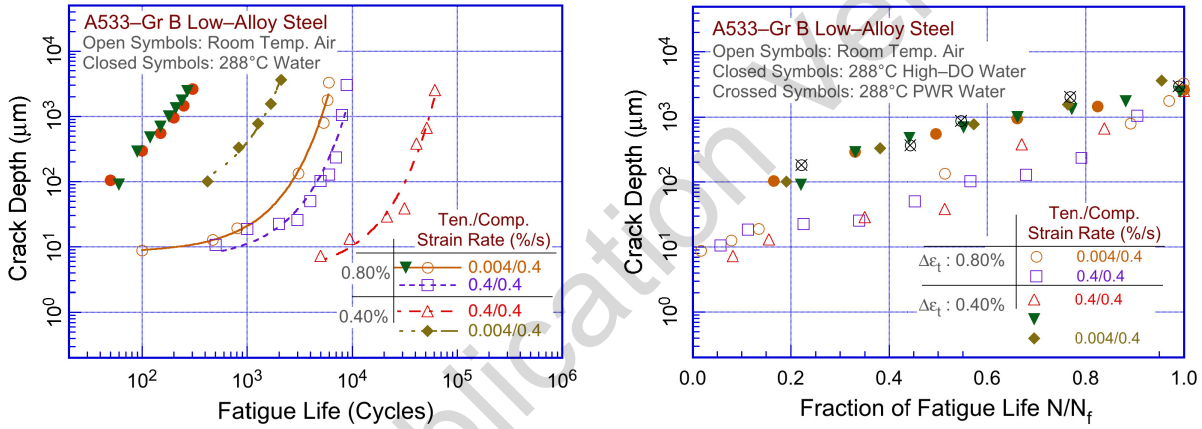

(a) (b)

Figure 2-11 Depth of largest crack plotted as a function of (a) fatigue cycles and (b) fraction of fatigue life for A533–Gr B low-alloy steel in air and water environments (Ref. 11).

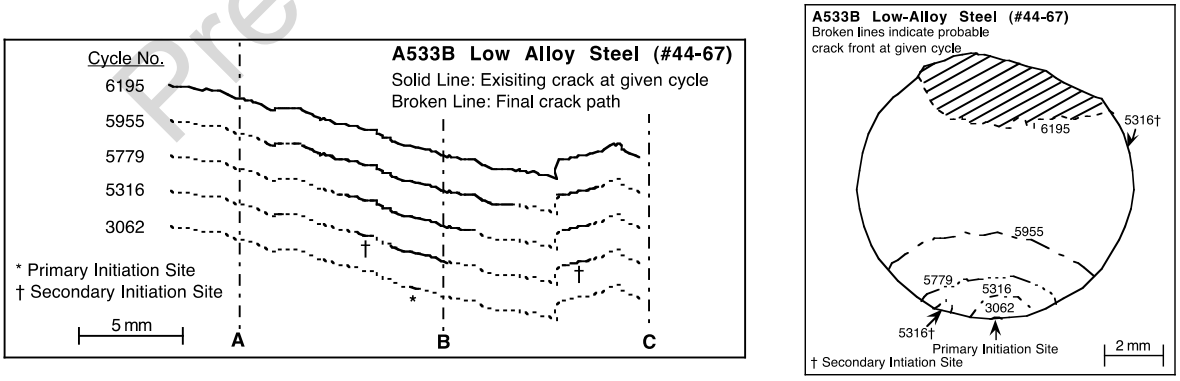

(a) (b)

Figure 2-12 (a) Morphology and length of surface crack after various numbers of cycles for A533–Gr. B steel in air at room temperature, and (b) fracture surface and probable crack front for surface cracks shown in (a) (Ref. 11).

Figure 2-13 plots the CGRs corresponding to the data shown in Figure 2-12 as a function of crack depth. The results indicate that, in LWR environments, the period spent in the growth of MSCs is decreased. At approximately 0.8% strain range, only 30-50 cycles are needed to form a 100-μm crack in high-DO water, whereas approximately 450 cycles are required to form a 100-μm crack in a low-DO PWR environment and more than 3,000 cycles are required to form a 100-μm crack in air. These values correspond to average growth rates of approximately 2.5, 0.22, and 0.033 μm/cycle in high-DO water, low-DO PWR environment, and air, respectively. The results also indicate that, relative to air, CGRs in high-DO water are nearly two orders of magnitude higher during the initial stages of fatigue life (i.e., for crack sizes less than 100 μm) and are one order of magnitude higher for crack sizes greater than 100 μm.

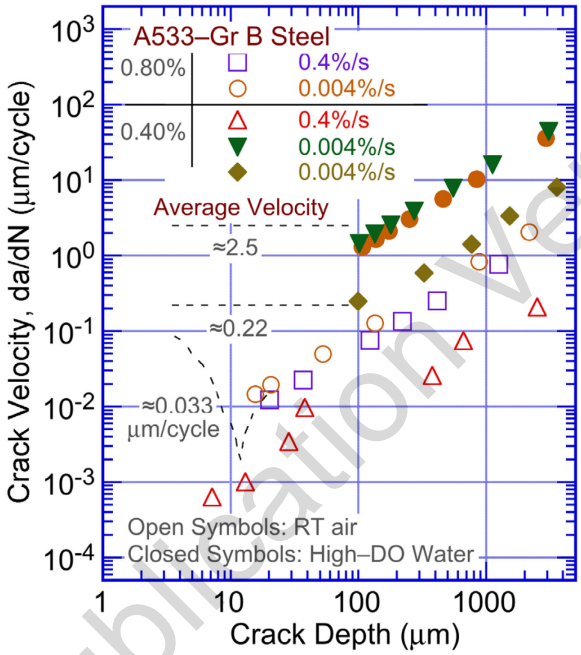

Figure 2-13 Crack growth rates plotted as a function of crack depth for A533–Gr B low-alloy steel tested in air and water environments (Ref. 11).

The surface crack and fracture surface morphologies of the test specimens indicate that, in high-temperature, high-DO water with slow strain rates, the surface cracks appear to grow entirely in Stage II growth as Mode I tensile cracks normal to the stress axis (Figure 2-8 and Figure 2-9). In air and low-DO PWR environments, both Stage I and Stage II growths are observed. Surface cracks grow initially as Mode II (shear) cracks along planes 45° to the stress axis and, when the stress intensities are large enough to promote slip on axes other than the primary slip axis, they grow as Mode I (tensile) cracks normal to the stress axis. In addition, for A106-Gr. B carbon steel, Stage I crack growth in air and low-DO water occurs entirely along the soft ferrite grains, whereas in high-DO water, cracks propagate across both ferrite and pearlite regions. These results are consistent with the slip-oxidation/dissolution mechanism in high-DO water.

2.2.2 Austenitic Stainless Steels

Austenitic SSs exposed to LWR environments develop an oxide film that consists of two layers: (1) a fine-grained, tightly-adherent, chromium-rich inner layer, and (2) a crystalline, nickel–rich outer layer composed of large and intermediate-sized particles. Figure 2-14 shows

photomicrographs of the gauge surface of Type 316NG specimens tested in simulated PWR water and high-DO water. The inner layer forms by solid-state growth, whereas the crystalline outer layer forms by precipitation or deposition from the solution. Figure 2-15 shows a schematic representation of the surface oxide film.

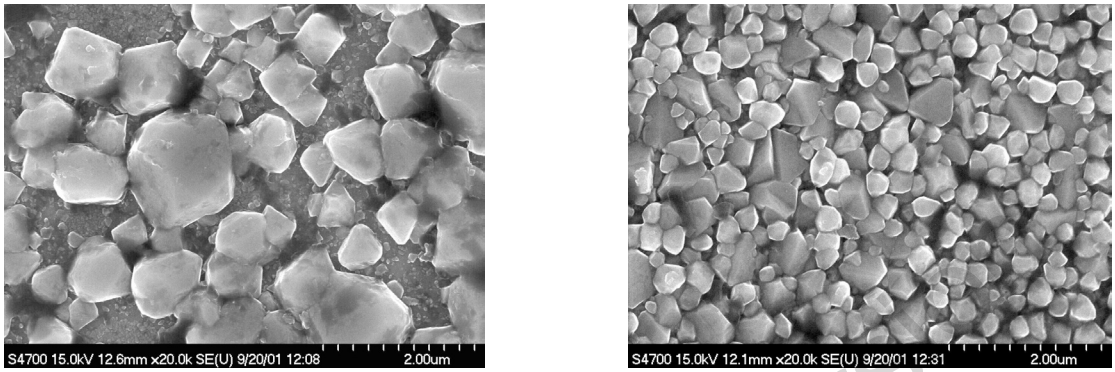

(a) (b)

Figure 2-14 Photomicrographs of oxide films that formed on Type 316NG SS in (a) simulated PWR water and (b) high-DO water (Ref. 13).

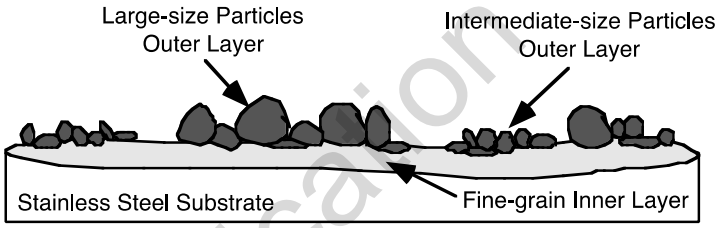

Figure 2-15 Schematic of the corrosion oxide film formed on austenitic SSs in LWR environments.

Several studies characterized the oxide films that form on austenitic SSs in LWR environments.[199-205] The inner layer consists of a chromium-rich spinel ($Ni_xCr_yFe_{3-x-y}O_4$) with a nonstoichiometric composition; the actual composition of spinels varies with environmental conditions. Da Cunha Belo et al.[203] determined that the inner layer that formed on Type 316L SS in a PWR environment at 350°C consisted of mixed chromium oxides (Cr_2O_3 + $FeCr_2O_4$) and Fe_3O_4. Nakayama and Oshida[205] characterized the oxide film on SSs exposed to high-DO (8 ppm) water at 300°C as chiefly composed of $NiO{\cdot}(Cr,Fe)_2O_3$ and/or $NiFe_2O_4$, which may be formed by a solid reaction between NiO and $(Cr,Fe)_2O_3$ or α-Fe_2O_3. Kim[199,200] identified the $FeCr_2O_4$ spinel chromite (or $Fe_xCr_{3-x}O_4$), along with $NiFe_2O_4$, in the inner layer formed on Types 304 and 316 SSs exposed at 288°C under BWR normal water chemistry (NWC) or BWR hydrogen water chemistry (HWC) conditions. Kim also noted that the inner oxide layer formed in an NWC BWR environment contained a lower concentration of chromium than that formed in an HWC low-DO environment. Such differences were attributed to chromium oxidation in high-DO water.

The structure and composition of the crystalline outer layer vary with the water chemistry. In BWR environments, the large particles in the outer layer are primarily composed of γ-Fe_2O_3 hematite in NWC, and Fe_3O_4 magnetite in HWC.[199,200] The intermediate particles in the outer

layer are composed of α-Fe_2O_3 in NWC and Fe_3O_4 in HWC. The structure of the outer layer varies when the water chemistry is cycled between NWC and HWC. In PWR environments, the large particles were identified as $Ni_{0.75}Fe_{2.25}O_4$ spinel and the intermediate particles as $Ni_{0.75}Fe_{2.25}O_4$ + Fe_3O_4.[203] Section 2.2.2.1 discusses the possible effects of minor differences in the surface oxide film on fatigue crack initiation.

2.2.2.1 Effects of Surface Micropits

The characteristics of the surface oxide films that form on austenitic SSs in LWR water environments influence the mechanism and kinetics of corrosion processes and thereby influence the initiation stage (i.e., the growth of MSCs). As discussed earlier, the reduction of fatigue lives in high-temperature water may be due to the presence of surface micropits. To investigate the effect of surface micropits, fatigue tests were conducted on Type 316NG (Heat P91576) specimens that were preexposed to either low-DO or high-DO water and then tested in air or water environments.[13] Figure 2-16 plots the results of these tests, as well as data obtained earlier on this heat and Heat D432804 of Type 316NG SS in air and low-DO water at 288°C. The fatigue lives of specimens preoxidized in high-DO water and then tested in low-DO water were identical to those of specimens tested without preoxidation. In addition, fatigue lives of specimens preoxidized at 288°C in low-DO water and then tested in air were identical to those of unoxidized specimens (Figure 2-16). If micropits were responsible for the reduction in life, the preexposed specimens should have shown a decrease in life. Furthermore, the fatigue limit of these steels should have also been lower in water than in air, but the data indicate that this limit was the same in both water and air environments. These results indicate that surface micropits or minor differences in the composition or structure of the surface oxide film had little or no effect on the formation of fatigue cracks.

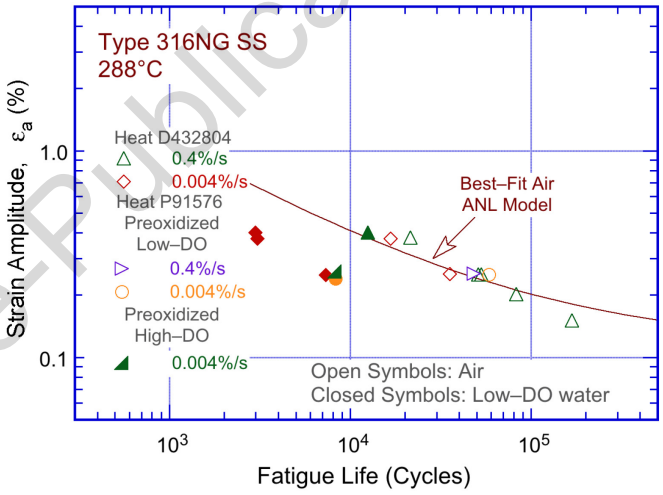

Figure 2-16 Effects of environment on formation of fatigue cracks in Type 316NG SS in air and low-DO water at 288°C (Preoxidized specimens were exposed for 10 days at 288°C in water that contained either less than 5-ppb DO and approximately 23 cm^3/kg dissolved H_2 or approximately 500-ppb DO and no dissolved H_2 (Ref. 13).

2.2.2.2 Mechanisms of Corrosion Fatigue

Both the slip oxidation/dissolution and the hydrogen-induced cracking mechanisms depend on the rates of oxide rupture, passivation, and liquid diffusion. Therefore, it is difficult to differentiate between the two processes or to establish their relative contribution to fatigue cracking in LWR environments. However, for austenitic SSs, lower fatigue lives in low-DO water vs. high-DO water are difficult to reconcile in terms of the slip-oxidation/dissolution mechanism, which assumes that CGRs increase with increasing DO in the water. Metallographic examination of fatigue test specimens suggested that hydrogen-induced cracking may have played an important role in environmentally assisted reduction in fatigue lives of austenitic SSs.[47] For example, hydrogen can cause localized crack tip plasticity by reducing the stress required for dislocation motion, which leads to higher rates and larger steps of oxide film rupture. Thus, fatigue lives may be decreased, not because of increased growth rates but because of increased film rupture frequency.

A detailed metallographic evaluation of austenitic SS fatigue test specimens was performed to characterize the crack and fracture morphology of the various heats under various heat treatment conditions.[47] Figure 2-17 presents photomicrographs of the crack morphology of Type 304 SS specimens under all test and environmental conditions. In all cases, the tensile axis was vertical (parallel to the plane of each photomicrograph). For austenitic SSs, the fatigue crack surface morphology was similar to that observed for carbon and low-alloy steels. In an air environment, fatigue cracks were more likely to be oblique, approaching 45° with respect to the tensile axis. By contrast, the cracks that formed in either BWR or PWR environments tended to be perpendicular to the tensile axis.

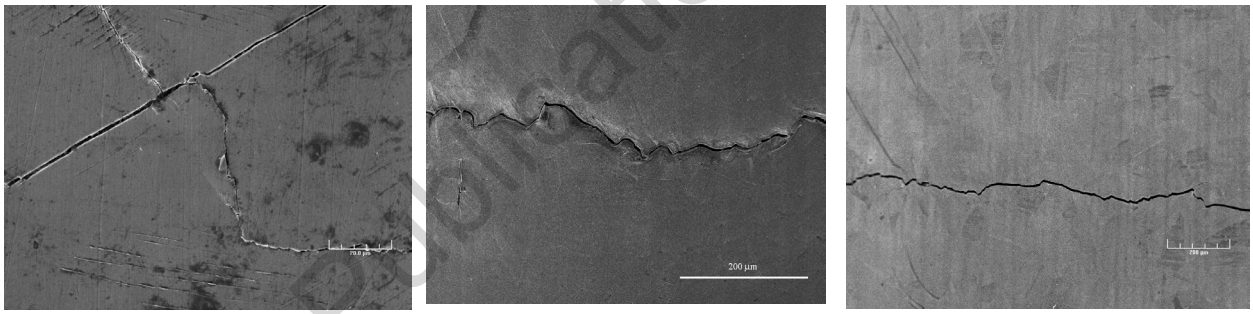

(a) (b) (c)

Figure 2-17 Photomicrographs of the fatigue crack morphology of Type 304 SS in (a) air, (b) high-DO BWR water, and (c) low-DO PWR water at 289°C (Ref. 47).

Figure 2-18 presents photomicrographs of the crack morphology of Type 304 SS under all test and environmental conditions. In air, the fracture mode for crack initiation (i.e., crack depths up to 200 μm) and crack propagation (i.e., crack depths greater than 200 μm) was transgranular (TG), most likely along crystallographic planes, leaving behind relatively smooth surfaces. With an increasing degree of sensitization, cleavage-like, or stepped, TG fracture and ridge structures were observed on the smooth surfaces. In simulated NWC BWR environments, the initial crack appeared intergranular (IG) under all heat treatment conditions, implying a weakening of the grain boundaries. The extent of IG fracture increased with the degree of sensitization. Nevertheless, for crack depths beyond 200 μm, the initial IG mode transformed into a TG mode with cleavage-like features. In simulated PWR environments, however, fatigue cracks initiated and propagated in a TG mode irrespective of the degree of sensitization.

Prominent features of the fracture surfaces included highly angular, cleavage-like fracture facets that exhibited well-defined “river” patterns.[47] IG facets were rarely observed; however, when they were found, it was mostly in the more heavily sensitized alloys.

In addition, fatigue striations normal to the crack advance direction were clearly visible beyond approximately 200-μm crack depths on the fracture surfaces of all materials under all environmental conditions. Figure 2-19 shows an example of the fatigue striations observed in Type 304 SS in different environments. Striations were found on both the TG and IG facets of the samples tested under BWR NWC conditions, or coexisting with the “river” patterns specific to the samples tested in the PWR environments. However, the striations on specimens tested in PWR water were quite faint compared to those tested in NWC BWR water. Furthermore, examination of the specimens after chemical cleaning suggested that some striations were produced by rupture of the surface oxide film rather than the formation of double notches or “ears” at the crack tip.

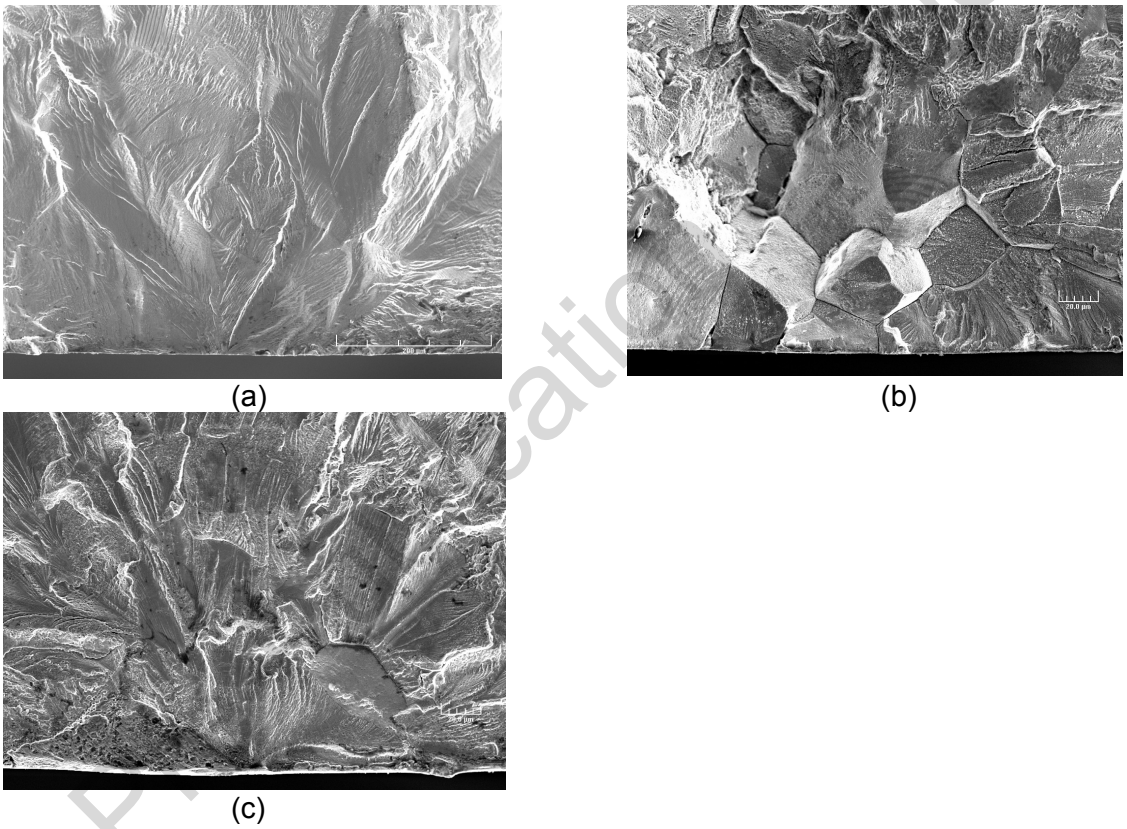

Figure 2-18 Photomicrographs showing sites of fatigue crack initiation on fracture surfaces of Type 304 SS tested at 289°C in (a) air, (b) high-DO BWR water, and (c) low-DO PWR water (Ref. 47).

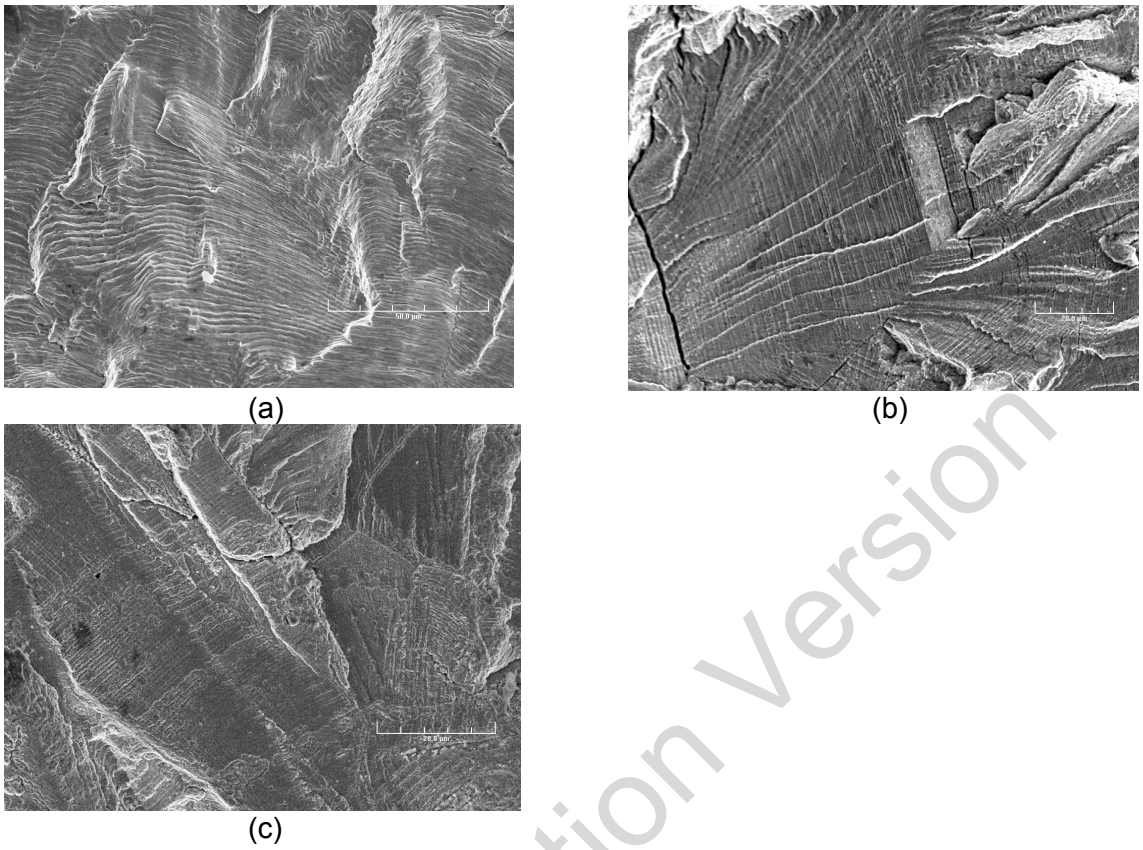

Figure 2-19 Photomicrographs showing fatigue striations on fracture surfaces of Type 304 SS tested at 289°C in (a) air, (b) high-DO BWR water, and (c) low-DO PWR water (Ref. 47).

The characterization of surface cracks and fracture morphology in austenitic SSs suggests that, in LWR environments, although film rupture was apparent, the formation and growth of fatigue cracks were primarily caused by hydrogen-induced cracking.

2.2.2.3 Effects of Dynamic Strain Aging

DSA was observed in austenitic SSs in air at strain rates below 0.3%/s and temperatures in the range of 300–600°C; the peak effects occurred at 500–600°C.[206] The fatigue life of a heat of Type 316LN SS at low strain rates was greater at 600°C than at 500°C. Typically at temperatures above 400°C, the fatigue life of austenitic SSs decreased with an increase in temperature or a decrease in strain rate.[57] DSA increased the dislocation density at slow strain rates, which enhanced the degree of inhomogeneity of deformation during fatigue loading.

DSA was also observed in Type 304L SS under LWR operating conditions. At a 0.4%/s strain rate, the fatigue life and fatigue limit in air were higher at 300°C than at 150°C (due to secondary strain hardening at 300°C).[58] A similar behavior was observed for this heat of SS in PWR water. At 0.4%/s, fatigue life decreased in PWR water relative to that in air at 150°C, but not at 300°C. This difference was identified as secondary hardening at 300°C, which was not observed at 150°C. The secondary hardening at 300°C may be due to DSA, although the temperature was relatively low.

2.2.2.4 Crack Growth Rates in Smooth Fatigue Specimens

Studies on the formation and growth characteristics of short cracks in smooth fatigue specimens of austenitic SSs in LWR environments indicated that, although the growth rates of mechanically small cracks were greater in water than in air, the decrease in fatigue lives was caused predominantly by the effects of the environment on the growth of MSCs.[44] Figure 2-20 shows the growth of the largest crack in austenitic SSs with respect to fatigue cycles in air and water environments. In the figure, the crack length for the test in air at 288°C and 0.75% strain range was measured only near the end of the test. The data obtained by Orbtlik, et al.[207] for Type 316L SS in air at 25°C and approximately 0.2% strain range were used to estimate the crack growth in air at 0.75% strain range. Similar studies on carbon and low-alloy steels indicate[11,165-167] that the fatigue crack size at various life fractions was independent of strain range, strain rate, and temperature; consequently, the depth of the largest crack at various life fractions was approximately the same at strain ranges of 0.75% and 0.3%. The curve for the test in air at 0.75% (shown as a dashed line in Figure 2-20) was calculated from the best-fit equation of the experimental data for Type 316L SS at 0.3% strain range. As expected, at a given strain range (i.e., 0.75%), more fatigue cycles are needed to reach a specific crack depth in air than in water. Conversely, for a specific number of cycles, the crack depth is longer in high-DO (BWR) water than in air, and the crack depth in low-DO PWR water is longer than in high-DO (BWR) water (i.e., After 1,500 cycles, the crack depth in air, high-DO (BWR) water, and low-DO (PWR) water was approximately 40, 300, and 1,100 μm, respectively). The growth of cracks during the initiation stage (i.e., growth of MSCs) was enhanced in water; the fatigue cycles needed to form a 500-μm crack were a factor of approximately 12 lower in low-DO water than in air. Figure 2-20 shows that the number of cycles required to produce a 500-μm crack is 800, 3,000, and 9,000 in low-DO (PWR) water, high-DO (BWR) water, and air environments, respectively; therefore, the number of cycles was more than a factor of 10 lower in low-DO water than in air.

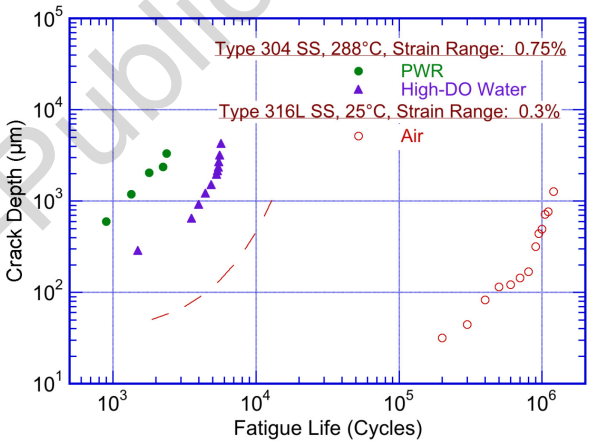

Figure 2-20 Depth of largest crack plotted as a function of fatigue cycles for austenitic SSs in air and water (Refs. 13 and 207).

Figure 2-21 plots the CGRs during the propagation stage (i.e., growth of mechanically small cracks) in air and water environments as a function of crack length; these rates were calculated from the best fit of the data in Figure 2-20. The CGRs in high-DO water for the specimen with a 24-hour soak period (closed diamonds in Figure 2-21) were determined from measurements of fatigue striations. The CGRs were a factor of 2 to 6 higher in water than in air. Growth rates in

PWR water or high-DO water with a 24-hour soak period were higher than those in high-DO water with a 120-hour soak period. At a crack length of approximately 1,000 μm, the CGRs in air, high-DO water, and low-DO water were 0.30, 0.64, and 1.05 μm/cycle, respectively. For the 0.75% strain range and 0.004%/s strain rate, these values corresponded to growth rates of approximately 1.6×10^{-9}, 3.4×10^{-9}, and 5.6×10^{-9} m/s in air, high-DO water, and low-DO water, respectively. Thus, growth rates were a factor of 3.5 greater in low-DO water than in air.

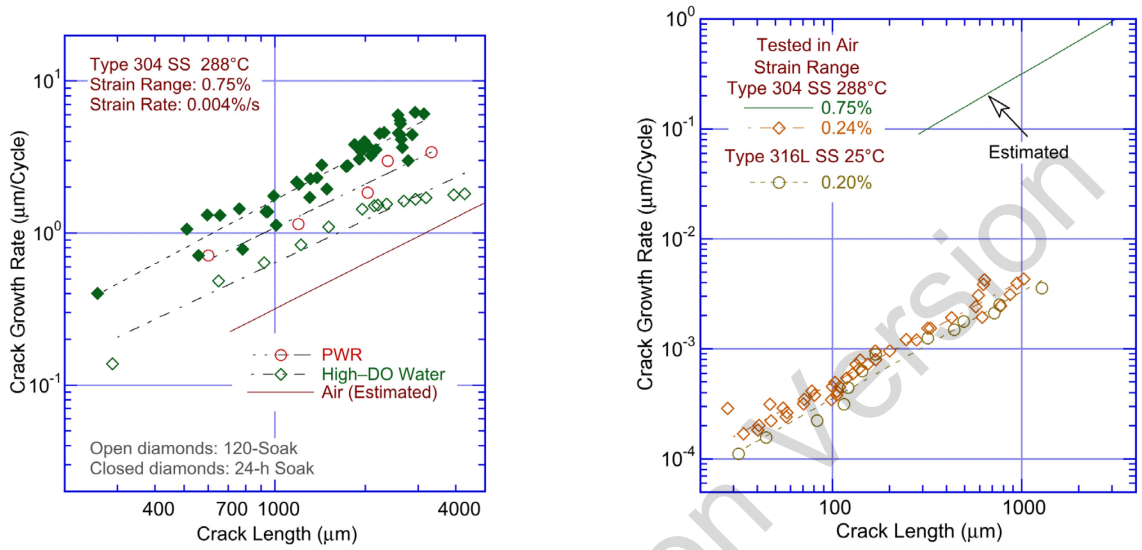

(a) (b)

Figure 2-21 Crack growth rates plotted as a function of crack length for austenitic SSs in (a) water and (b) air environments (Refs. 13, 44, and 207).

Shack and Kassner[208] reviewed fatigue crack growth (da/dN) data obtained from fracture-mechanics tests on CT specimens of wrought and cast SSs in LWR environments. The results indicate significant enhancement of CGRs in high-DO water; at CGRs of less than 10^{-10} m/s in air, the rates in BWR NWC conditions exceeded the air curve in ASME Code Section III by a factor of approximately 20 to 30. Figure 2-22(a) plots the experimental CGRs for sensitized Type 304 SS in high-DO water and those predicted in air for the same mechanical loading conditions. The fatigue CGRs in air, $\dot{a}_{air}$, (meters per second), were determined from a correlation at 288°C given by

$$\dot{a}_{air} = 3.43 \times 10^{-12}\, S(R)\, \Delta K^{3.3}/T_R, \qquad (15)$$

where the function S(R) is expressed as

$$\begin{aligned} S(R) &= 1.0 && R \le 0 \\ S(R) &= 1.0 + 1.8R && 0 < R \le 0.79 \\ S(R) &= -43.35 + 57.97R && 0.79 < R < 1.0, \end{aligned} \qquad (16)$$

and T_R is the rise time (seconds) of the loading waveform, R is the load ratio (K_{min}/K_{max}), and ΔK is $K_{max} - K_{min}$. The fatigue CGR in water [$\dot{a}_{env}$ (meters per second)] with 0.2-ppm DO

(i.e., BWR NWC) is expressed in terms of the fatigue CGR in air ($\dot{a}_{air}$) by the relationship

$$\dot{a}_{env} = \dot{a}_{air} + 4.5\times10^{-5} (\dot{a}_{air})^{0.5}. \quad (17)$$

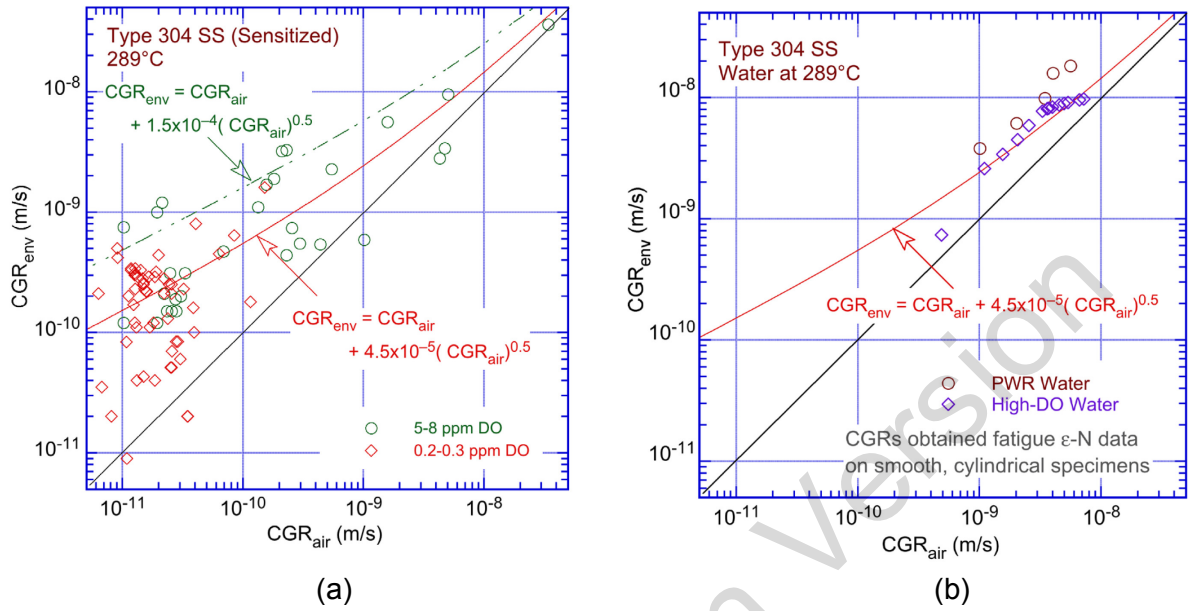

Figure 2-22 Crack growth rate data for Type 304 SS in high temperature water determined from (a) fracture mechanics CT specimens and (b) smooth cylindrical fatigue specimens (Ref. 208).

The CGR data from fracture-mechanics tests in low-DO PWR environments (Figure 2-22(b)) are sparse, particularly at rates that are less than 10^{-9} m/s. At high CGRs, the observed enhancement in both low- and high-DO environments was relatively small, and the magnitude of the enhancement under the same loading conditions was comparable in the two environments. At the time, few data were available for low CGRs in simulated PWR water. Therefore, Shack and Kassner[208] recommended that the environmental enhancement represented by Equation 17 for 0.2 ppm DO water should also be considered for PWR environments.[A]

Figure 2-22(b) plots the CGRs determined from fatigue ε–N tests on smooth, cylindrical specimens in high-DO and low-DO (PWR) water environments at 289°C. The rates in high-DO and low-DO (PWR) water represent the measured values shown as open diamonds and circles, respectively, from Figure 2-21(a). The CGRs in air for the same loading conditions (i.e., the same crack length) were determined from the estimated rates in air, shown by the solid line in Figure 2-21(a). The results from fatigue ε–N tests showed good agreement with the data obtained from the fracture–mechanics tests. The CGRs in high-DO water were consistent with the trend predicted from Equation 17. The rates in low-DO water were slightly higher.

A Since the study by Shack and Kassner was completed, American Society of Mechanical Engineers Boiler and Pressure Vessel Code (ASME Code) Case 809, "Reference Fatigue Crack Growth Rate Curves for Austenitic Stainless Steels in Pressurized Water Reactor Environments," dated June 23, 2015, has been approved. ASME Code Case 809 is based on a more extensive data base than the Shack and Kassner expressions. While there are differences in the CGR parameters used in the Code Case and the Shack and Kassner expressions, these differences are not expected to affect the conclusions drawn in this section on the importance of the effects of environment on the growth of MSCs.

The large reductions in fatigue life of austenitic SSs in PWR environments cannot be explained entirely on the basis of enhanced CGRs during the propagation stage (i.e., growth of mechanically small cracks). For example, the CGRs in low-DO water are a factor of 1.6 greater than those in high-DO water, but fatigue lives are approximately a factor of 4 lower in low-DO water than in high-DO water. As indicated by the results shown in Figure 2-21(a), the decrease in fatigue lives of austenitic SSs in PWR environments was caused predominantly by the effects of environment on the growth of MSCs. Thus, the reduction in fatigue life in LWR environments relative to that in air cannot be explained on the basis of enhanced CGRs in LWR environments. In LWR environments, the growth of MSCs is increased much more than the growth of mechanically small cracks. The data in Figure 2-21(a) demonstrate that the environmental effects on the growth of cracks less than or equal to 200 μm (i.e., Stage I of crack initiation) are significantly higher than on the growth of cracks greater than 200 μm (i.e., Stage II of crack initiation).

3 FATIGUE STRAIN VS. LIFE BEHAVIOR IN AIR

During the 1990s, the Pressure Vessel Council (PVRC) Working Group on ε–N Curve and Data Analysis compiled existing strain vs. life (ε–N) fatigue data developed at various establishments and research laboratories worldwide. The database, used in the Argonne National Laboratory (ANL) studies, and presented in the original version of NUREG/CR-6909, "Effect of LWR Coolant Environments on the Fatigue Life of Reactor Materials—Final Report," issued February 2007, was an extended version of the PVRC database. The reanalysis of the fatigue ε–N data presented in this report is based on a much larger fatigue ε–N database. The additional data include the Japan Nuclear Energy Safety Organization (JNES) data summarized in JNES-SS-1005, "Environmental Fatigue Evaluation Method for Nuclear Power Plants," issued March 2011, on carbon and low-alloy steels, wrought and cast austenitic stainless steels (SSs), nickel-chromium-iron (Ni-Cr-Fe) alloys, and their associated weld metals tested in air and light-water reactor (LWR) environments.[136] Additional data was also obtained from open literature fatigue ε–N test results on several heats of carbon and low-alloy steels tested in boiling-water reactor (BWR) environments.[138-146] Nearly 60% of the data in the more recent JNES database were included in the old JNUFAD[210] database. The JNUFAD database formed a portion of the PVRC database, which was used in the original version of the NUREG/CR-6909 report.

Unless otherwise mentioned, the fatigue database was obtained from smooth cylindrical gauge specimens that were tested under strain control with fully reversed loading (i.e., strain ratio, R, of -1). Tests on notched specimens or at R values other than -1 were excluded from the fatigue ε–N data analysis performed for this report. For the previous fatigue testing performed at ANL, the estimated uncertainty in the strain measurements was about 4% of the reported values. For the data obtained in other laboratories, the uncertainty in the reported values of strain is unknown but was assumed to be small enough such that the results were not significantly impacted.

In nearly all tests, fatigue life was defined as the number of cycles necessary for the tensile stress to drop 25% from its peak or steady-state value, N_{25}. As discussed in Section 1.1, for the specimen sizes used in these studies (e.g., 5.1 to 9.5 mm (0.2 to 0.375 in.) diameter cylindrical specimens) failure corresponds to an approximately 3-mm-deep crack. Some of the earlier tests in air were carried out to complete failure of the specimens; in some other tests, fatigue lives were defined as the number of cycles for peak tensile stresses to decrease by 10 or 50%. Therefore, fatigue lives defined by a criterion other than a 25% load drop were converted to consistent N_{25} values according to the following formula:

$$N_{25} = N_X/(0.947 + 0.00212X), \tag{18}$$

where X is the failure criterion (e.g., 10, 50 or 100% decrease in peak tensile stress).[10] The estimated uncertainty in fatigue life determined by this procedure is about 2%, which is within the strain measurement uncertainty.

The 25% load-drop criterion was not used for the tests that were performed using tube specimens. For tube specimens, fatigue lives were represented by the number of cycles to develop a leak because, with the exception of a few specimens, all tube specimens had 3-mm wall thicknesses.

3.1 Carbon and Low-Alloy Steels and Weld Metals

3.1.1 Experimental Data

The primary sources of fatigue ε–N data for carbon and low-alloy steels are the tests performed by General Electric Company (GE) in a test loop at the Dresden Nuclear Power Station, Unit 1;[14,15] work sponsored by the Electric Power Research Institute (EPRI) at GE;[16,17] the work of Terrell at Materials Engineering Associates (MEA);[48-50] the work at ANL on fatigue of pressure vessel and piping steels;[10-13,40-47] the large JNES database;[136] studies at Ishikawajima-Harima Heavy Industries (IHI), Hitachi, and Mitsubishi Heavy Industries (MHI) in Japan;[18-36] and the studies at Kraftwerk Union Laboratories (KWU) and Materialprufungsanstalt (MPA) in Germany.[55,56] From these sources, the total database for fatigue tests in air comprises 684 tests—254 tests on carbon steels and 430 tests on low-alloy steels. Carbon steels include 19 heats of A106-Grs. B and C, A333-Gr. 6, A508-Gr. 1, and A333-Gr. 6 weld metals. Low-alloy steels include 22 heats of A302-Gr. B, A508-Grs. 2 and 3, and A533-Gr. B steel. Table 3-1 summarizes the sources included in the updated database used for the present analyses, as categorized by material type and test environment. Appendix B provides other material information such as chemical composition, heat treatment, and room temperature tensile properties of the various types and heats of materials.

Table 3-1 Sources of the Fatigue ε–N Data on Carbon and Low-alloy Steels in an Air Environment.

ANL Mat. ID	Material Specification	Sulfur Content (wt.%)	Test Temperature (°C)	Number of Data Points	Source	Applicable Reference
Carbon Steels						
1	A106-Gr.B	0.015	25, 288	3, 17	ANL	10
3	A106-Gr.B	0.020	25, 288	13, 12	MEA	48-50
4	A106-Gr.C (STS480)	0.006	25	5	JNES (Kanasaki)	136
-	A106-Gr.C (STS480)	0.003	25	2	JNES (Kanasaki)	136
6	A106-Gr.B (STS49)	0.007	25	9	JNES (Higuchi)	136
9	A333-Gr.6 (STS42)	0.015	25, 250, 290	13, 7, 3	JNES (Higuchi)	136
10	A333-Gr.6 (STS42)	0.014	25	7[a]	JNES (Higuchi)	136
11	A333-Gr.6	0.006	288	1	JNES (Higuchi)	136
12	A333-Gr.6 (STS410)	0.012	25, 100, 200, 288	5, 4, 4, 2	JNES (Nakao), ANL	136,10
13	A333-Gr.6	0.030	25, 288	7, 6	GE	14-17
14	A333-Gr.6 (STS410)	0.008	25, 289	24, 10	JNES (Hirano)	136
15	A333-Gr.6 (STS410)	0.016	25, 289	12, 5	JNES (Hirano)	136
18	A508-Gr.1 (SFVC2B)	0.004	25, 289	6, 5	JNES (Hirano)	136
19	A508-Gr.1[b]	0.008	25	14	JNES (PLEX)	136
24	CS	-	25, 170	10, 28	MPA	55, 56
Carbon Steel Weld Metals						
-	A336-Gr.6 (STS410)	0.001	25, 288	6, 4	JNES (Hirano)	136
-	A336-Gr.6 (STS410)	0.010	25, 289	5, 5	JNES (Hirano)	136
Low-alloy Steels						
1	A302-Gr.B	0.027	288	7	ANL	10
2	A508-Gr.2	0.003	25	9	JNES (Nakao/Higuchi)	136
6	A508-Gr. 3 (SFVV3)	0.003	25, 288	6, 14	JNES (Nagata)	136

ANL Mat. ID	Material Specification	Sulfur Content (wt.%)	Test Temperature (°C)	Number of Data Points	Source	Applicable Reference
7	A508-Gr. 3 (SFVV3)	0.002	25, 288	7, 8	JNES (Narumoto)	136
8	A508-Gr. 3 (SFVV3)	0.003	25	8	JNES (Narumoto)	136
9	A508-Gr. 3 (SFVV3)	0.005	25, 200	31, 2	JNES (Ikemoto, Iwadate, Kou, Nihei, Fukakura)	136
10	A508-Gr. 3 (SFVV3)	0.003	150, 200, 290	18, 15, 13	JNES (Kou, Fukakura, Iida)	136
11	A508-Gr. 3 (SFVV3)	0.003	25, 200, 290	11, 17, 24	JNES (Nihei, Kou, Fukakura, Iwadate,)	136
12	A508-Gr. 3 (SFVV3)	0.003	25	10	JNES (Higuchi, Endou)	136
13	A508-Gr. 3 (SFVV3)	0.008	25	8[b]	JNES (Kanasaki)	136
14	A508-Gr. 3	0.002	288	14	Wu & Katada	141
16	A533-Gr. B	0.012	25, 288	6, 16	ANL	10,11,12
17	A533-Gr. B (SQV2A)	0.007	25, 288	14, 14	JNES (Nagata), Wu & Katada	136,141
18	A533-Gr. B (SQV2A)	0.001	25, 350	34, 10	JNES (Kazuo Toyam)	136
19	A533-Gr. B (SQV2A)	0.003	25, 300	6, 6	JNES (Narumoto)	136
20	A533-Gr. B (SQV2A)	0.002	25, 286	9, 8	JNES (Narumoto)	136
21	A533-Gr. B (SQV2A)	0.010	25	18[c]	JNES (Iida)	136
22	A533-Gr. B (SQV2A)	0.008	25, 150, 200, 250, 289	19,[b] 1, 1, 1, 4	JNES (Hirano)	136
23	A533-Gr. B	0.013	288	7	Wu & Katada	143
28	A533-Gr. B	0.014	270	2	MPA	55,56
29	LAS	-	25, 170	16, 16	MPA	55,56
31	17MnMoV64	0.018	200	3	S/KWU	55,56

[a] Six tests performed under load control were excluded.

[b] Includes test results for thermally aged materials.

[c] Tests performed using a sine waveform, and data include results for thermally aged materials.

In air, the fatigue lives of both carbon and low-alloy steels depend on steel type; temperature; and, for some compositions, applied strain rate and sulfide morphology. Figure 3-1 shows fatigue ε–N data from various investigations on carbon and low-alloy steels. The plots in this figure also include the best-fit air curves based on the ANL models (i.e., Equations 24 and 25 from Section 3.1.6) and the mean–data air curves at room temperature from Section III, "Rules for Construction of Nuclear Facility Components," of the American Society of Mechanical Engineers Boiler and Pressure Vessel Code (ASME Code) (i.e., Equations 7 and 8 from Section 1.2). The results indicate that, although significant scatter is apparent due to material variability, the fatigue lives of these steels are comparable at less than $5x10^5$ cycles, and those of low-alloy steels are greater than carbon steels for greater than $5x10^5$ cycles. In addition, the fatigue life at 10^6 cycles of low-alloy steels is higher than that of carbon steels.

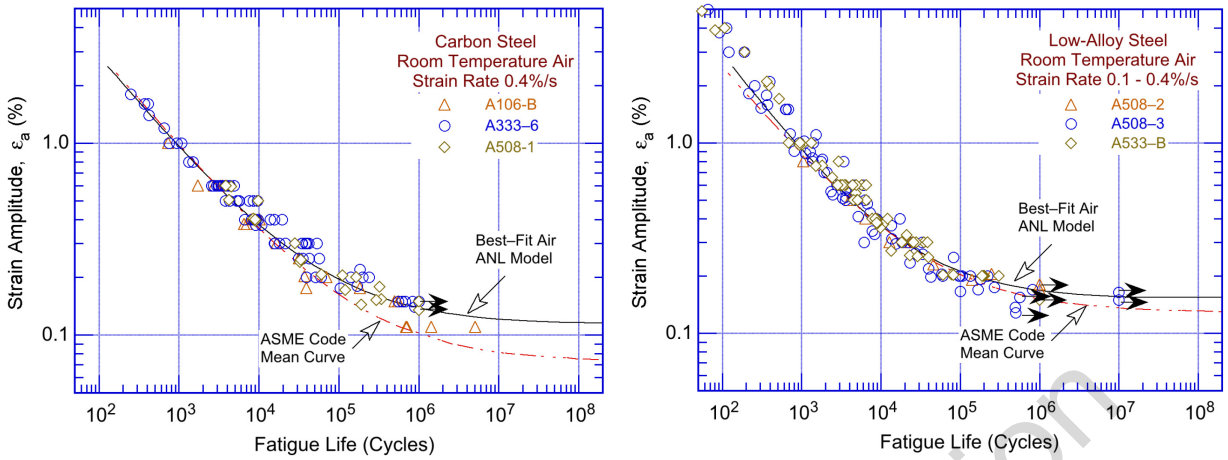

Figure 3-1 Fatigue strain vs. life data for carbon and low-alloy steels in air at room temperature (JNUFAD database and Refs. 10, 18, 19 and 48).

The results also indicate that the existing fatigue ε–N data for low-alloy steels are in good agreement with the ASME Code mean-data curve. The existing data for carbon steels are consistent with the ASME Code mean-data curve for fatigue lives below 5×10^5 cycles, and are above the ASME Code mean-data curve at longer lives. Thus, for carbon steels above 5×10^5 cycles, the ASME Code mean-data curve is conservative with respect to the existing fatigue ε–N data.

- *The ASME Code mean-data air curves for carbon and low-alloy steels (Equations 7 and 8) are either consistent with the existing fatigue ε–N data or are somewhat conservative under some conditions.*

3.1.2 Temperature

In air, the fatigue lives of both carbon and low-alloy steels decrease with increasing temperature; however, the effect is relatively small (less than a factor of 1.5). Figure 3-2 shows the existing fatigue ε–N data in air at 25–290°C. As discussed in Section 3.1.1 for each grade of steel, the data represent several heats of material. The solid lines in the plots represent the temperature dependence defined by Equation 22 in Section 3.1.6. The results indicate a factor of approximately 1.5 decrease in fatigue lives of both carbon and low-alloy steels as the temperature is increased from room temperature to 300°C.

- *Variations in the fatigue lives in air due to the effects of temperature for carbon and low-alloy steels were accounted for in the subfactor for "data scatter and material variability."*

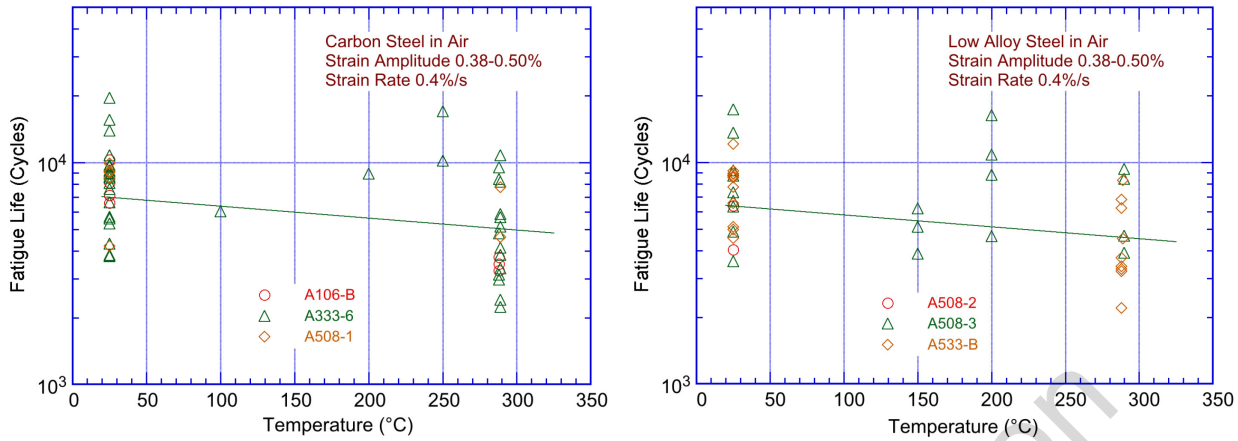

Figure 3-2 The change in fatigue lives of carbon and low-alloy steels in air as a function of temperature.

3.1.3 Strain Rate

The effect of strain rate on the fatigue lives of carbon and low-alloy steels in air appears to depend on the material composition. The existing data indicate that in the temperature range of dynamic strain aging (200–370°C), some heats of carbon and low-alloy steels were sensitive to strain rate; with decreasing strain rate, the fatigue lives in air were either unaffected,[10] decreased for some heats,[211] or increased for others.[212] The carbon and nitrogen contents in the steel are considered to have an important influence on strain rate effects. Inhomogeneous plastic deformation can result in localized plastic strains. This localization retards blunting of propagating cracks that is usually expected when plastic deformation occurs and can result in higher crack growth rates.[211] The increases in fatigue lives were attributed to retardation of CGRs due to crack branching and suppression of the plastic zone.[212] Furthermore, as discussed earlier, the formation of cracks may be enhanced in the presence of dynamic strain aging (DSA).

- *Variations in fatigue lives in air due to the effects of strain rate for carbon and low-alloy steels were accounted for in the subfactor for "data scatter and material variability."*

3.1.4 Sulfide Morphology

Some high-sulfur steels exhibit very poor fatigue properties in certain orientations because of structural factors such as the distribution and morphology of sulfides in the steel. For example, fatigue tests on a high-sulfur heat of A302–Gr. B steel in three orientations[B] in air at 288°C indicated that the fatigue life and fatigue limit in the radial (T2) orientation are lower than those in the rolling (R) and transverse (T1) orientations.[10] At low strain rates, fatigue lives in the T2 orientation were nearly one order of magnitude lower than in the R orientation. In the orientation

[B] The three orientations were represented by the direction that was perpendicular to the fracture plane. Both T1 and T2 directions were perpendicular to the R direction, but the fracture plane was across the thickness of the plate in the T1 orientation and parallel to the plate surface in the T2 orientation.

with poor fatigue resistance, crack propagation occurred preferentially along the sulfide stringers and was facilitated by sulfide cracking.

- *Variations in fatigue lives in air due to differences in sulfide morphology for carbon and low-alloy steels were accounted for in the subfactor for "data scatter and material variability."*

3.1.5 Cyclic Strain Hardening Behavior

The cyclic stress-strain response of carbon and low-alloy steels varies with steel type, temperature, and strain rate. In general, these steels show initial cyclic hardening followed by cyclic softening or a saturation stage at all strain rates. Carbon steels, with a pearlite and ferrite structure and low monotonic yield stress, exhibit significant initial hardening. Low-alloy steels, with a tempered bainite and ferrite structure and a relatively high monotonic yield stress, show little or no initial hardening and may exhibit cyclic softening with continued cycling. For both steels, the maximum stress increases as applied strain increases and generally decreases as temperature increases. However, at 200–370°C, these steels exhibited DSA, which resulted in enhanced cyclic hardening, a secondary hardening stage, and negative strain rate sensitivity.[211,212] The temperature range and extent of DSA varied with composition and structure.

Figure 3-3 shows the effects of strain rate and temperature on the cyclic stress response of A106-Gr. B carbon steel and A533–Gr. B low-alloy steel. For both steels, cyclic stresses were higher at 288°C than at room temperature. At 288°C, all steels exhibited greater cyclic and secondary hardening because of DSA. The extent of hardening increased as the applied strain rate decreased.

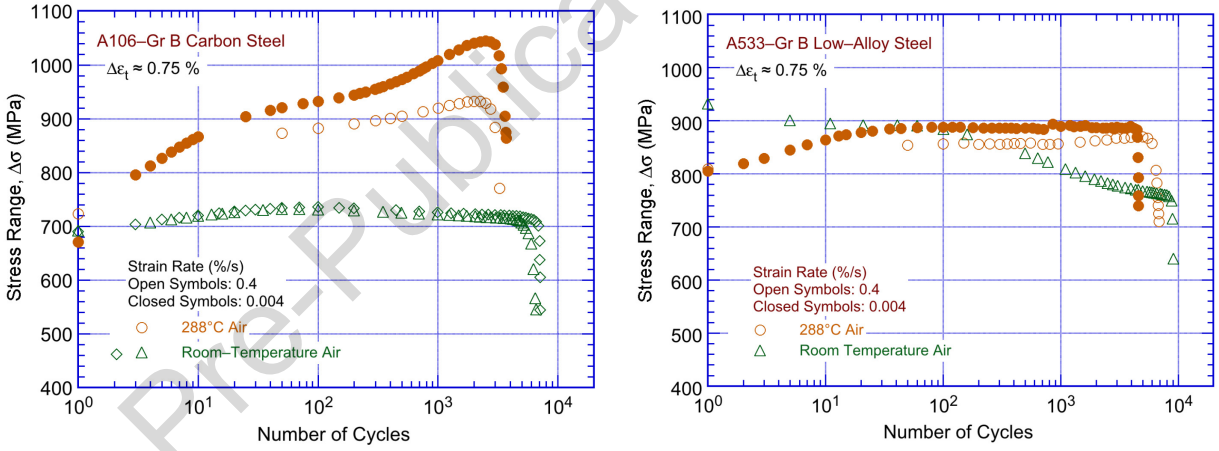

Figure 3-3 Effect of strain rate and temperature on cyclic stress of carbon and low-alloy steels.

- *Cyclic strain hardening behavior influenced the fatigue limits of materials; variations in fatigue lives in air due to the effects of strain hardening for carbon and low-alloy steels were accounted for in the subfactor for "data scatter and material variability."*

3.1.6 Fatigue Life Model

American Society for Testing and Materials Standard E739, "Standard Practice for Statistical Analysis of Linear or Linearized Stress-Life (S–N) and Strain-Life (ε–N) Fatigue Data,"[4] issued May 2016, treats fatigue life, N (or the logarithm of the fatigue life), as the dependent variable, and either of the controlled variables (e.g., stress or strain) as the independent variable. The coefficients of a "linear" model are commonly established through least-squares curve-fitting of the data using fatigue life as the dependent variable. An optimization program sets the coefficients to minimize the sum of the square of the residual errors, which are the differences between the predicted and actual values of N or ln(N). However, such an approach may not adequately determine the optimum coefficients for a nonlinear expression such as the Langer curve (Equation 6), which includes a constant term, C, related to the fatigue limit. The model does not address the fact that at low strain amplitudes, most of the error in life is due to uncertainty associated with either measurement of stress or strain or variation in threshold strain caused by material variability. A predictive model based on a least-squares fit on N or ln(N) is biased for low strain amplitude (ε_a). In addition, the data obtained at strain amplitudes less than the constant C in Equation 6 (e.g., most runouts) cannot be included in the analysis. On the other hand, a least-squares fit on ε_a does not work well for higher strain amplitudes. The two kinds of models are transformations of each other, although the precise values of the coefficients differ.

In the statistical model presented in References 130 and 10, the two approaches were combined by minimizing the sum of the squared Cartesian distances from the data points to the predicted curve (Figure 3-4). For low ε_a, this is very close to optimizing the sum of squared errors in predicted ε_a; at high ε_a, this is very close to optimizing the sum of squared errors in predicted life; and at medium ε_a, this model combines both factors. Therefore, the use of this model addresses the weaknesses identified previously for the model based on residual errors alone. To perform this alternate optimization, it was necessary to normalize the x and y axes by assigning relative weights that are used in combining the error in life and strain amplitude because the x and y axes are not in comparable units. In this analysis, errors in strain amplitude (%) were weighted 20 times as heavily as errors in ln(N). A value of 20 was selected for two related reasons. First, this factor led to approximately equal weighting of low and high strain amplitude data in the least-squared error computation of model coefficients. Second, when the factor was applied to the model to generate probability curves, it yielded a standard deviation on strain amplitude comparable to that obtained from the best fit of the high-cycle fatigue data to Equation 1.[130] Because there was judgment applied in the selection of this value, a sensitivity analysis was performed that demonstrated that the coefficients of the model do not change significantly for weight factors between 10 and 25.

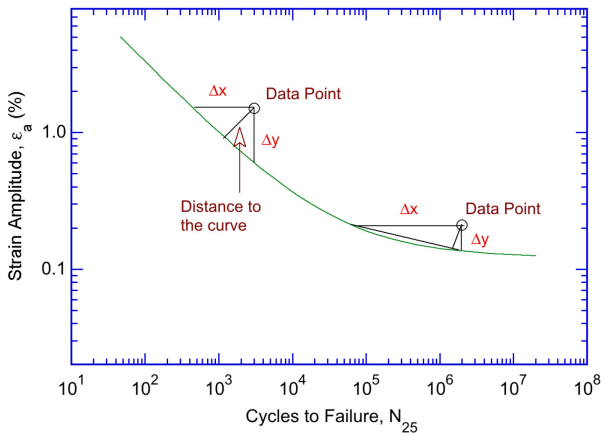

Figure 3-4 Schematic diagram of the best-fit of the experimental data by minimizing the distance between the data point and the S–N curve.

The normal distance from the best-fit curve was estimated as

$$D = \{(x-\hat{x})^2 + [k(y-\hat{y})]^2\}^{1/2}, \quad (19)$$

where $\hat{x}$ and $\hat{y}$ represent predicted values, and k = 20. Although R-squared is only applicable for linear regression, an approximate value for combined R-squared was derived for illustrative purposes. The combined R-squared was defined as

$$1 - \left(\frac{\Sigma D^2}{\Sigma Z^2}\right), \quad (20)$$

where

$$Z = \{(x-x')^2 + [k(y-y')]^2\}^{1/2} \quad (21)$$

and x' and y' represent the 25th percentile of x and y, respectively. The 25th percentile is selected instead of the mean because the mean values are exaggerated due to the nonlinearity of the equations, and because higher values are less influential to the model. The value from Equation 20 is not a true R-squared value, but often falls between the x-based R-squared and the y-based R-squared values; therefore, it is considered to be a better qualitative measure of the model's predictive accuracy because it is not distorted in the way x-based R-squared and y-based R-squared measures would be.

Fatigue life models presented in the original version of NUREG/CR-6909 for estimating the fatigue lives in air of carbon and low-alloy steels in air were developed at ANL as best fits of a Langer curve to an updated version of the PVRC database.[10,46] From those best fits, the fatigue lives, N, of carbon steels was represented by

$$\ln(N) = 6.614 - 0.00124\,T - 1.975\,\ln(\varepsilon_a - 0.113), \quad (22)$$

and that of low-alloy steels by

$$\ln(N) = 6.480 - 0.00124\,T - 1.808\,\ln(\varepsilon_a - 0.151), \quad (23)$$

where ε_a is applied strain amplitude (%), and T is the test temperature (°C). Thus, in room-temperature (25°C) air, the fatigue lives of carbon steels were expressed as

$$\ln(N) = 6.583 - 1.975 \ln(\varepsilon_a - 0.113), \quad (24)$$

and that of low-alloy steels, by

$$\ln(N) = 6.449 - 1.808 \ln(\varepsilon_a - 0.151). \quad (25)$$

Note that Equations 24 and 25 were based on incorporation of additional fatigue data and the analysis presented in Section 4.1.7 of Reference 137; the values of the constant A in the equations were updated from the values reported in NUREG/CR-6583, "Effects of LWR Coolant Environments on Fatigue Design Curves of Carbon and Low-Alloy Steels," issued February 1998,[10] and NUREG/CR-6815, "Review of the Margins for ASME Code Design Curves—Effects of Surface Roughness and Material Variability," issued September 2003.[46] As in these earlier analyses, the current analysis includes all reported runout data. Section 3.1.7 of this report further discusses the heat-to-heat variability of these equations. Relative to the models presented in NUREG/CR-6583, the fatigue lives predicted by the models in the original version of NUREG/CR-6909 were approximately 2% higher for carbon steel and approximately 16% lower for low-alloy steels. The predicted fatigue lives showed good agreement with the experimental values; the experimental and predicted values were within a factor of 3. Figure 3-5 shows the experimental and predicted fatigue lives of carbon and low-alloy steel data using the expressions defined by Equations 24 and 25. As discussed in Section 3.1.7, the greater-than-observed fatigue lives for A106-Gr. B steel at room temperature and for A216-Gr. WCC at 325°C appear to be due to heat-to-heat variability and not temperature effects.

- *The fatigue life models for carbon and low-alloy steels represent mean values of fatigue lives in air for specimens tested under fully reversed strain-controlled loading. The effects of parameters (such as mean stress, surface finish, size and geometry, and loading history) known to influence fatigue lives were accounted for in the several subfactors that were applied to the mean-data air curve to obtain the fatigue design air curve.*

3.1.7 Heat-to-heat Variability

Several factors, such as small differences in material composition and structure, can change the tensile and fatigue properties of materials. Sections 3.1.5 and 3.1.4 discuss the effect of interstitial element content on DSA and the effect of sulfide morphology on fatigue lives, respectively. The effect of tensile strength on fatigue lives was included in the expression for the ASME Code mean-data air curve described in the ASME Code Section III criteria document (i.e., constant A_f in Equation 2). In addition, the material fatigue limit was correlated with tensile strength (e.g., the fatigue limit increases with increasing monotonic tensile yield stress).[213]

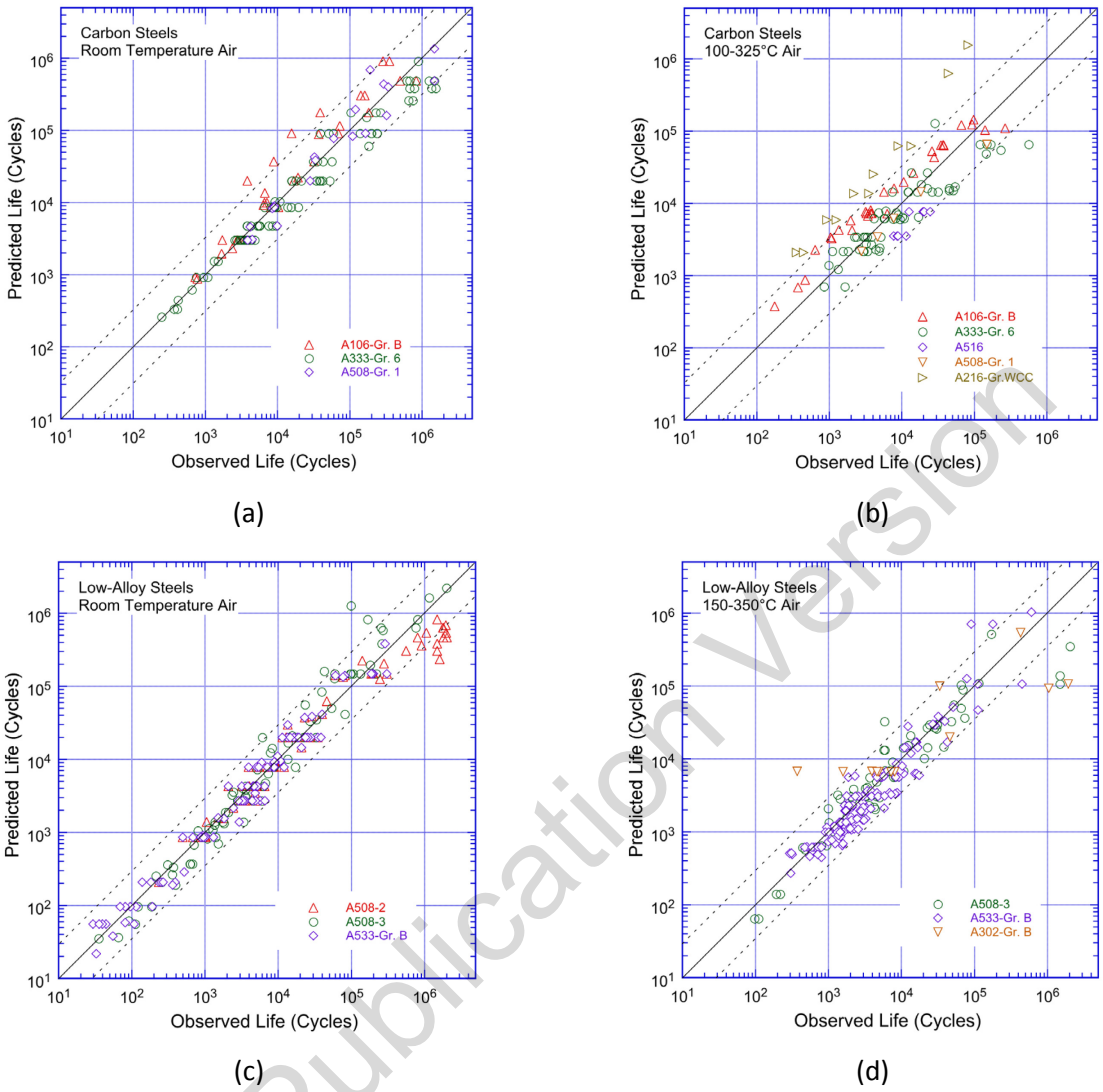

Figure 3-5 Experimental and predicted fatigue lives of (a,b) carbon steels and (c, d) low-alloy steels in air.

The effects of material variability and data scatter must be included in the data evaluation to ensure that the resulting design curves not only describe the available test data adequately but also adequately describe the fatigue lives of the much larger number of heats of material that are found in the field compared to the limited number of heats used for testing. The effects of material variability and data scatter are often evaluated by comparing the experimental data to a specific model for fatigue crack initiation (e.g., the best fit (in some sense) to the data). The adequacy of the evaluation depends on the sample of data used in the analysis. For example, if most of the data were obtained from a heat of material that has poor resistance to fatigue damage or under loading conditions that show significant environmental effects, the results may be conservative for most of the materials or service conditions of interest. Conversely, if most data are from a heat of material with a high resistance to fatigue damage, the results may be nonconservative for many heats in service.

Another method to assess the effect of material variability and data scatter is to consider the best-fit curves determined from tests on individual heats of materials or loading conditions as samples of a

much larger population of heats of materials and service conditions of interest. To do this, the fatigue behavior of each of the heats or loading conditions was characterized by the value of the constant A in Equation 6. The values of A for the various datasets were rank-ordered, and median ranks were used to estimate the cumulative distribution of A for the population.[214,215] The distributions were fit to lognormal curves. No rigorous statistical evaluation was performed for these curves, but the fits appeared reasonable and described the observed variability adequately. The data were normalized to room-temperature values using Equations 22 and 23 (Section 3.1.6). The median value of the constant A reported in the original version of NUREG/CR-6909 was 6.583 and 6.449, respectively, for the fatigue lives of carbon steels and low-alloy steels in room-temperature air. Figure 3-6 shows the estimated cumulative distributions of constant A in the ANL model for fatigue lives for heats of carbon and low-allow steels included in the original version of NUREG/CR-6909 and those included in this report.

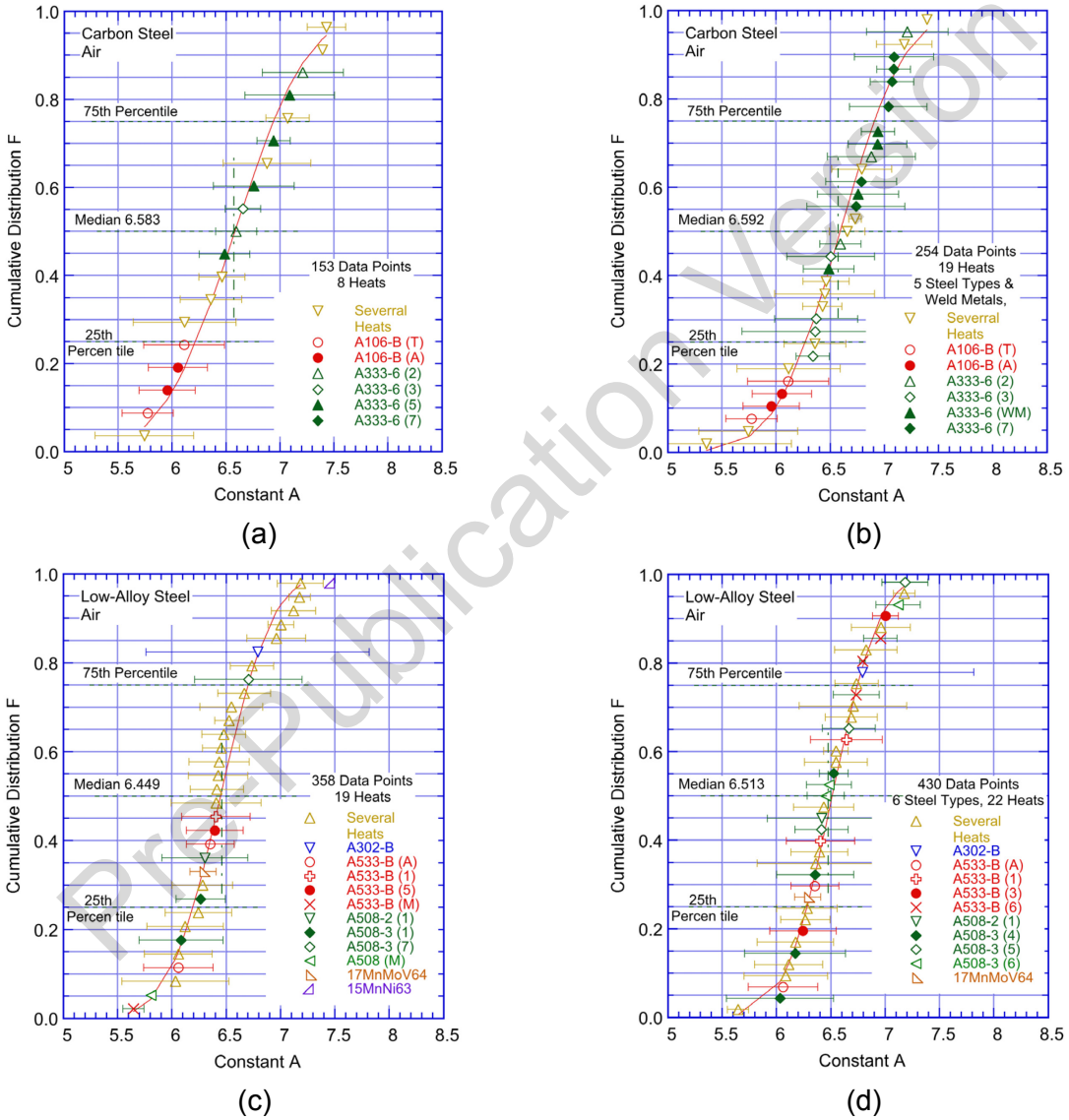

Figure 3-6 Estimated cumulative distribution of constant A in the ANL models for fatigue life data in the original version of NUREG/CR 6909 (a,c) and in this report (b,d) for heats of carbon steels (a,b) and low-alloy steels (c,d) in air.

The results indicate that the ANL fatigue models presented in the original version of NUREG/CR-6909 for predicting fatigue lives of carbon and low-alloy steels in air remain valid. In

spite of a significant increase in the number of data points, the median value of the constant A in Equation 6 did not change significantly for carbon steels (changed from 6.583 to 6.593) or for low-alloy steels (changed from 6.449 to 6.513). Note that the two heats of A106–Gr. B carbon steel were in the 10th to 25th percentile of the data (i.e., the fatigue lives of these heats were much lower than the average value for carbon steels). In addition, the average value of the constant A for the A216-Gr. WCC steel at 325°C (after adjusting for temperature effects) was 4.899, which is significantly lower than the median value of 6.583 for carbon steels. Therefore, it was not included in the reanalysis of the updated fatigue ε–N database, and Figure 3-6 does not show the value of the constant A for A216-Gr. WCC.

As discussed in the original version of NUREG/CR-6909, the A values that describe the 5th percentile of these distributions give fatigue ε–N curves that are expected to bound the fatigue lives of 95% of the heats of the materials tested. The cumulative distributions of A values in Figure 3-6 contain two potential sources of error. The means and standard deviations of the populations must be estimated from the means and standard deviations of the samples,[216] and confidence bounds must be obtained on the population means and standard deviations in terms of the sample means and standard deviations. Secondly, even these conditions did not fully address the uncertainties in the distributions because of the large uncertainties in the sample values themselves (i.e., the "horizontal" uncertainty in the actual value of A for a heat of material as indicated by the error bars in Figure 3-6). Therefore, a Monte Carlo analysis was performed to address both sources of uncertainty. The results for the median values and standard deviations of the constant A from the Monte Carlo analysis did not differ significantly from those determined directly from the experimental values.

Table 3-2 and Table 3-3 summarize the results for carbon and low-alloy steels, respectively, in terms of values for the constant A that provide bounds for the portion of the population and the confidence that is desired in the estimates of the bounds. In air, the 5th-percentile value of constant A at a 95% confidence level was 5.559 for carbon steels and 5.689 for low-alloy steels. Because the reanalysis did not change the constants significantly, the median values of the constant A for carbon and low-alloy steels were not changed in this report. Thus, constant A for the sample remains 6.583 for carbon steels and 6.449 for low-alloy steels, and the 95/95 values of the factor to account for material variability and data scatter are 2.8 and 2.1 on life for carbon and low-alloy steels, respectively. These factors provide 95% confidence that the resultant lives are greater than those observed for 95% of the materials of interest.

- *The mean-data air curves for carbon and low-alloy steels used to develop the fatigue design air curves represented the average fatigue behavior; heat-to-heat variability was included in the subfactor that was applied to the mean-data air curve to obtain the fatigue design air curve to account for "data scatter and material variability."*

Table 3-2 Values of Constant A in the ANL Fatigue Life Model for Carbon Steels in Air and the Factors on Life as a Function of Confidence Level and Percentage of the Population Bounded.

Confidence	Percentage of Population Bounded (Percentile Distribution of A)				
Level	95 (5)	90 (10)	75 (25)	67 (33)	50 (50)
			Values of Constant A		
50	5.798	5.971	6.261	6.373	6.583
75	5.700	5.883	6.183	6.295	6.500
95	5.559	5.756	6.069	6.183	6.381
			Factors on Life		
50	2.2	1.8	1.4	1.2	1.0
75	2.4	2.0	1.5	1.3	1.1
95	2.8	2.3	1.7	1.5	1.2

Table 3-3 Values of Constant A in the ANL Fatigue Life Model for Low-Alloy Steels in Air and the Factors on Life as a Function of Confidence Level and Percentage of the Population Bounded.

Confidence	Percentage of Population Bounded (Percentile Distribution of A)				
Level	95 (5)	90 (10)	75 (25)	67 (33)	50 (50)
			Values of Constant A		
50	5.832	5.968	6.196	6.284	6.449
75	5.774	5.916	6.150	6.239	6.403
95	5.689	5.840	6.085	6.175	6.337
			Factors on Life		
50	1.9	1.6	1.3	1.2	1.0
75	2.0	1.7	1.3	1.2	1.0
95	2.1	1.8	1.4	1.3	1.1

3.1.8 Fatigue ε–N Behavior of Weld Metals

Figure 3-7 plots available fatigue ε–N data for carbon and low-alloy steel weld metals in air at room temperature and 289°C. The results indicated that, in air, the fatigue lives of carbon and low-alloy steel weld metals were slightly lower than the mean ε–N behavior of nonwelded carbon or low-alloy steel test specimens. Except for one data set for CM-US-56B/MF-27 weld metal for which fatigue lives were a factor two lower than the mean-data curves, the fatigue lives of the other datasets were marginally lower. The results also indicated that the fatigue lives at 289°C were slightly lower than at room temperature. Despite these observations, the available fatigue ε–N data for carbon and low-alloy steel weld metals were insufficient to accurately establish their fatigue behavior relative to the mean-data air curve for carbon steels or low-alloy steels, respectively.

- *Until additional fatigue ε–N data for carbon and low-alloy steel weld metals are available, the fatigue mean air curves for carbon steel or low-alloy steels may also be used for weld metals.*

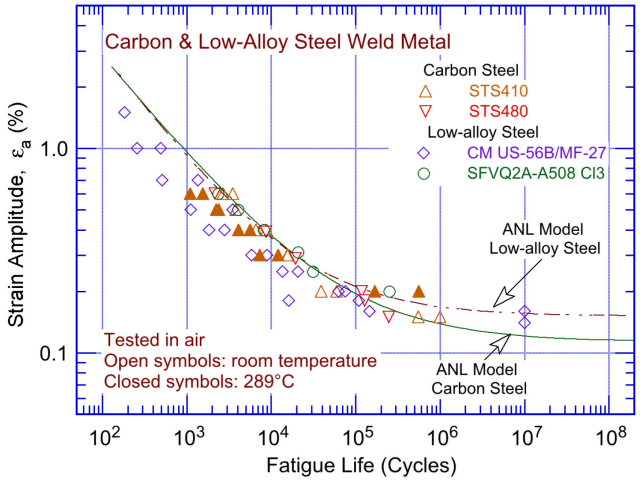

Figure 3-7 Fatigue ε–N behavior for carbon and low-alloy steel weld metals in air at room temperature and 289°C (Ref. 136).

3.1.9 Surface Finish

The effect of surface finish was considered to account for the difference in fatigue lives expected in an actual component with an industrial-grade surface finish compared to the smooth, polished surface of test specimens. Fatigue lives are sensitive to surface finish; cracks can initiate at surface irregularities that are normal to the axis of applied stress. The height, spacing, shape, and distribution of surface irregularities are important for crack initiation. The most common measure of roughness is average surface roughness, R_a, which is a measure of the height of the irregularities. Investigations of the effects of surface roughness on the low-cycle fatigue of Type 304 SS in air at 593°C indicated that fatigue lives decreased as surface roughness increased.[217,218] The effect of roughness on crack initiation, $N_i(R)$, is given by

$$N_i(R) = 1012\, R_q^{-0.21}, \tag{26}$$

where the root-mean-square (RMS) value of the average surface roughness, R_q, is in micrometers. Typical values of R_a for surfaces finished by different metalworking processes in the automotive industry[219] indicated that a value of R_a of 3 μm (or an R_q of 4 μm) represented the maximum surface roughness for drawing/extrusion, grinding, honing, and polishing processes, and a mean value for the roughness range for milling or turning processes. For carbon or low-alloy steels, an R_q of 4 μm in Equation 26 would decrease fatigue life by a factor of 3.7 (i.e., the R_q of a smooth polished specimen is approximately 0.0075 μm).[217]

A fatigue test was conducted on an A106–Gr. B carbon steel specimen that was intentionally roughened in a lathe under controlled conditions with 50-grit sandpaper to produce circumferential scratches with an average roughness of 1.2 μm and an R_q of 1.6 μm (approximately 62 μin.).[46] Figure 3-8 shows the results for smooth and roughened specimens. In air, the fatigue life of a roughened A106–Gr. B specimen was a factor of approximately 3 lower than that of smooth specimens. Another study of the effect of surface finish on the fatigue lives of carbon steels in room–temperature air showed a factor of 2 decrease in life when R_a was increased from 0.3 to 5.3 μm.[220] These results are consistent with Equation 26. Thus, a

factor of 2 to 3 on cycles is necessary to account for surface finish effects on the fatigue lives of carbon and low-alloy steels.

- *The effect of surface finish was included as part of the "surface finish and environment" subfactor that was applied to the mean-data air curves to obtain the fatigue design air curves for carbon and low-alloy steels.*

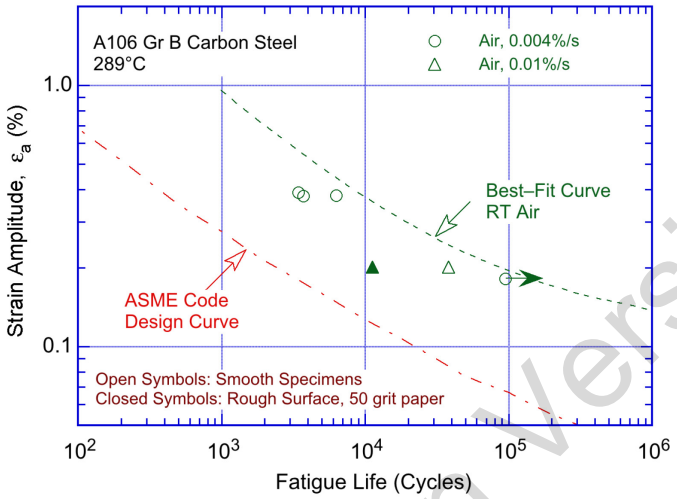

Figure 3-8 Effect of surface finish on the fatigue life of A106–Gr. B carbon steel in air at 289°C (Ref. 46).

3.1.10 Extension of the Best-Fit Mean Curve from 10^6 to 10^{11} Cycles

The experimental fatigue ε–N air curves that were used to develop the fatigue design air curve for carbon and low-alloy steels in the 2011 Addenda of ASME Code Section III were based on low-cycle fatigue data (less than 2×10^5 cycles). The design air curves proposed in this report were developed from a larger database that included fatigue lives up to 10^8 cycles. Both the ASME Code mean air curves and the ANL models in this report used the modified Langer equation to express the best-fit mean air curves; they are not recommended for estimating fatigue lives beyond the range of the experimental data (i.e., in the high-cycle fatigue regime).

An extension of the current high-cycle fatigue design curves in Section III and Section VIII of Division 2 of the ASME Code for carbon and low-alloy steels from 10^6 to 10^{11} cycles was proposed by O'Donnell to the ASME Section III Subgroup on Fatigue Strength.[C] In the high-cycle regime at temperatures not exceeding 371°C (700°F), the stress amplitude (S_a) vs. life relationship is expressed as

$$S_a = E\varepsilon_a = C_1 N^{-0.05}, \quad (27)$$

where ε_a is applied strain amplitude, E is the elastic modulus, N is the fatigue life, and C_1 is a constant. A fatigue life exponent of -0.05 was selected based on the fatigue stress range vs.

[C] W.J. O'Donnell, "Proposed Extension of ASME Code Fatigue Design Curves for Carbon and Low-Alloy Steels from 10^6 to 10^{11} Cycles for Temperatures Not Exceeding 700°F," was presented to the ASME Subgroup on Fatigue Strength on December 4, 1996.

fatigue life data on plain plates, notched plates, and typical welded structures given in Welding Research Council (WRC) Bulletin 398, "Reduction of S–N Curves for Ship Structural Details," issued January 1995.[221] Because the data were obtained from load-controlled tests with an R ratio of zero, they take into account the effect of maximum mean stresses and may overestimate the effect of mean stress under strain-controlled loading conditions. In addition, the fatigue data presented in WRC Bulletin 398 extend only up to 5×10^6 cycles; extrapolation of the results to 10^{11} cycles using a fatigue life exponent of -0.05 may yield overly conservative estimates of fatigue life. Finally, ASME received feedback from the evaluation of plant trouble reports, laboratory tests of socket welded joints, and plant operating experience that supported its use of Equation 27.

Manjoine and Johnson[213] developed fatigue design curves up to 10^{11} cycles for carbon steels and austenitic SSs from inelastic and elastic strain relationships, which were correlated with ultimate tensile strength. The log-log plots of the elastic strain amplitudes vs. fatigue life data were represented by a bilinear curve. In the high-cycle regime, the elastic strain vs. life curve had a small negative slope instead of a fatigue limit.[213] For carbon steel data at room temperature and 371°C (700°F) and fatigue lives extending up to 4×10^7 cycles, Manjoine and Johnson obtained an exponent of -0.01. The fatigue ε–N data used in this report at room temperature and with fatigue lives up to 10^8 cycles yielded a fatigue life exponent of approximately -0.007 for both carbon and low-alloy steels. Because the data are limited, the more conservative exponent value (i.e., -0.01) obtained by Manjoine and Johnson[213] was used in the original version of NUREG/CR-6909. In the high-cycle regime, the applied stress amplitude was expressed by the relationship

$$S_a = E\varepsilon_a = C_2 N^{-0.01}. \quad (28)$$

In the original version of NUREG/CR-6909, Equation 28 was used to extend the best-fit mean air curves beyond 10^6 cycles (in the high-cycle regime); therefore, the mean stress-life curves exhibited a small negative slope instead of the fatigue limit predicted by the modified Langer equation. The selection of a smaller value for the fatigue life exponent to extend the best-fit curve was based on evaluation of thermal fatigue data, which are bounded by Equation 28. However, the high-cycle thermal fatigue data are limited, and the data do not consider mechanical fatigue (i.e., vibration).

As discussed earlier in this report, the classical fatigue limit for ferrous alloys is a consequence of performing fatigue tests at constant cyclic stress or strain range and determining the threshold range below which cracks cannot propagate beyond microstructural barriers and fatigue failures do not occur. Miller and O'Donnell[222] discussed the causes that lead to elimination of the fatigue limit, including the introduction of transitory cyclic processes or time-dependent mechanisms that permit a previously nonpropagating crack to grow across microstructural barriers. The authors argued that the most probable significant condition for engineering plants designed to last beyond 10^6 cycles is the introduction of very low cyclic stress vibrations at high mean stress levels, with or without other mechanisms such as corrosion or time-dependent mechanisms. Therefore, in this report, to better accommodate the vibration data (e.g., Ref. 221), the extension of the fatigue stress or strain-life curves beyond 10^6 cycles is based on the more conservative Equation 27 rather than Equation 28 (i.e., an exponent of -0.05 is used). The value of constant C_1 was determined from the value of strain amplitude at which the slope of the curve expressed by Equation 27 is the same as that of the fatigue ε–N curve expressed by Equation 24 for carbon steels or Equation 25 for low-alloy steels.

- *The fatigue design air curves for carbon and low-alloy steels were extended beyond 10^6 cycles using Equation 27, which is consistent with the methodology used to*

develop the fatigue design air curve for carbon and low-alloy steels in the 2011 Addenda of ASME Code Section III.

3.1.11 Fatigue Design Curves

Although the two equations for the ASME Code mean air curves for carbon and low-alloy steels (i.e., Equations 7 and 8) are significantly different (because the mean stress correction is much larger for the low-alloy steels), the differences between the curves are much smaller when mean stress corrections are considered. Thus, ASME Code Section III provides one common fatigue design air curve for both carbon and low-alloy steels. The ASME Code fatigue design air curves for carbon and low-alloy steels were obtained from the best-fit curves in air (i.e., Equations 7 and 8, respectively) by first correcting for mean stress effects by using the modified Goodman relationship, followed by reducing the mean stress adjusted curves by factors of 2 on stress or 20 on cycles, whichever was more conservative. The discussions presented in Section 7.5 of the original version of NUREG/CR-6909 indicated that the current ASME Code requirement of a factor of 20 on cycles to account for the effects of material variability and data scatter, specimen size, surface finish, and loading history was conservative by at least a factor of 1.7 for these steels. To reduce this conservatism, separate fatigue design air curves based on the ANL models for carbon and low-alloy steels were developed using factors of 12 on life and 2 on stress. Figure 3-9 shows the fatigue design air curves developed following this approach for carbon and low-alloy steels. The difference between the design air curves based on the ANL models and the ASME Code design air curve is due to the difference in the factor on life used to obtain these curves (i.e., 20 for the ASME Code curve and 12 for the ANL curves). In addition, for the carbon steel design air curve, the conservatism in the high-cycle regime was corrected in the ANL models.

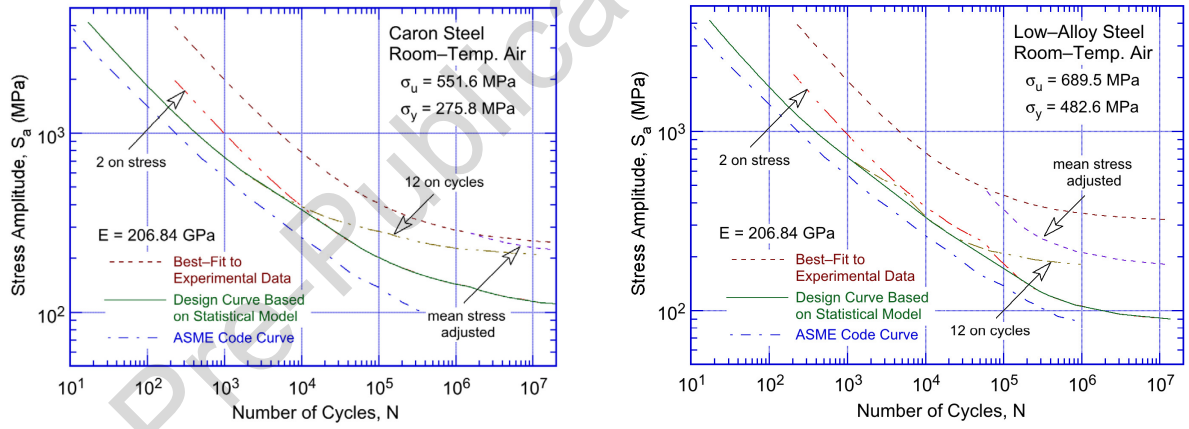

Figure 3-9 Fatigue design curves based on the ANL model for (a) carbon steels and (b) low-alloy steels in air.

The ASME Code fatigue design air curve for carbon and low-alloy steels with ultimate tensile strength (UTS) less than 552 MPa (80 ksi) included an extension of the design curve to 10^{11} cycles, which was proposed by O'Donnell and was based on Equation 27 in this report. In the original version of NUREG/CR-6909, the fatigue design air curves developed based on the ANL fatigue ε–N models were extended in the high-cycle regime beyond 10^6 cycles using Equation 28 instead of Equation 27. However, as discussed in Section 3.1.10, and to better

accommodate the field vibration data, the extension of the fatigue design curves beyond 10^6 cycles is based on Equation 27. Table 3-4 lists the values of stress amplitude (S_a) vs. cycles for the ASME Code Section III fatigue design air curve with O'Donnell's extension, and the design curve based on Equation 27 with either the ANL fatigue life models from Equation 24 for carbon steels or Equation 25 for low-alloy steels. Figure 3-10 and Figure 3-11 show the corresponding fatigue design air curves for carbon and low-alloy steels, respectively. For comparison, Table 3-5 presents the values of stress amplitude vs. cycles from the original version of NUREG/CR-6909 for the fatigue design air curves based on the ANL fatigue ε–N models and Equation 28.

- *Separate fatigue design air curves were developed for carbon and low-alloy steels from the ANL models using factors of 12 on life and 2 on stress. The results indicated that the ASME Code Section III fatigue design air curve for carbon and low-alloy steels for ultimate tensile strengths less than 552 MPa (80 ksi) was conservative with respect to the existing fatigue ε–N data, particularly for carbon steels. In this report, the extension of the fatigue design air curves beyond 10^6 cycles was based on Equation 27 instead of Equation 28 as in the original version of NUREG/CR-6909.*

Table 3-4 Fatigue Design Curves for Carbon and Low-Alloy Steels Including the Proposed Updated Extension to 10^{11} Cycles.

	Stress Amplitude (MPa/ksi)				Stress Amplitude (MPa/ksi)		
Cycles	ASME Code Curve	Eqs. 24 & 27 Carbon Steel	Eqs. 25 & 27 Low-alloy Steel	Cycles	ASME Code Curve	Eqs. 24 & 27 Carbon Steel	Eqs. 25 & 27 Low-alloy Steel
1 E+01	3999 (580)	5355 (777)	5467 (793)	2 E+05	114 (16.5)	176 (25.5)	141 (20.5)
2 E+01	2827 (410)	3830 (556)	3880 (563)	5 E+05	93.1 (13.5)	154 (22.3)	116 (16.8)
5 E+01	1896 (275)	2510 (364)	2438 (354)	1 E+06	86.2 (12.5)	142 (20.6)	106 (15.4)
1 E+02	1413 (205)	1820 (264)	1760 (255)	2 E+06		130 (18.9)	98 (14.2)
2 E+02	1069 (155)	1355 (197)	1300 (189)	5 E+06		120 (17.4)	94 (13.6)
5 E+02	724 (105)	935 (136)	900 (131)	1 E+07	76.8 (11.1)	115 (16.7)	91 (13.2)
1 E+03	572 (83)	733 (106)	720 (104)	2 E+07		110 (16.0)	88 (12.7)
2 E+03	441 (64)	584 (84.7)	576 (83.5)	5 E+07		105 (15.2)	84 (12.2)
5 E+03	331 (48)	451 (65.4)	432 (62.7)	1 E+08	68.5 (9.9)	101 (14.7)	81 (11.8)
1 E+04	262 (38)	373 (54.1)	342 (49.6)	1 E+09	61.1 (8.8)	90 (13.1)	72.3 (10.5)
2 E+04	214 (31)	305 (44.2)	276 (40.0)	1 E+010	54.4 (7.9)	81 (11.7)	64.4 (9.3)
5 E+04	159 (23)	238 (34.5)	210 (30.5)	1 E+011	48.5 (7.0)	72 (10.4)	57.4 (8.3)
1 E+05	138 (20.0)	201 (29.2)	172 (24.9)				

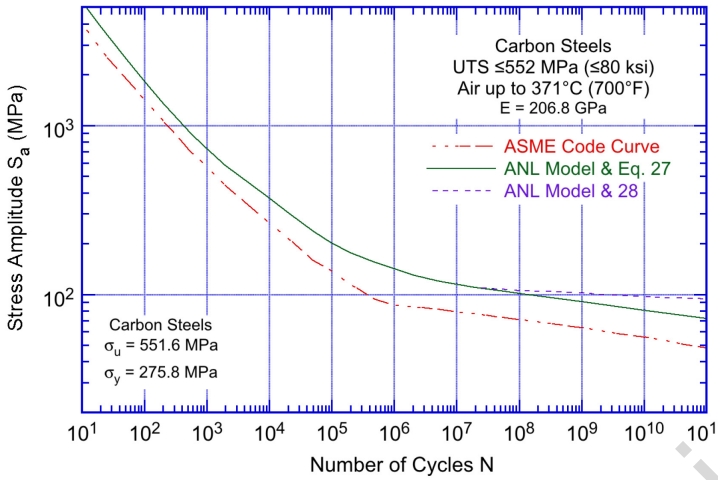

Figure 3-10 Fatigue design curve for carbon steels in air (The curve developed from the ANL model is based on factors of 12 on life and 2 on stress).

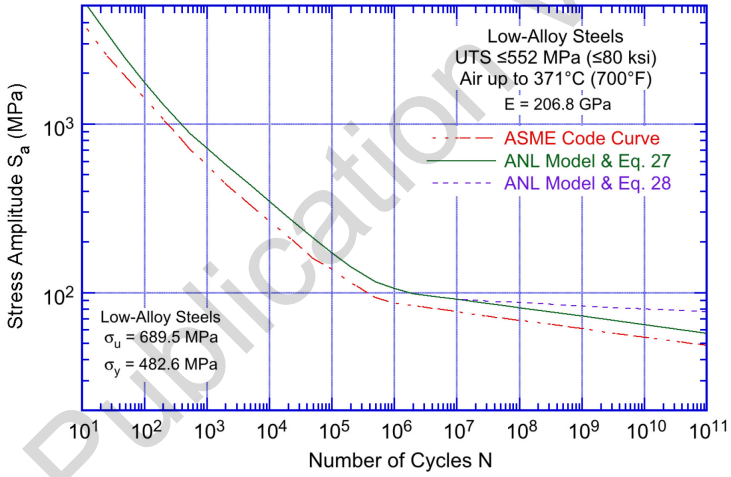

Figure 3-11 Fatigue design curve for low-alloy steels in air (The curve developed from the ANL model is based on factors of 12 on life and 2 on stress).

Table 3-5 Fatigue Design Curves for Carbon and Low-Alloy Steels and the Extension to 10^{11} Cycles Proposed in the Original Version of NUREG/CR 6909.

	Stress Amplitude (MPa/ksi)				Stress Amplitude (MPa/ksi)		
Cycles	ASME Code Curve	Eqs. 24 & 28 Carbon Steel	Eqs. 25 & 28 Low-alloy Steel	Cycles	ASME Code Curve	Eqs. 24 & 28 Carbon Steel	Eqs. 25 & 28 Low-alloy Steel
1 E+01	3999 (580)	5355 (777)	5467 (793)	2 E+05	114 (16.5)	176 (25.5)	141 (20.5)
2 E+01	2827 (410)	3830 (556)	3880 (563)	5 E+05	93 (13.5)	154 (22.3)	116 (16.8)
5 E+01	1896 (275)	2510 (364)	2438 (354)	1 E+06	86 (12.5)	142 (20.6)	106 (15.4)
1 E+02	1413 (205)	1820 (264)	1760 (255)	2 E+06		130 (18.9)	98 (14.2)
2 E+02	1069 (155)	1355 (197)	1300 (189)	5 E+06		120 (17.4)	94 (13.6)
5 E+02	724 (105)	935 (136)	900 (131)	1 E+07	76.5 (11.1)	115 (16.7)	91 (13.2)
1 E+03	572 (83)	733 (106)	720 (104)	2 E+07		110 (16.0)	90 (13.1)
2 E+03	441 (64)	584 (84.7)	576 (83.5)	5 E+07		107 (15.5)	88 (12.8)
5 E+03	331 (48)	451 (65.4)	432 (62.7)	1 E+08	68.3 (9.9)	105 (15.2)	87 (12.6)
1 E+04	262 (38)	373 (54.1)	342 (49.6)	1 E+09	60.7 (8.8)	102 (14.8)	83 (12.0)
2 E+04	214 (31)	305 (44.2)	276 (40.0)	1 E+010	54.5 (7.9)	97 (14.1)	80 (11.6)
5 E+04	159 (23)	238 (34.5)	210 (30.5)	1 E+011	48.3 (7.0)	94 (13.6)	77 (11.2)
1 E+05	138 (20.0)	201 (29.2)	172 (24.9)				

3.2 Wrought and Cast Austenitic Stainless Steels and Weld Metals

3.2.1 Experimental Data

The relevant fatigue ε–N data used to evaluate wrought and cast austenitic SSs in air include the large JNES database;[136] data developed at ANL[45] and GE;[14,15] results of Keller;[63] and the data[64,65,70,73] compiled by Jaske and O'Donnell[61] for developing fatigue design criteria for pressure vessel alloys. The database comprises 770 tests from which 622 data points were obtained—332 tests (267 data points) on Type 304 SS, 315 tests (244 data points) on Type 316 SS, 96 tests (77 data points) on SS weld metals (i.e., 34 tests (23 data points) on Type 304 SS weld metals and 62 tests (54 data points) on Type 316 SS weld metals), and 37 tests (34 data points) for CF-8M grade of cast austenitic SSs. Both low-carbon and high-carbon grades of Types 304 and 316 SS are included in the database. Out of these, 432 data points were obtained at room temperature, 7 data points were obtained at 100–200°C, and 183 data points were obtained at 250–325°C. Another 70 data points obtained at temperatures of 400°C and above were not included in the present reanalysis to verify the fatigue ε–N expression for austenitic SSs in air because they were outside of the temperature range experienced in LWRs. As discussed in Section 3.2.4, the fatigue ε–N data for austenitic SSs shows some temperature dependence above 460°C. Table 3-6 summarizes the points included in the updated database used for the present analyses, as categorized by material type and test environment. Appendix B presents other material information such as chemical composition, heat treatment, and room temperature tensile properties of the various types and heats of materials. Please note that grades of austenitic SSs that have better fatigue resistance, particularly the titanium- or niobium-modified SSs, were not considered in the analysis. Fatigue lives for such alloys are expected to be greater than the proposed fatigue design curve.

Table 3-6 Sources of the Fatigue ε–N Data on Wrought and Cast Austenitic SSs in an Air Environment.

ANL Mat. ID	Material Heat Designation[a]	Carbon Content (wt.%)	Test Temperature (°C)	No. of Data Points	Source	Applicable Reference
Type 304 Stainless Steels						
1	304-1	0.050	288	10	JNES (Tokimasa)	136
2	304-30, 31	0.050	25	10, 4	JNES (Yamanaka),	136
3	304-3H	0.060	25	8	JNES (Enomoto),	136
4	304-4B	0.050	25	10	JNES (Kitigawa)	136
5	304-5B	0.060	25	3	JNES (Sakamoto)	136
6	304-6B	0.060	25	11	JNES (Tsunenari)	136
7	304-7B	0.059	25	10	JNES (Kasahara)	136
8	304-8B	0.060	25	6	JNES (Ichihara)	136
10	304-10, 10H	0.060	25, 300, 100	2, 7, 2	JNES (Usami)	136
11	304-11H	0.070	25	7	JNES (Yamanaka)	136
12	304-12	-	25	11	JNES (Nishijima)	136
13	304-13	0.026	21	10	Jaske & O'Donnell	64
14	304-14	0.026	21	9	Jaske & O'Donnell	64
15	304-15	-	21	6	Jaske & O'Donnell	63
16	304-16	0.060	21	8	Jaske & O'Donnell	70
17	304-17	-	21	6	Jaske & O'Donnell	65
18	304-18	0.020	27	8	Jaske & O'Donnell	73
20	304-G	0.060	25, 260	9, 9[b]	GE	14,15
21	304-A2	0.060	288	4	ANL	45
22	304-21, 21T	0.060	25, 325	2, 7	JNES (Kanasaki, Tsutsumi)	136
23	304-32	0.070	300	3	JNES (Endo)	136
24	304-35	0.070	25, 289	8,[c] 5	JNES (Hirano)	136
26	304HP-1	0.050	25	6	JNES (Nishijima)	136
27	304HP-2	0.060	25	17,[c] 14[c,d]	JNES (Nishijima)	136
28	304L-E	0.039	150,300	5, 11	Solomon	58-60
29	304L-1	0.017	25	5	JNES (Hirano)	136
30	304L-G	0.022	260	7	GE	14,15
31	304L	0.013	25	9	JNES (Suzuki)	136
Type 316 Stainless Steels						
32	316-1H	0.055	25, 290	7, 8	JNUFAD (Tokimasa)	210
33	316-2	0.050	25	6	JNES (Kaneo)	136
34	316-3H	0.040	25	6	JNES (Ikemoto)	136
35	316-4	0.060	21	4	Jaske & O'Donnell	63
38	316-7	-	21	8	Jaske & O'Donnell	61
39	316-8	-	22	3	Jaske & O'Donnell	61
40	316-9	-	21	5	Jaske & O'Donnell	61
41	316-10	-	21	4	Jaske & O'Donnell	61
42	316-12T, 25T	0.060	325, 25	7, 5	JNES (Kanasaki, Tsutsumi)	136
45	316-25, -25, -27T	0.040, 0.060	25, 325, 25	4, 6, 6	JNES (EFT, PLEX)	136
46	316-26T	0.057	25	10[e]	JNES (EFT)	136
47	316-1H, 316L-1H	0.055, 0.015	25, 290	7, 7	JNES (Tokimasa)	136

ANL Mat. ID	Material Heat Designation[a]	Carbon Content (wt.%)	Test Temperature (°C)	No. of Data Points	Source	Applicable Reference
48	316N-1	0.010	25, 288	25[b], 18[b]	JNES (Yamauchi, Matsuno, Tokimasa)	136
50	316N-3H	0.012	25, 290	7, 7	JNES (Tokimasa)	136
51	316N-6	0.007	25	12	JNES (Higuchi)	136
52	316N-7	0.008	25, 290	25, 14	JNES (Utsunomiya, Nagata, Higuchi, Kanasaka, Ogawa)	136
53	316N-8	0.011	25, 289	5, 8	JNES (Hirano)	136
54	316N-A	0.013	22, 288, 320	12, 6, 3	ANL	45
Stainless Steel Weld Metals						
55	304HP-WM-1	0.058	25	7[d], 10	JNES (Nishijima)	136
56	304-WM-2	0.034	25	6	JNES (Kanasaki)	136
57	316-WM	0.020	25	6[f]	JNES (EFT)	136
58	316N-WM-1	0.018	25, 290	13, 11	JNES (Ogawa, Nagata)	136
59	316N-WM-2	0.017	25, 289	10, 7	JNES (Hirano)	136
60	316N-WM-3	0.002	25	7	JNES (Kanasaki)	136
Cast Austenitic Stainless Steels						
61	CF–8M-1	0.053	325	12	JNES (Tsutsumi)	136
62	CF–8M-2	0.050	25	10	JNES (Hirano)	136
63	CF–8M-3	0.050	25	6	JNES (Kanasaki)	136
68	CF–8M-8	0.064	288	5[b]	ANL	45
69	CF–8M-9	0.065	288	1[b]	ANL	45

[a] The last letter at the end of the material heat designation refers to the following: H = hourglass specimens, T = tube specimens, and B = bending tests.

[b] This data point Includes thermally aged specimens.

[c] Half of the tests were performed on hourglass specimens.

[d] Tests were performed in axial load-control using a sinusoidal waveform.

[e] Five tests each were performed on solid cylindrical specimens and tube specimens.

[f] Tests were performed on tube specimens.

Figure 3-12 shows the fatigue ε–N data for Types 304, 304L, 316, and 316NG SSs in air at temperatures between room temperature and 400°C. The plots in this figure include the best–fit air curve based on the updated ANL fatigue life model (Equation 29 in Section 3.2.6) and the mean-data air curve from ASME Code Section III before publication of the 2009 Addenda. The results indicated that the fatigue lives of Types 304, 304L, and 316 SS are comparable and generally show good agreement with the ANL model with respect to the mean-data air curve. The fatigue lives of Type 316NG are slightly higher than those for Types 304, 304L, and 316 SS at high strain amplitudes.

A few heats of Type 304L and 316NG show poor agreement with the ANL best-fit curve. Typically, for such heats, the slope of the fatigue ε–N curve is steeper; therefore, fatigue lives are slightly longer at high strain amplitudes and lower at low strain amplitudes. This behavior is also observed in PWR environments, as shown in Figure 4-28 and Figure 4-30 in Section 4.2.1. Because the methodology is applicable to several grades, heat-treatments, and compositions of materials, a single slope of the fatigue ε–N curve is assumed for all materials.

However, all of the data are evenly distributed within the scatter band along the ANL mean air curve for austenitic SSs. Some of the tests on Type 316 SS in room–temperature air were conducted in load-control mode at stress levels in the range of 190–230 MPa. The data are

shown as triangles in Figure 3-12, with strain amplitudes of 0.1 to 0.12% and fatigue lives in the range of $7x10^4$ to $3x10^7$ cycles. For these tests, the strain amplitude was calculated only as elastic strain rather than also including the portion of the strain from plastic loading. When plastic strain was considered, based on cyclic stress vs. strain correlations for Type 316 SS,[45] actual strain amplitudes for these tests ranged from 0.23 to 0.32%. Therefore, these results were excluded from the analysis of the fatigue ε–N data to develop the model for estimating the fatigue lives of these steels in air to ensure that an inconsistent bias would not be interjected in the evaluation.

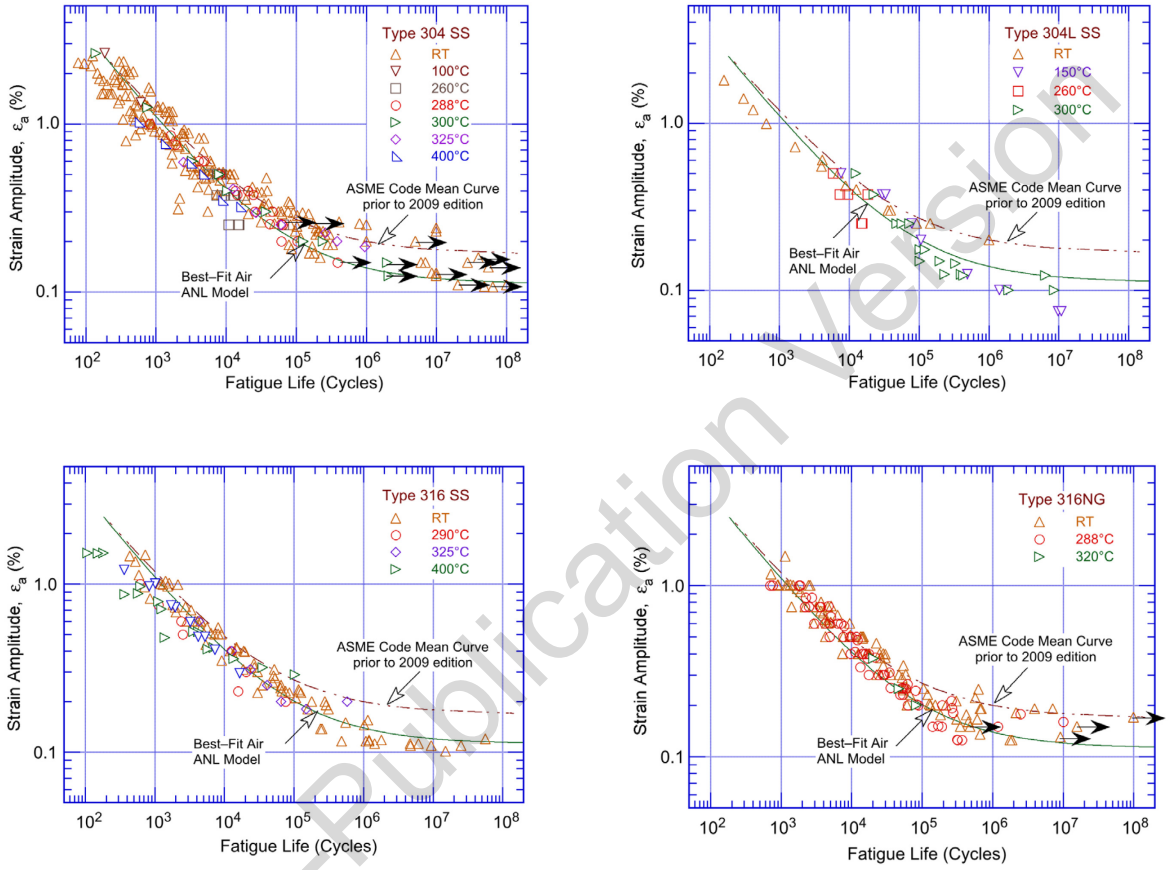

Figure 3-12 Fatigue ε–N behavior for Types 304, 304L, 316, and 316NG austenitic SSs in air at various temperatures up to 400°C (Refs. 13, 42, 47, 61, and 136).

The results in Figure 3-12 indicated that the mean-data air curve in ASME Code Section III before publication of the 2009 Addenda was not consistent with the existing fatigue ε–N data for austenitic SSs. At strain amplitudes less than 0.3% (i.e., stress amplitudes less than 585 MPa (84.9 ksi)), the ASME Code mean air curve predicted significantly longer fatigue lives than those observed experimentally for several heats of austenitic SSs with compositions and tensile strengths within the ASME Code specifications. The difference between the ASME Code Section III mean air curve and the best fit of the available experimental data was caused by differences in the tensile strengths of the steels. The ASME Code Section III mean air curve represents SSs with relatively high tensile strengths; the fatigue ε–N data obtained during the last 30 years were obtained on SSs with lower tensile strengths. Furthermore, for the mean air curve in ASME Code Section III before publication of the 2009 Addenda, the 10^6-cycle fatigue

limit (i.e., the stress amplitude at a fatigue life of 10^6 cycles) was 389 MPa, which is greater than the upper range of the room-temperature monotonic yield strength of austenitic SSs used for the mean stress correction in this report (approximately 303 MPa in Table B-2 in Appendix B). Consequently, the fatigue design air curve for austenitic SSs in ASME Code Section III did not include a mean stress correction for fatigue lives below 10^6 cycles. Studies by Wire et al.[223] and Solomon et al.[58] on the effects of residual stress on fatigue lives demonstrated that mean stress decreased the 10^6-cycle fatigue limit of materials; the extent of these effects depended on the cyclic-hardening behavior of the materials and the resultant decreases in strain amplitudes developed during load-controlled cycling. Strain hardening is more pronounced at high temperatures (e.g., 288–320°C) or at high mean stress values (e.g., greater than 70 MPa); therefore, as observed by Wire et al. and Solomon et al., fatigue lives for load-controlled tests with mean stress were actually increased at high temperatures or large values of mean stress. In both studies, under load controlled conditions, mean stress effects were observed at low temperatures (150°C) or at relatively low mean stress values (less than 70 MPa).

Wire et al.[223] performed fatigue tests on two heats of Type 304 SS to establish the effects of mean stress under both strain-controlled and load-controlled conditions. The strain-controlled tests indicated that "an apparent reduction of up to 26% in strain-amplitude occurred in the low and intermediate cycle regime ($<10^6$ cycles) for a mean stress of 138 MPa." However, the results were affected by both mean stress and cold work. Although the composition and vendor-supplied tensile strengths for the two heats of Type 304 SS were within ASME Code specifications, the measured mechanical properties showed much larger variations than indicated by the vendor properties. Wire et al. stated, "[a]t 288°C, monotonic yield strength varied from 152–338 MPa. These wide variations are attributed to variations in [cold] working from the surface to the center of the thick cylindrical forgings." After separating the individual effects of mean stress and cold work, the Wire et al. results indicated a 12% decrease in strain amplitude for a mean stress of 138 MPa. These results were consistent with the predictions based on conventional mean stress models such as the Goodman correlation.

The current ASME Code Section III fatigue design air curve (i.e., 2009 Addenda or later editions of the ASME Code) is based on the ANL model presented in Equation 29. This curve is consistent with the extensive fatigue ε–N data analyzed in this report. Section 3.2.6 presents additional details of the analysis.

- *The ASME Code Section III fatigue design air curve is now based on the ANL model and is consistent with the existing fatigue ε–N data for austenitic SSs.*

3.2.2 Specimen Geometry and Type of Loading

Figure 3-13 shows the influence of specimen geometry (hourglass vs. gauge-length specimens) on the fatigue lives of Types 304 and 316 SS. At temperatures up to 300°C, specimen geometry had little or no effect on the fatigue lives of austenitic SSs; the fatigue lives of hourglass specimens were comparable to those of gauge specimens.

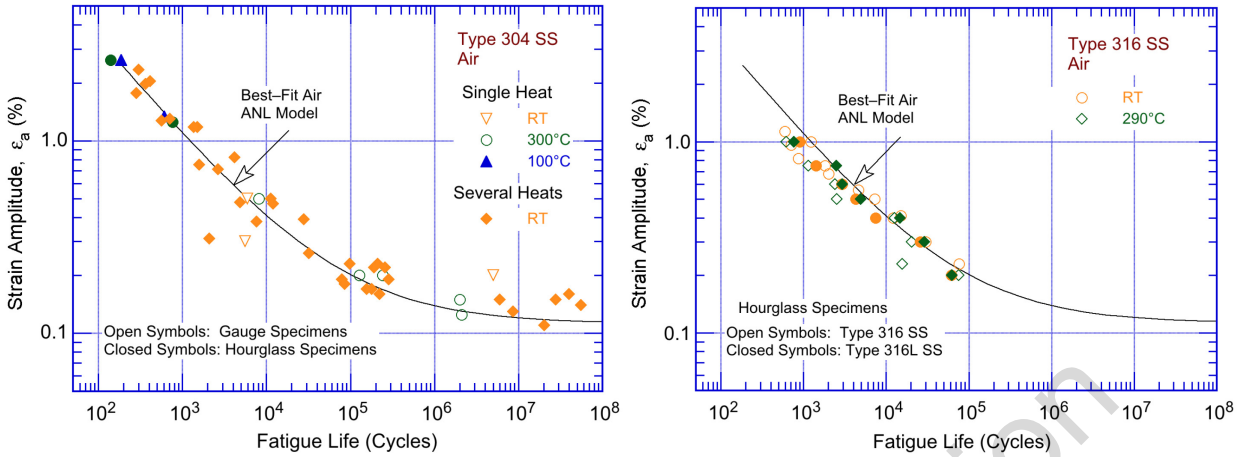

Figure 3-13 Influence of specimen geometry on fatigue lives of Types 304 and 316 SSs (JNUFAD data).

Figure 3-14 shows the results of strain-controlled bending fatigue tests tested on rectangular bar specimens of Type 304 SS in room-temperature air. Although all of the fatigue tests were performed at high strain amplitudes (i.e., producing fatigue lives less than 10^4 cycles), the bending-test data were evenly distributed along the ANL mean-data air curve for austenitic SSs.

- *Fatigue ε–N data obtained on hourglass specimens, straight gauge specimens, or bending test specimens may be used to develop the fatigue design air curves.*

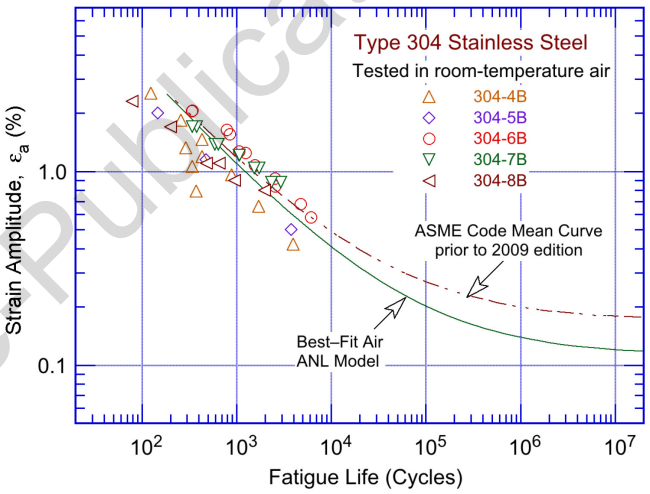

Figure 3-14 Influence of bending loading on fatigue lives of Types 304 and 316 SSs (JNUFAD data).

3.2.3 Strain Rate

A statistical analysis of the fatigue ε–N data presented in Reference 45 indicated that the fatigue lives of austenitic SSs in an air environment decreased with decreasing strain rate at temperatures between 400 and 430°C. However, studies at Électricité de France (EdF) indicated that variations in strain rate in the range of 0.4 to 0.008%/s had no effect on the

fatigue lives of SSs at temperatures up to 400°C.[57] Thus, for the fatigue data analysis presented in this report, strain rate effects on fatigue lives in air were considered insignificant.

- *Effects of strain rate on the fatigue lives of austenitic SSs in air were considered insignificant.*

3.2.4 Temperature

Figure 3-12 plots the fatigue lives of austenitic SSs in air at temperatures between room temperature and 400°C. The results indicated that the fatigue lives of Types 304, 304L, 316, and 316NG SS did not show any dependence on temperature from room temperature up to 400°C. These results are consistent with the observation of Amzallag et al.[57]

Figure 3-15 plots additional fatigue data at temperatures between 427 and 456°C.[61-63] The results indicated that the fatigue ε–N data at temperatures between 400 and 460°C were evenly distributed along the ANL best-fit air curve. Furthermore, for austenitic SSs, DSA is typically observed at temperatures of 500-600°C.[206] Therefore, for these results, the fatigue ε–N data for austenitic SSs in air are well represented by a single curve, the ANL model.

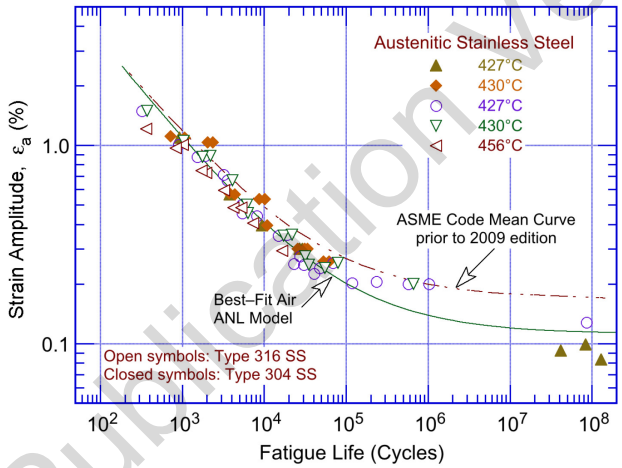

Figure 3-15 Influence of temperature on fatigue lives of austenitic SSs in air (Refs. 61-63).

However, studies at GE by Solomon et al. indicate that temperature influenced the fatigue limit of austenitic SSs because of differences in the secondary hardening behavior of the material.[60] Secondary hardening is the transformation of retained austenite to martensite causing an increase in hardness. This frequently occurs in high-alloy steels due to precipitation of carbides during the tempering process.

- *Temperature had no significant effect on the fatigue lives of austenitic SSs in air at temperatures below 400°C. Limited additional data also showed no temperature effects up to 450°C. However, the existing fatigue data are inadequate to establish the effects of secondary hardening on fatigue life, especially at temperatures above 400°C. In the proposed methodology, these secondary hardening effects are accounted for in the factor applied on stress that was applied to obtain the design curve from the mean-data curve.*

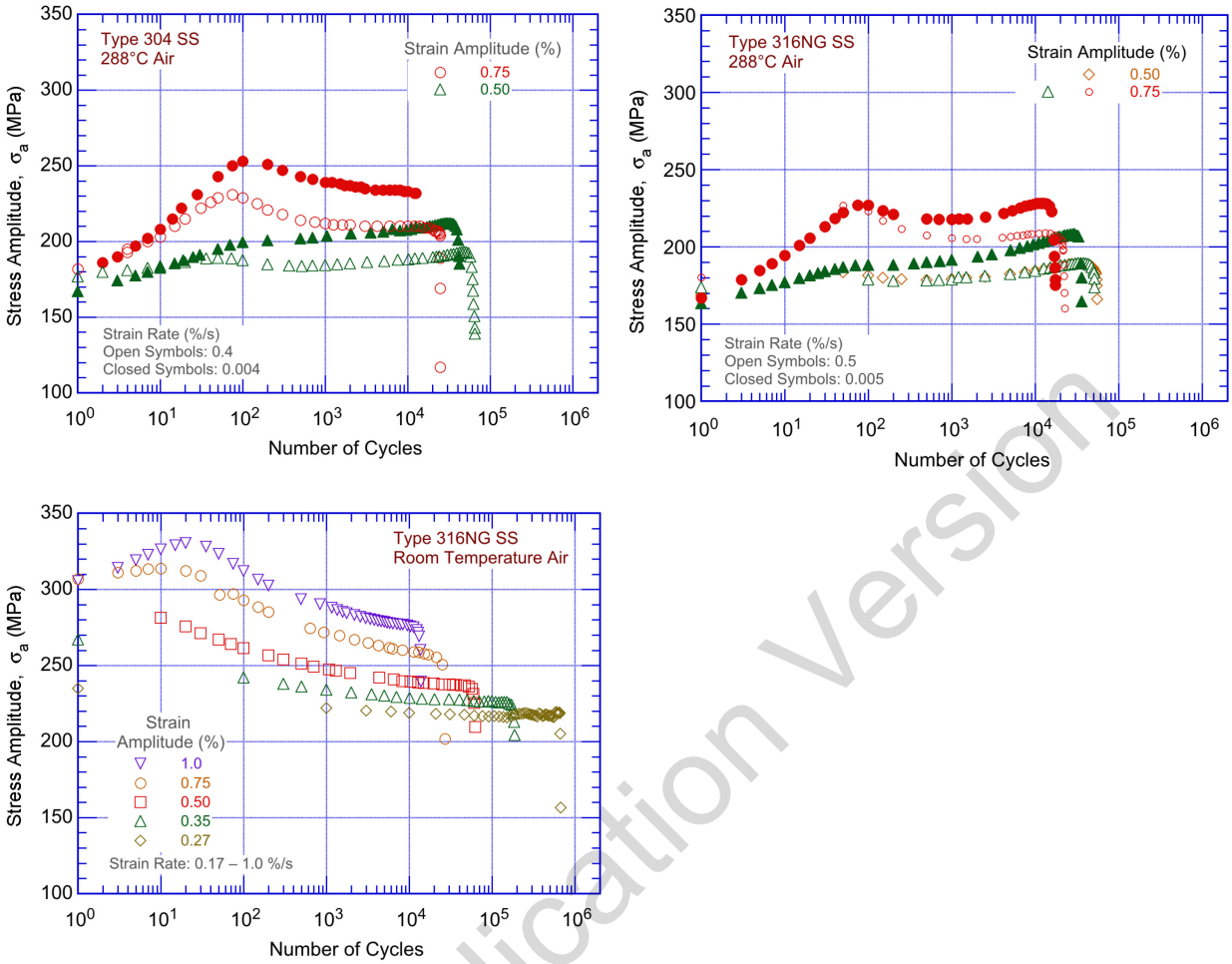

Figure 3-16 Effects of strain amplitude, temperature, and strain rate on cyclic strain–hardening behavior of Types 304 and 316NG SSs in air at 288°C and room temperature.

3.2.5 Cyclic Strain Hardening Behavior

Under cyclic loading, austenitic SSs exhibited rapid hardening during the first 50 to 100 cycles. As shown in Figure 3-16, the extent of hardening increased with increasing strain amplitude and decreasing temperature and strain rate.[45] The initial hardening was followed by a softening and saturation stage at high temperatures and by continuous softening at room temperature.

Figure 3-17 shows the cyclic stress vs. strain curves for Types 316, 304, and 316NG SSs at room temperature and 288°C. In this figure, cyclic stress corresponds to the value at half-life at a strain rate of 0.4%/s. For the various steels, cyclic stresses increased in magnitude in the following order: Types 316NG, 304, and 316.[45]

- *Cyclic strain hardening behavior influenced the fatigue lives of SS materials. The ASME Code accounted for variations in fatigue lives due to such effects by applying the factor of 2 on stress to obtain the design air curve from the mean-data air curve.*

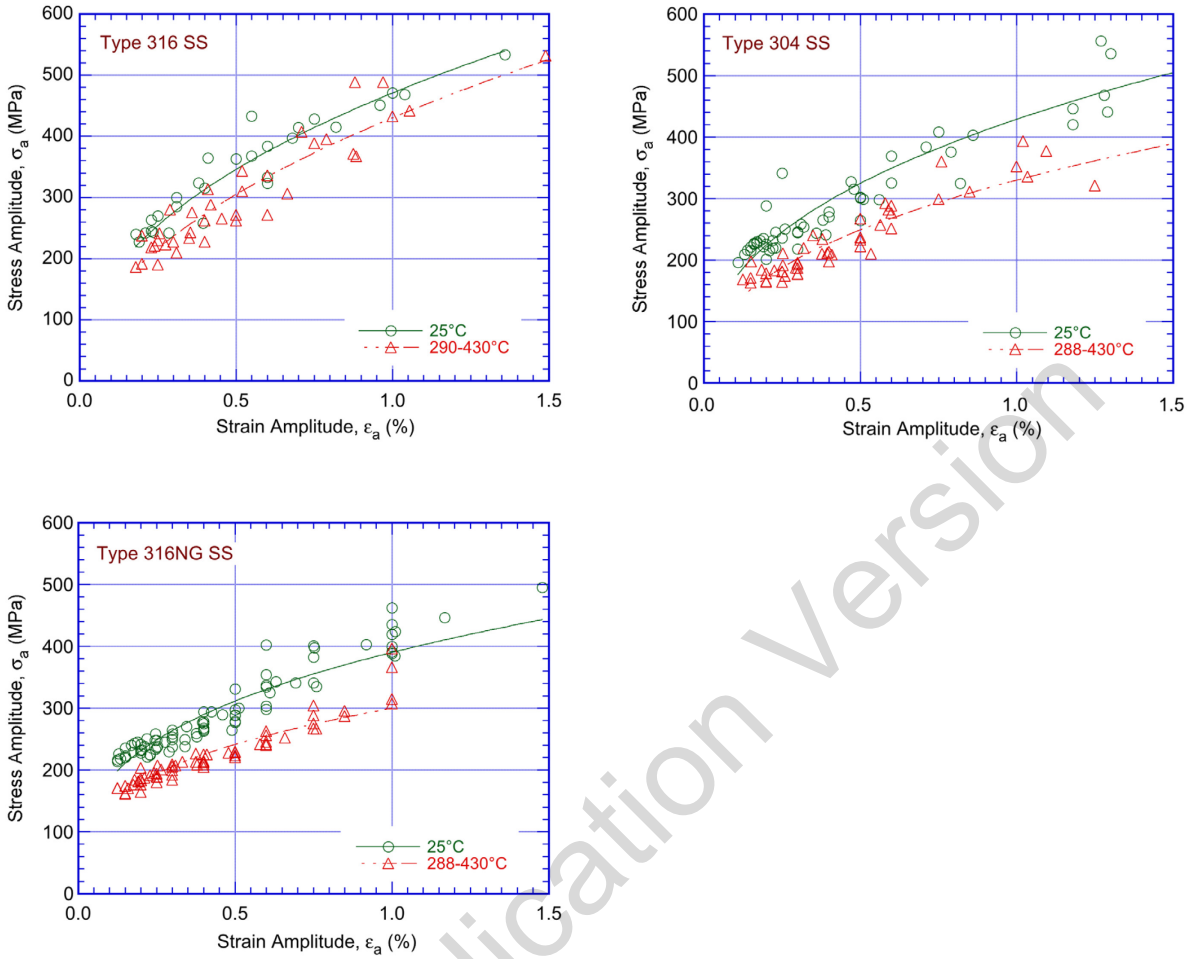

Figure 3-17 Cyclic stress-strain curves for Types 316, 304 and 316NG SSs in air at room temperature and 288°C.

3.2.6 Fatigue Life Model

In the original version of NUREG/CR-6909,[137] an updated version of the PVRC database was used to develop the best-fit mean air curve for austenitic SSs. The sources were listed in Table 1 of the report. The data were obtained on smooth specimens tested under strain-controlled conditions with fully reversed loading (i.e., R = -1) in compliance with consensus standard approaches used for the development of such data. The database consisted of 520 tests on Types 304, 316, 304L, 316L and 316NG SSs; approximately 220 of the tests were for Type 304 SS; 150 tests were for Type 316 SS; and 150 tests were for Types 316NG, 304L, and 316L SSs. The austenitic SSs used in these studies complied with the compositional and strength requirements of ASME Code specifications. The best-fit methodology described in Section 3.1.6 for carbon and low-alloy steels was also used for the analysis of the fatigue ε–N data for austenitic SSs.

Several different best-fit mean ε–N curves for austenitic SSs were previously proposed in the literature. Examples include Jaske and O'Donnell,[61] Diercks,[224] Chopra,[45] Tsutsumi et al.,[34] and Solomon and Amzallag.[225] These curves differ by up to 50%, particularly in the regime of 10^4 to 10^7 cycles. The constant C in Equation 6 (related to the fatigue limit of the material) varied from

a value of 0.110 proposed by Tsutsumi et al., a value of 0.112 proposed by Jaske and O'Donnell, and a value of 0.167 proposed in the original ASME Code Section III mean air curve. The differences primarily occurred because different databases were used in developing these models for the mean ε–N curves. The analyses by Jaske and O'Donnell and by Diercks were based on Jaske and O'Donnell's data.

Tsutsumi et al. used the JNUFAD data, which are included in the JNES database.[136] In the original version of NUREG/CR-6909, the updated PVRC data were analyzed to develop the ANL model for austenitic SSs; the updated PVRC data included the JNUFAD database. In addition, unlike the earlier ANL reports that proposed separate expressions for high-carbon and low-carbon grades of SSs, a single expression was developed for the fatigue ε–N behavior of austenitic SSs. The model assumed that fatigue lives in air were independent of temperature and strain rate. Consistent with the models proposed by Tsutsumi et al.[34] and by Jaske and O'Donnell,[61] the value of the constant C in the modified Langer equation (Equation 6) was lower than that in earlier reports (i.e., 0.112 instead of 0.126). The proposed curve yielded an R^2 value of 0.851 when compared with the updated PVRC data; the R^2 values for the mean curves derived by Tsutsumi et al., Jaske and O'Donnell, and the ASME Code were 0.839, 0.826, and 0.568, respectively.

In air at temperatures up to 400°C, the fatigue lives for Types 304, 304L, 316, 316L, and 316NG SSs were represented by the following expression:

$$\ln(N) = 6.891 - 1.920 \ln(\varepsilon_a - 0.112) \quad (29)$$

where ε_a is applied strain amplitude (%). Figure 3-18 plots the experimental values of fatigue lives and those predicted by Equation 29 for austenitic SSs in air. The predicted lives showed good agreement with the experimental values; for most tests, the differences between the experimental and predicted values were within a factor of 3. For some tests, the observed fatigue lives at low strain amplitudes (i.e., amplitudes that yielded fatigue lives greater than $5x10^4$ cycles) were significantly longer than the predicted values.

- *The ANL fatigue life model for austenitic SSs represents mean values of fatigue lives in air. The effects of parameters (such as mean stress, surface finish, size and geometry, and loading history) known to influence fatigue lives were accounted for in the factors of 12 on life and 2 on stress that were applied to the mean-data air curve to obtain the fatigue design air curve.*

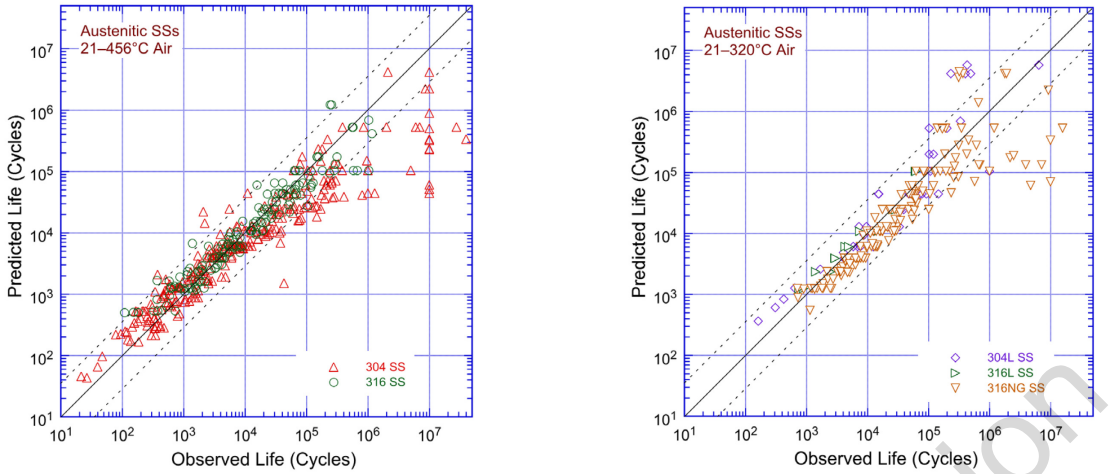

Figure 3-18 Experimental and predicted fatigue lives (using the ANL model) for austenitic SSs in air.

3.2.7 Heat-to-heat Variability

The effects of material (heat-to-heat) variability and data scatter were included in the fatigue model to ensure that the design curves adequately describe both the available test data and the fatigue lives of the much larger number of heats of materials found in the field compared to the limited numbers of heats tested in the laboratory. As mentioned earlier for carbon and low-alloy steels, heat-to-heat variability and data scatter in the fatigue ε–N data for austenitic SSs were also evaluated by considering the best–fit curves determined from tests on individual heats of materials or loading conditions as samples of the much larger population of heats of materials and service conditions of interest. The fatigue lives of each of the heats or loading conditions were characterized by the value of the constant A in Equation 6. The values of A for the various datasets were rank-ordered, and median ranks were used to estimate the cumulative distribution of A for the population. The distributions were fit to lognormal curves. Figure 3-19 shows the estimated cumulative distributions of constant A in the ANL model for fatigue lives of heats of wrought and cast austenitic SSs included in the original version of NUREG/CR-6909 and those included in this report. Note that the new updated database used in this report consisted of 622 data points, which is a significant increase (74%) compared to the 357 data points used in the original version of NUREG/CR-6909. The data were obtained on five types of austenitic SSs, four types of associated SS weld metals, and one type of cast austenitic SS. There are a total of 86 different heats of these materials.

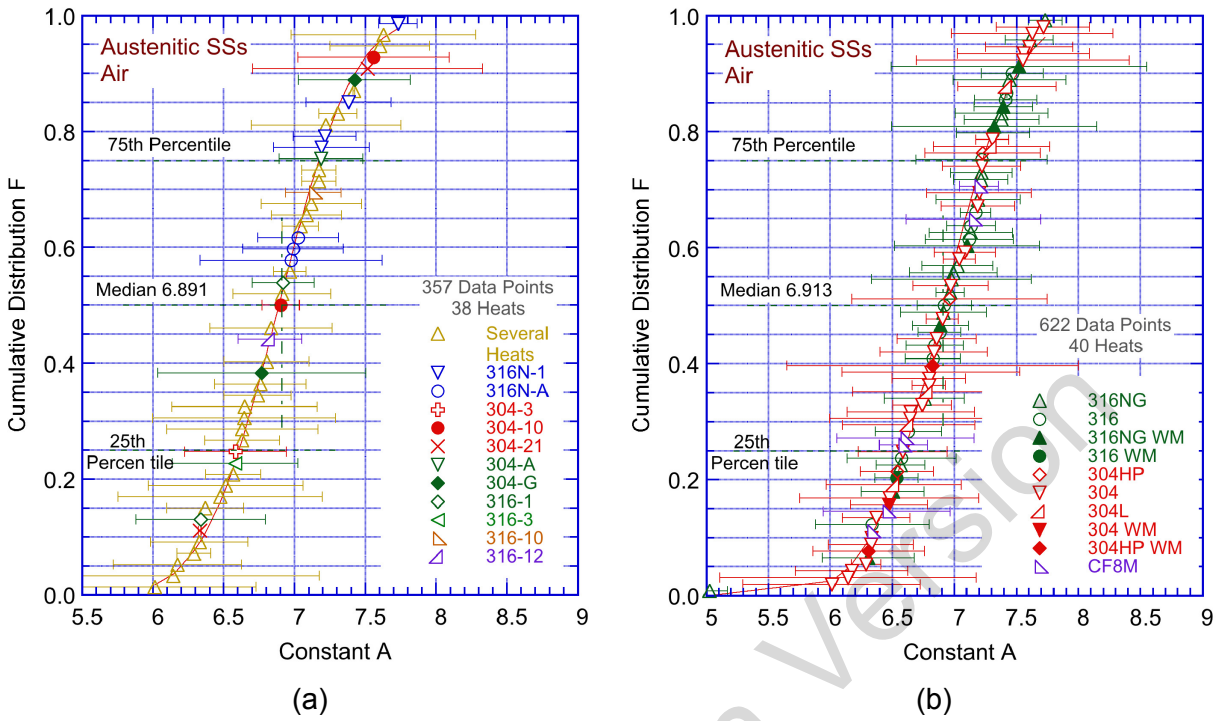

Figure 3-19 Estimated cumulative distribution of constant A in the ANL model for fatigue lives for heats of austenitic SSs in air included in (a) the original version of NUREG/CR 6909 and (b) those included in this report.

The results of the reanalysis indicated that the ANL fatigue model presented in the original version of NUREG/CR-6909 for predicting fatigue lives of austenitic SSs in air was adequate and remains representative of the updated (larger) database. Despite the significant increase in data, the reanalysis of the much larger updated database yielded an insignificant change in the median value of the constant A in Equation 6. The constant A increased from 6.891 to 6.913. In addition, Figure 3-19 indicates that the various heats of wrought austenitic SSs and the associated SS weld metals were evenly distributed about the median value of constant A. The few heats of CF–8M cast austenitic SS were in the 15th to 30th percentile of the data (i.e., the fatigue lives of the heats of CF–8M were lower than the average values for austenitic SSs). However, this does not necessarily indicate that cast CF–8M materials have marginally lower fatigue lives than the average wrought SS material. This behavior is representative for this specific sample. Additional fatigue ε–N data are needed on cast austenitic SSs to better establish the typical fatigue behavior of cast SS materials.

The values of the constant A that describe the 5th percentile of the statistical distributions produced a fatigue ε–N curve that bounded the fatigue lives of 95% of the heats of austenitic SSs. A Monte Carlo analysis was performed to address the data uncertainties in the median value and standard deviation of the sample used for the analysis. For austenitic SSs, Table 3-7 summarizes the values for A that provided bounds for the portion of the population and the confidence that was desired in the estimates of the bounds. Because the reanalysis summarized in Figure 3-19 and Table 3-7 indicated that the constant A did not change significantly from the original version of NUREG/CR-6909, the median value of the constant A for austenitic SSs remains 6.891, and was not changed in this report. Also from Table 3-7, the 95/95 value of the factor to account for material variability and data scatter is 2.3 on life. This factor is needed to provide reasonable confidence that the resultant lives are greater than those

observed for 95% of the SS materials of interest. Note that a relatively large value of 2.3 for the adjustment factor for material variability and data scatter is due to the fact that the ASME Code fatigue design curve for SSs is applicable to a wide range of material grades; heat-treatments; and compositions, particularly the low-C and high-C grades of SSs.

Table 3-7 Values of Constant A in the ANL Fatigue Life Model for Austenitic SSs and the Factors on Fatigue Lives for Austenitic SSs in Air as a Function of Confidence Level and Percentage of the Population Bounded.

Confidence Level	Percentage of Population Bounded (Percentile Distribution of A)				
	95 (5)	90 (10)	75 (25)	67 (33)	50 (50)
			Values of Constant A		
50	6.205	6.356	6.609	6.707	6.891
75	6.152	6.309	6.569	6.668	6.851
95	6.075	6.241	6.510	6.611	6.793
			Factors on Life		
50	2.0	1.7	1.3	1.2	1.0
75	2.1	1.8	1.4	1.2	1.0
95	2.3	1.9	1.5	1.3	1.1

- *The mean-data air curve for austenitic SSs used to develop the fatigue design air curve represented the average fatigue behavior; heat-to-heat variability was included in the subfactor that was applied to the mean-data air curve to obtain the fatigue design air curve to account for "data scatter and material variability."*

3.2.8 Fatigue ε–N Behavior of Cast Austenitic Stainless Steels

Available fatigue ε–N data[29,34,43,45] indicated that the fatigue lives of cast CF–8M SSs in air were similar to those of wrought austenitic SSs. Figure 3-20 plots the fatigue ε–N data for CF–8M cast austenitic SS in air, at temperatures between room temperature and 325°C. The results indicated that the fatigue lives of cast SSs were evenly distributed along the ANL best-fit curve for the mean data for wrought austenitic SSs.

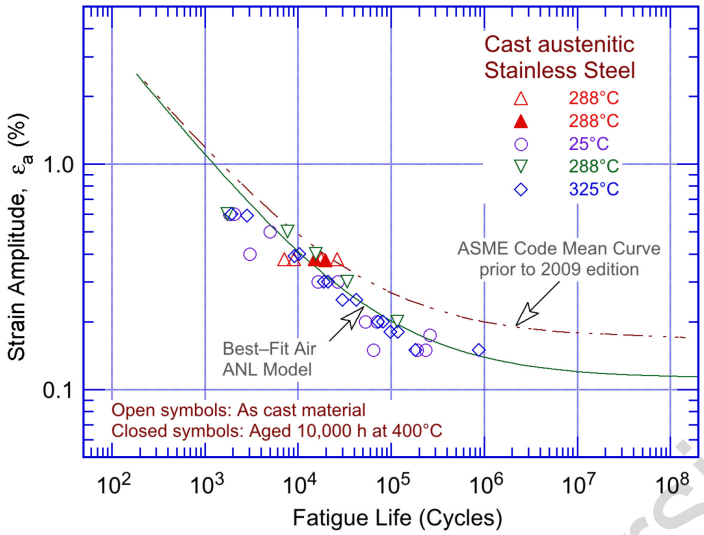

Figure 3-20 Fatigue ε–N behavior for several heats of CF-8M cast austenitic SSs in air at various temperatures.

The effects of thermal aging at 250–400°C on the fracture toughness properties of cast austenitic SSs are well established. Fracture toughness decreased significantly after thermal aging because of the spinodal decomposition of the ferrite phase to form a Cr-rich α' phase.[229-232] The cyclic-hardening behavior of cast austenitic SSs was also influenced by thermal aging.[45] The spinodal decomposition of the ferrite phase during thermal aging at 400°C strengthened the ferrite phase and increased cyclic hardening. At 288°C, cyclic stresses of cast SSs aged for 10,000 hours at 400°C were higher than those for unaged material or wrought SSs. The existing data were too sparse to establish the effects of thermal aging on strain-rate effects on the fatigue lives of cast SSs in air.

- *The fatigue mean-data air curve for wrought austenitic SSs may be used for cast austenitic SSs.*

3.2.9 Fatigue ε–N Behavior of Weld Metals

Figure 3-21 plots available fatigue ε–N data for Types 304, 304HP (i.e., high purity), 316, and 316NG weld metals in air at room temperature. The results indicated that the fatigue lives of SS weld metals were slightly lower than the mean ε–N air curve for austenitic SSs in the low-cycle fatigue regime (i.e., fatigue lives less than 10^4 cycles) and generally longer in the high-cycle regime. However, the weld metal data were within the scatter band for the various grades and heats of austenitic SSs such that the differences between the weld and base materials are not significant enough to warrant a separate weld metal curve without the development of additional data.

- *The limited fatigue ε–N air data indicate that the mean-data air curve for wrought austenitic SSs may be used for SS weld metals.*

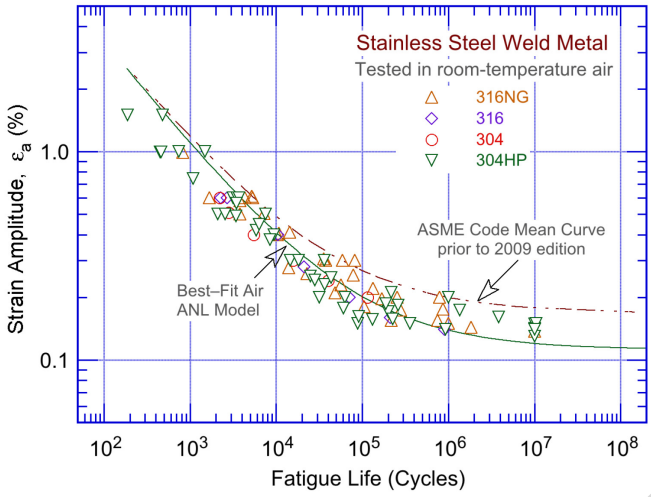

Figure 3-21 Fatigue ε–N behavior for austenitic SS weld metals in air at room temperature.

3.2.10 Surface Finish

Fatigue tests were conducted on Types 304 and 316NG SS specimens that were intentionally roughened in a lathe under controlled conditions with 50-grit sandpaper to produce circumferential scratches with an average surface roughness of 1.2 μm.[46] Figure 3-22(a) and (b) show the results for Types 316NG and 304 SS, respectively. For both steels, the fatigue lives of the roughened specimens were a factor of approximately 3 lower than those of the smooth specimens.

- *The effect of surface finish was included as part of the "surface finish and environment" subfactor that was applied to the mean-data air curve to obtain the fatigue design air curve for austenitic SSs."*

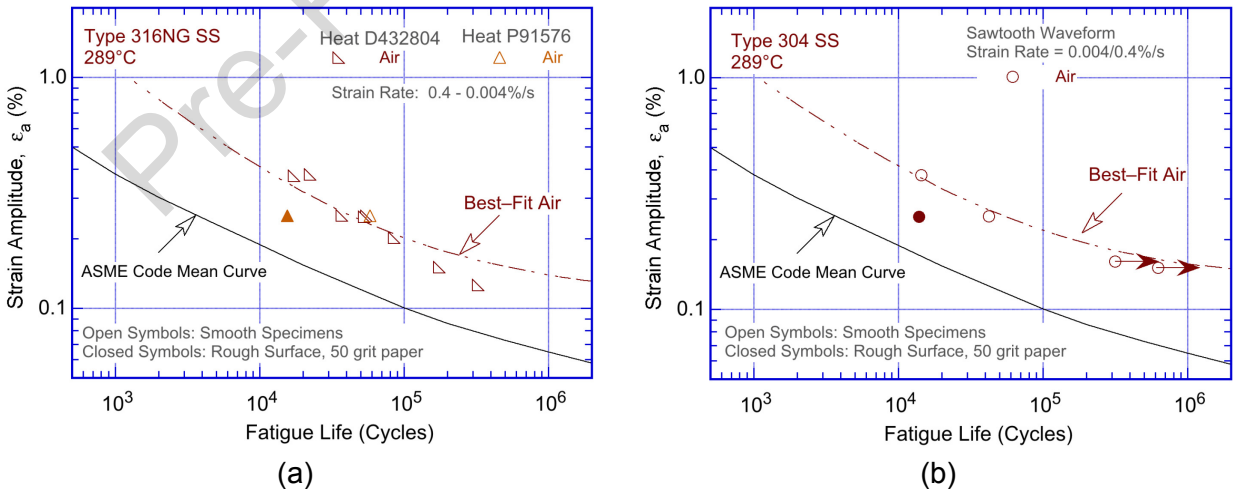

Figure 3-22 Effects of surface roughness on fatigue lives of (a) Type 316NG and (b) Type 304 SSs in air (Ref. 46).

3.2.11 Fatigue Design Curve

As discussed in Section 3.2.1, the ASME Code mean data that were used to develop the current ASME Code Section III fatigue design air curve were not consistent with the existing fatigue ε–N data. Therefore, a fatigue design air curve that was consistent with the existing database was derived from the ANL model (Equation 29) by following the same procedure that was used to develop the ASME Code Section III fatigue design air curve. The discussion presented in Section 5.5 indicated that the current ASME Code Section III requirement for a factor of 20 on cycles to account for the effects of material variability and data scatter, specimen size, surface finish, and loading history was conservative by at least a factor of 1.7. Therefore, to reduce this conservatism, an fatigue design air curve based on the ANL model for austenitic SSs (Equation 29) was developed by correcting for mean-stress effects using the modified Goodman relationship and then by lowering the mean-stress-adjusted curve by a factor of 2 on stress and 12 on cycles, whichever was more conservative. The resulting fatigue design air curve and the fatigue design air curve in ASME Code Section III before publication of the 2009 Addenda were presented in the original version of NUREG/CR-6909. The two fatigue design air curves were identical beyond 10^8 cycles. In 2009, the new fatigue design air curve that was based on the ANL model for austenitic SSs was adopted into Mandatory Appendix I of ASME Code Section III. Figure 3-23 shows both of the ASME Code Section III air fatigue design air curves,[D] and Table 3-8 lists the values of stress amplitude vs. cycles for the current and the proposed design air curves.

- *A new fatigue design air curve for austenitic SSs that is consistent with the existing data was developed from the ANL model using factors of 12 on life and 2 on stress. This curve is the same as the ASME Code Section III fatigue design air curve implemented in 2009.*

Table 3-8 The ASME Code Fatigue Design Curves for Austenitic SSs in Air.

No. of Applied Cycles	Stress Amplitude MPa (ksi)	
	Current ASME Code Design Curve	ASME Code Design Curve Prior to 2009
1 E+01	6000 (870)	4881 (708)
2 E+01	4300 (624)	3530 (512)
5 E+01	2748 (399)	2379 (345)
1 E+02	1978 (287)	1800 (261)
2 E+02	1440 (209)	1386 (201)
5 E+02	974 (141)	1020 (148)
1 E+03	745 (108)	820 (119)
2 E+03	590 (85.6)	669 (97.0)
5 E+03	450 (65.3)	524 (76.0)
1 E+04	368 (53.4)	441 (64.0)
2 E+04	300 (43.5)	383 (55.5)
5 E+04	235 (34.1)	319 (46.3)
1 E+05	196 (28.4)	281 (40.8)
2 E+05	168 (24.4)	248 (35.9)
5 E+05	142 (20.6)	214 (31.0)
1 E+06	126 (18.3)	195 (28.3)
2 E+06	113 (16.4)	157 (22.8)
5 E+06	102 (14.8)	127 (18.4)
1 E+07	99 (14.4)	113 (16.4)
2 E+07		105 (15.2)
5 E+07		98.6 (14.3)
1 E+08	97.1 (14.1)	97.1 (14.1)
1 E+09	95.8 (13.9)	95.8 (13.9)
1 E+10	94.4 (13.7)	94.4 (13.7)
1 E+11	93.7 (13.6)	93.7 (13.6)

[D] Because the data used in developing the fatigue design curve (Figure 3-23) were obtained from strain-controlled tests, the fatigue ε–N curve is valid up to 371°C, as stated in the figure. However, when converting the strain to a pseudo-stress, the elastic modulus used for the conversion should be a function of temperature as required by ASME Code Section III.

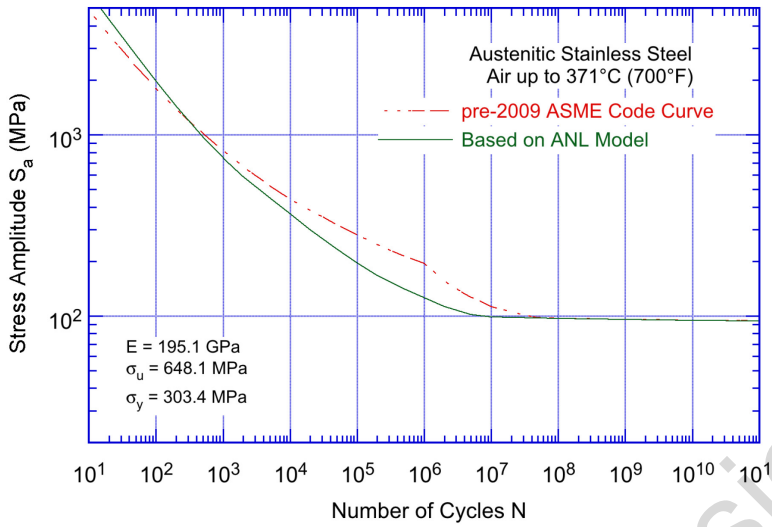

Figure 3-23 Fatigue design curves for austenitic SSs in air.

3.3 Ni-Cr-Fe Alloys and Weld Metals

The relevant fatigue ε–N data in air environments for Ni-Cr-Fe alloys, their weld metals, and limited Alloy 800 heats, include the data compiled by Jaske and O'Donnell[61] for developing fatigue design criteria for pressure vessel alloys; the JNES database from Japan, which included studies by Mitsubishi Heavy Industries (MHI), Ishikawajima-Harima Heavy Industries (IHI), and Hitachi;[39,136,210] studies by Bettis Atomic Power Laboratory,[70] Knolls Atomic Power Laboratory,[67,68] the National Aeronautics and Space Administration (NASA),[73] Battelle's Columbus Laboratories,[69] and GE;[71,72,14] work sponsored by EPRI at Westinghouse Electric Corporation,[66] and the tests performed by Van Der Sluys et al.[75] The database comprises 588 tests from which 559 data points were obtained—191 data points for 17 heats of Alloy 600, 17 data points for 3 heats of Alloy 690, 23 data points for 2 heats of Alloy 800, 196 data points for 7 heats of Alloy 718; and 140 tests of Ni-Cr-Fe weld metals from which 132 data points were obtained for 1 heat of Alloy 690 weld metal, 5 heats of Alloy 82 weld metal, 4 heats of Alloy 182 weld metal, and 6 heats of other Ni-Cr-Fe weld metals. Out of these, 427 data points were obtained from tests conducted at room temperature, 40 data points were obtained from tests conducted at 260–316°C, and 92 data points were obtained from tests conducted at 427°C. Table 3-9 summarizes the sources included in the updated database used for this report, as categorized by material type and test environment. Appendix B provides other material information such as chemical composition, heat treatment, and room temperature tensile properties of these various alloys and associated weld metals.

Table 3-9 Sources of the Fatigue ε–N Data in an Air Environment for Ni Cr Fe Alloys, Their Weld Metals, and Limited Alloy 800 Heats.

ANL Mat. ID	Material Heat Designation[a]	Monotonic Yield Strength (MPa)	Test Temperature (°C)	No. of Data Points	Source	Applicable Reference
Alloy 600						
1	Alloy 600-1	310	25	12	JNES (Higuchi)	136
2	Alloy 600-2	294	25	9	JNES (Nakao),	136
3	Alloy 600-3	-	25	6	JNES (Hirano),	136
4	Alloy 600-4	289	25	6	JNES (Hirano)	136
5	Alloy 600-5	264	25	11	JNES (Hirano)	136
6	Alloy 600-6	303	25	6	JNES (Kanasaki)	136
7	Alloy 600-7	253	24, 93, 204, 316	5, 5, 10, 7	KAPL (Dinerman)	67
8	Alloy 600-8	-	24	8[a]	KAPL (Mowbray)	68
9	Alloy 600-9	-	24	10[a]	KAPL (Mowbray)	68
10	Alloy 600-10	-	24	8[a]	KAPL (Mowbray)	68
11	Alloy 600-11	-	24	13[a]	KAPL (Mowbray)	68
12	Alloy 600-12	-	24	7[a]	KAPL (Mowbray)	68
13	Alloy 600-13	-	24, 316	9, 9	EPRI (Jacko)	66
14	Alloy 600-14	-	21	19	Bettis (McGowan&Faber)	70
15	Alloy 600-15	386	260	6	GE (Hale)	14
16	Alloy 600-16	-	21	15	Jaske & O'Donnell	61
17	Alloy 600-17	-	24, 83	5, 5	Jaske & O'Donnell	61
Alloy 690						
20	Alloy 690-1	280	25	6	JNES (Kanasaki)	136
21	Alloy 690-2	-	25	5	PVP (Higuchi)	39
22	Alloy 690-3	-	315	6	PVP (Van der Sluys)	75
Alloy 800						
25	Alloy 800-1	-	21	7	BMI (Jaske et al.)	69
26	Alloy 800-2	-	427	6, 10	BMI (Jaske et al.), GE (Conway)	69,71
Alloy 718						
30	Inconel 718-1	-	21	18	ASME Data File	210
31	Inconel 718-2	-	21	4	J. Miller (J of Mat.)	72
32	Inconel 718-3	-	24, 427	17, 31	ASME Data File	61
33	Inconel 718-4	-	24, 427	30, 10	ASME Data File	61
34	Inconel 718-5	-	21, 427	34, 4	ASME Data File	61
35	Inconel 718-6	-	27, 427	12, 8	ASME Data File, NASA (Natchigall)	61,73
36	Inconel 718-7	-	22, 427	5, 23	ASME Data File	61
Ni-Cr-Fe Alloy Weld Metals						
38	Alloy 690 WM	431	25	6	JNES (Kanasaki)	136
39	Alloy 62	-	24	9[a]	KAPL (Mowbray)	68
40	Alloy 82-1	-	24	8[b]	KAPL (Mowbray)	68
41	Alloy 82-2	-	24	8[a]	KAPL (Mowbray)	68
42	Alloy 82-3	-	24	17[a]	KAPL (Mowbray)	68
43	NiCrFe WM-1	-	24	9	Higuchi, Iida	SGFS 1988
44	Arcaloy 8N12	-	24	6[a]	KAPL (Mowbray)	68

ANL Mat. ID	Material Heat Designation[a]	Monotonic Yield Strength (MPa)	Test Temperature (°C)	No. of Data Points	Source	Applicable Reference
45	NiCrFe WM-2	-	25	9, 5	JNUFAD (Higuchi, Nakao)	210
46	Alloy 82-4	322	260	7	KAPL (Mowbray)	68
47	Alloy 182-1	-	25	13	PVP (Higuchi)	39
48	Alloy 182-2	456	290	7	JNES (Higuchi)	136
49	Alloy 182-3	405	25	5	JNES (Nakao)	136
50	Alloy 182-4	409	25	6	JNES (Kanasaki)	136
51	Alloy 82-5	339	315	5	PVP (Van der Sluys)	75
52	Alloy 152	-	25	6	PVP (Higuchi)	39
53	Alloy 132	-	25	6	PVP (Higuchi)	39

[a] The tests were performed under bending fatigue.

[b] Six tests performed under bending fatigue, and four were performed under rotating bending.

3.3.1 Experimental Data

Figure 3-24 shows the fatigue ε–N data for Ni-Cr-Fe alloys such as Alloys 600, 690, and Alloy 800 in air at temperatures between room temperature and 427°C. Figure 3-25 presents the fatigue ε–N data for Alloys 62, 82, 132, 152, 182, and other Ni-Cr-Fe alloy weld metals in air at temperatures between room temperature and 315°C. Figure 3-26 shows the fatigue ε–N data for Inconel 718 in air at room temperature and 427°C. Fatigue CUF evaluations for Ni-Cr-Fe alloy and Alloy 800 components are performed using the fatigue design air curve for austenitic SSs because ASME Code Section III does not have a separate curve for these materials. Therefore, these three figures include the best–fit air curve for austenitic SSs based on the ANL model (Equation 29 in Section 3.2.6). The results indicated that, although the data for Alloys 690 and 800 are limited, the fatigue lives of these alloys were comparable to those of Alloy 600 (Figure 3-24). The fatigue ε–N data for Ni-Cr-Fe alloy weld metals indicated that the fatigue lives of the various weld metals were comparable, although the data for Alloy 82 at 260 to 315°C showed significant scatter (Figure 3-25).

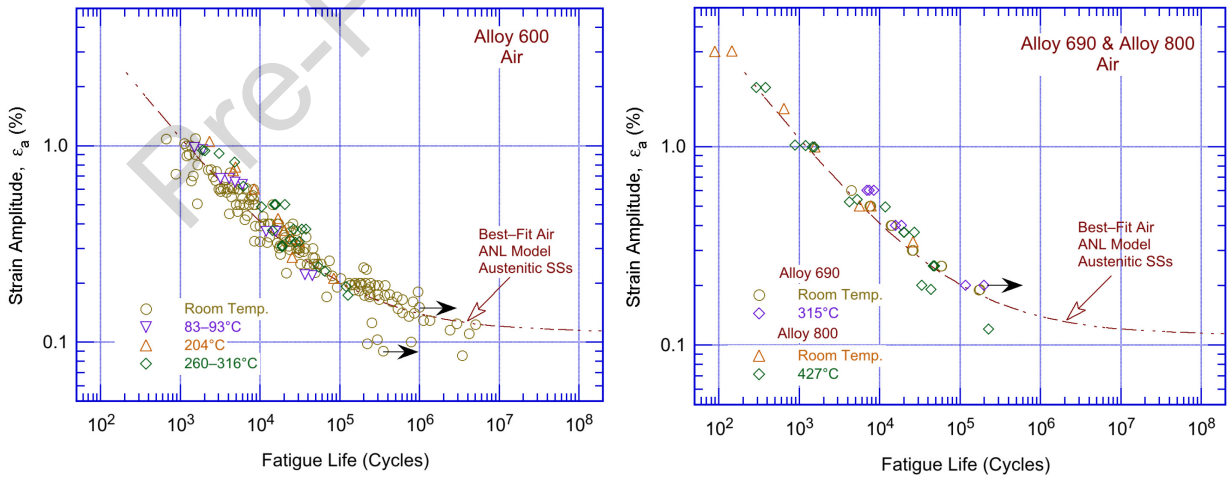

Figure 3-24 Fatigue ε–N behavior for Alloys 600, 690 and 800 in air at temperatures between room temperature and 427°C (Refs. JNUFAD data, 61, and 66–75).

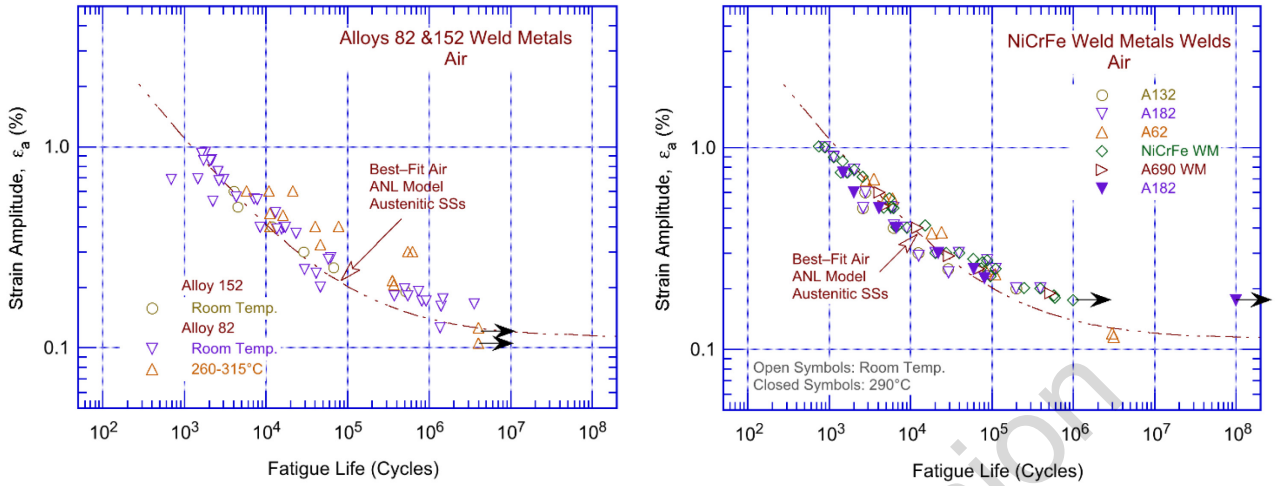

Figure 3-25 Fatigue ε–N behavior for Alloys 62, 82, 132, 152 and 182 welds in air at various temperatures (Refs. JNUFAD data, 61, and 66–75).

The fatigue lives of the Ni-Cr-Fe alloy weld metals were comparable to those of the wrought Alloys 600 and 690 in the low-cycle regime (i.e., less than 10^5 cycles) and were slightly superior to the lives of wrought materials in the high-cycle regime. The results also indicated that the fatigue limit for the weld metals was higher than that for wrought materials. Overall, the available fatigue ε–N data indicated that the fatigue lives of Ni-Cr-Fe alloys and Alloy 800 were represented by the fatigue design air curve for austenitic SSs; however, fatigue evaluations for Ni-Cr-Fe weld metals were conservative using these curves.

The fatigue ε–N data in Figure 3-26 indicate that the fatigue lives of Inconel 718 were greater than those for austenitic SSs and other Ni-Cr-Fe alloys and their weld metals, particularly at strain amplitudes less than 0.5% (i.e., in the high-cycle regime). The fatigue limit for Inconel 718 was much higher than that of austenitic SSs. Therefore, fatigue analyses for Inconel 718 that used the fatigue design air curve for austenitic SSs yielded conservative estimates of fatigue usage. To avoid this conservatism, Jaske and O'Donnell proposed the following expression for fatigue lives of Inconel 718 in air,

$$\ln(N) = 6.859 - 2.0 \ln(\varepsilon_a - 0.210). \quad (30)$$

Figure 3-26 also shows the Jaske and O'Donnell best-fit air curve for Inconel 718.

The available fatigue ε–N data for Ni-Cr-Fe alloys also indicated that, unlike austenitic SSs that do not show temperature dependencies of fatigue lives under LWR operating conditions, the fatigue lives of Alloy 600 were generally longer at high temperatures compared to those at room temperature, particularly for Alloy 82 weld metal (Figure 3-25(a)).[66-68] Similar behavior was observed for Inconel 718 (Figure 3-26). However, limited data for Alloy 690 (Figure 3-24(b)) and Alloys 62, 132, 182, and 690 weld metals (Figure 3-25(b)), indicated little or no effects of temperature on their fatigue lives. The existing data were insufficient to adequately determine the effect of strain rate on the fatigue lives of Ni-Cr-Fe alloys.

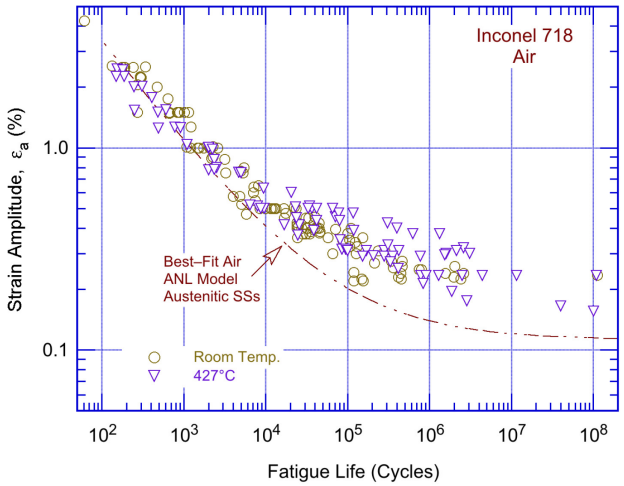

Figure 3-26 Fatigue ε–N behavior for Inconel 718 in air at room temperature and 427°C (Refs. 61, 72, 73, 136, and 210).

Overall, the results indicated that the best-fit mean air curve for austenitic SSs adequately represented the available fatigue ε–N data of Ni-Cr-Fe alloys, their weld metals, and Alloy 800 in the low-cycle regime (i.e., fatigue lives less than $5x10^4$ cycles) while these curves provided slightly conservative estimates of the fatigue lives for Ni-Cr-Fe alloys in the high-cycle regime (i.e., fatigue lives greater than $5x10^4$ cycles), particularly for Ni-Cr-Fe alloy weld metals. However, the best-fit mean-data curve for austenitic SSs yielded very conservative estimates of fatigue lives for Inconel 718 for fatigue lives greater than 10^4 cycles. A separate fatigue ε–N curve is needed within ASME Code Section III to reduce this conservatism and better represent the fatigue behavior of Inconel 718. In the interim, the fatigue design air curve for austenitic SSs for austenitic SSs in ASME Code Section (or equivalently the SS fatigue design air curve for austenitic SSs in this report) can be conservatively used for Inconel 718.

- *For Ni-Cr-Fe alloys and their welds, the ANL fatigue life air model proposed in this report for austenitic SSs (Equation 29) was either consistent or conservative with respect to the fatigue ε–N data. This curve is significantly conservative for Inconel 718.*

3.3.2 Fatigue Life Model

For Ni-Cr-Fe alloys (and Alloy 800), fatigue evaluations are based on the fatigue design air curve for austenitic SSs because it also applies to Ni-Cr-Fe alloys in ASME Code Section III. The rather limited fatigue ε–N data for Ni-Cr-Fe alloys (such as Alloys 600, 690, and 800 and their welds) were consistent with the best-fit mean air curve for austenitic SSs for fatigue lives less than 10^4 cycles. The data also showed longer fatigue lives than the estimated values for fatigue lives greater than 10^4 cycles. The data were comparable or slightly conservative with respect to the ANL model for austenitic SSs (e.g., Equation 29). Estimates of the cumulative distribution of constant A in the fatigue ε–N curve for the various heats of Alloys 600, 690, and 800, and their associated weld metals, yielded a median value of 7.129. This value was slightly greater than the value of constant A derived for austenitic SSs. In other words, the fatigue lives of these Ni-Cr-Fe alloys (and Alloy 800) were approximately 25% greater than those for austenitic SSs. Based on these findings, the current ASME Code Section III fatigue design air curve for austenitic SSs, which is the same as the ANL model presented in Figure 3-23 and

Table 3-8, appropriately represented (albeit slightly conservatively) the fatigue ε–N behavior of Ni-Cr-Fe alloys and their welds.

- *The ASME Code Section III fatigue design air curve for austenitic SSs, which is the same as the ANL air model for austenitic SSs, is applicable for Ni-Cr-Fe alloys, their welds, and Alloy 800. The current design fatigue air curve for austenitic SSs yielded conservative estimates of fatigue lives for Inconel 718.*

4 FATIGUE ε–N BEHAVIOR IN LWR ENVIRONMENTS

Several review articles[118-126] and ANL topical reports[10,12,13,45-47] present an analysis of the existing fatigue strain vs. life (ε–N) data and the procedures for incorporating environmental effects into the American Society of Mechanical Engineers Boiler and Pressure Vessel Code (ASME Code) fatigue evaluations. The key material, loading, and environmental parameters that influenced the fatigue lives of carbon and low-alloy steels and austenitic stainless steels (SSs) were identified, and the ranges of these key parameters where environmental effects were significant were defined. Sections 4.1, 4.2, and 4.3 discuss in detail how various material, loading, and environmental parameters affected fatigue lives and how these effects are incorporated into the ASME Code fatigue evaluations for carbon and low-alloy steels, wrought and cast SSs, and nickel-chromium-iron (Ni-Cr-Fe) alloys. As subsequently discussed, the environmental fatigue correction factor (F_{en}) approach presumes that the slope of the fatigue strain (or stress) vs. life curve is the same in air and water environments. Based on the totality of the data in the report, this assumption appears reasonable. If environmental effects increase with decreasing strain, the use of an adjustment factor would be a function of strain and the concept becomes more complex.

4.1 Carbon and Low-Alloy Steels

Fatigue life models for estimating the fatigue life of carbon and low-alloy steels in light-water reactor (LWR) environments presented in the original version of NUREG/CR-6909, "Effect of LWR Coolant Environments on the Fatigue Life of Reactor Materials—Final Report," issued February 2007, were based on the updated Pressure Vessel Research Council (PVRC) database available at that time. The effects of key parameters, such as temperature, strain rate, dissolved oxygen (DO) content in water, and sulfur content in the steel, were included in the correlations. The functional forms for the effects of strain rate, temperature, DO level in water, and sulfur content in the steel were based on the data trends. For both carbon and low-alloy steels, the model assumed threshold and saturation values of 1.0 and 0.001%/s, respectively, for strain rate; 0.001 and 0.015 weight percent (wt.%), respectively, for sulfur; and 0.04 and 0.5 parts per million (ppm), respectively, for DO. The model also considered a threshold value of 150°C for the temperature below which environmental effects were considered to be insignificant. The fatigue ε–N data in LWR environments were fitted to a modified version of Equation 6 expressed as

$$\ln(N) = A - B \ln(\varepsilon_a - C) + D\, S^*\, T^*\, O^*\, \dot{\varepsilon}^*, \tag{31}$$

where S^*, T^*, O^*, and $\dot{\varepsilon}^*$ are transformed sulfur content, temperature, DO level, and strain rate, respectively, and D is a constant. The slope, B, of the fatigue ε–N behavior in LWR environments was considered to be the same as in air, and the constant C was also considered the same because, as discussed in Section 4.1.3, environmental effects on fatigue were not observed below a threshold strain level. The constants A and D were determined from the best-fit of the fatigue ε–N data in LWR environments. The constant A in the Argonne National Laboratory (ANL) models presented in the original version of NUREG/CR-6909 differed from the value reported earlier in NUREG/CR-6583, "Effects of LWR Coolant Environments on Fatigue Design Curves of Carbon and Low-Alloy Steels," issued February 1998, and NUREG/CR-6815, "Review of the Margins for ASME Code Design Curves—Effects of Surface Roughness and Material Variability," issued September 2003. Relative to the earlier model, the fatigue lives predicted by the updated model in the original version of NUREG/CR-6909 were approximately 6% lower for carbon steels and approximately 2% higher for low-alloy steels.

The effects of water environments on fatigue lives were expressed in terms of an F_{en}, which was defined as the ratio of life in air at room temperature, N_{RTair}, to that in water at the service temperature, N_{water}. Values of F_{en} were obtained from the ANL fatigue life models, where

$$\ln(F_{en}) = \ln(N_{RTair}) - \ln(N_{water}). \quad (32)$$

Thus, because constants B and C are identical in both air and water environments, using Equation 6 for air and Equation 31 for water environment, Equation 32 can be rewritten for carbon and low-alloy steels as

$$\ln(F_{en}) = A_{air} - A_{water} - D_{water}\, S^*\, T^*\, O^*\, \dot{\varepsilon}^*. \quad (33)$$

In the original version of NUREG/CR-6909, fatigue lives in water were different for carbon and low-alloy steels. Therefore, separate F_{en} expressions were developed for carbon steels and for low-alloy steels. The F_{en} expressions developed in the original version of NUREG/CR-6909 for carbon and low-alloy steels are provided in Appendix E, Equations E0.27 and E0.28, respectively, and the transformed parameters are given in Appendix E, Equations E0.22– E0.25.

Section 4.2.7 of the original version of NUREG/CR-6909 notes that the effect of sulfur on the fatigue lives of carbon and low-alloy steels depended on the DO level in water. Therefore, the F_{en} determined from the expressions presented in the original version of the report probably yielded nonconservative estimates of fatigue life for low-sulfur (less than 0.005 wt.%) steels in high-temperature water containing greater than 1 ppm of DO. However, because this behavior was observed in laboratory data at DO concentrations (i.e., 2 ppm) that are much greater than those in LWR environments, the behavior is not likely to be applicable to LWR operating conditions.

During the time since the publication of the original version of NUREG/CR-6909, the U.S. Nuclear Regulatory Commission received several comments from interested stakeholders on the fatigue life models proposed therein. These comments have focused on the constants in the F_{en} expressions, which result in F_{en} values of approximately 2 even at temperatures below 150°C or at very high strain rates. Although this behavior seems inconsistent with the mechanisms that were proposed for environmental fatigue effects (because the calculated cumulative usage factor (CUF) step increases at the time environmental effects are applied), the constants were appropriate based on analyses of the fatigue ε–N data and assumed constraints that were applied in the data reduction and analysis. Figure 4-1 shows the fatigue ε–N behavior for carbon and low-alloy steels in air at room temperature and high-purity water at temperatures below 150°C. These results indicated that in environments of both pressurized-water reactors (PWRs) with low-DO and boiling-water reactors (BWRs) with normal water chemistry (NWC), the fatigue lives of carbon and low-alloy steels were a factor of 2 lower, thereby indicating the need for the constant terms in the F_{en} equations. Another comment received from interested stakeholders was in regards to the temperature range specified in the F_{en} expressions. The maximum temperature limit was specified as 350°C even though data on carbon and low-alloys steels at temperatures above 300°C were sparse.

In this report, the F_{en} expressions presented in the original version of NUREG/CR-6909 for incorporating environmental effects on the fatigue lives of carbon and low-alloy steels have been updated to address the stakeholders' comments using the much larger database described in Section 4.1.1. In LWR environments, the fatigue lives of carbon and low-alloy steels remain dependent on strain rate, DO level, temperature, and sulfur content of the steel. However, because the fatigue life of carbon and low-alloy steels is considered to be the same in

LWR environments, a single F_{en} expression is developed for both carbon and low-alloy steels. The sections below discuss the effects of various material and environmental parameters on the fatigue lives of these materials.

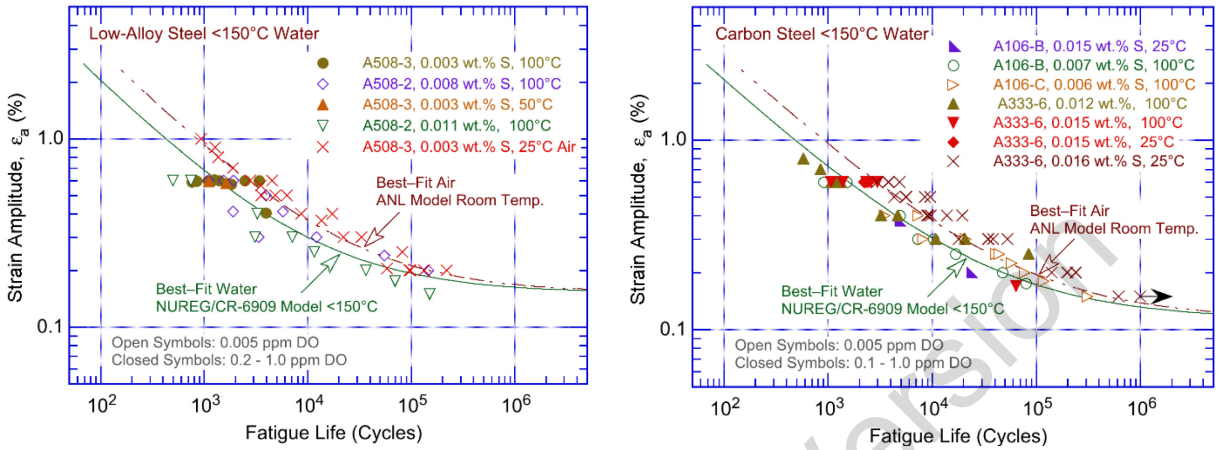

Figure 4-1 Fatigue ε–N behavior for carbon and low alloy steels in air at room temperature and high-purity water at temperatures below 150°C (Ref. 137).

4.1.1 Experimental Data

The primary sources of fatigue ε–N data for carbon and low-alloy steels in LWR environments are the tests performed by General Electric Company (GE) in a test loop at the Dresden Nuclear Power Station, Unit 1 reactor;[14,15] the work of Terrell at Materials Engineering Associates (MEA);[48-50] the work at ANL on fatigue of pressure vessel and piping steels;[10-13,40-47] the large Japan Nuclear Energy Safety Organization (JNES) database[136] that includes studies at Ishikawajima-Harima Heavy Industries, Hitachi, and Mitsubishi Heavy Industries (MHI) in Japan,[18-36] the work at Kraftwerk Union Laboratories (KWU) and Materialprufungsanstalt (MPA) in Germany;[55,56] and some recent investigations by Wu and Katada.[138-144] The database in LWR environments used in this report comprises a total of 1,174 tests, which represented 638 tests on carbon steels and 536 tests on low-alloy steels. The carbon steel tests included 21 heats of A106–Grs. B and C, A333–Gr. 6, A508–Gr. 1, A226 Cl. 4, A516–G70, and A516–KC70 steels. The low-alloy steel tests included 20 heats of A302–Gr. B, A508–Grs. 2 and 3, A533–Gr. B, 15MnNi63, and 17MnMoV64 steels. Table 4-1 summarizes the data sources for the updated database used in this report, as categorized by material type and test environment. Appendix B provides other material information, such as chemical composition, heat treatment, and room temperature tensile properties, for the various types and heats of materials.

Figure 4-2 presents a sampling of fatigue ε–N data on carbon and low-alloy steels in air and high-DO water at 288°C. The figure also shows curves based on the ANL air models (Equations 24 and 25 in Section 3.1.6). The fatigue data in LWR environments indicated a significant decrease in fatigue lives for carbon and low-alloy steels when the following four key threshold conditions were satisfied simultaneously: applied strain range (Δε) above a threshold value, service temperature above a threshold value, DO in the water above a minimum threshold level, and the loading strain rate below a threshold value. The sulfur content of the steel was also an important parameter for environmental effects on the fatigue lives for carbon and low-alloy steels. Although the microstructures and cyclic-hardening behavior of carbon and

low-alloy steels were significantly different, environmental degradation of the fatigue lives for these steels was nearly identical. As shown in Figure 4-2, for both steels, environmental effects on the fatigue lives were moderate for both steels (i.e., a factor of approximately 2 lower) if any one of the key threshold conditions was not satisfied.

Table 4-1 Sources of the Fatigue ε–N Data for Carbon and Low-Alloy Steels in LWR Environments.

ANL Mat. ID	Material Specifications	Sulfur Content (wt.%)	Dissolved Oxygen (ppm)	Test Temperature (°C)	No. of Data Points	Source	Applicable Reference
Carbon Steels							
1	A106-Gr.B[a]	0.015	0.001-8.0	288	35	ANL, JNES (Higuchi)	10-13,136
2	A106-Gr.B	0.007	0.005	100, 290	8, 7	JNES (Kanasaki)	136
3	A106-Gr.B	0.020	0.01	288	18	MEA	48
4	A106-Gr.C (STS480)	0.006	0.005	100, 290	12, 9	JNES (Tsutsumi)	136
5	A106-Gr.C (STS480)	0.020	0.005	290	4	JNES (Tsutsumi)	136
7	A226-Cl.4 (SFVC2B)	0.004	0.05-8.0	289	15	JNES (Hirano)	136
8	A333-Gr.6 (STS42)	0.015	8.0	250	8	JNES (Ishihara)	136
9	A333-Gr.6 (STS42)	0.015	0.01-8.0	100, 150, 200, 250, 290	6, 12, 11, 32, 13	JNES (Higuchi)	136
10	A333-Gr.6 (STS42)	0.014	0.2	288	12	JNES (Higuchi, Emnomoto)	136
11	A333-Gr.6 (STS410)	0.006	8.0	288	5	JNES (Higuchi)	136
12	A333-Gr.6 (STS410)[b]	0.012	0.01-8.0	25, 50, 100, 150, 200, 250, 288/290	1, 3, 18, 19, 22, 13, 62	JNES (Higuchi, Hirano, Kanasaki, Nakao), ANL	136,10-13
14	A333-Gr.6 (STS410)	0.008	0.01-8.0	50, 100, 150, 200, 250, 289/290	2, 1, 5, 5, 5, 105	JNES (Abe, Higuchi, Kanasaki, Hirano)	136
15	A333-Gr.6 (STS410)	0.016	0.01-8.0	100, 200, 250, 289/290	7, 12, 4, 91	JNES (Hirano, Higuchi, Kanasaki)	136
16	A333-Gr.6 (STS410)	0.026	0.05-8.0	289	12	JNES (Hirano)	136
17	A508-Gr.1 (SFVV1)	0.008	8.0	300	14	JNES (Kitagawa)	136
21	A516-KC70	0.033	0.2	260	14[c]	GE	14, 15
22	A516-G70 (SGV480)	0.002	8.0	290	3	JNES (Higuchi)	136
23	CS tube	0.025	0.01-8.0	240	13	S/KWU	55, 56
Low-alloy Steels							
1	A302-Gr.B	0.027	0.001-0.9	288	9	ANL	10-13
2	A508-Gr.2	0.003	0.2	288	21[d]	JNES (Nakao, Higuchi)	136

ANL Mat. ID	Material Specifications	Sulfur Content (wt.%)	Dissolved Oxygen (ppm)	Test Temperature (°C)	No. of Data Points	Source	Applicable Reference
4	A508-Gr.2[e]	0.008	0.05-8.0	200, 250, 289	6, 9, 39	JNES (Hirano)	136
5	A508-Gr.2[e]	0.008	0.005	100, 150, 200, 250, 290	10, 2, 10, 2, 13	JNES (Nomura)	136
6	A508-Gr. 3 (SFVV3)	0.003	0.1	288	9	JNES (Nagata)	136
12	A508-Gr. 3 (SFVV3)	0.003	0.05-8.0	50, 100, 150, 200, 250, 283/ 288/290	2, 12, 29, 27, 8, 60	JNES (Endou, Kasai, Higuchi)	136
14	A508-Gr. 3	0.002	0.1	288	16	Wu & Katada	141,143
15	A508-Gr. 3	0.018	0.5	285	3	MPA	55,56
16	A533-Gr. B	0.012	0.001-0.9	288	30	ANL	10-13
17	A533-Gr. B (SQV2A)	0.007	0.1, (0.01-4.0)	288, (20, 100, 147/150, 200, 250, 288)	8, (1, 4, 2, 2, 1, 23)	JNES (Nagata), Wu & Katada	136, 141,143
21	A533- Gr. B (SQV2A)	0.010	0.2-8.0	288/290	53[e]	JNES (Nakao, Higuchi)	136
23	A533-Gr. B	0.013	0.1	288	27	Wu & Katada	139,142, 143
24	A533-Gr. B	0.025	0.1	288	6	Wu & Katada	143
25	A533-Gr. B	0.038	0.1, 2.0	200, 288	6, 13	Wu & Katada	139
26	A533- Gr. B (SQV2A)	0.021	0.05-1.0	200, 289	5, 29	JNES (Higuchi)	136
27	A533-Gr. B Cl. 2	<0.001	1.0	289	3	JNES (Hirano)	136
28	A533-Gr. B	0.003, 0.005, 0.014	2.0	285	3, 2, 5	MPA	55,56
30	15MnNi63	0.003	0.4, 8.0	240	1, 4	MPA	55,56
31	17MnMoV64	0.018	0.45	210	21	S/KWU	55,56

[a] This material was tested at ANL and IHI (Higuchi).

[b] This material was also tested at ANL.

[c] Tests performed on rectangular bars under bending fatigue.

[d] Four tests performed under load control using sine waveform.

[e] Data include results for thermally aged materials.

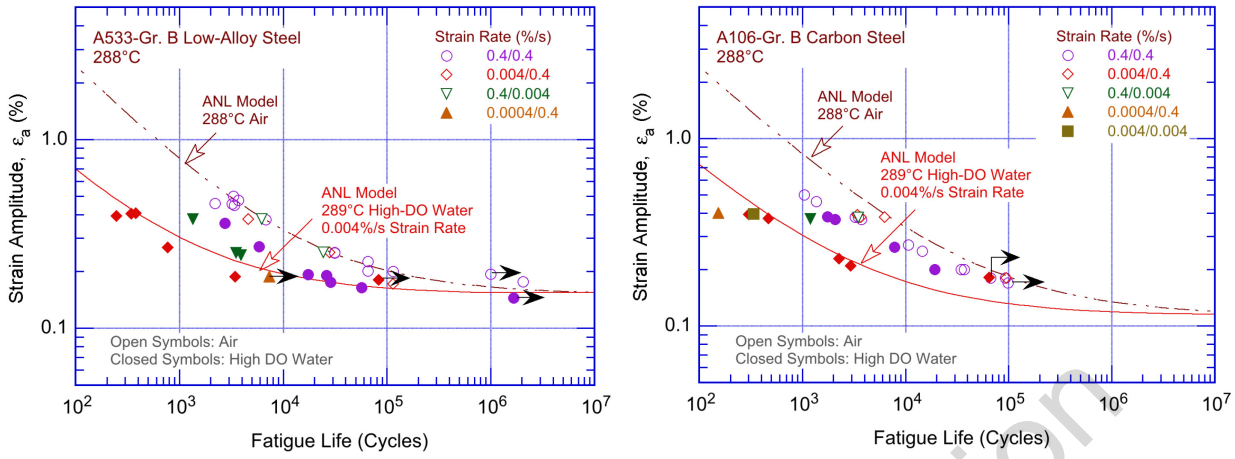

Figure 4-2 Strain amplitude vs. fatigue life data for (a) A533–Gr B and (b) A106–Gr B steels in air and high-DO water at 288°C (Ref. 10).

The existing fatigue data indicated that slow strain rates applied during tensile–loading cycles were primarily responsible for environmentally assisted reduction in the fatigue lives of these steels.[10] The mechanism of environmentally assisted reduction in the fatigue lives of carbon and low-alloy steels was termed strain-induced corrosion cracking (SICC).[78,85,86] Slow strain rates applied during both the tensile–load and compressive–load portions of load cycles (i.e., slow/slow strain rate test) did not further decrease the fatigue lives, e.g., refer to the solid diamond and solid square symbols in Figure 4-2(b) for A106–Gr B carbon steel. Limited data from fast/slow tests indicated that slow strain rates during compressive load cycles also decreased fatigue lives. However, the decrease in life was relatively small. For fast/slow strain rate tests, the major contribution of environment occurred during the slow reducing strain, but just after the peak tensile condition. For example, the fatigue lives of A533–Gr B low-alloy steels at 288°C, 0.7 ppm DO, and approximately 0.5% strain range decreased by factors of 5, 8, and 35 for the fast/fast, fast/slow, and slow/fast tests, respectively, i.e., refer to the solid circle, diamond, and inverted triangle symbols in Figure 4-2(a). Similar results were observed for A333–Gr. 6 carbon steel;[23] relative to the fast/fast test, the fatigue lives for the slow/fast and fast/slow tests at 288°C, 8 ppm DO, and 0.6% strain amplitude decreased the fatigue lives by factors of 7.4 and 3.4, respectively.

Environmental effects on the fatigue lives of carbon and low-alloy steels were consistent with the slip oxidation/dissolution mechanism for crack propagation, particularly at slow strain rates.[189,190] A critical concentration of sulfide (S^{2-}) or hydrosulfide (HS^{-}) ions, which is produced by the dissolution of sulfide inclusions in the steel, is required at the crack tip for environmental effects to occur. For this mechanism, a model for the initiation or cessation of environmentally assisted cracking (EAC) of these steels in low-DO PWR environments was also proposed.[182] Initiation of EAC requires a critical concentration of S^{2-} ions at the crack tip, which is supplied with the S^{2-} ions as the advancing crack intersects the sulfide inclusions, and the inclusions dissolve in the high-temperature water. Thus, environmental fatigue is controlled by the synergistic effects of sulfur content, environmental conditions, and flow rate. The EAC initiation/cessation model was used to determine the minimum crack extension and crack growth rates (CGRs) that are required to maintain the critical S^{2-} ion concentration at the crack tip and sustained environmental enhancement of growth rates.

- *LWR environments have significant effects on the fatigue lives of carbon and low-alloy steels; such effects were not considered in the original ASME Code fatigue design curves. Environmental effects for carbon and low-alloy steels may be incorporated into ASME Code fatigue evaluations using the F_{en} expression given in Equation 34 (Section 4.1.11).*

4.1.2 Strain Rate

The effects of strain rate on the fatigue lives of carbon and low-alloy steels in LWR environments were determined to be significant when other key threshold conditions (e.g., strain amplitude, temperature, and DO content), were satisfied. When any one of the threshold conditions was not satisfied (e.g., if low-DO PWR environments or temperatures less than 150°C were not present), the effects of strain rate were consistent with those observed in air.

When all threshold conditions were satisfied, the fatigue lives of carbon and low-alloy steels decreased logarithmically with decreasing strain rate. Figure 4-3 plots the fatigue lives of A106–Gr B and A333–Gr. 6 carbon steels and A533–Gr B low-alloy steel[10,23] as a function of strain rate. The lines in this figure represent the predicted fatigue lives determined from the updated F_{en} expressions presented later in Section 4.1.10 (for water for the two DO values identified on each plot) and either Equations 24 or 25 (for air). The decrease in fatigue lives in simulated (low-DO) PWR environments (e.g., DO levels ≤ 0.04 ppm) was less than in high-DO environments (i.e., a maximum of a factor of 3.5 to 4.5 lower). For the heats of A106–Gr. B and A333-Gr. 6 carbon steel and A533–Gr. B low-alloy steel, the effects of strain rate on fatigue lives saturated between values of 0.004 and 0.0004%/s strain rate. Although the data for A333–Gr. 6 carbon steel at 250°C and 8 ppm DO did not indicate saturation for strain rates up to 0.0001%/s, the results were comparable to those for the other two steels. The F_{en} expressions proposed by JNES for incorporating environmental effects on the fatigue lives of carbon and low-alloy steels recommended a saturation strain rate of 0.0004%/s for DO levels up to 0.7 ppm and 0.0001%/s above 0.7 ppm. Based on the data shown in Figure 4-3, the saturation strain rate in the ANL model was also changed to 0.0004%/s for all DO levels.

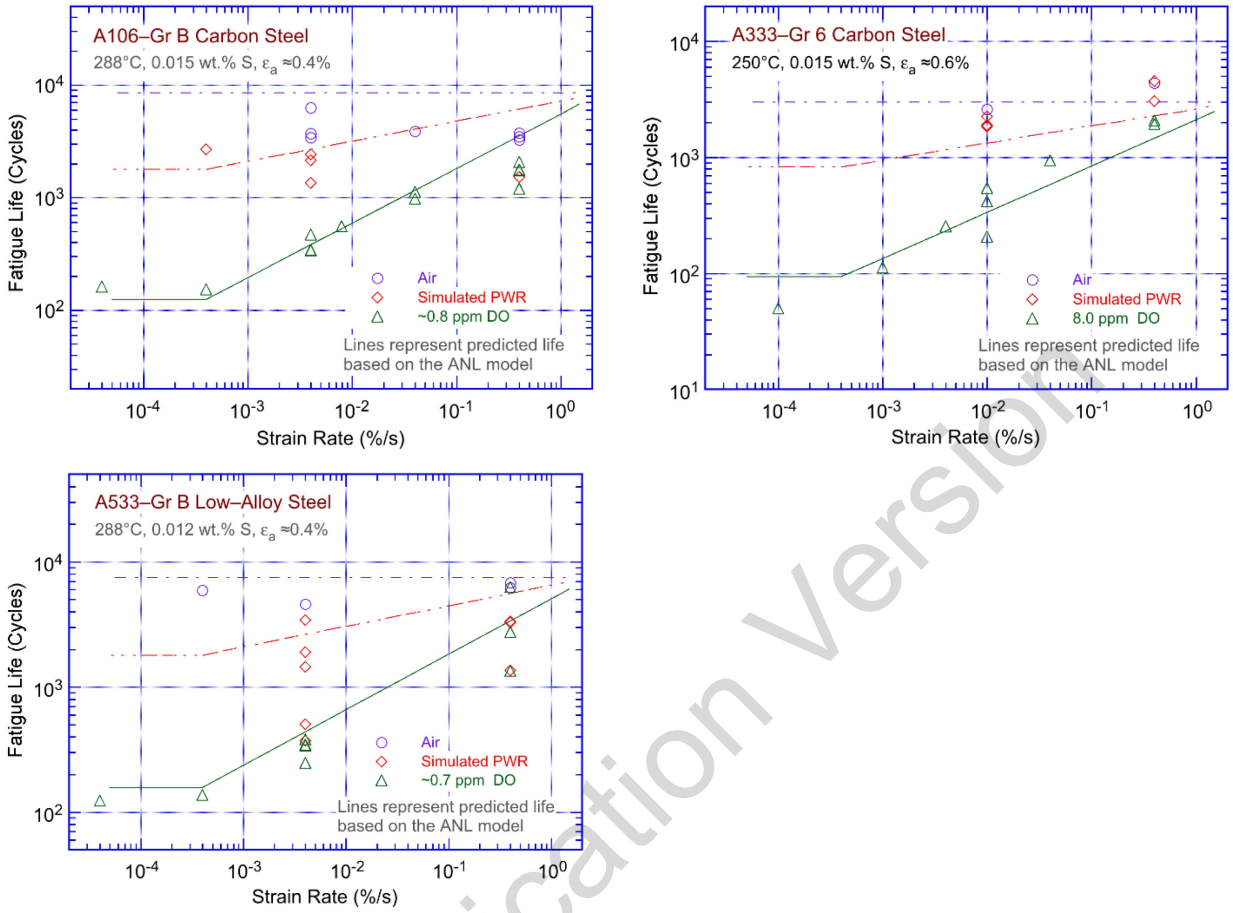

Figure 4-3 Dependence of fatigue lives of carbon and low-alloy steels on strain rate (Refs. 10 and 23).

For carbon and low-alloy steels, the potential effects of dynamic strain aging (DSA) are also likely to affect fatigue lives. Figure 4-4 shows the strain-rate dependence of fatigue life of A533-Gr. B low-carbon steel at 288°C and 200°C in high-purity water with 0.1 and 2.0 ppm DO. The lines represent the predicted fatigue lives based on the revised F_{en} expressions given in Equation 34. The results indicated that the predicted fatigue lives at 0.001%/s strain rate were greater than the experimental values, particularly at 200°C (i.e., the ANL models yielded nonconservative estimates for these environmental and loading conditions). This behavior was attributed to DSA. However, the difference between the estimated and experimental values was a factor of 2, which is within the range of data scatter for the fatigue ε–N data for carbon and low-alloy steels in LWR environments. Therefore, no additional adjustments were made to accommodate DSA effects in the revised ANL model for carbon and low-alloy steels.

Section 4.4 discusses the methodology for calculating F_{en} under conditions where temperature and strain rate are changing (i.e., actual load transients), and guidance is provided for defining the strain rate for a specific load cycle or load set pair.

- *The effect of strain rate on the fatigue lives of carbon and low-alloy steels in LWR environments were explicitly considered in the F_{en} expression given in Equation 34 (Section 4.1.11); the saturation strain rate limit was changed from the value of 0.001%/s, specified in the original version of NUREG/CR-6909, to 0.0004%/s to more appropriately reflect the data in the updated database.*

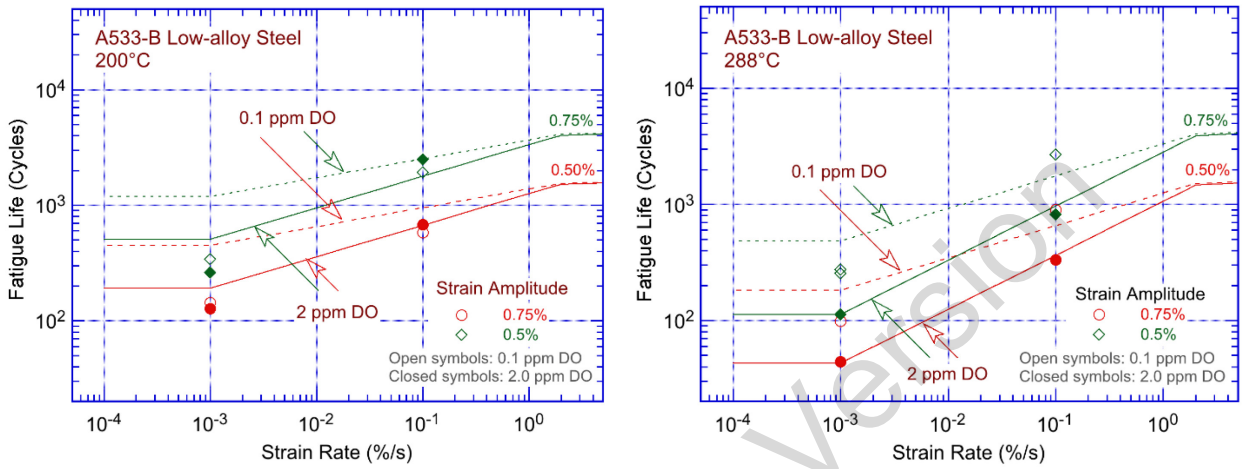

Figure 4-4 Fatigue life of A533–Gr. B low-alloy steel as a function of strain rate in high-purity water with 0.1 or 2.0 ppm DO (Refs. 141 and 143).

4.1.3 Strain Amplitude

The fatigue lives of carbon and low-alloy steels in LWR environments were observed to be lower than those in air. However, limited data indicated that at strain amplitudes below 0.3%, the fatigue lives of A533-Gr. B and A508-3 low-alloy steels were greater than those in air Figure 4-5). The reasons for this behavior were not clear. However, under the environmental and loading conditions that resulted in such behavior, estimates of fatigue lives of low-alloy steels were conservative. Therefore, in this report, this behavior was not explicitly addressed in the F_{en} methodology for estimating environmental effects on fatigue lives.

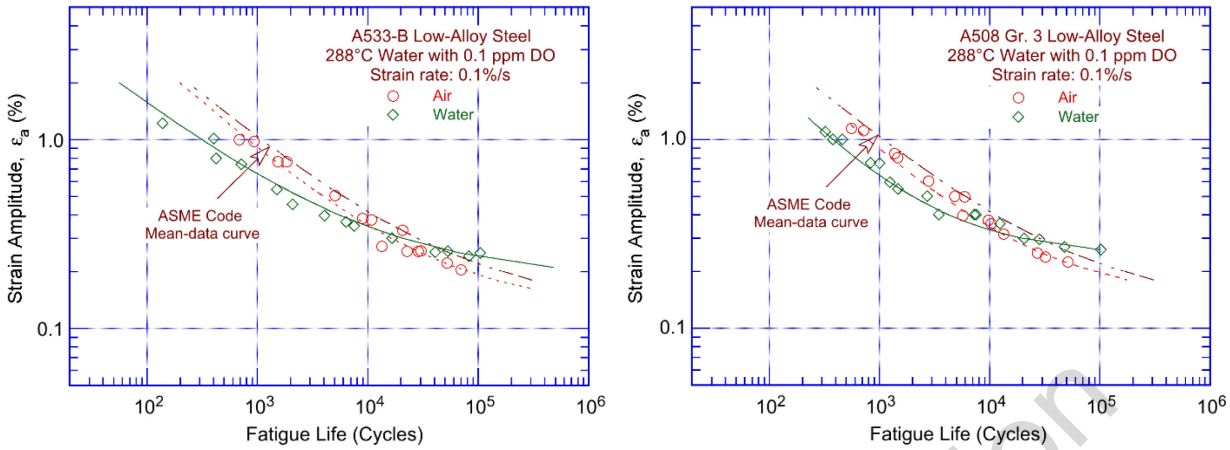

Figure 4-5 Fatigue strain-life behavior of A533–Gr. B and A508–Gr. 3 low-alloy steels at 288°C in air and high-purity water with 0.1 ppm DO (Ref. 151).

The available small-scale laboratory fatigue test data indicated that a minimum threshold strain range, $\Delta\varepsilon_{th}$, was required to cause an environmentally assisted decrease in fatigue lives (i.e., LWR water environments had no effect on the fatigue lives of these steels at strain ranges below the threshold value). Figure 4-2 shows the fatigue lives of A533–Gr B and A106–Gr B steels in high-DO water at 288°C and various strain rates.[10] Fatigue tests at low strain amplitudes were rather limited. Because environmental effects on fatigue lives increased with decreasing strain rates, fatigue tests at low strain amplitudes and strain rates that would result in significant environmental effects are restrictively time consuming. For the limited data that were available, the threshold strain amplitude (one-half of the threshold strain) was slightly above the fatigue limits for these steels.

Exploratory fatigue tests with changing strain rate were conducted to determine the $\Delta\varepsilon_{th}$ beyond which environmental effects were significant. The tests were performed with waveforms in which slow strain rates were applied during a portion of the tensile loading cycles (Figure 4-6).[10,24] Figure 4-7 summarizes the results for A106–Gr B steel tested in air and low- and high-DO environments at 288°C and approximately 0.75% strain range. The loading waveforms implemented in the tests consisted of segments of loading and unloading at fast and slow strain rates. Figure 4-7 plots the variation in fatigue lives of two heats of carbon steel and one heat of low-alloy steel[10,24] as a function of the fraction of the loading strain at slow strain rate. Open symbols indicate tests where the slow strain rate loading occurred near the maximum tensile strain, and closed symbols indicate tests where the slow strain rate loading occurred near the maximum compressive strain. If the relative damage was the same at all strain levels, fatigue lives should have decreased linearly from A to C along the chain–dot lines in Figure 4-7. Instead, the results indicated that, during a strain cycle, the relative damage due to slow strain rate occurred only after the strain level exceeded a threshold value. The $\Delta\varepsilon_{th}$ for these steels was in the range of 0.32 to 0.36%.

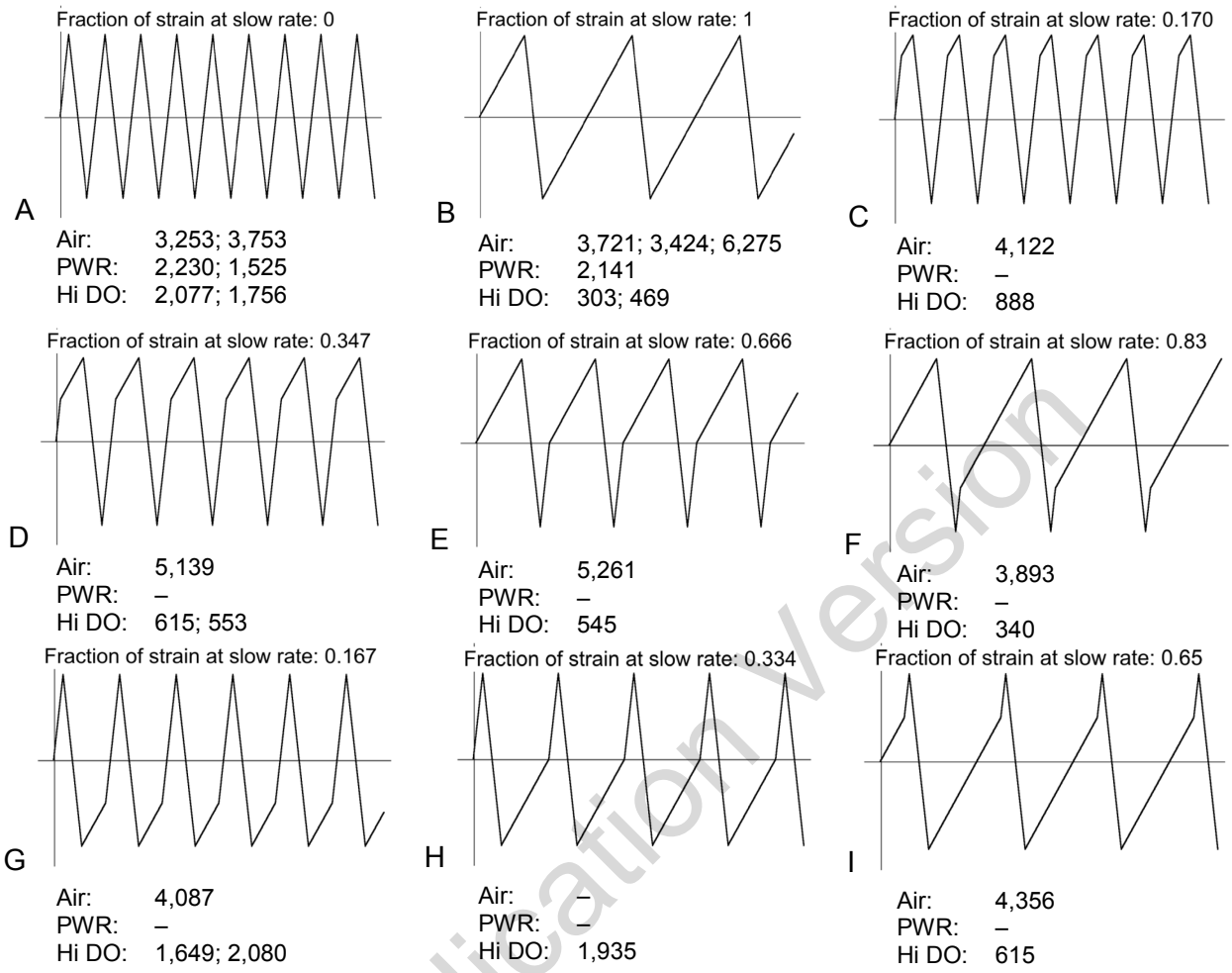

Figure 4-6 Fatigue life of A106–Gr B carbon steel at 288°C and 0.75% strain range in air and water environments under different loading waveforms (Ref. 10).

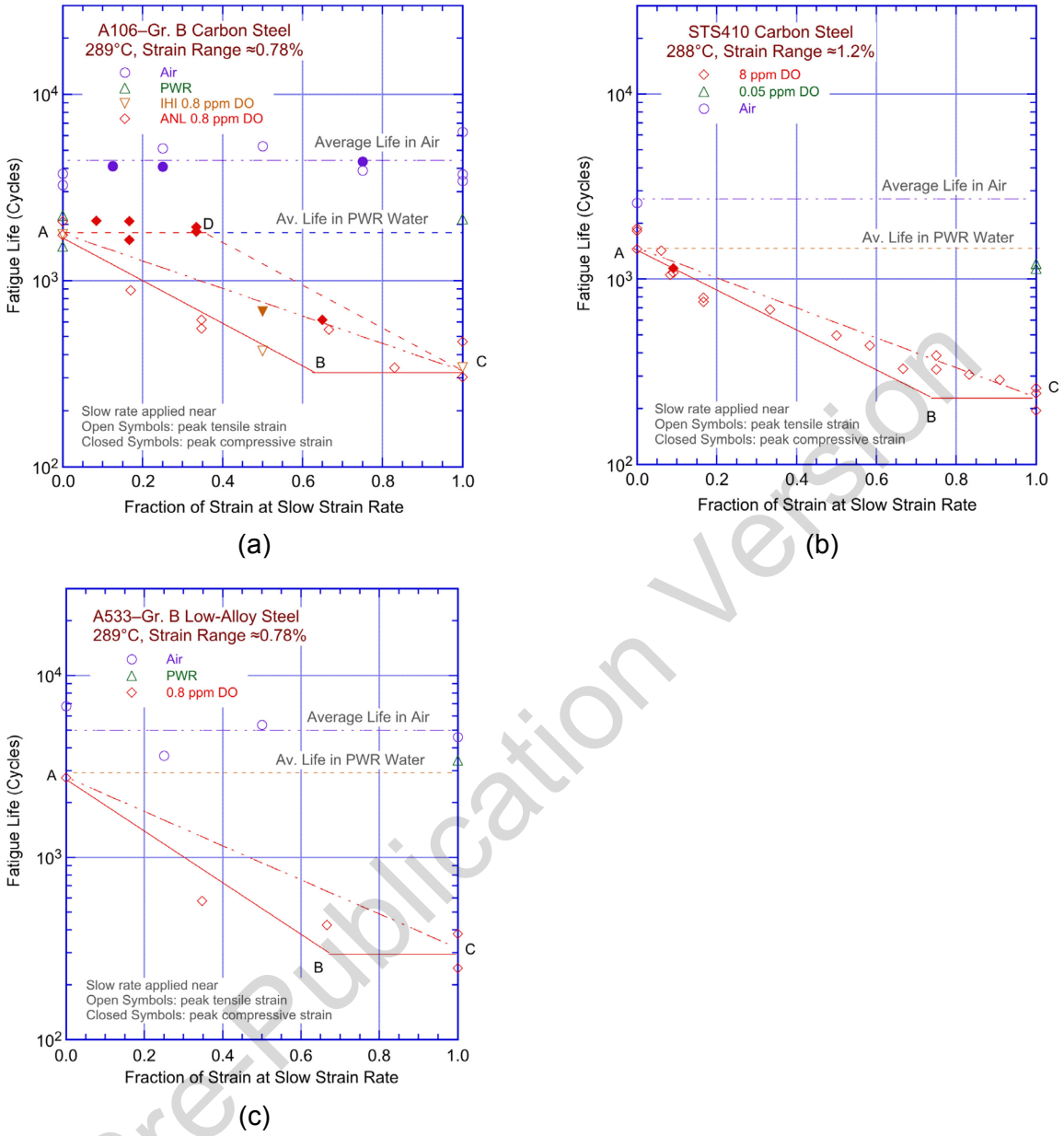

Figure 4-7 Fatigue lives of carbon and low-alloy steels tested with loading waveforms where slow strain rate was applied during a fraction of the tensile loading cycle (Refs. 10 and 24).

Loading histories with slow strain rate applied near the maximum tensile strain (i.e., waveforms C, D, E, or F in Figure 4-6) showed continuous decreases in fatigue lives (lines AB in Figure 4-7), followed by saturation when a portion of the slow strain rate occurred at strain levels below the threshold value (lines BC in Figure 4-7). In contrast, loading histories with slow strain rates applied near the maximum compressive strain (i.e., waveforms A, G, H, or I in Figure 4-6) did not produce any fatigue damage (line AD in Figure 4-7(a)) until the fraction of the strain was sufficiently large such that the slow strain rates occurred at strain levels greater than the threshold value. However, tests with such loading histories often showed lower fatigue lives than the predicted values (e.g., the solid inverted triangle or solid diamond symbols in

Figure 4-7(a)). The fatigue ε–N data presented in Figure 4-2 indicated that the threshold strain was between 0.25 and 0.40%. As discussed in Section 4.2.2, similar tests on austenitic SSs in PWR environments also showed the existence of a strain threshold below which the material was insensitive to environmental effects.[35] The $\Delta\varepsilon_{th}$ was independent of material type (weld metal or base metal) and temperature in the range of 250–325°C, but it tended to decrease as the strain range was decreased. For austenitic SSs, the threshold strain was expressed in terms of $\Delta\varepsilon$ (Equation 42 in Section 4.2.3). At a low strain amplitude (e.g., 0.3%), the proposed expression yielded a strain threshold of approximately 0.28%. Because the contribution of strain threshold was more significant at low strain amplitudes, a value of 0.28% was proposed in the original version of NUREG/CR-6909. After applying a factor of 2 on strain to account for the uncertainties associated with material variability and experimental scatter, a threshold "strain amplitude" of 0.07% (or a stress amplitude of 145 MPa (21 ksi)) was specified in the original version of NUREG/CR-6909 for use when performing ASME Code fatigue CUF evaluations for both carbon and low-alloy steels. The modified rate approach, described in Section 4.4, was used to predict the results from tests on A106-B and A333-6 carbon steels and A533-Gr. B low-alloy steel that were conducted with changing strain rate in high-DO water (0.8 to 8.0 ppm DO) at 289°C.[136]

Figure 4-8 shows the experimental values of fatigue lives and those predicted from the modified rate approach, with and without the consideration of a threshold strain. Most of the scatter in the data was due to heat-to-heat variations. The results indicated that estimates of fatigue lives based on the modified rate approach, without the consideration of a strain threshold, were in good agreement with the experimental values for A106-B and A333-6 carbon steels (Figure 4-8(a)). However, the data for A533-Gr. B low-alloy steel (shown as circular symbols in Figure 4-8) show an unusual behavior. First, the material showed a very strong dependence of environmental effects on applied strain amplitude. For example, for the tests with no strain rate change (shown by closed symbols), the fatigue lives at 0.6% strain amplitude (i.e., fatigue lives in the range of 100 to 800 cycles) showed excellent agreement with the experimental values.

However, the predicted fatigue lives at 0.4% strain amplitude (i.e., fatigue lives in the range of 250 to 1,500 cycles) were a factor of 2 higher and, at 0.3% strain amplitude (i.e., fatigue lives in the range of 350 to 3,300 cycles), the predicted fatigue lives were more than a factor of 3 higher. In addition, nearly all fatigue tests where slow strain rates were applied near the compressive strain peak, particularly the tests at 0.4% or 0.3% strain amplitudes, exhibited unusually low fatigue lives. The reasons for such a dependence of environmental effects on applied strain amplitude are not understood.

The results shown in Figure 4-8(b) included a threshold strain of 0.28%. It was assumed that, during a strain cycle beginning from the peak compressive strain, environmental effects on fatigue lives occurred only when the strain exceeded the strain threshold (i.e., the F_{en} was determined in accordance with the modified rate approach). Once again, the results for A106-B and A333-6 carbon steel either showed little or no changes in the resulting fatigue lives, or showed better agreement with the experimental values; however, the data for A533-Gr. B low-alloy steel, particularly for tests with slow strain rate imposed at the peak compressive strain, exhibited an unusual behavior. These results indicated that the modified rate approach, without consideration of a strain threshold, yielded the best estimates of fatigue lives of carbon and low-alloy steels in LWR environments.

- *Section 4.1.11 describes the procedure for calculating F_{en} in LWR water environments and Section 4.4 discusses the modified rate approach. However, while using the modified rate approach to determine F_{en} for a stress cycle or load set pair, inclusion of a threshold strain may yield nonconservative estimates for fatigue lives.*

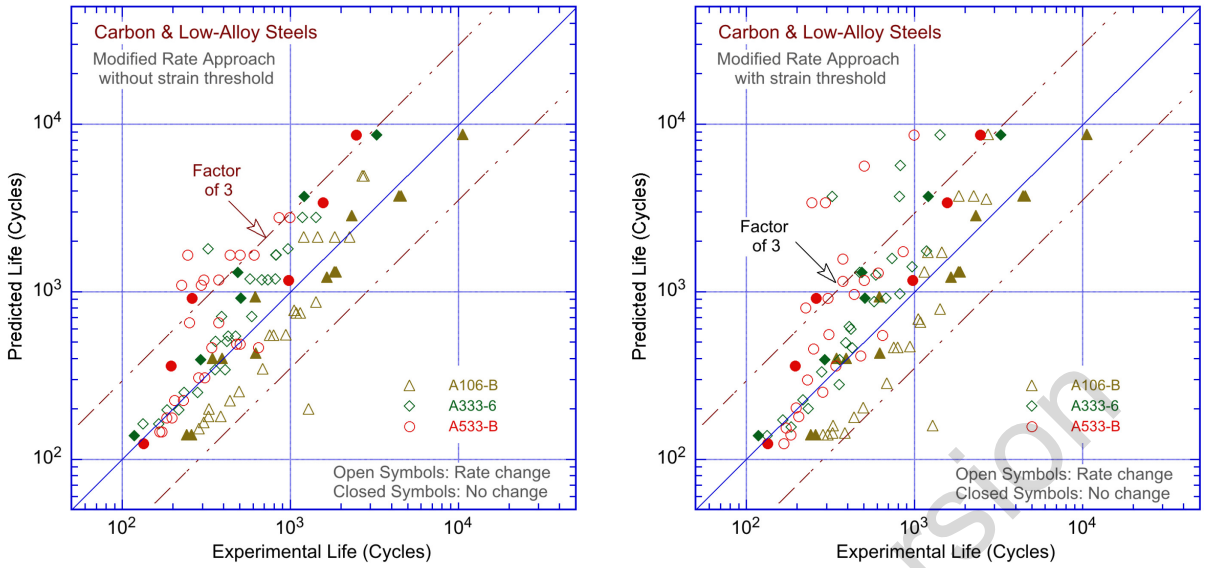

Figure 4-8 Experimental values of fatigue life and those predicted from the modified rate approach (a) without and (b) with consideration of a threshold strain (Ref. 136).

4.1.4 Temperature

Figure 4-9 shows the change in fatigue lives of two heats of A333–Gr. 6 carbon steel[18,19,22] as a function of test temperature at different levels of DO and strain rates. The sulfur content of the two heats of A333-Gr. 6 carbon steel was 0.015% and 0.012 wt.%. For all these tests, the strain amplitude was 0.6%, which is above the threshold strain limit for environmental effects. In air, both heats had a fatigue life of 2,993 cycles. The results indicated a threshold temperature of 150°C, above which the environment decreased the fatigue life if the DO content in the water was also above the critical level of 0.05 ppm. An artificial neural network (ANN) was used to find patterns and identify the threshold temperature below which environmental effects were moderate.[226] The main benefits of the ANN approach were that estimates of lives were based purely on the data and not on preconceptions and that, by learning trends, the network interpolated effects where data were not present. The factors that affected fatigue lives had synergistic effects on one another. The neural network detected and used these effects in its predictions. The training of the neural network was all based on the same dataset, but the order in which the data were presented to the ANN for training was varied, and the initial ANN weights were randomized to guard against overtraining and to ensure that the network did not arrive at a solution that was a local minimum. The results indicated that at high strain rates (0.4%/s), fatigue lives were relatively insensitive to temperature. At low strain rates (0.004%/s), fatigue lives decreased with an increase in temperature beyond a threshold value of approximately 150°C.[226] The precision of the data indicated that this trend was present in the data used to train the ANN. Only a moderate decrease in fatigue lives was observed in water at temperatures below the threshold value of 150°C or at DO levels less than or equal to 0.05 ppm. Under these conditions, fatigue lives in water were a factor of approximately 2 lower than in air. Figure 4-9 shows an average life of approximately 2,000 cycles for the 0.015 wt.% sulfur steel and approximately 1,200 cycles for the 0.012 wt.% sulfur steel.

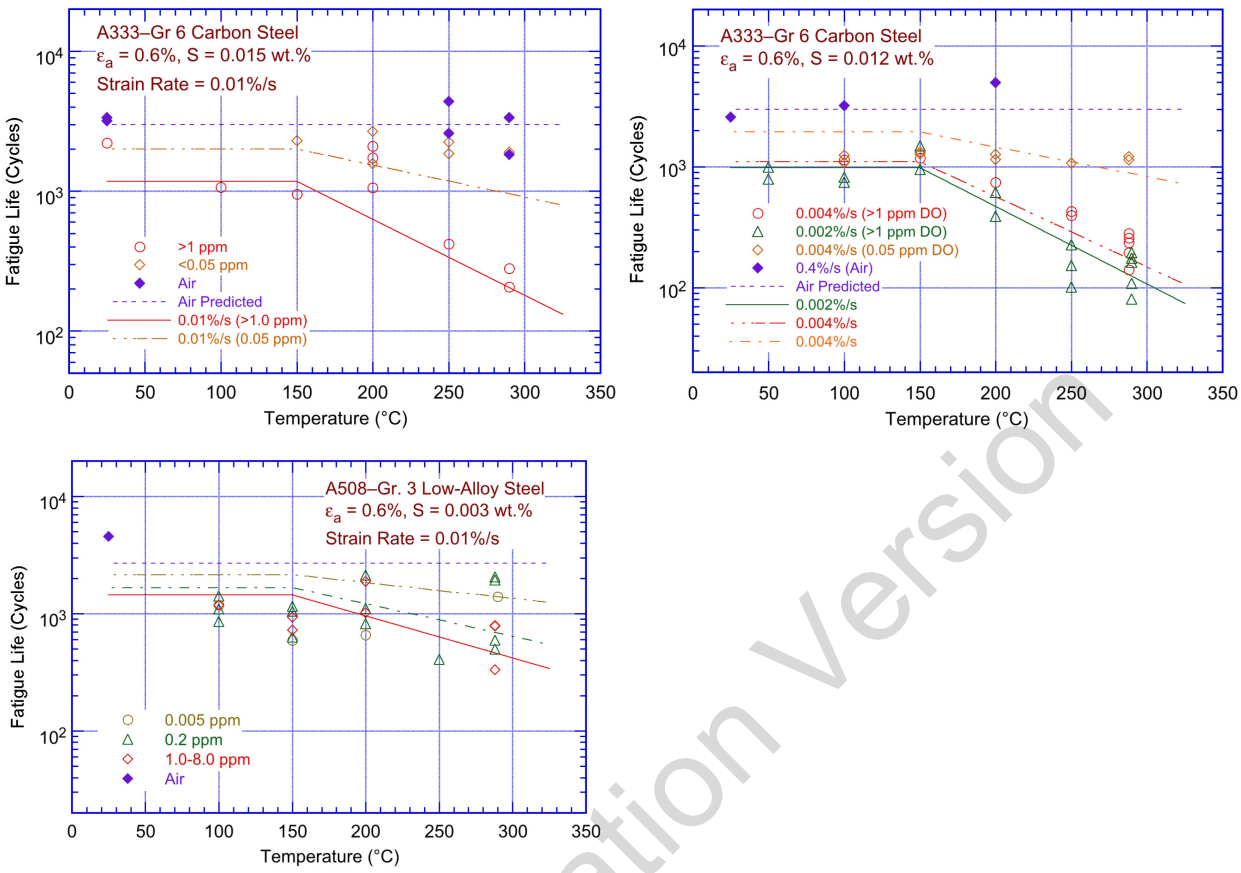

Figure 4-9 Change in fatigue life of A333–Gr. 6 carbon steel and A508 Gr. 3 low-alloy steel with temperature and DO (Ref. 136).

At temperatures above 150°C, the logarithm of fatigue life decreased linearly with temperature; the decrease in fatigue life was greater at higher temperatures and DO levels. However, as mentioned earlier, the temperature range specified in the original version of NUREG/CR-6909 for environmental effects for carbon and low-alloy steels in LWR environments extended beyond the range of actual fatigue ε–N data. An insignificant amount of fatigue ε–N data were available at temperatures above 290°C. Consequently, as discussed in Section 1.5, item xix and Section 4.1.11, the maximum temperature limit was extended slightly to 325°C as a reasonable bound to cover most anticipated LWR operating conditions. This is adequate for expected operating LWR conditions, especially when considering the use of average temperature.

Nearly all of the fatigue ε–N data available for evaluation for this report were obtained under loading histories with constant strain rates, temperatures, and strain amplitudes. However, the operating experience for U.S. LWRs indicates that the actual loading histories encountered during normal operation involves variable loading and environmental conditions. Some fatigue tests were conducted in Japan on 12 mm outer diameter tube specimens (1- and 3-mm wall thicknesses) of A333–Gr. 6 carbon steel in oxygenated water under combined mechanical and thermal cycling.[21] Triangular waveforms were used for both strain and temperature cycling. Two sequences were selected for temperature cycling (Figure 4-10): (1) an in-phase sequence in which the temperature cycling was synchronized with the mechanical strain cycling and (2) another sequence in which the temperature and strain cycling were out of phase (i.e., the maximum temperature occurred at the time of minimum strain level and vice versa). Three

temperature ranges, 50–290°C, 50–200°C, and 200–290°C, were selected for the tests. The results are shown in Figure 4-11; an average temperature was used to plot the thermal cycling tests. Because environmental effects on fatigue lives were moderate and independent of temperature below 150°C, the temperatures for the tests cycled in the ranges of 50–290°C or 50–200°C were determined from the average of the threshold temperature of 150°C and the maximum temperature of the test (i.e., 220°C and 175°C, respectively). The results (Figure 4-11) indicated that load cycles involving variable temperature conditions represented by an average temperature (e.g., the fatigue lives from variable temperature tests were comparable with those from constant temperature tests).

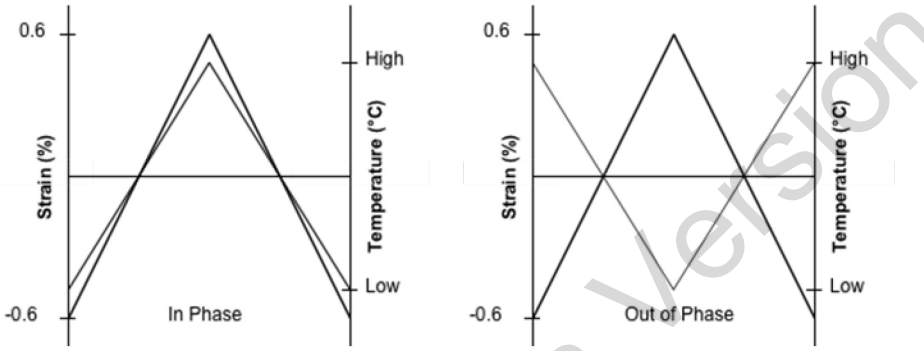

Figure 4-10 Waveforms for changes in temperature and strains during exploratory fatigue test (Ref. 21).

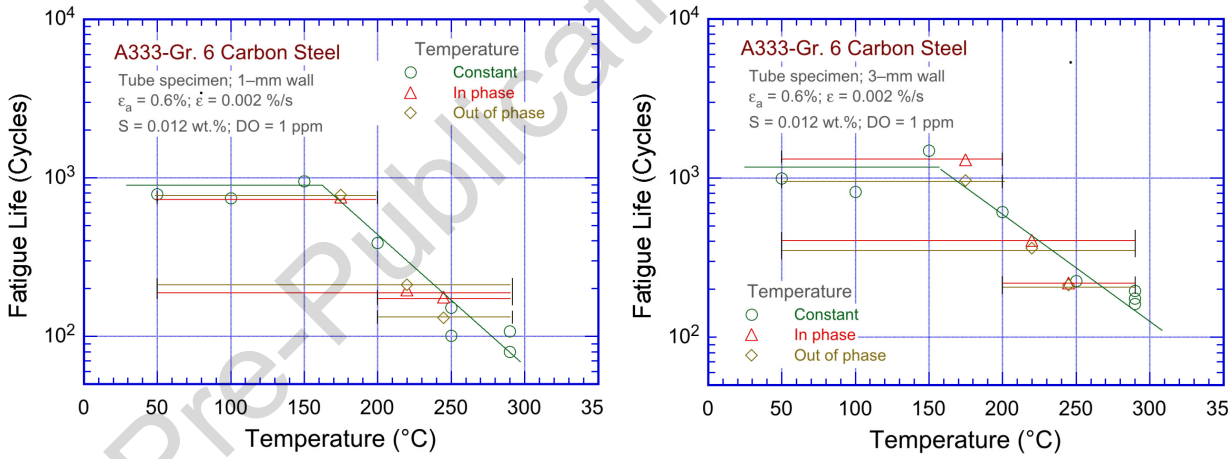

Figure 4-11 Fatigue lives of A333–Gr. 6 carbon steel tube specimens under varying temperature conditions, as indicated by horizontal bars (Ref. 21).

However, nearly identical fatigue lives were obtained from the in-phase and out-of-phase tests. Assuming that the tensile–load cycle was primarily responsible for the observed environmentally assisted reductions in fatigue lives, and that the applied strains and temperatures must be above a minimum threshold value for environmental effects to occur, the fatigue lives obtained from the out-of-phase tests were expected to be longer than those obtained from the in-phase tests. This expectation was based on the premise that the applied strains above the threshold strain occurred at temperatures above 150°C for the in-phase tests, whereas the applied strains above the threshold strain occurred at temperatures below 150°C for the out-of-phase tests. Under the assumption that

environmental effects on fatigue lives were considered to be minimal below the 150°C temperature and 0.28% strain threshold values, the average temperatures for the out-of-phase tests at 50–290°C, 50–200°C, and 200–290°C were 195, 160, and 236°C, respectively, instead of 220, 175, and 245°C, as plotted in Figure 4-11. Thus, the fatigue lives from out-of-phase tests were expected to be at least 50% higher than those from the in-phase tests. Such differences in environmental conditions were therefore assumed to be offset by the difference in the cyclic hardening behavior of the material for the out-of-phase and in-phase tests. From those observations, it was concluded that estimates of fatigue lives for actual nuclear power plant transients based on an average temperature may yield nonconservative estimates.

- *The effects of temperature on the fatigue lives of carbon and low-alloy steels in LWR environments were explicitly considered in F_{en} defined in Equation 34 (Section 4.1.11). For simple, linear transients, an average temperature that considers the threshold temperature of 150°C may be used to calculate F_{en} for a specific stress cycle or load set pair. Complex thermal transients that have multiple increasing and decreasing temperature excursions should be evaluated using the maximum temperature for the specific stress cycle or load set pair unless information is available to justify the use of an average temperature.*

4.1.5 Dissolved Oxygen

Figure 4-12 shows the dependence of fatigue lives of carbon and low-alloy steels on the DO content in water.[18,19,22] For the tests summarized in this figure, the temperatures, applied strain amplitudes, and sulfur contents in the steels tested were above, and the strain rates were below, the critical threshold values. The results indicated a minimum DO level of 0.04 ppm above which the environment decreased the fatigue lives of the steels tested. The effect of DO content on fatigue lives saturated at 0.5 ppm (i.e., increases in DO levels above 0.5 ppm did not cause further decreases in fatigue lives). In Figure 4-12, for DO levels between 0.04 and 0.5 ppm, fatigue lives decreased logarithmically with DO. Estimates of fatigue lives from the trained ANN also showed a similar effect of DO on the fatigue lives of carbon steels and low-alloy steels.

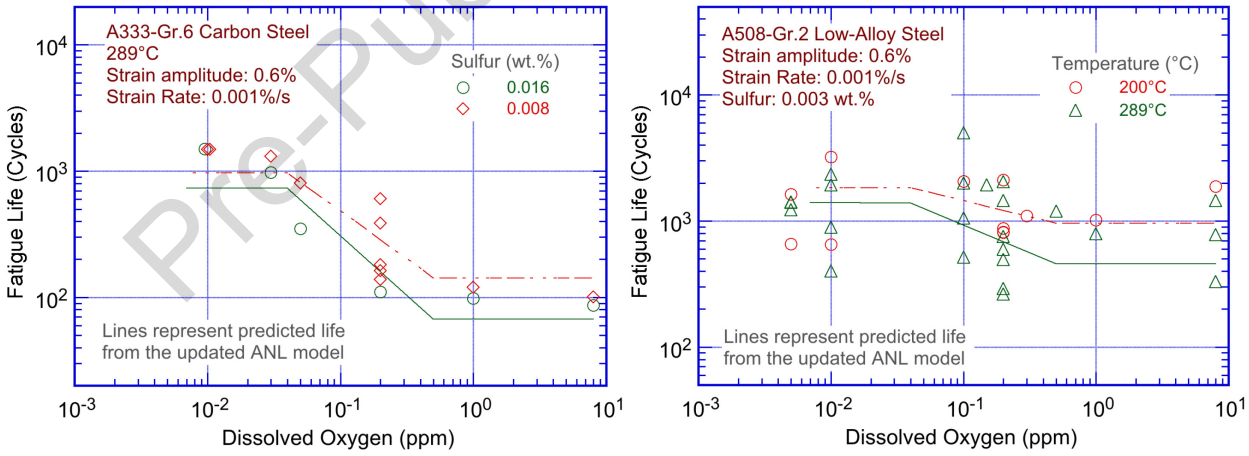

Figure 4-12 Dependence on DO of the fatigue lives of carbon and low-alloy steels in high-purity water (Refs. 18, 19, and 22).

Environmental effects on the fatigue lives of carbon and low-alloy steels were insignificant at DO levels of 0.04 ppm and strain rates greater than or equal to 1%/s; they increased with decreasing

strain rate (F_{en} was about 2 at 320°C, 0.010% S, 0.04 ppm DO, and 0.04%/s strain rate). In contrast, environmental enhancement of CGRs was observed in low-alloy steels even in low-DO water.[182] This apparent inconsistency of fatigue ε–N data with the CGR data was attributed to differences in the environmental conditions locally at the crack tip. As discussed earlier in Section 2.2.1.2, environmentally assisted enhancement of CGRs in low-alloy steels required a critical level of sulfides at the crack tip.[182] The development of this critical sulfide concentration required a minimum crack extension of 0.33 mm and CGRs in the range of 1.3×10^{-4} to 4.2×10^{-7} mm/s. These conditions were not achieved under the majority of the available fatigue ε–N tests. Thus, environmental effects on fatigue lives are expected to be insignificant in low-DO environments for carbon and low-alloy steels.

- *The effects of DO levels on the fatigue lives of carbon and low-alloy steels in LWR environments were explicitly considered in the F_{en}, defined in Equation 34 (Section 4.1.11).*

4.1.6 Water Conductivity

In most of the studies reviewed for this report, the DO level in water was considered as the key environmental parameter that affected the fatigue lives of materials in LWR environments. Studies on the effects of the concentration of anionic impurities in water (expressed as the overall conductivity of water) were limited. The limited data indicated that the fatigue lives of WB36 low-alloy steel at 177°C in water with approximately 8 ppm DO decreased by a factor of approximately 6 when the conductivity of the water was increased from 0.06 to 0.5 μS/cm.[78,227] Similar behavior was also observed in another study of the effects of conductivity on the initiation of short cracks.[228]

- *U.S. LWRs are unlikely to accumulate significant fatigue cycles during off–NWC conditions. Thus, the effects of water conductivity on fatigue lives were not considered in the determination of F_{en} for carbon and low-alloy steels.*

4.1.7 Sulfur Content in Steel

Sulfur content and morphology were the most important material-related parameters that determined susceptibility of low-alloy steels to environmentally enhanced fatigue CGRs.[184-188] A critical concentration of S^{2-} or HS^- ions was required at crack tips for environmental effects to occur. The corrosion fatigue CGRs and threshold stress intensity factor, ΔK_{th}, were both a function of the sulfur content in the range 0.003–0.019 wt.%.[187] The probability of environmental enhancement of fatigue CGRs in precracked specimens of low-alloy steels, diminished markedly for sulfur contents less than 0.005 wt.%.

The available fatigue ε–N data for carbon and low-alloy steels also indicated a dependence of fatigue lives on sulfur content. When all the threshold conditions were satisfied, the environmental effects on the fatigue lives of these materials increased with increased sulfur content. Figure 4-13 plots the fatigue lives of A508–Cl. 3 low-alloy steels with 0.003 and 0.008 wt.% sulfur and A333–Gr. 6 carbon steels with 0.008 and 0.016 wt.% sulfur as a function of strain rate,. The available datasets were too sparse to establish a functional form for dependence of fatigue lives on sulfur content and to define either a threshold for sulfur content below which environmental effects were unimportant or an upper limit above which the effects of sulfur on fatigue lives may saturate. A linear dependence of fatigue life vs. sulfur content was assumed in proposed correlations for estimating the fatigue lives of carbon steels and low-alloy steels in LWR environments.[10,118] The limited data indicated that, in high-purity water with

0.2 ppm DO at 289°C, the fatigue lives of carbon steels with 0.016 and 0.026 wt.% sulfur at 0.001%/s strain rate and 0.3% strain amplitude were comparable. Similar behavior was observed for low-alloy steels with greater than 0.0125 wt.% sulfur. Therefore, fatigue lives of carbon and low-alloy steels were assumed to saturate at sulfur contents above 0.015 wt.%.[10]

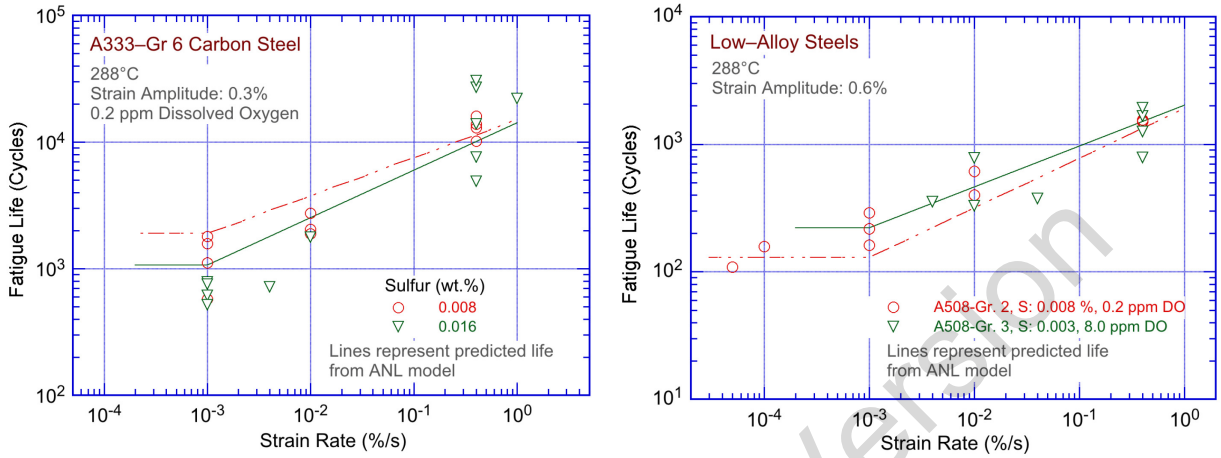

Figure 4-13 Effect of strain rate on fatigue life of low-alloy steels with different sulfur contents (Refs. 10 and 136).

The existing fatigue ε–N data also indicated significant reductions in fatigue lives for some heats of carbon steels with sulfur levels as low as 0.002 wt.%. Figure 4-14 plots the fatigue lives of several heats of A333–Gr. 6 carbon steels with sulfur contents of 0.002–0.016 wt.% in high-DO water at 288°C and 0.6% strain amplitude were plotted as a function of strain rate.[10] Environmental effects on the fatigue lives of these steels were independent of sulfur contents in the range of 0.002–0.015 wt.%. The fatigue lives of carbon steel in air-saturated water (approximately 8 ppm DO) were relatively insensitive to sulfur contents in very high-DO water. Under these conditions, the effects of DO dominated fatigue lives.

- *The effects of steel sulfur content on the fatigue lives of carbon and low-alloy steels in LWR environments were explicitly considered in the F_{en}, defined in Equation 34 (Section 4.1.11). Evaluation of experimental data on low-sulfur steels (less than 0.005 wt.% sulfur) in water with more than 1 ppm DO should be performed with caution because, in some cases, the effects of sulfur were observed to be larger than those predicted by Equation 34.*

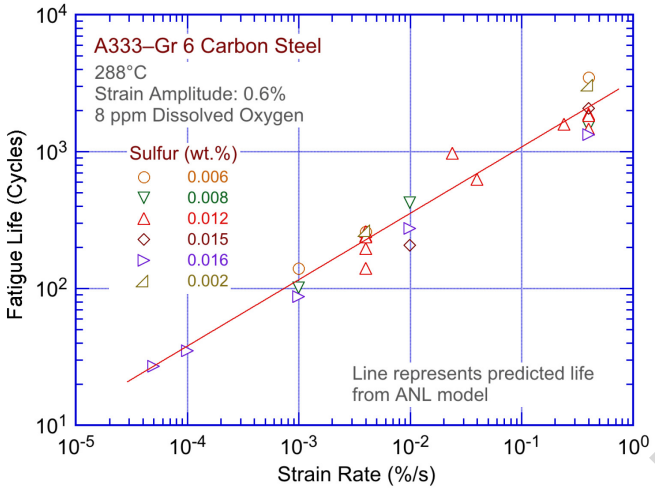

Figure 4-14 Effect of strain rate on the fatigue lives of A333–Gr. 6 carbon steels with different sulfur contents (Ref. 10).

4.1.8 Hold Periods

Fatigue tests conducted using trapezoidal loading waveforms indicated that hold periods at peak tensile strains decreased the fatigue lives of carbon steels in high-DO water at 289°C.[10,24] However, examination of the data indicated that these results were caused by limitations of the test procedures or by frequency effects. Figure 4-15 plots loading waveforms, hysteresis loops, and fatigue lives for the tests on A106–Gr B carbon steel in air and water environments.[10] A 300–s hold period was sufficient to reduce fatigue lives by approximately 50% (approximately 2,000 cycles without a hold period and approximately 1,000 cycles with a hold period); a longer hold period of 1800 s resulted in lower fatigue lives than those obtained with a 300–s hold period. For example, two 300–s hold tests at 288°C and approximately 0.78% strain range in oxygenated water with 0.7 ppm DO yielded fatigue lives of 1,007 and 1,092 cycles; the fatigue life from a 1,800–s hold test was 840 cycles. These tests were conducted in stroke–control mode and were different from conventional hold–time tests in a strain–controlled mode where the total strain in the sample was held constant during the hold period. However, a portion of the elastic strain was converted to plastic strain because of stress relaxation. In the stroke–controlled tests, the occurrence of additional plastic strains in the samples was due to relaxation of elastic strains from the load trains (Figure 4-15). Consequently, significant strain changes occurred during the hold periods; the measured plastic strains during the hold periods were approximately 0.028% from relaxation of the gauge and 0.05–0.06% from relaxation of the load trains. These conditions resulted in strain rates of 0.005–0.02%/s during the hold periods. The reductions in fatigue lives were attributed to slow strain rates during the hold periods. In addition, frequency effects decreased the fatigue lives obtained from hold time tests. For example, in air, the fatigue lives of stroke-controlled tests with hold periods were approximately 50% lower than those without the hold periods.

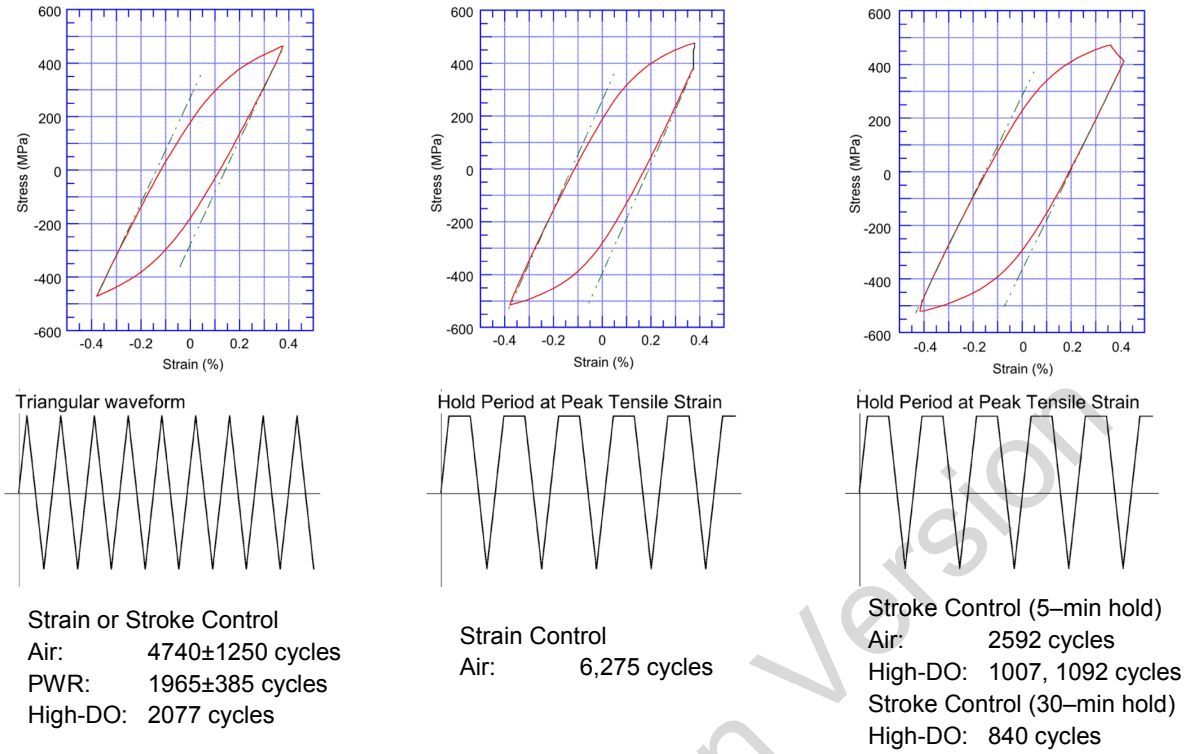

Figure 4-15 Fatigue lives of A106–Gr B steel in air and water environments at 288°C, 0.78% strain range, and hold periods at peak tensile strain (Ref. 10); (Hysteresis loops are for tests in air).

Hold time tests were also conducted on STS410 carbon steel at 289°C in water with 1 ppm DO (Figure 4-16).[24] The most significant observation was that, for strain hold periods at peak tensile strain, reduction in fatigue lives were significant in tests that were conducted at fast strain rates (e.g., 0.4%/s). The reduction in fatigue lives with hold periods decreased at lower strain rates with insignificant reductions in fatigue lives at 0.004%/s strain rate. The results also indicated that the decrease in fatigue lives with extended hold periods saturated at values that were comparable to fatigue lives at slow strain rates (e.g., 0.004%/s).

The most significant observation of these data was that little or no decreases in fatigue lives were observed when the hold periods were below the peak strain during the decreasing strain portions of the fatigue cycles (i.e., 0.06% below the peak strain of 0.24%). Based on these results, Higuchi et al.[24] concluded that the procedures for calculating F_{en} did not need revision.

The JNES report[136] investigated hold time effects and reported that, in the high-temperature water environments, the fatigue lives of carbon and low-alloy steels were reduced due to strain hold times at the peak (local maximum value). Fatigue life reductions caused by strain hold times at the peak were significant at higher strain rates; however, they were reduced as the strain rate decreased. There were little or no observed fatigue life reductions at strain rates of 0.004%/s or less. JNES concluded that the extent of fatigue life reduction depended on the length of the hold time, and that fatigue life reductions tended to be saturated as the hold time became longer. A threshold was observed at a strain rate of 0.004%/s. For carbon steels, the effects of strain hold times were negligible at strain rates of 0.004%/s or lower. Fatigue life reductions caused by strain hold times in low-alloy steels were smaller than those in carbon steels. Although fatigue lives were reduced due to strain hold times at the peak (local maximum

value), no reduction in fatigue lives was observed when strain was held at 0.06% below the peak strain after overshoot, although tensile stresses corresponding to the yield point still remained. From these results, JNES concluded that the effects of strain hold times in the actual components were not necessary because the peak thermal stress generated by actual operating thermal transients is not considered to exceed the monotonic yield stress significantly; however, for strain rates exceeding 0.004%/s, evaluations should be performed assuming a threshold strain rate of 0.004%/s while considering fatigue life reduction caused by strain holding when the strain is at the peak and held under the internal pressure condition that accompanies elastic followup.

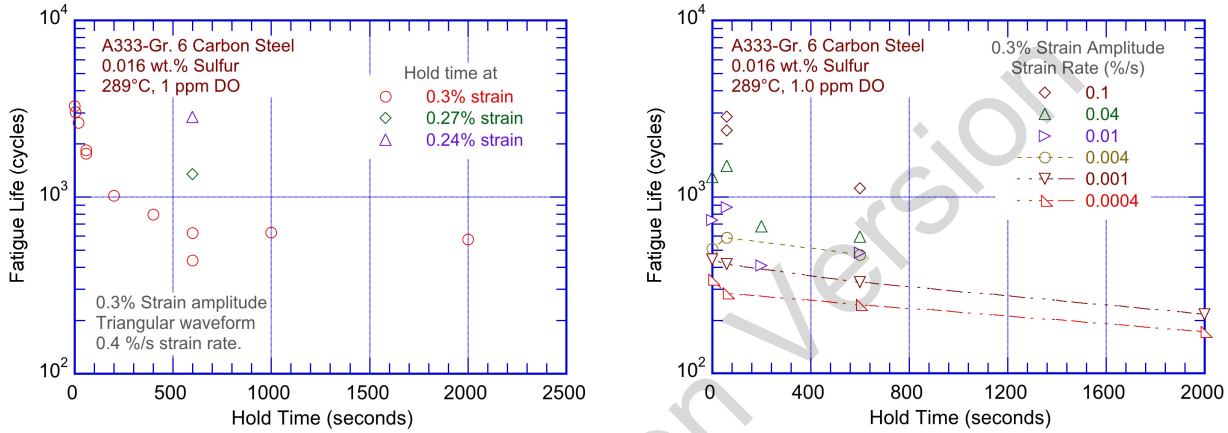

(a) (b)

Figure 4-16 Effect of hold periods on the fatigue lives of A333–Gr. 6 carbon steel at 289°C in water with 1 ppm DO (Ref. 24).

As discussed in Section 4.1.11, the differences in fatigue lives observed in the JNES tests were generally within the data scatter for the fatigue ε–N data in LWR environments. Thus, the effects of hold time from available data are inconclusive and, until such time as sufficient data are available, the updated F_{en} methodology does not address these effects. Further research of these effects is recommended.

- *The available ε–N data investigated in this report were not fully conclusive with respect to the effects of hold time periods on the fatigue lives of carbon and low-alloy steels in LWR environments. Thus, the updated F_{en} methodology did not explicitly address hold time effects.*

4.1.9 Flow Rate

Nearly all of the laboratory fatigue ε–N data for LWR environments were obtained at very low water flow rates. Recent test data indicated that, under the environmental conditions typical for operating BWRs, environmental effects on the fatigue lives of carbon steels were lower at high flow rates (7 m/s) compared to the fatigue lives under very low flow rate conditions similar to those flow rates where most of the data were obtained.[25,26,55] Figure 4-17 shows the effects of water flow rate on the fatigue lives of high- and low-sulfur A333–Gr. 6 carbon steel and A533-Gr. B low-alloy steel in high-purity water at 289°C tested at different strain amplitudes and strain rates.

The results indicated that the effects of increased flow rates were modest. The benefits were greater for high-sulfur steels at high strain amplitudes and high strain rates (e.g., 0.4%/s).[25,26] At

0.3% strain amplitude and 0.01%/s strain rate, for all DO levels, fatigue lives were increased by a factor of approximately 2 when the flow rate was increased from approximately 10^{-5} to 7 m/s. At 0.6% strain amplitude and 0.001%/s strain rate, fatigue lives were increased by a factor of approximately 6 in water with 0.2 ppm DO and by a factor of approximately 3 in water with 1.0 or 0.05 ppm DO.

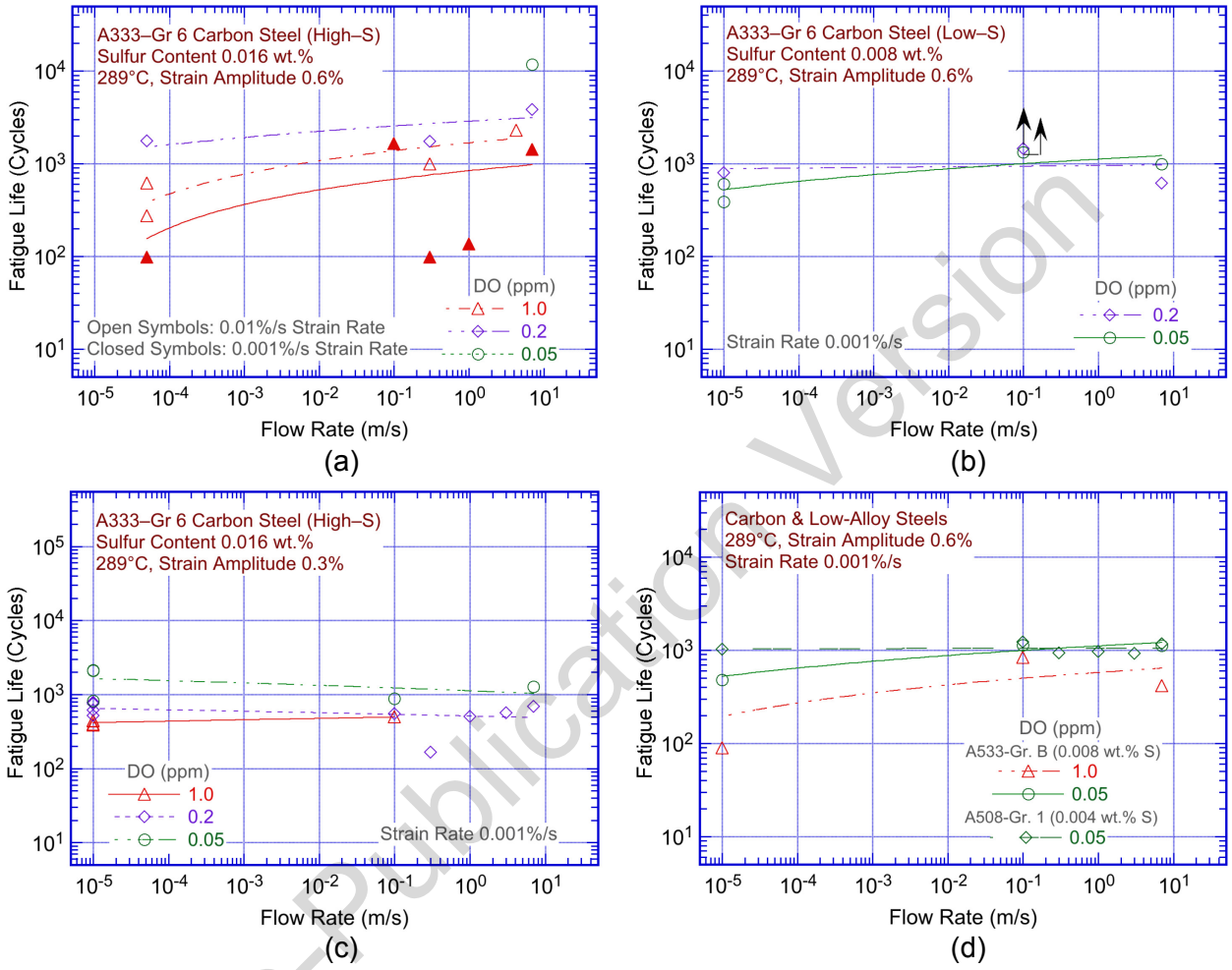

Figure 4-17 Effects of water flow rate on fatigue lives of A333–Gr. 6 and A508 Gr. 1 carbon steels and A533 Gr. B low-alloy steel at 289°C and 0.3 or 0.6% strain amplitudes and various strain rates (Refs. 25 and 26).

Under similar loading conditions (i.e., 0.6% strain amplitude and 0.001%/s strain rate), a low-sulfur (0.008 wt.%) heat of A333–Gr. 6 carbon steel showed a factor of approximately 2 increase in fatigue life with increased flow rates. Note that the beneficial effects of flow rate were determined from a single test on each material at very low flow rates; data scatter in LWR environments is typically a factor of approximately 2. A factor of 2 increase in fatigue lives was observed (Figure 4-18) at KWU during component tests with 180° bends of carbon steel tubing (0.025 wt.% sulfur) when internal flow rates of up to 0.6 m/s were established.[55] The tests were conducted at 240°C in water that contained 0.2 ppm DO.

- *Because of the uncertainties in the flow conditions at or near the locations of crack initiation, the updated F_{en} methodology did not explicitly consider the potentially beneficial effects of flow rates on the fatigue lives of carbon and low-alloy steels.*

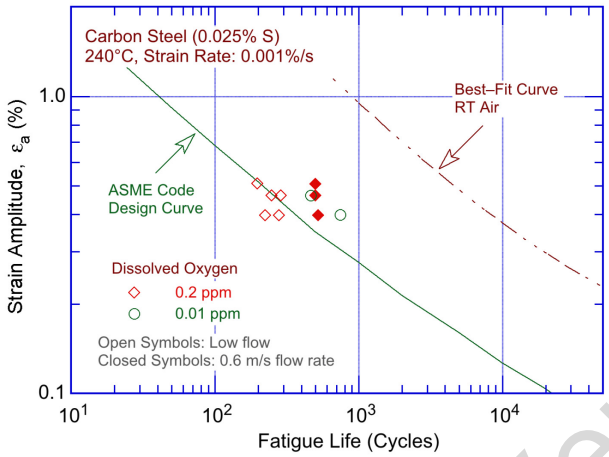

Figure 4-18 Effect of flow rate on low-cycle fatigue of carbon steel tube bends in high-purity water at 240°C (Ref. 55) (RT is room temperature).

4.1.10 Fatigue Life Model

As discussed in the beginning of Section 4.1, the fatigue life models for estimating the fatigue lives of carbon and low-alloy steels in LWR environments presented in the original version of NUREG/CR-6909 were based on an analysis of the updated PVRC database using an approach expressed by Equations 31-33. For this report, more recently available data were fit to a modified version of the Langer equation expressed by Equation 6, which included a term for environmental effects on fatigue lives. The environmental term included the effects of key parameters, such as temperature, strain rate, DO content in the water, and sulfur content in the steel on the fatigue lives of carbon and low-alloy steels, and considered revised constraints based on stakeholder comments and experience with implementation of the F_{en} methodology in industry analyses. However, a single F_{en} was determined for both carbon and low-alloy steels, from Equation 31 assuming that all three constants A, B, and C were the same as in air. The constant D and the functional forms of the dependencies and constraints of the transformed sulfur content, temperature, DO level, and strain rate were determined from the best fit of Equation 31 to the experimental data for carbon and low-alloy steels in LWR environments. The details are given in the next section.

- *The ANL fatigue life models for carbon and low-alloy steels represent the mean values of fatigue life as a function of applied strain amplitude, temperature, strain rate, DO level in the water, and sulfur content of the steel. The models did not include the effects of parameters (such as mean stress, surface finish, size and geometry, and loading history) known to influence fatigue lives; the effects of these parameters were considered in the development of the fatigue design curves, as discussed in Chapter 5.*

4.1.11 Environmental Fatigue Correction Factor

To incorporate environmental effects into ASME Code Section III fatigue evaluations, the original version of NUREG/CR-6909 specified that the fatigue usage for a specific stress cycle or load set pair based on the current ASME Code Section III fatigue design curves was multiplied by the F_{en} for carbon steels and low-alloy steels. Appendix A, "Incorporating Environmental Effects into Fatigue Evaluations," to the original version of NUREG/CR-6909 provides further details for incorporating environmental effects into fatigue evaluations.

The original F_{en} expressions for carbon and low-alloy steels have been updated in this report using the larger fatigue ε–N database described in Table 4-1 to remove some of the conservatism in the F_{en} methodology and to reflect the additional data available since the initial publication of NUREG/CR-6909. As discussed previously, an additional objective of the reevaluation was to investigate the significance of the constant terms in the previous expressions. The updated evaluation addressed stakeholders' concerns related to (1) the constants in the F_{en} expressions that result in F_{en} values of approximately 2 even when strain rate is very high or temperature is very low and (2) the temperature dependence of F_{en} for carbon and low-alloy steels.

The available fatigue ε–N data for carbon and low-alloy steels were reanalyzed using a different dependence of fatigue lives on strain rate, DO, and temperature such that F_{en} is equal to 1 at high strain rates (i.e., greater than 2.2%/s). A single F_{en} expression was developed for both carbon and low-alloy steels. The functional form of the new F_{en} expression and for the dependence of F_{en} on the sulfur content in the steel were comparable to the expressions proposed by JNES.[136] In addition, a maximum temperature limit was selected at 325°C as a reasonable extension to cover most anticipated LWR operating conditions. This is adequate for expected operating LWR conditions considering the use of average temperature (as discussed in Section 4.4 and shown in Figure 4-67). In addition, the limit for the saturation strain rate was decreased from 0.001 to 0.0004%/s. A best fit of the experimental data yielded the following expression for F_{en}, which was defined as the ratio of fatigue life in air at room temperature (25°C (77°F)) to that in water at the service temperature, for both carbon and low-alloy steels:

$$F_{en} = \exp((0.003 - 0.031\dot{\varepsilon}^*)\, S^* T^* O^*), \tag{34}$$

where S^*, T^*, O^*, and $\dot{\varepsilon}^*$ are the transformed sulfur content, temperature, DO level, and strain rate, respectively, defined as follows:

$$\begin{aligned} S^* &= 2.0 + 98\,S && (S \le 0.015 \text{ wt.\%}) \\ S^* &= 3.47 && (S > 0.015 \text{ wt.\%}) \end{aligned} \tag{35}$$

$$\begin{aligned} T^* &= 0.395 && (T < 150°C) \\ T^* &= (T - 75)/190 && (150°C \le T \le 325°C) \end{aligned} \tag{36}$$

$$\begin{aligned} O^* &= 1.49 && (DO < 0.04 \text{ ppm}) \\ O^* &= \ln(DO/0.009) && (0.04 \text{ ppm} \le DO \le 0.5 \text{ ppm}) \\ O^* &= 4.02 && (DO > 0.5 \text{ ppm}) \end{aligned} \tag{37}$$

$$\begin{aligned} \dot{\varepsilon}^* &= 0 && (\dot{\varepsilon} > 2.2\%/s) \\ \dot{\varepsilon}^* &= \ln(\dot{\varepsilon}/2.2) && (0.0004\%/s \le \dot{\varepsilon} \le 2.2\%/s) \\ \dot{\varepsilon}^* &= \ln(0.0004/2.2) && (\dot{\varepsilon} < 0.0004\%/s). \end{aligned} \tag{38}$$

Figure 4-19 and Figure 4-20 plot the experimental values of fatigue lives compared to those predicted by Equation 34 and the expressions contained in the original version of NUREG/CR-6909 for carbon and low-alloy steels, respectively. The results indicate that the new F_{en} expressions represent a better fit of the experimental data relative to the fit for the expressions in the original version of NUREG/CR-6909; the regression (R-squared) values increased from 0.80 to 0.85 for carbon steels and from 0.83 to 0.84 for low-alloy steels. The new expressions typically underestimated environmental effects for operating conditions that resulted in very large F_{en} values (i.e., greater than 40) and in the high-cycle fatigue regime (i.e., fatigue lives above 50,000 cycles). However, such conditions are not typical of the thermal transients encountered during reactor operation or evaluated in most ASME Code CUF calculations. A threshold strain amplitude (one-half of $\Delta\varepsilon$) is also defined, below which LWR water environments have an insignificant effect on fatigue life. The threshold strain amplitude is specified as 0.07% or a 145 MPa (212 ksi) for both carbon and low-alloy steels.

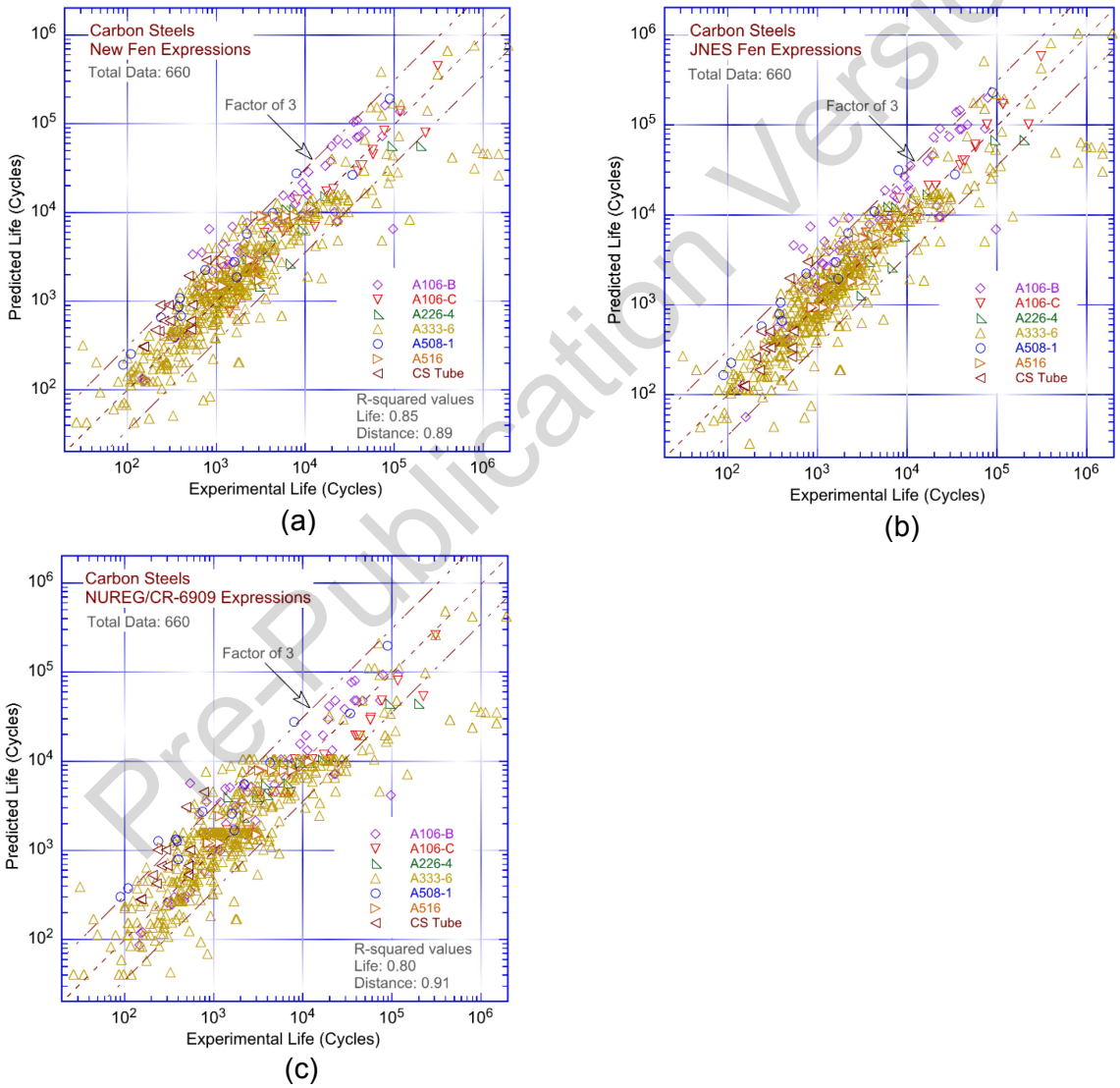

Figure 4-19 Experimental fatigue lives of carbon steel in LWR environments vs. fatigue lives predicted from the (a) new expression, (b) JNES expression, and (c) the previous NUREG/CR-6909 expression.

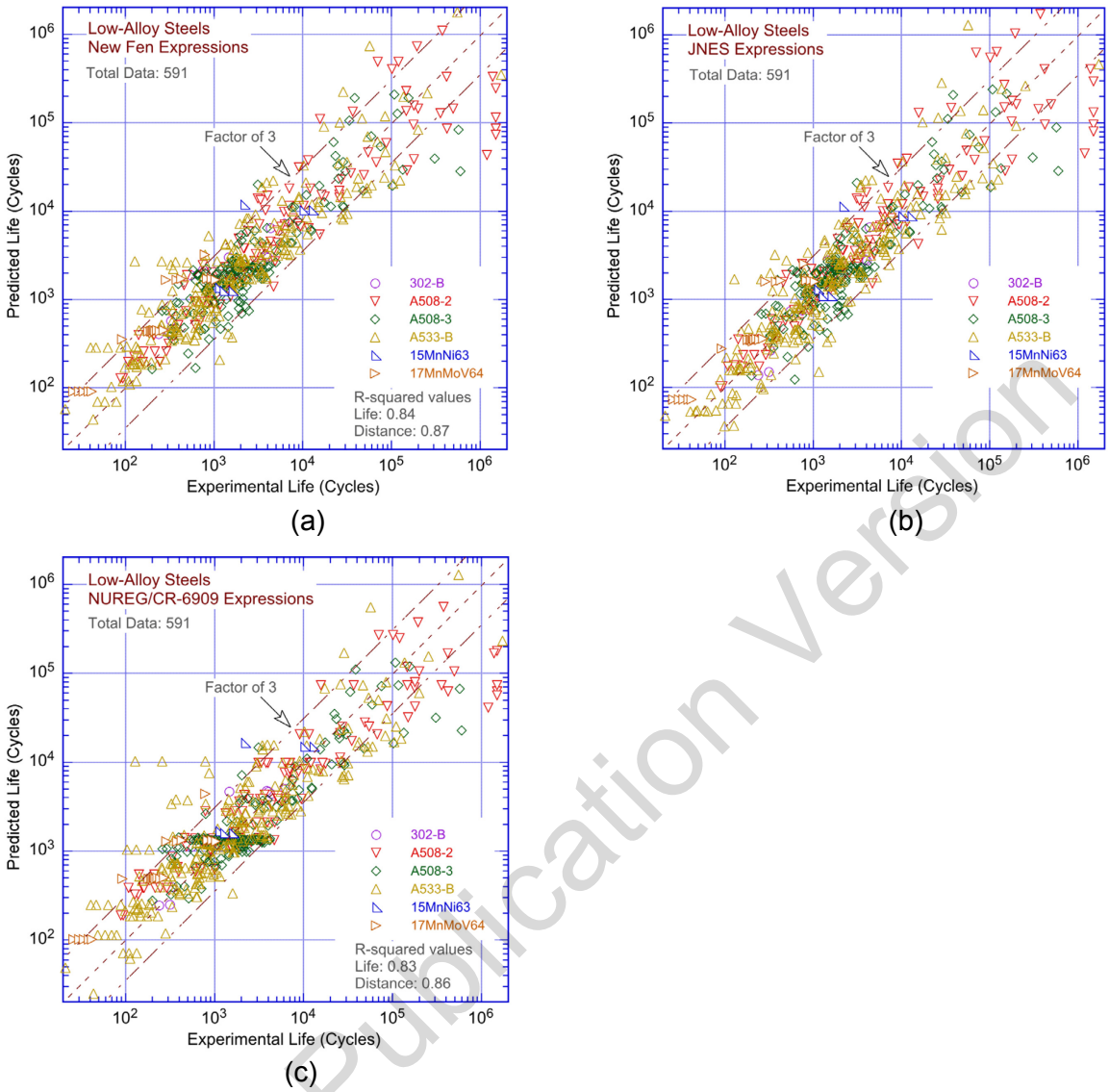

Figure 4-20 Experimental fatigue lives of low-alloy steels in LWR environments vs. fatigue lives predicted from the (a) new expression, (b) JNES expression, and (c) the previous NUREG/CR 6909 expression.

Figure 4-21 shows a comparison that was made of the fatigue lives predicted for carbon and low-alloy steels using the new F_{en} expressions and the JNES F_{en} expressions. In general, F_{en} values calculated from the new ANL expression were marginally lower than those obtained from the JNES expression in Reference 136; the fatigue lives predicted by the new ANL expressions were either comparable to or slightly longer than those predicted from the JNES expressions. However, there were a few data points for carbon steels and several data points for low-alloy steels for which the fatigue lives predicted by the JNES expression were significantly lower than those predicted by the new ANL expression (bottom left corner of the plots in Figure 4-21). As discussed previously, the new ANL F_{en} expression was optimized under environmental and loading conditions that are anticipated during reactor operation (i.e., conditions that yield F_{en} values less than 40). This optimization limitation explains the differences observed between the two expressions because the predicted F_{en} values for nearly all of these data points were above 60. The tests associated with these points were conducted in air-saturated water (8 ppm DO) at very low

strain rates. Considering this, the ANL and JNES expressions are in very good agreement, which is remarkable given that the development approaches used were different.

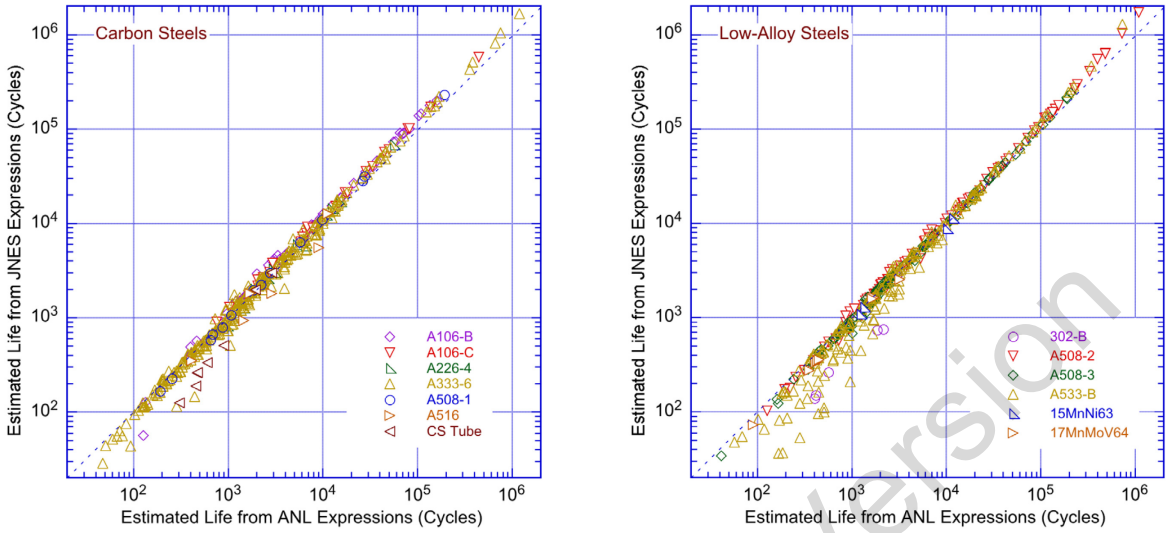

Figure 4-21 Comparison of the fatigue lives of carbon and low-alloy steels predicted from the new Fen expression and the JNES Fen expression.

Upon completion of the modeling phase, the residual errors (i.e., the Cartesian distance of each data point from the mean prediction curve) did not show significant patterns, such as heteroskedasticity (changing variance), or a nonzero slope. The residual errors for each variable, grouped by steel type, were plotted and are shown in Figure 4-22 and Figure 4-23 for carbon and low-alloy steels, respectively. The residuals were determined from the difference between the logarithms of the estimated lives and predicted lives. Thus, negative residual errors indicated conservative estimates of fatigue lives and positive residual errors indicated nonconservative estimates of fatigue lives (i.e., predicted lives were greater than the observed fatigue lives). However, if the residuals for a specific heat were not evenly distributed about zero, it did not necessarily indicate any deficiency in the predictive models. Such results indicated that the specific heat was either superior or inferior to the average behavior predicted by the model. For example, a positive residual indicated that the heat was inferior (i.e., the constant A from Equation 6 for the heat was smaller than the median value of A determined for the model) and a negative residual indicated that the heat was superior to the average behavior for the material. Section 4.1.13 discusses this behavior further.

The results presented in Figure 4-22 and Figure 4-23 did not show any unexplained patterns. In general, high variance tended to be associated with longer lives and lower strain amplitudes. Furthermore, biases were traceable to heat-to-heat variations. For example, the heats of A108-Gr. B, A508-Gr. 1, and A516-KC70 had inferior fatigue resistances and two heats of A333-Gr. 6 (ANL Material Identifications (IDs) 8 and 10 in Table 4-1) had superior fatigue resistances compared to the average behavior represented by the fatigue ε–N model (Equations 39 and 40).

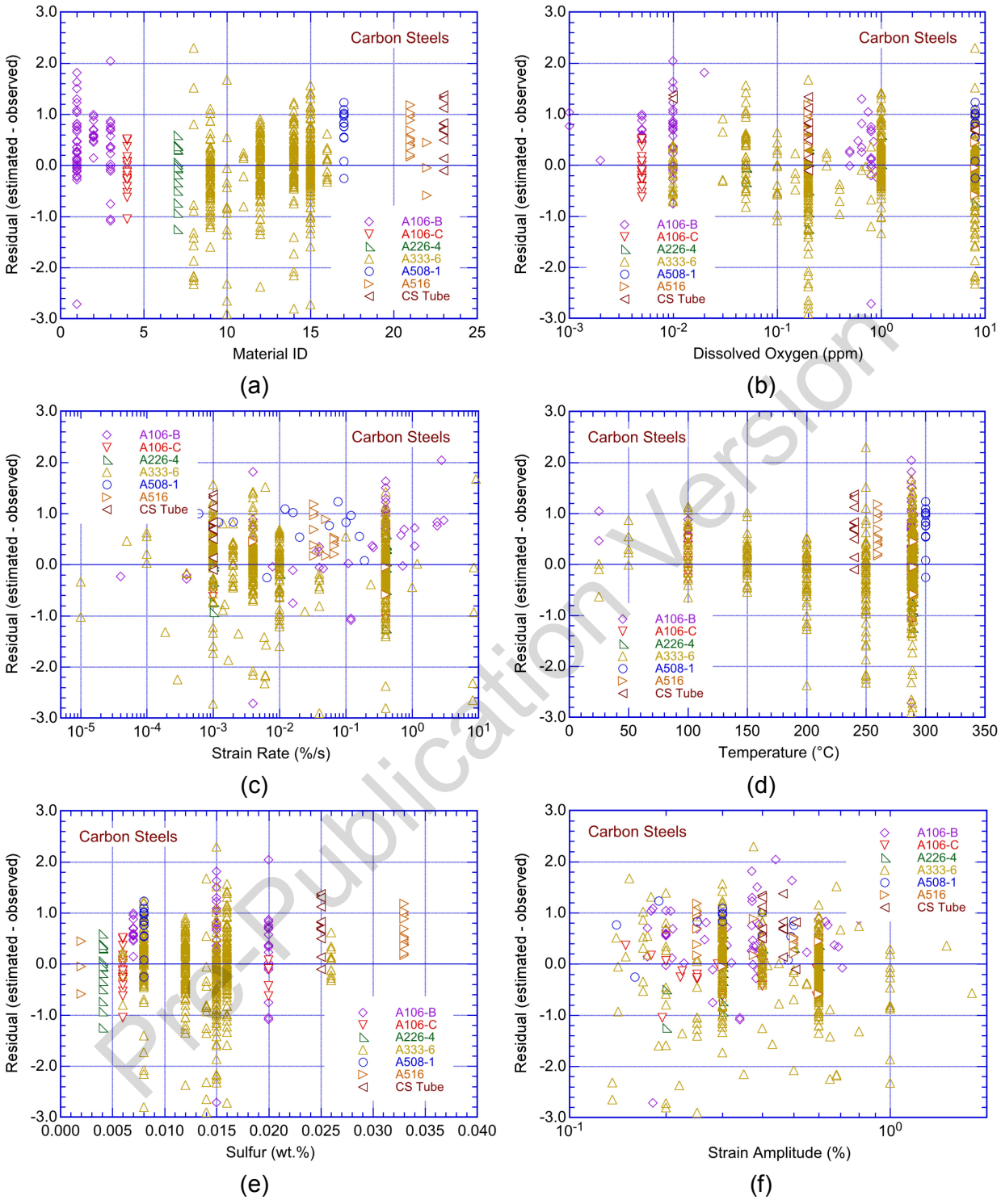

Figure 4-22 Residuals for predicted fatigue lives of carbon steels as a function of (a) Material ID, (b) water DO content, (c) strain rate, (d) temperature, (e) steel sulfur content, and (f) strain amplitude.

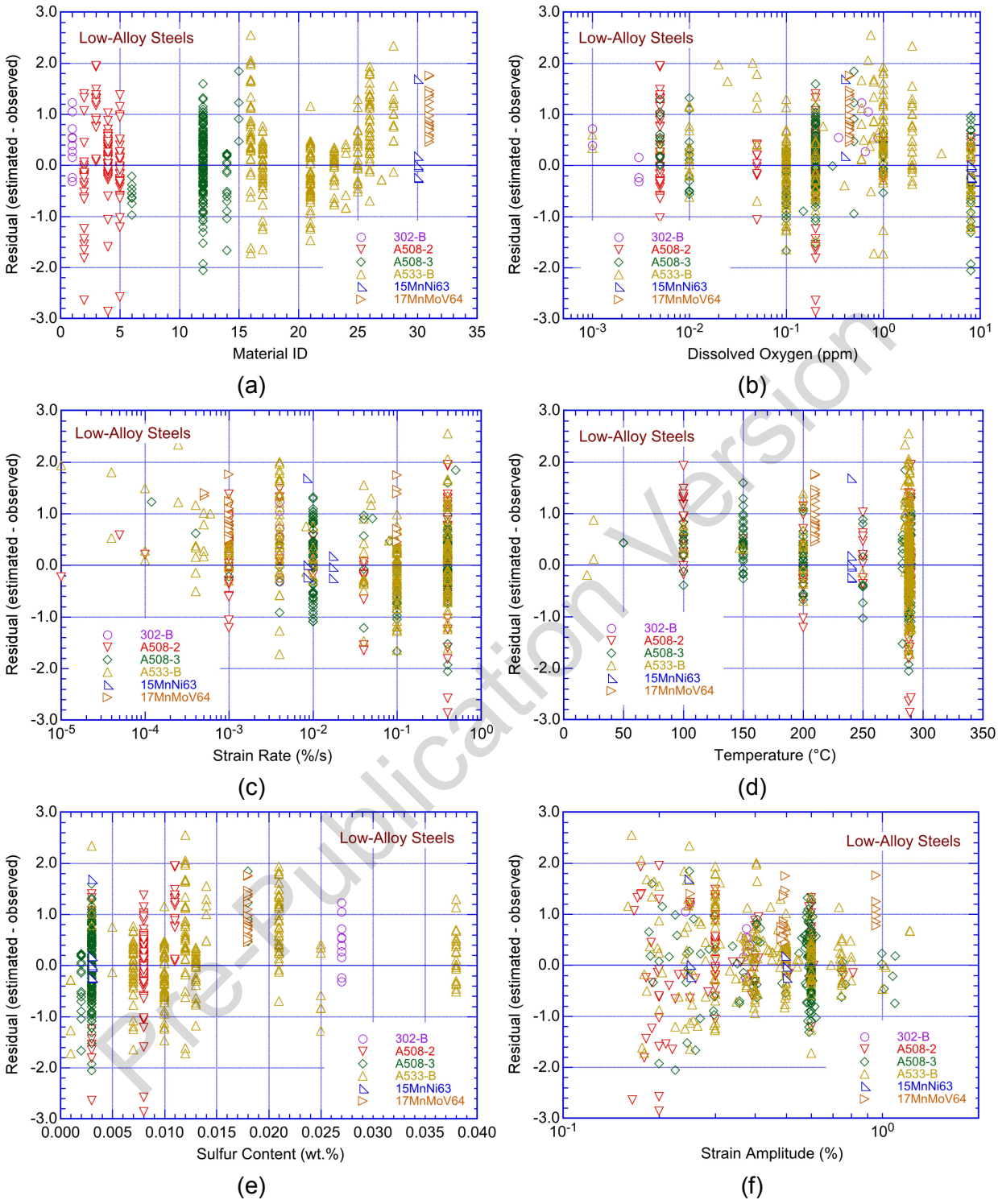

Figure 4-23 Residuals for predicted fatigue lives of low-alloy steels as a function of (a) Material ID, (b) water DO content, (c) strain rate, (d) temperature, (e) steel sulfur content, and (f) strain amplitude.

Some of the heats of carbon and low-alloy steels were also tested in air. The residual errors for the best fit of the fatigue ε–N data for carbon and low-alloy steels in air were plotted as a

function of the ANL Material ID, as shown in Figure 4-24. Most of the data subsets for fatigue tests in air followed the same trends observed in LWR environments; data subsets that yielded positive residuals in LWR environments also showed positive residuals in air, and vice versa.

The exception was ANL Material ID 21, which yielded a positive residual in an LWR environment but a negative residual in an air environment. However, the total data in air were quite limited for this heat of A516-KC70 carbon steel; therefore, quantitative conclusions were not made.

- *The F_{en} approach should be used to incorporate environmental effects into ASME Code, Section III fatigue evaluations for carbon and low-alloy steels. Appendix C of this report presents a sample application of F_{en} using the NB-3200 methodology.*

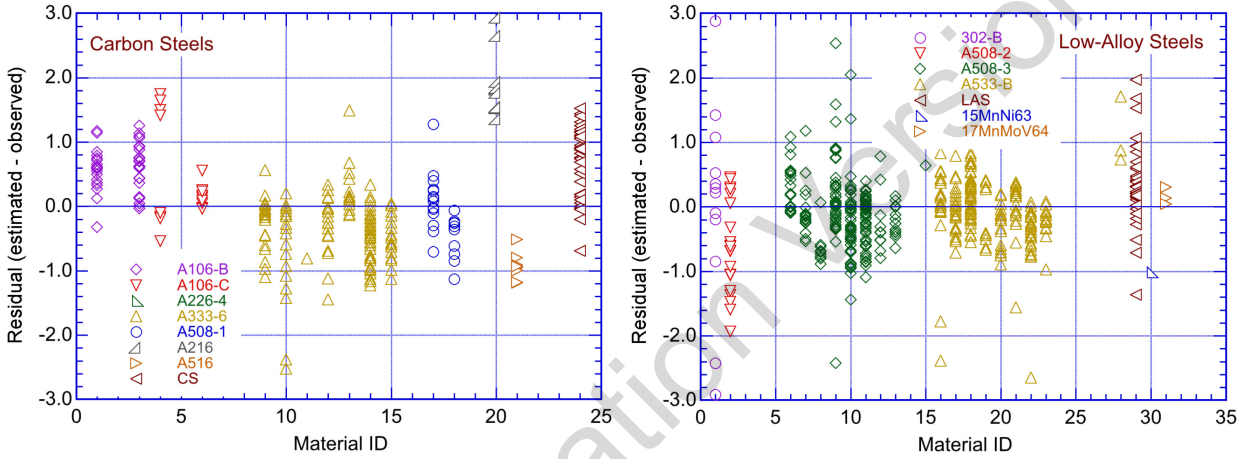

Figure 4-24 Residuals for predicted fatigue lives in air of carbon and low-alloy steels as a function of Material ID.

4.1.12 Surface Finish

Fatigue tests were conducted on specimens of carbon and low-alloy steels that were intentionally roughened in a lathe under controlled conditions with 50-grit sandpaper to produce circumferential scratches with an average surface roughness, R_a, of 1.2 μm and a root-mean-square surface roughness, R_q, of 1.6 μm (approximately 62 μin.).[46] Figure 4-25 shows the results for A106–Gr B carbon steel and A533–Gr B low-alloy steel. In air, the fatigue lives of rough A106–Gr B specimens were a factor of 3 lower than that of smooth specimens, and, in high-DO water, were the same as those of smooth specimens. In low-DO water, the fatigue lives of the roughened A106–Gr B specimen were slightly lower than those for smooth specimens. The effects of surface finish on the fatigue lives of A533–Gr B low-alloy steel were similar to those for A106–Gr B carbon steel; in high-DO water, the fatigue lives of both rough and smooth specimens were the same. The results in water were consistent with a mechanism of growth by a slip oxidation/dissolution process, which was not affected by surface finish. Surface roughness is expected to influence fatigue lives in LWR environments. However, additional data are needed to accurately establish the combined effects of surface finish and water environment on the fatigue life of carbon and low-alloy steels used in LWRs.

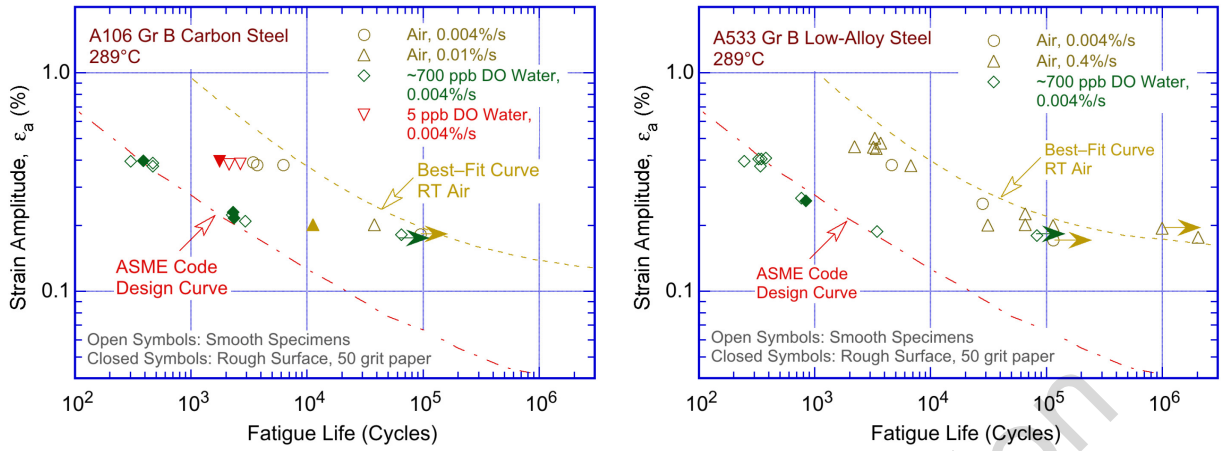

Figure 4-25 Effect of surface finish on the fatigue lives of (a) A106–Gr B carbon steel and (b) A533 low-alloy steel in air and high-purity water at 289°C (Ref. 46).

The potential additional impact of strain rate on the observed surface finish effects on the fatigue lives of low-alloy steels were also investigated (Figure 4-26).[144] The results showed a strong influence of strain rate on surface finish effects. At high strain rates, relative to smooth specimens, the fatigue lives of A533-Gr. B low-alloy steel decreased significantly even with slight increases in surface roughness, whereas at slow strain rates, because fatigue lives were already low, any further decrease in fatigue lives occurred only for very rough surfaces. The different behavior was attributed to the differences in the mechanism for corrosion fatigue of carbon and low-alloy steels in LWR environments. As discussed in Section 2.2.1.2, the corrosion fatigue mechanism changed from hydrogen-induced cracking to a slip-oxidation/dissolution mechanism with decreasing strain rates. During cyclic loading in high-temperature water, plastic deformation induced slip bands at the crack tip along the maximum shear directions or the preferred slip directions, which ruptured the protective oxide film at the crack tip. Furthermore, the slip bands were the favored paths for hydrogen transportation and the matrix/inclusion interfaces were the preferred traps for hydrogen. As a result, at high strain rates, fatigue cracking preferentially occurred along the slip bands and the matrix/inclusions interfaces, which resulted in macroscopically tortuous fatigue cracks and a rough fracture surface. However, at low strain rates, fatigue crack growth in high-temperature water was controlled by the film-rupture/oxidation-dissolution mechanism, which resulted in a macroscopically straight, relatively flat, featureless fracture surface.

The results in Figure 4-25 were also observed to be consistent with strain rate effects; the surface finish of the specimens that were tested at slow strain rates were not sufficiently rough to further decrease the fatigue lives.

- *The effects of surface finish were not explicitly included in the F_{en} for carbon and low-alloy steels; instead, they were included in the subfactor for "surface finish and environment" that was applied to the mean-data air curve to develop the fatigue design curve in air.*